INTERPLAY BETWEEN THE RETROVIRAL STRUCTURAL PROTEIN GAG AND THE PLASMA MEMBRANE DURING RETROVIRAL ASSEMBLY

A Dissertation

Presented to the Faculty of the Graduate School

of Cornell University

In Partial Fulfillment of the Requirements for the Degree of

Doctor of Philosophy

by

Yi Wen

August 2019

INTERPLAY BETWEEN THE RETROVIRAL STRUCTURAL PROTEIN GAG AND THE PLASMA MEMBRANE DURING RETROVIRAL ASSEMBLY

Yi Wen, Ph. D.

Cornell University 2019

The retroviral structural protein Gag is the primary driving force of assembly of retroviruses. Gag contains three major domains: the N-terminal Matrix domain (MA) for association with the inner leaflet of the plasma membrane (PM), the Capsid domain (CA) for Gag multimerization, and the C-terminal Nucleocapsid domain (NC) for packaging two copies of genomic RNA. The Gag-RNA, Gag-Gag, and Gag-membrane interactions together result in viral assembly. The work presented in this thesis focuses on human immunodeficiency virus type-1 (HIV-1) and Rous sarcoma virus (RSV) Gag interactions with membranes, aiming to understand how Gag binds to the inner leaflet of the PM and how the biophysical properties of the PM contribute to Gag assembly.

For membrane association, Gag may exploit electrostatic interactions, hydrophobic interactions, recognition of specific lipid headgroups, protein multimerization, and sensitivity to membrane order. HIV-1 Gag is naturally myristoylated while RSV Gag is not. HIV-1 MA is reported to be sensitive to membrane order, but the mechanism remains elusive. In a comparative study to probe effects of membrane charge and membrane order on Gag-membrane interactions, I developed model membranes with equal phosphatidylserine (PS) concentrations in both disordered (Ld) and ordered (Lo) phases. I found that RSV MA membrane association is primarily based on electrostatic interactions, being only sensitive to

membrane charge but not to membrane order. In contrast, myristoylated HIV-1 MA, and proteins containing hydrophobic regions, such as MARCKS, all show preference for disordered membranes.

Phosphatidylinositol 4,5-bisphosphate (PIP2) comprises approximately 2 mol% of total inner leaflet lipid. HIV-1 is hypothesized to assemble at PIP2-rich microdomains. To probe whether PIP2-rich domains exist under physiological conditions, I exploited inner leaflet model membranes and used biophysical methods such as self-quenching. I discovered that PIP2 forms clusters at remarkably low concentrations in a multivalent cation-dependent manner. Under physiological cation conditions, free PIP2 and cation-bridged PIP2 clusters can co-exist. Interestingly, I found that HIV-1 not only targets PIP2 clusters, but also further enriches PIP2 at assembly sites as Gag multimerizes in model membranes. I propose that PIP2 cation-bridged cluster formation and protein-induced PIP2 clusters could explain the distinct pools of PIP2 in biological membranes.

BIOGRAPHICAL SKETCH

Yi Wen was born on March 18th, 1991 and was raised in Kunming, the capital city of Yunnan province in southwest China, which is also known as the spring city. Richly endowed with natural resources, Yunnan has the greatest variety of both animal and plant species among all provinces in China. Yi was always full of curiosity and loved nature in her childhood. When she was offered an exam-free admission into the top senior high school in her hometown, she naturally chose to major in science. It was also during senior high school that Yi participated in a biological science project and learned about viruses and vaccines. This experience reminded her of the outbreak of severe acute respiratory syndrome (SARS) in 2003, when people had to wear thick masks all the time in public.

Due to an interest in the fascinating world of viruses, Yi chose biological sciences as a major in college, Minzu University of China in Beijing. To develop a comprehensive understanding of virology, Yi started a summer internship early in college at the Institute of Medical Biology of Chinese Academy of Medical Science, where she participated in project to manufacture and assess the effectiveness of inactivated H1N1 influenza virus vaccines derived from chicken embryos. This special experience deepened her fascination with viral infection and host immunity mechanisms against viruses at the molecular and cellular level. After finishing all courses within the first 3 years, Yi was determined to find a research lab to work on viruses. Since the start of the human immunodeficiency virus (HIV-1) epidemic in the 1980s, more than 70 million people have been infected and about 35 million people have died of AIDS. After the first Chinese HIV-1 outbreak, Yunnan has been the most affected area in the nation. Wanting to contribute her effort to HIV-1 research, Yi took a full-time position as a research assistant in Linqi Zhang's lab at the Comprehensive AIDS research center in Tsinghua University. She worked on a gene therapy-based

project that could ultimately provide a protected reservoir of CD4+ T cells resistant to HIV-1 infection, an essential first step towards a functional cure of AIDS. She employed transcription activator-like effector nucleases (TALENs) to knock out CCR5/CXCR4, the essential co-receptors for HIV-1 entry in human cells. The resulting cells exhibited robust, stable and heritable protection against many different HIV-1 subtypes.

After arriving at Cornell, Yi has had a unique opportunity of being co-mentored by two professors to work on collaborative and interdisciplinary projects. She studied biochemistry and virology with Dr. Volker Vogt and she learned membrane biophysics from Dr. Jerry Feigenson. Her research goal has been to understand how retroviruses interact with cell membranes during viral particle assembly and release. During her graduate studies, she presented a talk and several posters at major scientific conferences, and published her research work in peer-reviewed journals. She was awarded the Harry and Samuel Mann outstanding graduate student award of 2017. After her six-year PhD, she plans to take a postdoctoral position in the field of immunology, with the long term goal of applying her training in vaccine development and immunotherapy.

ACKNOWLEDGMENTS

First, I would like to thank Volker Vogt and Jerry Feigenson for their constant support and guidance throughout the PhD. I have been fortunate to have both of them as advisors. They have encouraged my research and helped me to grow as a research scientist. I am especially grateful for all the joint group meetings over the years that inspired me with ideas. I would like to express my sincere gratitude to Volker and Jerry for their insightful questions and comments to help guide me in developing critical thinking skills; for their continuous support in allowing me to attend many conferences to expand my knowledge; for their patient investment in teaching me to be a better writer; for their feedback and encouragement to help me improve as a public speaker; and for their enthusiasm, humility, generosity, and kindness in teaching me to be a better human being.

Second, I would like to thank the rest of my thesis committee, Warren Zipfel and John Parker, for their thoughtful suggestions about my research projects and for their caring encouragement about my career plans. I would also like to express my gratitude to other faculty members who have provided me with professional guidance during my graduate studies, including Bill Brown, Maurine Linder, Michael A. Rutzke, Hector Aguilar-Carreno, and Scott Emr.

Third, my sincere appreciation also goes to all of those with whom I have had the pleasure to work with in both Vogt and Feigenson labs. I thank my colleagues for the stimulating scientific discussions and fun personal conversations over the past six years, including Michael Weiner, David Ackerman, Thais Azevedo Enoki, Milka Doktorova, Naveen Mohideen, Aaron Troy, and Thomas Torng in Feigenson lab, and Jackie Dokko, Alejandro Rodriguez, Brian Jacobs, Danni Jin, and Ava Jarvis in Vogt lab.

Last but not the least, I would like to thank my husband, colleague, and life

partner Robert Dick for his help and support in the lab, and his love and caring for me in life. You are always there to motivate and encourage me when my confidence is low; you are always there to cheer me up when I am feeling down; and you are always there to celebrate and share joys with me when I accomplish even little things in life. I would also like to thank my parents for supporting me throughout my PhD and my life in general. I deeply appreciate everything you have done to help and support me. I could not have accomplished any of this without you.

TABLE OF CONTENTS

LIST OF FIGURES

LIST OF TABLES

LIST OF ABBREVIATIONS

acquired immunodeficiency syndrome (AIDS)

adult T-cell leukemia (ATL)

amphipathic helix (AH)

AP180 N-terminal homology (ANTH)

attenuated total reflection Fourier transform infrared (ATR-FTIR)

atomic force microscopy (AFM)

avian leukosis virus (ALV)

avian sarcoma/ leukosis viruses (ASLV)

Bin-Amphiphysin-Rvs (BAR)

capsid (CA)

cholesterol (Chol)

circular dichroism (CD)

clathrin-mediated endocytosis (CME)

critical micelle concentration (CMC)

critical PIP2 concentration (CPC)

C-terminal domain of capsid (CA-CTD)

cyclophilin A (CypA)

cytopathic effect (CPE)

cytoplasmic tail (CT)

cytoskeleton-associated protein (CAP23)

dehydroergosterol (DHE)

detergent-resistant membranes (DRMs)

diacylglycerol (DAG)

direct stochastic optical reconstruction microscopy (dSTORM)

double stranded DNA (dsDNA)

Ebola virus (EBOV)

electron microscopy (EM)

electron spin resonance (ESR)

endogenous retroviruses (ERVs)
endoplasmic reticulum (ER)
endosomal sorting complexes required for transport (ESCRT)
envelope (Env)
Epsin N-terminal homology (ENTH)
equine infectious anemia virus (EIAV)
Evectin2 (Ev2)
feline immunodeficiency virus (FIV)
FK506 binding protein (FKBP)
fluorescence correlation spectroscopy (FCS)
fluorescence photoactivation localization microscopy (FPALM)
fluorescence recovery after photobleaching (FRAP)
Foot and-mouth disease virus (FMDV)
Förster resonance energy transfer (FRET)
giant unilamellar vesicles (GUVs)
growth associated protein (GAP43)
HTLV-1 associated myelopathy/tropical spastic paraparesis (HAM/TSP)
hemagglutinin (HA)
Hepatitis C virus (HCV)
hexakisphosphate (IP6)
highly basic region (HBR)
human immunodeficiency virus type 1 (HIV-1)
human T-cell leukemia virus type 1 (HTLV)
inductively coupled plasma optical emission spectroscopy (ICP-OES)
inositol trisphosphate (IP3)
integrase (IN)
isopropyl -D-1-thiogalactopyranoside (IPTG)
L-a-phosphatidylinositol (liver PI)
L-a-phosphatidylinositol-4,5-bisphosphate (brain-PI(4,5)P2)
large unilamellar vesicles (LUVs)

liquid-disordered (Ld)

liquid-ordered (Lo)

lissamine rhodamine 18:1,18:1-PE (LR-DOPE)

long terminal repeats (LTR)

large unilamellar vesicle (LUVs)

major homology domain (MHR)

Marburg virus (MARV)

Mason-Pfizer monkey virus (MPMV)

matrix (MA)

methyl β-cyclodextrin (MβCD)

microtubule organizing center (MTOC)

monomeric neon green (mNG)

mouse mammary tumor virus (MMTV)

multilamellar vesicles (MLVs)

murine leukemia virus (MLV)

myristoylated alanine-richC kinase substrate (MARCKS)

naphtho[2,3-a]pyrene (naphthopyrene)

N-terminal domain of capsid (CA-NTD)

nuclear localization signal (NLS)

nuclear magnetic resonance (NMR)

nucleocapsid (NC)

open reading frame (ORF)

packaging signal (Ψ)

phenylmethylsulfonyl fluoride (PMSF)

PI transfer proteins (PITPs)

plasma membrane (PM)

pleckstrin homology (PH)

phosphatidylinositol 4-phosphate 5-kinase (PIP5K)

phosphatidylcholine (PC)

phosphatidylethanolamine (PE)

phosphatidylinositol (PI)

Phosphatidylinositol-3-phosphate [PI(3)P]

Phosphatidylinositol-4-phosphate [PI(4)P]

Phosphatidylinositol-4-phosphate [PI(5)P]

phosphatidylinositol 3,4-bisphosphate [PI(3,4)P2]

phosphatidylinositol 3,5-bisphosphate [PI(3,5)P2]

phosphatidylinositol 4,5-bisphosphate [PI(4,5)P2]

Phosphatidylinositol (3,4,5)-trisphosphate [PI(3,4,5)P3]

phosphatidylserine (PS)

phosphoinositides (PIPs)

phospholipase C (PLC)

polyethyleneimine (PEI)

polymerase (Pol)

polyphosphoinositide 5-phosphatase IV (5PtaseIV)

pre-integration complexes (PICs)

protease (PR)

rapid solvent exchange (RSE)

reverse transcriptase (RT)

reverse-transcription complexes (RTCs)

ribonuclease (RNase)

ribonucleoprotein (RNP)

Rous sarcoma virus (RSV)

single-stranded RNA (ssRNA)

simian immunodeficiency virus (SIV)

solid-gel (Lβ)

spacer peptide (SP)

sparsely tethered bilayer lipid membranes (stBLMs)

sphingomyelin (SM)

stimulated-emission depletion microscopy (STED)

surface (SU)

surface plasmon resonance (SPR)

transmembrane (TM)

thin-layer chromatography (TLC)

tris(2-carboxyethyl)-phosphine (TCEP)

untranslated regions (UTR)

Vesicular stomatitis virus (VSV)

virological synapse (VS)

virus-like-particles (VLPs)

walleye dermal sarcoma virus (WDSV)

wild type (WT)

Wiskott-Aldrich Syndrome protein (WASP)

yeast N-terminal myristoyl transferase (yNMT)

1,2-distearoyl-sn-glycero-3-phosphocholine (DSPC)

1,2-dipalmitoyl-sn-glycero-3-phospho-L-serine (DPPS)

1,2-dioleoyl-sn-glycero-3-phosphocholine (DOPC)

1,2-dioleoyl-sn-glycero-3-phospho-L-serine (DOPS)

1-palmitoyl-2-oleoyl-sn-glycero-3-phosphoethanolamine (POPE)

1-palmitoyl-2-oleoyl-sn-glycero-3-phospho-L-serine (POPS)

1-palmitoyl-2-oleoyl-sn-glycero-3-phosphocholine (POPC)

1-oleoyl-2-{6-[4-(dipyrromethene boron difluoride)butanoyl] amino}hexanoyl-sn-glycero-3-phosphoinositol-4,5-bisphosphate) (TF-PIP2)

1-oleoyl-2-(6-((4,4-difluoro-1,3-dimethyl-5-(4-methoxyphenyl)-4- bora-3a,4a-diaza-s-indacene-2-propionyl)amino)hexanoyl)-sn-glycero-3- phosphoinositol-4.5-bisphosphate (TMR-PIP2)

3,3'-dilinoleyloxacarbocyanine perchlorate (Fast DiO)

CHAPTER 1

INTRODUCTION TO RETROVIRUS ASSEMBLY

RETROVIRUS INTRODUCTION

Retroviruses are a family of enveloped, single-stranded (ss) positive-sense RNA viruses. They infect a wide variety of host vertebrates from fish, chickens, horses to humans; and they have been found to link to a wide spectrum of pathologies including many types of cancers and immunodeficiencies. Retroviruses are named for their own enzyme called reverse transcriptase, which was discovered independently in 1971 by Howard Temin and David Baltimore (1). Different from most viruses, retroviruses utilize reverse transcriptase to transcribe genomic RNA into DNA. This process makes it possible for the new DNA to be incorporated into the genome of infected cells by the viral integrase. A virus genome that is integrated into the DNA of a host cell is defined as a provirus or proviral DNA (2). Once the retrovirus has infected the host, the infection will persist indefinitely.

Two human retroviruses are especially important pathogens: human immunodeficiency virus type 1 (HIV-1), and the human T-cell leukemia virus type 1 (HTLV). HIV-1 is the pathogenic agent causing acquired immunodeficiency syndrome (AIDS). Since the beginning of the epidemic, an estimated 77.3 million people have become infected with HIV and 35.4 million people have died of AIDS-related illnesses. At the end of 2017, there were approximately 36.9 million people living with HIV globally, and a quarter of them are not aware of their infection status.

HTLV-1 is the causative agent of a type of cancer called adult T-cell leukemia (ATL) and also a demyelinating disease called HTLV-1 associated myelopathy/tropical spastic paraparesis (HAM/TSP), both of which are generally severe and progressively incapacitating (3). Globally, approximately 20 million people are thought to be infected with HTLV-1.

RETROVIRUS HISTORY

Retroviruses were first discovered in chickens more than 100 years ago. In 1908, Ellermann and Bang found that chicken leukemia was caused by a virus, which turned out to be avian leukosis virus (ALV) (4, 5). Only 3 years later, Peyton Rous reported the cell-free transmission of a sarcoma in chickens and successfully isolated the virus, which was named Rous sarcoma virus (RSV) (6). Together, the discovery avian sarcoma/ leukosis viruses (ASLV) paved the road for future discoveries of human retroviruses. During the next few decades, many other tumor-inducing viruses that cause neoplastic disease were discovered among mammalian species, including mice, cattle, and monkeys (7). Several viruses isolated during this period became important model systems still used today. The first pathogenic human retrovirus, HTLV-1, was reported by Robert C. Gallo and coworkers in 1980 and reconfirmed by Yorio Hinuma and coworkers in 1981 (3, 8, 9). The first successful isolation of HTLV-1 was from cultures of human leukemia T cells (10, 11). The HTLV-1 genome encodes several viral regulatory proteins (Tax and Rex), and so it became the prototype of a complex retrovirus (12).

At the similar time of HTLV-1 isolation, AIDS epidemics arose in several developed countries. The isolation of what is now called HIV-1 (also be referred to as HIV, LAV, IDAV-1, IDAV-2, LAV-1, HTLV-III and ARV) was from a patient with lymphadenopathy, using the protocol previously described for HTLV-1 by Gallo. Sequencing results showed that the HIV-1 genome is capable of coding for several regulatory proteins in addition to the standard retroviral proteins. Initial electron micrographs showed that the HIV-1 particles have a conical core structure, not resembling the spherical core seen in HTLV-1 particles. Following immunofluorescence and anti-sera experiments that distinguished HIV-1 from HTLV-1, HIV-1 was discovered as a brand-new human retrovirus (13, 14). HIV-1 was quickly found to be the causative pathogen of AIDS, which only took two and half years after its initial identification (15). Of note, HIV-1 belongs to the lentivirus family, which is characterized by long incubation periods. More than a century ago, the first descriptions of two lentiviral diseases, equine infectious anemia, and Visna, a sheep neurological disease (Sigurdsson 1954) gave rise to the concept of slow viral infections (7). Several lentiviruses were later learned to induce immunodeficiency in various species of mammals, including apes, cows, goats, cats, and humans (16, 17).

CLASSIFICATION OF RETROVIRUSES

The retroviruses encompass a large family called Retroviridae, which shares common virion structure and viral replication mode. The family Retroviridae is now divided into two subfamilies: Orthoretrovirinae and Spumaretrovirinae (Fig. 1.1). The Orthoretrovirinae subfamily currently includes six genera. Alpharetrovirus is a genus

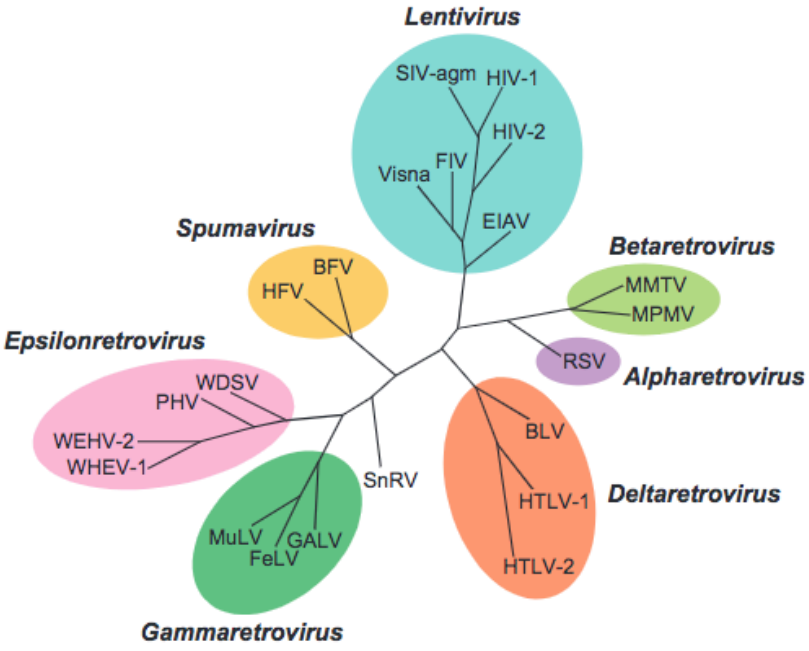

Fig 1.1 Retrovirus classification. The family Retroviridae is divided into two subfamilies Orthoretrovirinae and Spumaretrovirinae and seven genera. Images are adapted from Virus Taxonomy: Ninth Report of the International Committee on Taxonomy of Viruses. King, A.M., Adams, M.J., Carstens, E.B., Lefkowitz, E.J., Copyright © 2012 International Committee on Taxonomy of Viruses. Published by Elsevier Inc.

of avian retroviruses that was first discovered, including Rous sarcoma virus (RSV). Betaretroviruses infect mammals and include mouse mammary tumor virus (MMTV) and Mason-Pfizer monkey virus (MPMV). Gammaretrovirus members also infect mammals and murine leukemia virus (MLV) is an example. Deltaretrovirus is the genus that includes the human pathogen HTLV-1 and also the related HTLV-II. Epsilonretrovirus members can infect fish, such as walleye dermal sarcoma virus (WDSV). Lastly, Lentivirus (Latin: lentus, slow), characterized by its slow disease progression, causes immunodeficiency in many mammals, such as in cats (feline immunodeficiency virus, FIV), in primates (simian immunodeficiency virus, SIV and HIV types 1 and 2), and in horses (equine infectious anemia virus, EIAV). Alpha-, Beta-, Gammaretrovirus are considered simple retroviruses, while Epislonretrovirus, Deltaretrovirus and Lentivirus are considered complex due to their additional viral regulatory and accessory proteins. Viruses in the Spumaretrovirinae subfamily are also known as foamy viruses due to the characteristic 'foamy' appearance of the cytopathic effect (CPE) induced in the infected cells. Spumaviruses contain significant amounts of double-stranded full-length DNA, and many of them assemble and bud through the endoplasmic reticulum (ER) instead of the plasma membrane (PM) (18). There are many differences between Orthoretroviruses and Spumaviruses in the viral life cycle. Therefore, the topics covered in the remainder of this thesis refer exclusively to Orthoretroviruses, unless otherwise noted.

Retroviruses are also classified based on their morphological types under the electron microscope as Type- A, B, C and D (19). The Type-A viruses bud intracellularly in the ER, and have an "immature" morphology, which features an

electron lucent core and one or two concentric electro-dense rings. Type-B viruses have an eccentric round core with MMTV as the prototype. Type-C viruses have a central electron-dense “mature” core, and most of tumor-inducing viruses are of this type, such as MLV. The D-type viruses all have a bar-shaped or cone-shaped core, including MPMV and all Lentiviruses.

Retroviruses can also exist in two forms: exogenous and endogenous. Exogenous retroviruses are infectious and mostly pathogenic, and are transmitted horizontally among individuals. Endogenous retroviruses (ERVs) are discrete genetic loci in vertebrate genomes that bear homology to retroviral proviral gene sequences and organization (20). Many ERVs have persisted in the host genomes for millions of years, so they are considered remnants of ancestral infections. ERVs have acquired mutations during host DNA replication that make them no longer produce virions. Unlike exogenous retroviruses, the majority of ERVs are not pathogenic. The abundance of ERVs suggests that a near-constant presence of retroviruses throughout the vertebrate evolution.

THE RETROVIRAL GENES

The retroviral genome is single stranded, positive sense RNA, about 7000-12,000 nucleotides long. The coding region is flanked by 5' and 3' untranslated regions (U5 and U3), and also by a short repeated (R) sequence at both termini (Fig. 1.2). Similar to a typical eukaryotic mRNA, the retroviral RNA genome contains a 5' cap and 3' poly-A tail. However, after reverse transcription, the double stranded

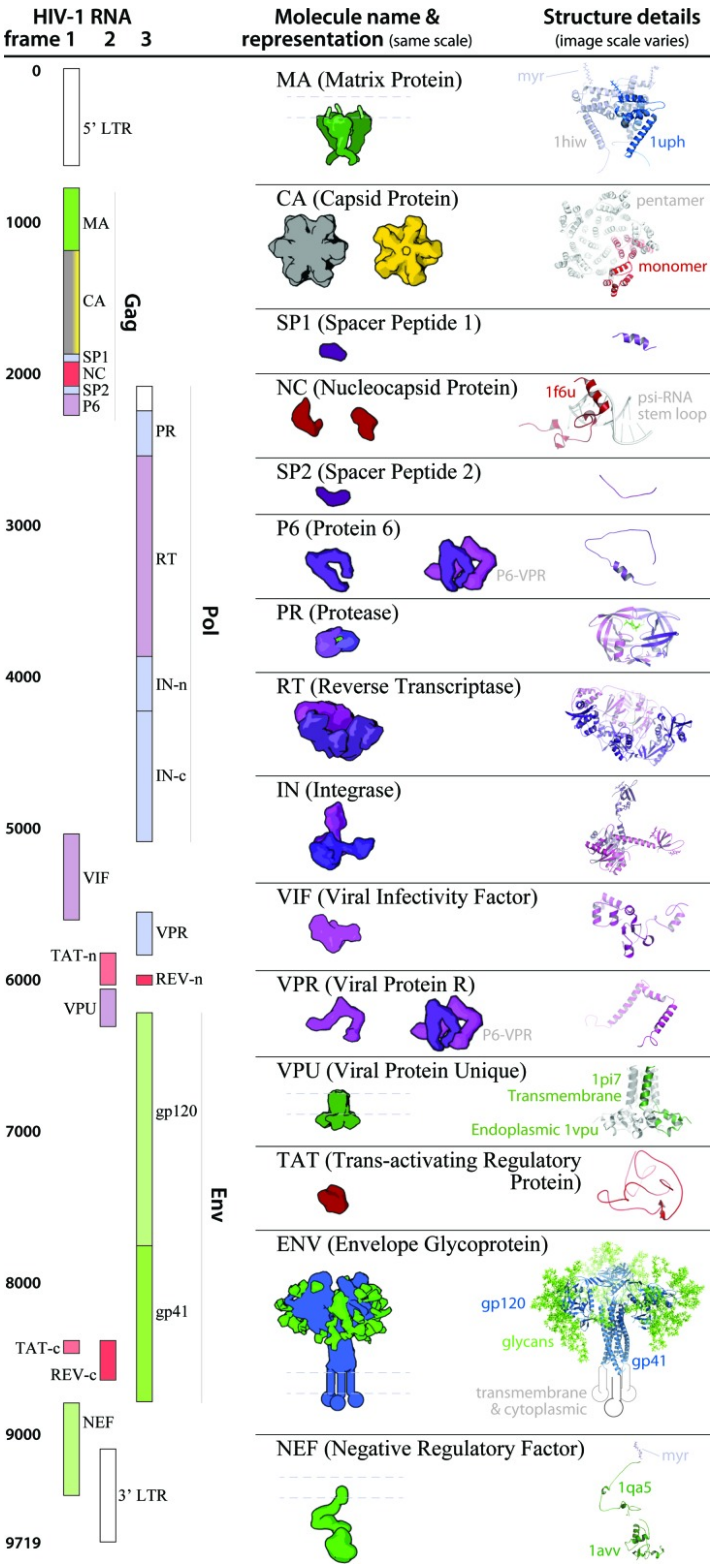
HIV-1 RNA
frame 1 2 3
Molecule name & representation (same scale)
Structure details (image scale varies)
0
5' LTR
1000
MA
CA
SP1
NC
SP2
P6
Gag
2000
PR
RT
IN-n
IN-c
Pol
3000
4000
5000
VIF
VPR
TAT-n
REV-n
6000
VPU
gp120
gp41
Env
7000
8000
TAT-c
REV-c
NEF
9000
3' LTR
9719
MA (Matrix Protein)
myr
1hiw
1uph
CA (Capsid Protein)
pentamer
monomer
SP1 (Spacer Peptide 1)
NC (Nucleocapsid Protein)
1f6u
psi-RNA stem loop
SP2 (Spacer Peptide 2)
P6 (Protein 6)
P6-VPR
PR (Protease)
RT (Reverse Transcriptase)
IN (Integrase)
VIF (Viral Infectivity Factor)
VPR (Viral Protein R)
P6-VPR
VPU (Viral Protein Unique)
1pi7
Transmembrane
Endoplasmic 1vpu
TAT (Trans-activating Regulatory Protein)
ENV (Envelope Glycoprotein)
gp120
glycans
gp41
transmembrane & cytoplasmic
NEF (Negative Regulatory Factor)
myr
1qa5
1avv

Fig 1.2 HIV genome organization and viral proteins. The HIV-1 genome is about 9.7 kb, which comprises two LTRs (long terminal repeats) flanking the internal unique sequence. The HIV-1 genome contains 9 open reading frames that produce 15 proteins with molecular representations and structural details shown above. The Gag polyprotein is proteolytically cleaved to generate the matrix (MA), capsid (CA), nucleocapsid (NC), and p6 proteins. The *gag-pol* encodes protease (PR), reverse transcriptase (RT), and integrase (IN). In addition, The HIV-1 *env* gene encodes gp120 and gp41. HIV-1 also encodes two important regulatory elements: Tat and Rev and a few important accessory proteins Vif, Vpr, Nef, and Vpu (in HIV-1) or Vpx (in HIV-2). Figure is from Johnson, G.T., Goodsell, D.S., Autin, L., Forli, S., Sanner, M.F. and Olson, A.J., 2014. 3D molecular models of whole HIV-1 virions generated with cellPACK. Faraday discussions, 169:23-44 - Published by The Royal Society of Chemistry.

proviral DNA genome is longer than its corresponding RNA genome. The additional long terminal repeats (LTR) are composed of U3, R and U5 elements ("U" for unique to that end) (21). The LTR harbors sequences that are important for further integration and transcription.

All retroviral genomes contain four conserved genes: *gag, pro, pol*, and *env* (Fig. 1.2). The *gag* gene encodes a structural polyprotein called Gag, which will eventually be cleaved into three conserved domains called matrix (MA), capsid (CA), nucleocapsid (NC), and additional peptides in some viruses. The *pro* gene encodes the viral protease (PR) that proteolytically cleaves Gag during maturation. The location of the *pro* gene varies, either in the 3' end of the *gag*, the 5' of the pol or between *gag* and *pol*. The *pol* gene encodes the reverse transcriptase (RT) that generates a proviral DNA copy from the viral RNA genome, and the integrase (IN) that inserts the proviral DNA into the host chromosome. The *env* gene encodes the envelope protein, which is cleaved in the Golgi apparatus to yield two glycosylated polypeptides called surface (SU) and transmembrane (TM), both of which form a complex that mediates viral entry by first interacting specifically with cellular receptor proteins, and then fusing the viral and cellular membranes. Retroviruses that harbor only *gag*, *pro*, *pol*, and *env* genes are simple retroviruses, while others that contain additional accessory genes are complex retroviruses, such as HIV-1 and HTLV-1. Some of these encoded accessory proteins are critical for viral replication. Some retroviruses also carry oncogenes that have been acquired from host cells, which enable these viruses to transform cells oncogenically or induce tumors in animals. RSV, for example, has acquired the *v-src* gene, derived from cellular *c-src*, allowing it to cause tumors in infected chickens.

THE RETROVIRAL LIFE CYCLE

The life cycle of retroviruses (Fig. 1.3) can be divided into two distinct stages: early and late stage (22). The early stage includes viral binding and entry, uncoating, reverse transcription, nuclear import, and integration . The late stage includes transcription, nuclear export, packaging and translation, viral particle assembly, budding and maturation.

Entry

The retroviral life cycle begins when the SU protein on the viral envelope recognizes and binds to specific receptors on the host cell PM (23). In addition to CD4 found on T-helper lymphocytes, HIV-1 entry also requires an additional co-receptor called CCR5 or CXCR4 (24, 25). Receptor/co-receptor binding triggers conformation changes in viral Env proteins, which leads to dissociation of SU from TM, and induces the fusogenic domain within TM to contact the host PM (26). Entry of virions into the cell is achieved by retroviral TM proteins inserting into the target membrane, forming a six-helix bundle. Full fusion of viral and cellular membranes allows the release of the viral core into the cytoplasm.

Uncoating

After its release into the cytoplasm, the viral core undergoes a disassembly process known as uncoating. However, it still remains unclear what the precise timing and location are for this event (27). Viral uncoating depends on capsid stability and

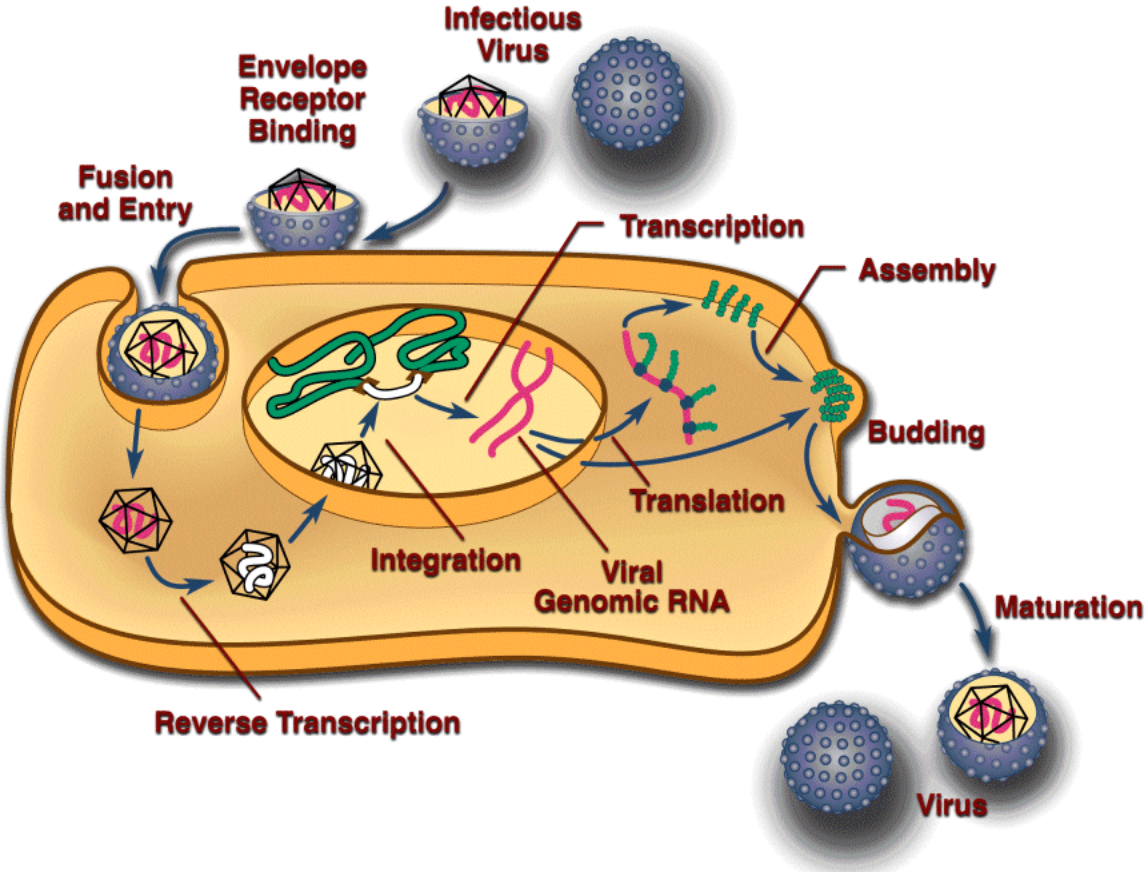

Fig 1.3 An overview of retrovirus life cycle. Virions enter the host cells by interaction of the viral Env to a specific cellular receptor. Following a fusion event, the viral core is released into the cell cytoplasm. Reverse transcription of the viral genomic RNA results in a dsDNA that is integrated into the host DNA. Cellular machinery-mediated transcription and translation of viral RNA and protein lead to retroviral assembly at the inner leaflet of the plasma membrane. Cellular ESCRT proteins are recruited to the budding site to facilitate the release of virus particles from cells. During or following fission, viral protease becomes active and cleaves Gag proteins at multiple sites. Progeny virions undergoes a maturation process to become infectious. Images are adapted from Retroviruses, John M. Coffin, Stephen H. Hughes, and Harold E. Varmus, Copyright © 1997, Cold Spring Harbor Laboratory Press.

interaction with host factors (28). Premature or delayed uncoating affects viral DNA production and nuclear import, and reduces viral infection. Interactions with cellular proteins, such as the cellular protein cyclophilin A (CypA) for HIV-1, have been shown to stabilize or destabilize viral capsid, depending on the cell and the retrovirus type (28).

Reverse Transcription

Uncoating leads to the generation of subviral particles called reverse-transcription complexes (RTCs) and pre-integration complexes (PICs). The net result of reverse transcription is the synthesis of a double-stranded DNA copy from the viral RNA genome by RT (1, 29, 30). RT has two distinctive enzymatic functions. A DNA polymerase function is to utilize DNA or RNA as a template for DNA synthesis. RT also harbors a ribonuclease H (RNase H) function that specifically cleaves RNA in RNA–DNA hybrids. Using tRNA as a primer, the minus strand DNA is synthesized first. Then a short RNase H-resistant, purine-rich RNA is produced as a primer for positive strand DNA synthesis. After carrying out displacement synthesis, a blunt-ended linear duplex proviral DNA is produced, with the characteristic LTR at both ends. RT has no proofreading activity, which results in frequent mutation and recombination, which promote viral evolution and diversification (31, 32).

Nuclear Import

The PIC is trafficked through the cytoplasm, possibly by hijacking cytoskeletal components. For some retroviruses, the PICs are able to actively cross the nuclear

through the nuclear pore (HIV-1), while for others, the PICs must wait for the breakdown of the nuclear membrane during cell mitosis (MLV) (33, 34).

Integration

Once inside the nucleus, the proviral DNA is integrated into the host genome by IN (35, 36). After trimming overhangs, short single-strand gaps are soon filled and ligated by cellular enzymes. The integrated provirus is flanked by a 4–6-bp duplication relative to the preintegration site in host DNA. Proviral insertion sites are not specific, so it is possible to cause a loss-of-function or a gain-of-function mutation in the host genome. Integration stabilizes the proviral DNA against degradation, and ensures efficient generation of viral genome and mRNAs using cellular machinery. Evidence suggests that there are strong biases in HIV-1 DNA integration site selection, which facilitate aggressive HIV-1 replication (37, 38).

Transcription and nucleus export

As soon as integration takes place, the retroviral life cycle enters the late stage. Viral DNA is transcribed as a full-length RNA product, mediated by RNA polymerase II (39). Complex retroviruses encode trans-activators to enhances gene transcription, Tat and Tax in the case of HIV-1 and HTLV-1, respectively (40, 41). Retroviral RNA contains splice donor and acceptor signals that utilize cellular splicing machinery to produce unspliced mRNAs as well as singly (and in complex retroviruses multiply) spliced mRNAs. Complex retroviruses also encode viral proteins like Rex (HTLV-1) and Rev (HIV-1) to mediate transport of unspliced RNAs to the cytoplasm (42, 43).

Translation

To achieve translation in the cytoplasm, retroviruses again exploit cellular translation machinery (44). The full-length transcript is used to synthesize the structural Gag polyprotein and PR, RT, and IN as part of the Gag-pro-pol polyprotein. Retroviruses have developed two distinctive mechanisms that permit production of Gag-pol that can be automatically incorporated into the virus together with Gag (39, 45). The result is the production of about 20 Gag polypeptides to 1 Gag–pro-pol polypeptide. The first mechanism, used by most retroviruses, is ribosomal frameshifting. During translation of *gag*, ribosomes slip backward one nucleotide, leave the *gag* open reading frame (ORF), and shift to the overlapping region of pro-pol ORF. The second mechanism, used by gamma retroviruses, is readthrough termination, in which the stop codon in Gag is misread as a sense codon to allow the translation to continue into pro-pol ORF. For many retroviruses, the Gag protein as well as the Gag-pro-pol proteins are modified by the addition of a 14-carbon fatty acid to the terminal glycine after the initial methionine removal (46, 47, 48). The myristate is crucial for Gag binding to the PM (49, 50, 51).

On the other hand, the large Env polyprotein is synthesized from a spliced transcript, and follows the same path as other secreted proteins. The translation of Env begins on cytoplasmic free ribosomes, which is then transported to the rough ER, mediated by a small hydrophobic signal peptide (52, 53). Once Env is synthesized, post-translational modifications take place on both the SU and TM subunits. SU is glycosylated for all retroviruses, while TM is glycosylated for most retroviruses. Env

oligomerizes into a trimer and is then trafficked through the Golgi apparatus. During this transit, a furin-like protease cleaves Env into the two domains, which remain non-covalently associated (52, 54-56). This process generates a hydrophobic fusion peptide at the amino terminus of TM. During the trafficking through the Golgi apparatus, additional sugars are added to SU, which contributes to the overall the heterogeneity of Env (57). Finally, the trimeric Env complexes are transported to the PM, where they are incorporated into assembling viral particles.

Membrane binding and assembly

Retroviral assembly begins in the cytosol. In summary, retroviral assembly is a combined process of multimerization of thousands of Gag molecules, interacting with the PM, and packaging two copies of viral genomic RNA (58-61). How Gag proteins target to the PM among all available cellular membranes is intriguing. Gag protein alone is sufficient to drive assembly and budding of virus-like-particles (VLPs) (62). During assembly, Gag associates with the host membrane via the MA domain, Gag multimerizes via the CA domain, and specifically binds and packages retroviral genomic RNA via the NC domain (Fig. 1.4). And these interactions facilitate each other. For example, RNA binding brings multiple Gag together in the proper elongated conformation, which enhances Gag-Gag interactions, and further increases overall Gag membrane binding (63). More details of retroviral assembly will be discussed in the following section.

Budding

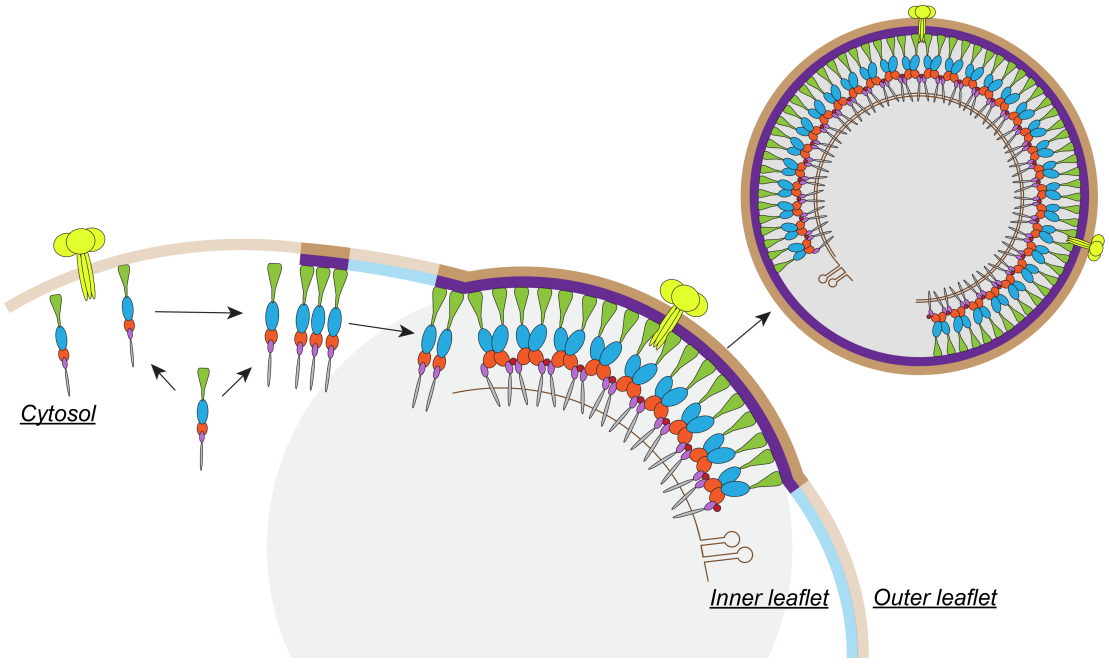

Fig 1.4 An illustration of HIV-1 assembly at the PM. Synthesized in cytosol, Gag targets and binds to the inner leaflet of the PM, as Gag multimerizes and packages genomic viral RNAs. HIV-1 seems to assemble at microdomains enriched in phosphatidylinositol 4,5-bisphosphate [PI(4,5)P2] shown as dark purple regions at the PM, and the released HIV-1 particle has enriched PI(4,5)P2 in viral membranes.

The viral budding has two stages. First is membrane deformation, with the membrane wrapping around the assembling Gag lattice. Second is membrane fission, in which retroviruses hijack the endosomal sorting complexes required for transport (ESCRT) machinery to facilitate the liberation of virus particles, similar to many other enveloped viruses (60, 64). The recruitment of ESCRT requires a short motif in Gag called the late domain, such as P(T/S)AP (HIV-1), PPXY (RSV), and YPXL (EIAV) (65-67). Many lentiviruses also harbor a secondary late domain. Viruses like HIV-1 appear to recruit multiple ESCRT-associated factors such as TSG101, ALIX, and NEDD4L in a stepwise fashion to achieve viral budding (68-70). How Env glycoproteins expressed on cell surface are incorporated into viral particles is not fully understood (52).

Maturation

During or immediately after viral budding, Gag and Gag–Pol proteins are cleaved into their mature forms by the viral PR, which then leads to a dramatic change in the virion core by protein reorganization (60, 71, 72). All retroviruses require this maturation process to become infectious. After Gag undergoes PR cleavage, MA remains associated with the viral membrane, NC packages the viral RNA genome that dimerizes, and CA condenses into a mature capsid shell enclosing both the viral genome and enzymes. PR is an aspartic protease and the active form is a dimer (73-74). PR activation must be tightly controlled, because premature activation hinders proper assembly of viral particles. However, the exact timing and mechanism of PR activation are not known. The ordered processing of Gag might be important for

infectivity. The rate of cleavage at individual sites varies over wide range, due mostly to local sequence, but some evidence suggests that the cleavages have to take place in an ordered way (75, 76).

THE RETROVIRAL GAG PROTEIN

The Gag polyprotein is the primary retroviral structural protein that drives assembly of progeny viral particles (58, 77). Gag is composed of three conserved domains: MA, CA and NC, as well as a variety of short peptides or proteins depending on the viral genus. Even though there is low sequence similarity between different retroviruses, these canonical domains exhibit strong structural conservation (78). See Fig. 1.5 for an overview of Gag domain organization in the alpha-, beta-, gamma-, delta-, and lenti-virus genera.

MA domain

MA is the N-terminal domain of Gag that associates with the PM of the host cells. Even though only sharing little sequence similarity, all retroviral MA domains fold into similar alpha-helical structures, which expose patches of basic residues on their surfaces (79). Most retroviruses also contain an N-terminal 14-carbon fatty acid, called myristate. However, the alpharetrovirus RSV, and the lentivirus EIAV lack this myristoylation (80). Many retroviruses associate with membranes by exploiting both of the surface basic patches and the hydrophobic myristate. Studies have also shown that MA also is able to bind cellular RNA species, which regulates MA membrane binding (63, 81).

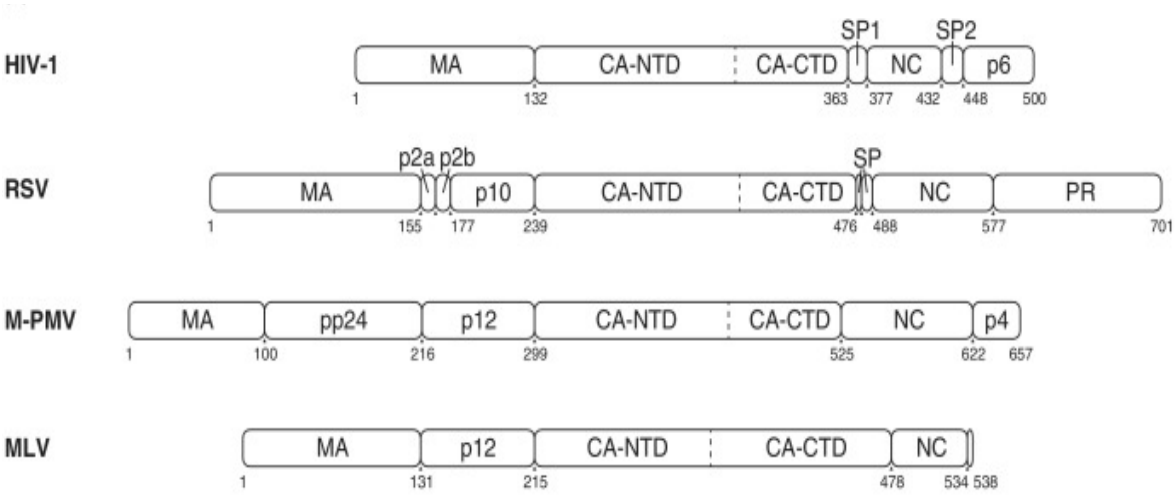

Fig 1.5 The retroviral Gag protein organization. A schematic depiction of Gag polyprotein in human immunodeficiency virus type 1 (HIV-1), Rous sarcoma virus (RSV), Mason-Pfizer monkey virus (M-PMV) and murine leukemia virus (MLV). Images are adapted from Mattei, Simone, Florian KM Schur, and John AG Briggs. 2016. Retrovirus maturation—an extraordinary structural transformation. Curr Opin Virol. 18:27-35. https://doi.org/10.1016/j.coviro.2016.02.008. This article is available under the terms of the Creative Commons Attribution License (CC BY). https://creativecommons.org/licenses/by/4.0/

CA domain

CA is critical for Gag multimerization. CA is the biggest domain and is the most conserved domain within Gag. An N- terminal subdomain called CA-NTD containing seven α-helices and a C- terminal subdomain called CA-CTD containing four α-helices are connected by a short flexible linker. Structures of both CA-NTD and CA-CTD have been solved in many retroviruses (79). CA contains a highly conserved region, about 20 amino acids, called the major homology domain (MHR), which is conserved among Orthoretrovirinae. Mutations in the MHR often compromise assembly and abrogate infectivity.

NC domain

NC recognizes, binds, and packages the viral genomic RNA. NC is the smallest conserved domain in Gag. In all retroviruses, except spumaviruses, NC has one or two characteristic "zinc finger" Cys-His motifs (CX2CX4HX4C), that allow NC to recognize and bind viral genomic RNA via the ψ element (psi) at the 5' UTR (82). This specific NC binding to psi is how retroviruses distinguish the viral genomic RNA from an abundant pool of cellular RNA (83-85). NC also harbors patches of basic residues that contribute to the nucleic acid binding. It has been proposed that retroviral assembly initiates when several Gag proteins bind to dimeric genomic RNA via NC domains. In vitro studies on RSV show that oligonucleotides that support Gag assembly must be at least 16 nucleotides in length. These oligonucleotides are long enough to accommodate two binding Gag molecules (86). The NC domain of RSV and HIV-1 replaced with a leucine zipper dimerization domain supports Gag assembly

(87, 88). These results suggest that a Gag dimer is the minimal multimeric state required to initiate retroviral assembly.

Minor domains

The minor domains cleaved from Gag vary for different retroviruses. The minor domains of RSV, HIV-1 are well studied. RSV Gag includes MA-p2-p10-CA-SP-NC-PR (see Fig.1.5). Both the p2 and p10 domains contain the late domain which recruits ESCRT for budding (65, 66, 89). There is evidence suggesting that the p10 domain plays a role in immature lattice formation (90, 91). SP is the spacer peptide between CA and NC domains, and is proposed to form helix bundles required for immature assembly. Unlike most other retroviruses, PR is encoded as a part of Gag in RSV. HIV-1 Gag organization is MA-CA-SP1-NC-SP2-p6 (see Fig. 1.5). HIV-1 SP1 is thought to play a similar role as RSV SP in facilitating immature core formation (92). SP2 is proposed to regulate the kinetics of Gag proteolytic processing by PR (59). Like the p10 domain, the p6 domain also contains the late domain. The p6 domain also binds to the HIV-1 accessory protein Vpr.

Immature Gag lattice

Recent technical improvements of cryo-electron tomography and sub-tomogram averaging methods have allowed the core structures of immature HIV-1 and RSV viral particles to be determined at very high resolution (91, 93-95). Within immature HIV-1 virions, the Gag lattice is incomplete, containing randomly distributed gaps (Fig. 1.6) (94). HIV-1 CA-NTDs are shown to form rings around the

hexameric center, while CA-CTDs form dimers (93). Below the CA-CTD, the spacer peptide SP1 appears as rod-like densities, which form a six-helix bundle. According to solved structures, CA-NTDs are believed to form extensive inter-hexameric and intra-hexameric contacts (93). Within immature RSV VLPs, CA-CTDs seem to adopt a similar arrangement as that in HIV-1. CA-CTD arrangement is mostly conserved, while CA-NTD is not (91). In contrast to HIV-1, RSV CA-NTDs exhibit strong dimeric contacts to ensure further hexamer-hexamer contacts (91). RSV also employs p10 to stabilize the immature CA lattice.

Mature Gag lattice

After PR cleaves Gag into individual domains, a dramatic structural rearrangement occurs that leads to the formation of a mature core that encapsulates the viral genomic RNA (Fig. 1.6). CA-CA interactions in the immature lattice are destabilized, and new CA-CA interactions form in the mature lattice with different protein contact surfaces. An amino terminal β-hairpin forms in the context of the mature CA protein after Gag cleavage. The β-hairpin structure in CA-NTD and the spacer peptide SP1 are considered to function as structural switches from the immature lattice to the mature lattice (96). The liberation of CA-SP1 from other domains during proteolytic processing disrupts the immature lattice, while cleavage between CA and SP1 is required to form the mature lattice (59). However, the architectural transition from immature to mature lattice is not fully understood. According to the “fullerene cone model”, a curved hexameric lattice requires

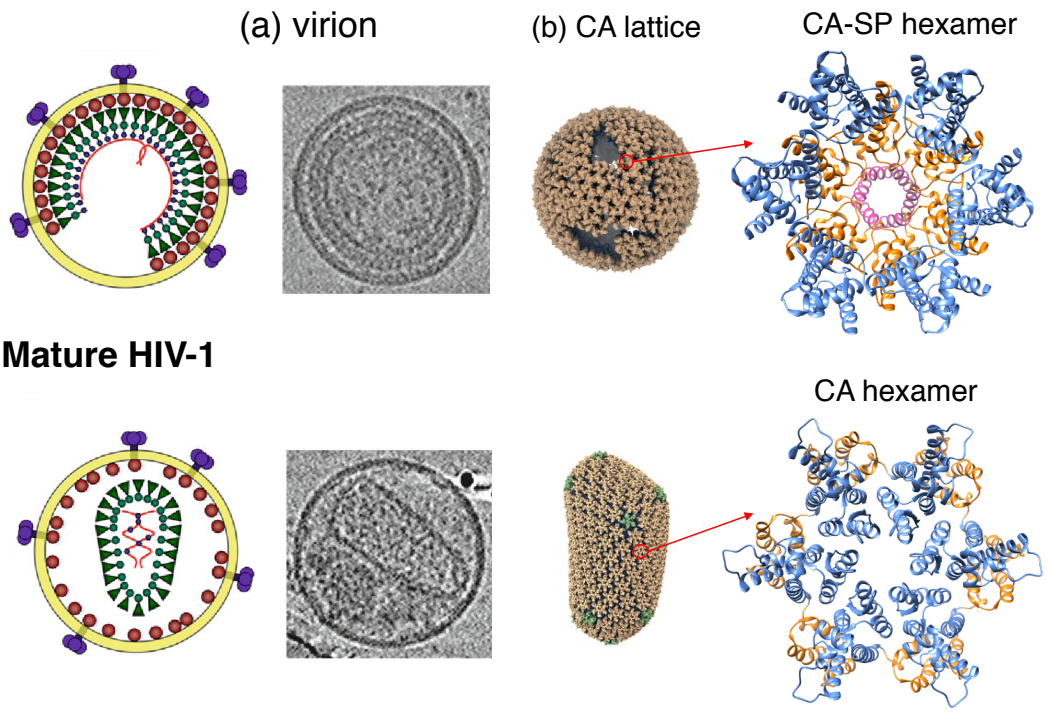

Fig 1.6 Immature and mature HIV-1. (a) Schematic models and negative staining EM images of the immature virion (top) and the mature virion (bottom). Images are adapted from Ganser-Pornillos, Barbie K., Mark Yeager, and Owen Pornillos. "Assembly and architecture of HIV." Viral molecular machines. Springer, Boston, MA, 2012. 441-465. (b) A pseudo-atomic model of the immature HIV-1 capsid core composed entirely of CA-SP hexamers structure (PDB:SL93) with gaps in the lattice (top). A pseudo-atomic model the mature HIV-1 conical-shaped capsid core (bottom) contains 286 hexamers (brown) and 12 pentamers (green), with a zoom-in structure of the mature CA hexamer (PDB: 5MCX). Images are adapted from Perilla, Juan R., and Angela M. Gronenborn. 2016. Molecular architecture of the retroviral capsid." Trends Biochem Sci. 41: 410-420.

incorporation of 12 pentamers to form a closed shell structure (97). Different retroviruses adopt distinct core geometries, which might be a result of different distribution of the pentamers within the hexameric lattice. For example, the HIV-1 conical core contains 12 pentamers with 5 at the tip and 7 at the base, while the RSV polyhedral core has 12 homogenously distributed pentamers (96, 98). In vitro studies suggest that the mature CA lattice is overall conserved, with larger spacing (about 10nm) between hexamer-hexamer contacts compared to the immature lattice. In the mature lattice, six CA-NTDs form a hexameric ring with a central helix bundle, and CA-CTDs beneath the hexameric ring form an external ring with dimeric inter-hexamer contacts that link hexamers together (96, 99). To form a mature HIV-1 conical cone, where variable local curvatures exist, it requires considerable structural flexibility of this CA lattice (100). Not all liberated CA assembles into the mature capsid, as studies show that CA is in both free and assembled forms (101).

HIV-1 ENVELOPE INCORPORATION

The incorporation of Env glycoproteins is an essential step in producing an infectious virus. The TM or gp41 subunit of most lentiviral Env glycoproteins has a very long cytoplasmic tail (CT) compared to those in other retroviruses (102). For example, the HIV-1 gp41 CT is about 150 residues long, and EIAV glycoprotein has even longer CT, about 200 residues. In contrast, the CT of the prototype alpharetrovirus, RSV CT is only 20 residues in length (52). Near membranes, the HIV-1 CT has a tyrosine-based sorting signal with a consensus sequence YxxL that interacts with the clathrin adaptor protein complex (AP-2) during clathrin-dependent

endocytosis, and basolateral sorting of Env in polarized cells (52). The C-terminal of CT contains three conserved amphipathic α-helical lentivirus peptides (102). These peptides have been shown to associate with the inner leaflet of the PM. Two palmitoylated Cys residues are involved in targeting HIV-1 Env to lipid rafts. Previous studies showed that truncation of the HIV-1 CT leads to a reduction in viral replication (103). This observation leads to a hypothesis that the CT of HIV-1 gp41 influences Env incorporation into virus particles (52, 104). Many investigations report a direct interaction between MA and the gp41 CT during particle assembly (104-106). Several HIV-1 MA mutants fail to colocalize with Env and to incorporate Env, but are still able to assemble. However, these defects can be rescued by large C-terminal truncations of the CT or further compensatory mutations in MA (107-109). HIV-1 Env with a truncated CT also fails to localize at viral assembly sites, which leads to Env-deficient particles. However, this defect can also be rescued by a compensatory MA point mutation, located at the trimer interface (110-112). Other investigations have reported that the HIV-1 MA organizes as trimers (113-115). Base on structural and mutation work, it is proposed that an interaction across the HIV-1 MA trimer interface is key to the rescue of Env incorporation. It is likely that HIV-1 MA trimerization is adapted to accommodate the long CT by enlarging the aperture at the hexameric center of the MA lattice (52). This result suggests that Gag multimerization significantly reduces the mobility of Env at assembly sites (116). To date, it seems that the CT of Env and MA are crucial for Env incorporation, but the exact mechanism still remains elusive. Future work is required to solve this long-standing mystery of Env incorporation.

GAG-MEMBRANE INTERACTIONS

Assembly of alpharetroviruses (RSV), gammaretroviruses (MLV), deltaretroviruses (HTLV), and lentiretroviruses (HIV-1) depends on multimerization of the Gag at the inner leaflet of the PM. By contrast, betaretroviruses (MPMV) pre-assemble immature viral cores near the microtubule organizing center (MTOC), which are then transported to the PM for budding as enveloped viral particles. My study is focused on retroviruses that assemble at the PM, especially HIV-1 and RSV. Several principles govern retroviral Gag-membrane interactions, including electrostatic interactions, hydrophobic insertion of the myristate into the membrane core, binding pockets in MA that recognize specific lipid head groups, preference to certain membrane order, and multimerization of Gag.

Electrostatic interactions

Even though they share only a low degree of sequence homology, the MA domains of retroviruses share a high degree of structural homology. The globular head of MA, composed of 5-6 major α-helices, contains several basic residues on the surface. Retroviruses have a basic patch in MA for association with negatively charged membranes. However, MA net surface charge varies. For example, it is neutral in equine infectious anemia virus (EIAV), +3 in RSV, and +6 in HIV-1 (80). This basic patch orients itself facing membranes, and interacts electrostatically with the positively charged inner leaflet of the PM, which is 20-30 mol% phosphatidylserine (PS), 5-10 mol% phosphatidylinositol (PI), and 1-2 mol%

phosphatidylinositol-4,5-bisphosphate (PI(4,5)P2). Altering the number of basic residues in MA alters Gag membrane binding, and consequentially inhibits virus release. In HIV-1, the I18K/L20K mutations increase Gag-membrane association by 2-fold in cells (117). The K29T/K31T mutations reduce viral release, while the K29E/K31E mutations relocate Gag onto Golgi membranes (117, 118). Furthermore, single mutation of K18, R20, or R22 also significantly lowers viral infectivity. Interestingly, the sequence comprising the first 31 residues of HIV-1 MA is capable of membrane binding independently, relying on both the basic residues and the myristate (119, 120).

Unlike HIV-1, RSV Gag is not naturally myristoylated, which makes it a simpler model to probe electrostatic interactions between MA and membranes. Single mutations of basic to acidic residues in RSV MA lead to a decrease of Gag PM localization and virion release, while double mutations result in a loss of Gag PM localization and virion release (121, 122). Interestingly, the virion release of a double basic to acidic mutant can be recovered by restoring the net surface charge of MA back to +3 by either mutating the same residues or other resides (121). This result implies that it is the overall surface net charge that matters, rather than the exact basic side chain in the structure. An RSV MA mutant with two basic residues mutated to neutral almost loses membrane binding (123). Furthermore, increasing the total negatively charged lipid PS in membranes also increases overall MA membrane association, as is true by the addition of highly charged phosphatidylinositol 4,5-bisphosphate [PI(4,5)P2] by liposome flotation (124, 125). Another way to probe electrostatic interactions between MA and membranes is to vary the ionic strength of

protein-membrane mixtures in flotation or pelleting assays in vitro. RSV MA membrane binding decreases dramatically when NaCl increases from 50mM to 150mM or 300mM (123, 125). In addition, another major component of the PM, cholesterol (Chol), can enhance Gag membrane binding by making the electrostatic potential at the membrane surface more negative, and by decreasing the penalty for lipid headgroup desolvation (126).

Previous studies suggest that tRNAs negatively regulate Gag membrane association by binding to MA (63). Nuclear magnetic resonance (NMR) chemical shift data show that the residues responsible for RNA and PI(4,5)P2 interaction overlap. More recent studies show that HIV-1 MA specifically binds to a subset of tRNAs in the cytosol, ensuring that MA targets to the inner leaflet of the PM by specifically targeting PI(4,5)P2 (63, 81). Cellular factors such as inositol hexakisphosphate (IP6) can also bind to both MA and NC domains, which might regulate Gag membrane association and Gag conformation (127).

Hydrophobic interactions

Most retroviral Gag proteins are myristoylated, a 14-carbon fatty acid modification that occurs co-translationally at the N-terminal Gly residue. The myristate is thought to be inserted into the hydrophobic core of the lipid bilayers. Mutation of the N-terminal Gly to Ala completely abrogates Gag PM localization and virion release, which indicates that Gag myristoylation is critical for membrane binding (128-130). In another in vivo study, a truncated Gag with the MA domain removed, but with an added ectopic myristate upstream of CA, is still capable of

membrane binding and budding (131, 132). This result indicates that the hydrophobic interaction mediated by the myristate is an essential signal for Gag membrane association. In vitro, a depletion of myristoylation results in a significant decrease in MA and full-length Gag liposome binding. Myristoylation is reported to increase HIV-1 MA membrane affinity by 10-fold on sparsely tethered bilayer lipid membranes (stBLMs) measured by surface plasmon resonance (SPR) (133). Some Gag proteins, such as those of alpharetroviruses (e.g., RSV) and the lentivirus equine infectious anemia virus (EIAV), are not myristoylated, and these rely only on other membrane binding signals.

Specific recognition and binding to lipid head groups

Early NMR data showed that HIV-1 MA specifically binds PI(4,5)P2 (134, 135). Mass spectrometric protein footprinting found that of the 21 Lys residues in HIV-1 Gag, only Lys29 and Lys31 bound to PI(4,5)P2 with the highest affinity (135). In PI(4,5)P2-depleted cells, Gag with this double mutation is localized to intracellular compartments (117). In vitro flotation data confirmed the critical role of Lys29 and Lys31, as these two Gag mutants bind PI(4,5)P2 less efficiently compared with WT Gag (136). A subsequent NMR study suggests that different basic residues, Arg21 and Lys26, form an interface for PI(4,5)P2 binding (134). The stretch of basic residues in HIV-1 MA that forms a highly basic region (HBR, with amino acid sequence KWEKIRLRPGGKKQYKLK) on the surface of MA is thought to mediate Gag-PI(4,5)P2 interactions. A Gag mutant with all of the Lys and Arg residues in HBR switched (HBR/RK switch) contains the same net surface charge but fails to bind

membranes containing PI(4,5)P2 in vitro (137, 138). This surprising result indicates that both the overall charge and specific amino acid sequence in the HBR are necessary for HIV-1 specific PI(4,5)P2 interactions. The specific interaction with PI(4,5)P2 is reported to increase non-myristoylated HIV-1 MA membrane affinity, to a level similar to that of myristoylation (133). It's challenging to prove the critical role of PI(4,5)P2 in MA and Gag membrane binding without perturbing the overall PI(4,5)P2 level in the PM. In a few studies, PI(4,5)P2 was depleted by overexpression of the polyphosphoinositide 5-phosphatase IV (5PtaseIV) in cells (124, 139). PI(4,5)P2 depletion dramatically reduced HIV-1 Gag membrane association and viral release. In contrast, under similar conditions, no significant changes were observed for RSV Gag (124). However, in another study with different conditions, RSV Gag did show slight sensitivity to PI(4,5)P2 depletion (139). What is consistent is that the presence of physiological levels of PI(4,5)P2 significantly enhances the binding of both RSV and HIV-1 MA in flotation and pelleting assays.

Previously, a model was proposed in a few NMR studies of HIV-1 MA, using PI(4,5)P2 with short acyl chains. They reported that the binding of PI(4,5)P2 to myristoylated MA triggers the myristate to flip out from the sequestered to the exposed conformation, while the sn-2 chain of PI(4,5)P2 flips out from the membrane and inserts into the hydrophobic cleft in MA (134, 140, 141). However, newer data based on PI(4,5)P2 with normally long chains in bicelles calls their previous model into question (142). They re-examined key residues in the cleft that interact with the sn-2 chains of the truncated PI(4,5)P2 in aqueous solution, and found that these residues do not respond to native PI(4,5)P2 in bicelles. In summary, upon membrane

binding, conserved basic residues of MA interact electrostatically and dynamically with multiple PI(4,5)P2 and phosphatidylserine (PS) molecules, and both acyl chains of PI(4,5)P2 remain anchored in the PM bilayer.

Gag multimerization

Gag lattice formation is thought to initiate when one or multiple Gag molecules dimerize upon NC binding to retroviral genomic RNAs in the cytosol. Retroviral genomic RNAs contain a 'packaging signal' ('Ψ') and are packaged in virus particles with very high selectivity among all cellular RNAs. However, in mammalian cells, Gag is able to assemble into virus-like particles (VLPs) when Ψ-containing genomic RNAs are absent, with similar amount of random cellular mRNA packaged instead (143). In vitro, purified Gag can assemble into VLPs in the presence of single-stranded nucleic acids that are long enough to support the binding of at least two Gag molecules, approximately 16 nt in the case of RSV (86, 88, 144,145). Further in vitro assembly studies found that HIV-1 full-length Gag but without myristate, only forms aberrant small spherical particles in vitro. However, the addition of inositol pentakisphosphate (IP5) could correct this size defect (144, 145). Recently, IP6, the most abundant phosphorylated inositol in mammalian cells has been found to be even more functionally robust (146, 147).

Deletion of the NC domain in RSV Gag abolishes viral assembly both in vivo and in vitro (87, 148); while deletion of NC domain in HIV-1 Gag only impairs viral assembly and introduces some defects in vivo (149, 150). The abrogation or reduction in viral assembly due to lack of NC domain could be rescued by replacing NC with a

dimer-forming leucine zipper domain (151-153). When NC is replaced with dimerizable Cys by chemicals or oxidation, HIV-1 Gag is also able to form VLPs (154). It is thought that retroviral genomic RNA drives Gag to form low-order multimers, but they might be dispensable for subsequent assembly events. However, a recent study found that intact Gag and dimerizable Gag without NC exhibit different subsequent assembly properties, specifically the speed of Gag cluster movement and the density clusters growing (155). One study reports that non-myristylated HIV-1 Gag adopts a compact, horseshoe conformation on supported bilayers. Upon the addition of short oligonucleotides, Gag takes on an extended conformation that is able to form proper Gag-Gag contacts (127). Collectively, these studies imply that the formation of dimers or small oligomers of Gag leads to the assembly of the full viral particle.

This initial Gag multimerizion is also dependent on Gag concentration (156). HIV-1 Gag is predominantly cytoplasmic (127, 157). As more Gag is produced in the cytosol, an increased PM-localized Gag was observed (157). In cells, HIV-1 Gag in the cytosol is found to be predominately monomeric or dimeric, while Gag on the PM is mostly found to be higher order multimers (157-159). As expected, monomeric HIV-1 MA is entirely cytoplasmic and some dimeric MA is partially localized to the PM (160). These multimerization effects in vivo have been further confirmed in vitro. HIV-1 MA dimerization is achieved by adding a dimerizable domain called FK506 binding protein (FKBP). As expected, this enhances MA membrane binding both in vitro and in vivo (161) Eliminating HIV-1 Gag membrane association by blocking myristoylation abolishes viral assembly. However, when this Gag reaches high enough

concentrations, viral assembly is observed in the cytosol (162). Taken together, these results demonstrate that Gag RNA-binding function, dimerization capacity, and membrane binding ability are critical but redundant factors for HIV-1 viral assembly. One defect among the three factors is still tolerable, but two or three defects kill assembly (130).

The SP1 region of HIV-1 Gag is 14 residues long and is highly conserved. Point mutations or deletions within this region, especially in the first 4 residues, is detrimental for correct viral assembly in cells, leading to formation of tubes or other misassembled structures (163-166). According to NMR, dynamics simulations and circular dichroism (CD), SP1 is almost unstructured in aqueous solution, only exhibiting a slight propensity to form an alpha helix (92, 167), although secondary structure predictions suggest that it can readily become helical. However, SP1 undergoes a dramatic conformational transition to an alpha-helix when its concentration reaches a critical level. Once SP1 becomes helical, its tendency to self-associate contributes to Gag multimerization (168). Thus, SP1 is proposed to act as a molecular switch, forming a six-helix bundle to promote HIV-1 viral assembly. A recent study found that IP6 facilitates the formation of the six-helix bundle and stabilizes it, further promoting the assembly of the immature HIV-1 Gag lattice (146). This is a result of six-fold symmetric interactions between six phosphate groups on IP6 and sidechains of the two Lys rings, with one in MHR and the other in the six-helix bundle. After PR proteolytic cleavage of Gag, IP6 further promotes assembly of the mature HIV-1 Gag lattice by supporting ionic interactions between six phosphate groups on IP6 and an alternative ring of Arg sidechains in CA-NTD (146). It's likely

that cellular IP6 facilitates the correct HIV-1 Gag conformation upon binding to the membranes, and promotes HIV-1 Gag multimerization by stabilization of the six-helix bundle.

Similar to HIV-1, RSV Gag multimerization also relies on a few key interactions. In RSV, MA is localized in the cytoplasm and the nucleus, because it harbors a nuclear localization signal (NLS) (169, 170). RSV MA dimerization is not sufficient to cause strong PM association in vivo, whereas hexamerization results in robust PM binding (161). RSV Gag is mostly large complexes that are not entirely Gag, prior to localization to the PM by the use of both fluorescence correlation spectroscopy (FCS) and Förster resonance energy transfer (FRET) (171). Abolishing Gag-membrane association leads to increased cytosolic interactions; while removal of NC domain results in loss of both Gag multimerization and membrane association. These results imply that RSV MA binds to RNA via NC first, leading to Gag multimerization in the cytosol, which then promotes efficient membrane association (171). In RSV, NC is dispensable for robust Gag membrane binding. Instead, a 24-residue spacer peptide assembly (SPA) domain is required (89, 172, 173). Residues essential for in vitro assembly are positioned on the hydrophobic faces of the helices. A single mutation I475A in SPA abrogates VLP assembly in vitro, and significantly reduces membrane binding (172, 173). RSV Gag membrane interaction is highly cooperative, which is attributed to SPA. In RSV, an intact SPA domain is required for cooperative membrane binding, while the NC domain is required for the viral assembly (63, 173). In summary, cooperative interplay between Gag-Gag contacts,

Gag-membrane association, and Gag-RNA binding lead to fully assembled viral particles.

Membrane order preference

Retroviral membranes are derived from the PM of the infected host cells. Several lipidomic studies report that the HIV-1 and RSV membrane is enriched in cholesterol and sphingolipids compared with the host PM from which HIV-1 and RSV buds (174-177). However, other groups do not report a significant enrichment of cholesterol in HIV-1 virions (178). Membrane rafts are microdomains enriched in cholesterol and high-melting phospholipids with a higher degree of membrane order compared with other regions of membranes. Nevertheless, these early lipidomic studies led to a hypothesis that HIV-1 buds from these membrane rafts, since HIV-1 viral membranes are enriched in lipids found enriched in rafts (179). Several studies suggest that depletion of cholesterol from the PM by adding methyl β-cyclodextrin (MβCD) leads to a great reduction in viral budding in cells expressing HIV-1 Gag (180). However, a depletion of such an essential component in the PM severely compromises cell viability. A few reports agree that HIV-1 envelopes contain a lipid composition different than the host PM. However, the degrees and types of lipid enrichment are not that consistent (51, 178, 181-184). These inconsistencies between studies might be due to variations in methods for lipid content measurement, limited success of isolating pure PM from other intracellular membranes, and the usage of different cell types.

If rafts do exist in the inner leaflet of the PM, the mechanism by which Gag targets them is not clear. One study reported that HIV-1 Gag is sensitive not only to the negative charge of membranes, but also to the hydrophobic core of lipid bilayers (185). HIV-1 Gag appears to prefer binding to membranes containing phosphatidylserines with unsaturated acyl chains as well as higher cholesterol concentration. This result suggests that retroviruses seem to select raft-like membrane regions for assembly.

REFERENCES

1. Coffin JM, Fan H. 2016. The discovery of reverse transcriptase. Annu Rev Virol. 3:29-51.
2. Varmus HE. 1982. Form and function of retroviral proviruses. Science. 216:812-820.
3. Coffin JM. 2015. The discovery of HTLV-1, the first pathogenic human retrovirus. Proc Natl Acad Sci. 112:15525-15529.
4. Rubin H. 2011. The early history of tumor virology: Rous, RIF, and RAV. Proc Natl Acad Sci. 108:14389-14396.
5. Payne LN, Nair V. 2012. The long view: 40 years of avian leukosis research. Avian Pathol. 41:11-19.
6. Weiss RA, Vogt PK. 2011. 100 years of Rous sarcoma virus. J Exp Med. 208:2351-2355.
7. Coffin JM, Hughes SH, Varmus HE. 1997. Retroviruses. Cold Spring Harbor Laboratory Press.
8. Gallo RC. 2005. History of the discoveries of the first human retroviruses: HTLV-1 and HTLV-2. Oncogene. 24: 5926-5930.
9. Vahlne A. 2009. A historical reflection on the discovery of human retroviruses. Retrovirology. 6:40-48.
10. Poiesz BJ, Ruscetti FW, Gazdar AF, Bunn PA, Minna JD, Gallo RC. 1980. Detection and isolation of type C retrovirus particles from fresh and cultured lymphocytes of a patient with cutaneous T-cell lymphoma. Proc Natl Acad Sci. 77:7415-7419.
11. Yoshida M, Miyoshi I, Hinuma Y. 1982. Isolation and characterization of retrovirus from cell lines of human adult T-cell leukemia and its implication in the disease. Proc Natl Acad Sci. 79:2031-2035.
12. Seiki M, Hattori S, Hirayama Y, Yoshida M. 1983. Human adult T-cell leukemia virus: complete nucleotide sequence of the provirus genome integrated in leukemia cell DNA. Proc Natl Acad Sci. 80:3618-22.
13. Gallo RC, Salahuddin SZ, Popovic M, Shearer GM, Kaplan M, Haynes BF,

Palker TJ, Redfield R, Oleske J, Safai B, White G, Foster P, Markham PD. 1984. Frequent detection and isolation of cytopathic retroviruses (HTLV-III) from patients with AIDS and at risk for AIDS. Science. 224:500-503.

14. Levy JA, Hoffman AD, Kramer SM, Landis JA, Shimabukuro JM, Oshiro LS. 1984. Isolation of lymphocytopathic retroviruses from San Francisco patients with AIDS. Science. 225:840-842.
15. Gallo RC, Montagnier L. 2003. The Discovery of HIV as the cause of AIDS. N Engl J Med. 349:2283-2285.
16. Narayan O, Clements JE. 1989. Biology and pathogenesis of lentiviruses. J Gen Virol. 70:1617-1639.
17. Miller RJ, Cairns JS, Bridges S, Sarver N. 2002. Human Immunodeficiency Virus and AIDS: Insights from Animal Lentiviruses. J Virol. 74:7187-7195.
18. Linial ML. 1999. Foamy Viruses Are Unconventional Retroviruses . J Virol. 73:1747-1755.
19. Weiss RA. 1996. Retrovirus classification and cell interactions. J Antimicrob Chemother. 37(suppl_B), 1-11.
20. Weiss RA. 2006. The discovery of endogenous retroviruses. Retrovirology. 3(1), 67.
21. Temin HM. 1982. Function of the retrovirus long terminal repeat. Cell. 28:3-5.
22. Nisole S, Saïb A. 2004. Early steps of retrovirus replicative cycle. Retrovirology. 1:9.
23. Chan DC, Kim PS. 1998. HIV entry and its inhibition. Cell. 93(5), 681-684.
24. Alkhatib G. 2009. The biology of CCR5 and CXCR4. Curr Opin HIV AIDS. 4:96.
25. Bleul CC, Wu L, Hoxie JA, Springer TA, Mackay CR. 1997. The HIV coreceptors CXCR4 and CCR5 are differentially expressed and regulated on human T lymphocytes. Proc Natl Acad Sci. 94:1925-1930.
26. Wilen CB, Tilton JC, Doms RW. 2012. HIV: Cell binding and entry. Cold Spring Harb Perspect Med 2:a006866.
27. Campbell EM, Hope TJ. 2015. HIV-1 capsid: The multifaceted key player in

HIV-1 infection. Nat Rev Microbiol. 13:471.

28. Rawle DJ, Harrich D. 2018. Toward the “unravelling” of HIV: Host cell factors involved in HIV-1 core uncoating. PLOS Pathog. 14:e1007270.
29. Hu WS, Temin HM. 1990. Retroviral recombination and reverse transcription. Science. 250:1227-1233.
30. Telesnitsky A, Goff S. 1997. Reverse Transcriptase and the Generation of Retroviral DNA. Retroviruses. 242:1168-1171.
31. Preston BD, Poiesz BJ, Loeb LA. 1988. Fidelity of HIV-1 reverse transcriptase. Science. 242:1168-1171.
32. Roberts JD, Bebenek K, Kunkel TA. 1988. The accuracy of reverse transcriptase from HIV-1. Science. 242:1171-1173.
33. Suzuki Y, Craigie R. 2007. The road to chromatin - Nuclear entry of retroviruses. Nat Rev Microbiol. 5:187-196.
34. Bukrinsky MI, Sharova N, Dempsey MP, Stanwick TL, Bukrinskaya AG, Haggerty S, Stevenson M. 1992. Active nuclear import of human immunodeficiency virus type 1 preintegration complexes. Proc Natl Acad Sci. 89:6580-6584.
35. Goff S. 2002. Genetics of retroviral integration. Annu Rev Genet. 26:527-544.
36. Craigie R, Bushman FD. 2012. HIV DNA integration. Cold Spring Harb Perspect Med. 2:a006890.
37. Schröder ARW, Shinn P, Chen H, Berry C, Ecker JR, Bushman F. 2002. HIV-1 integration in the human genome favors active genes and local hotspots. Cell.
38. Shih CC, Stoye JP, Coffin JM. 1988. Highly preferred targets for retrovirus integration. Cell. 110:521-529.
39. Karn J, Stoltzfus CM. 2012. Transcriptional and posttranscriptional regulation of HIV-1 gene expression. Cold Spring Harb Perspect Med. 2(2), a006916.
40. Frankel AD, Young JAT. 2002. HIV-1: fifteen proteins and an RNA. Annu Rev Biochem. 67:1-25.
41. Zimmermann K, Dobrovnik M, Ballaun C, Bevec D, Hauber J, Böhnlein E. 1991. trans-Activation of the HIV-1 LTR by the HIV-1 Tat and HTLV-I Tax

proteins is mediated by different cis-acting sequences. Virology. 182:874-878.

42. Hanly SM, Rimsky LT, Malim MH, Kim JH, Hauber J, Duc Dodon M, Le SY, Maizel J V., Cullen BR, Greene WC. 1989. Comparative analysis of the HTLV-I Rex and HIV-1 Rev trans-regulatory proteins and their RNA response elements. Genes Dev. 3:1534-1544.
43. Pollard VW, Malim MH. 2002. The HIV-1 Rev protein. Annu Rev Microbiol. 52:491-532.
44. Balvay L, Lastra ML, Sargueil B, Darlix JL, Ohlmann T. 2007. Translational control of retroviruses. Nat Rev Microbiol. 5:128-140.
45. Jacks T, Power MD, Masiarz FR, Luciw PA, Barr PJ, Varmus HE. 1988. Characterization of ribosomal frameshifting in HIV-1 gag-pol expression. Nature. 331:280-283.
46. Wills JW, Craven RC. 1991. Form, function, and use of retroviral Gag proteins. AIDS. 5:639-654.
47. Henderson LE, Krutzsch HC, Oroszlan S. 2006. Myristyl amino-terminal acylation of murine retrovirus proteins: An unusual post-translational protein modification. Proc Natl Acad Sci. 80:339-343.
48. Maurer-Stroh S, Eisenhaber F. 2004. Myristoylation of viral and bacterial proteins. Trends Microbiol. 12:178-185.
49. Provitera P, El-Maghrabi R, Scarlata S. 2006. The effect of HIV-1 Gag myristoylation on membrane binding. Biophys Chem. 119:23-32.
50. Li H, Dou J, Ding L, Spearman P. 2007. Myristoylation is required for human immunodeficiency virus type 1 Gag-Gag multimerization in mammalian cells. J Virol. 81:12899-12910.
51. Ono A. 2009. HIV-1 assembly at the plasma membrane: Gag trafficking and localization. Future Virol. 4:241-257.
52. Checkley MA, Luttge BG, Freed EO. 2011. HIV-1 envelope glycoprotein biosynthesis, trafficking, and incorporation. J Mol Biol. 410:582-608.
53. Merk A, Subramaniam S. 2013. HIV-1 envelope glycoprotein structure. Curr Opin Struct Biol. 23:268-276.

54. Chan DC, Fass D, Berger JM, Kim PS. 1997. Core structure of gp41 from the HIV envelope glycoprotein. Cell. 89:263-273.
55. Kwong PD, Wyatt R, Robinson J, Sweet RW, Sodroski J, Hendrickson WA. 1998. Structure of an HIV gp 120 envelope glycoprotein in complex with the CD4 receptor and a neutralizing human antibody. Nature. 393:648659.
56. Liu J, Bartesaghi A, Borgnia MJ, Sapiro G, Subramaniam S. 2008. Molecular architecture of native HIV-1 gp120 trimers. Nature. 455:109-113.
57. Lee JH, Ozorowski G, Ward AB. 2016. Cryo-EM structure of a native, fully glycosylated, cleaved HIV-1 envelope trimer. Science. 351:1043-1048.
58. Briggs JAGG, Simon MN, Gross I, Kräusslich HG, Fuller SD, Vogt VM, Johnson MC. 2004. The stoichiometry of Gag protein in HIV-1. Nat Struct Mol Biol. 11:672-675.
59. Ganser-Pornillos BK, Yeager M, Sundquist WI. 2008. The structural biology of HIV assembly. Curr Opin Struct Biol. 18:203-217.
60. Sundquist WI, Krausslich HH-G, Kräusslich HG. 2012. HIV-1 assembly , budding , and maturation. Cold Spring Harb Perspect Med. 2:a006924.
61. Freed EO. 2013. Advances in HIV-1 assembly and release. Adv HIV-1 Assem Release 1-221.
62. Bush DL, Vogt VM. 2014. In vitro assembly of retroviruses. Annu Rev Virol. 1:561-580.
63. Chukkapalli V, Oh SJ, Ono A. 2010. Opposing mechanisms involving RNA and lipids regulate HIV-1 Gag membrane binding through the highly basic region of the matrix domain. Proc Natl Acad Sci. 107:1600-1605.
64. Votteler J, Sundquist WI. 2013. Virus budding and the ESCRT pathway. Cell Host Microbe. 14:232-241.
65. Dilley KA, Gregory D, Johnson MC, Vogt VM. 2010. An LYPSL late domain in the Gag protein contributes to the efficient release and replication of Rous sarcoma virus. J Virol. 84:6276-6287.
66. Freed EO. 2002. Viral late domains. J Virol. 76:4679-4687.
67. Zhadina M, Bieniasz PD. 2010. Functional interchangeability of late domains,

late domain cofactors and ubiquitin in viral budding. PLoS Pathog. 6:e1001153.

68. Von Schwedler UK, Stuchell M, Müller B, Ward DM, Chung HY, Morita E, Wang HE, Davis T, He GP, Cimbora DM, Scott A, Kräusslich HG, Kaplan J, Morham SG, Sundquist WI. 2003. The protein network of HIV budding. Cell. 114:701-713.
69. Weiss ER, Göttlinger H. 2011. The role of cellular factors in promoting HIV budding. J Mol Biol. 410:525-533.
70. Martin-Serrano J, Neil SJD. 2011. Host factors involved in retroviral budding and release. Nat Rev Microbiol. 9:519-531.
71. Briggs JAG, Kräusslich HG. 2011. The molecular architecture of HIV. J Mol Biol. 410:491-500.
72. Bell NM, Lever AML. 2013. HIV Gag polyprotein: Processing and early viral particle assembly. Trends Microbiol. 21:136-144.
73. Brik A, Wong CH. 2003. HIV-1 protease: Mechanism and drug discovery. Org Biomol Chem. 1:5-14.
74. Nicholson LK, Yamazaki T, Torchia DA, Grzesiek S, Bax A, Stahl SJ, Kaufman JD, Wingfield PT, Lam PYS, Jadhav PK, Hodge CN, Domaille PJ, Chang CH. 1995. Flexibility and function in HIV-1 protease. Nat Struct Biol. 2:274-280.
75. Pettit SC, Lindquist JN, Kaplan AH, Swanstrom R. 2005. Processing sites in the human immunodeficiency virus type 1 (HIV-1) Gag-Pro-Pol precursor are cleaved by the viral protease at different rates. Retrovirology. 2:66.
76. Mattei S, Tan A, Glass B, Müller B, Kräusslich H-G, Briggs JAG. 2018. High-resolution structures of HIV-1 Gag cleavage mutants determine structural switch for virus maturation. Proc Natl Acad Sci. 115:E9401-E9410.
77. Freed EO. 1998. HIV-1 Gag proteins: diverse functions in the virus life cycle. Virology. 251:1-15.
78. de Marco A, Davey NE, Ulbrich P, Phillips JM, Lux V, Riches JD, Fuzik T, Ruml T, Krausslich H-G, Vogt VM, Briggs JAG. 2010. Conserved and Variable Features of Gag Structure and Arrangement in Immature Retrovirus

Particles. J Virol. 84:11729-11736.
79. Kingston RL, Fitzon-ostendorp T, Eisenmesser EZ, Schatz GW, Vogt VM, Post CB, Rossmann MG. 2000. Structure and self-association of the Rous sarcoma virus capsid protein. Structure. 8:617-628.
80. Dick RA, Vogt VM. 2014. Membrane interaction of retroviral Gag proteins. Front Microbiol. 5:1-11.
81. Kutluay SBB, Zang T, Blanco-melo D, Powell C, Jannain D, Errando M, Bieniasz PD. 2014. Global changes in the RNA binding specificity of HIV-1 Gag regulate virion genesis. Cell. 159:1096-1109.
82. De Guzman RN, Wu ZR, Stalling CC, Pappalardo L, Borer PN, Summers MF. 1998. Structure of the HIV-1 nucleocapsid protein bound to the SL3 ψ-RNA recognition element. Science. 279:384-388.
83. Comas-Garcia M, Davis SR, Rein A. 2016. On the selective packaging of genomic RNA by HIV-1. Viruses. 8:246-257.
84. Eckwahl MJ, Telesnitsky A, Wolin SL. 2016. Host RNA packaging by retroviruses: a newly synthesized story. MBio. e02025-15.
85. Comas-Garcia M, Kroupa T, Datta SA, Harvin DP, Hu W-S, Rein A. 2018. Efficient support of virus-like particle assembly by the HIV-1 packaging signal. Elife. 7:e38438.
86. Ma YM, Vogt VM. 2004. Nucleic Acid Binding-Induced Gag Dimerization in the Assembly of Rous Sarcoma Virus Particles In Vitro. J Virol. 78:52-60.
87. Johnson MC, Scobie HM, Ma YM, Vogt VM. 2002. Nucleic acid-independent retrovirus assembly can be driven by dimerization. J Virol. 76:11177-85.
88. Ma YM, Vogt VM. 2002. Rous sarcoma virus Gag protein-oligonucleotide interaction suggests a critical role for protein dimer formation in assembly. J Virol. 76:5452-5462.
89. Keller PW, Johnson MC, Vogt VM. 2008. Mutations in the spacer peptide and adjoining sequences in Rous sarcoma virus Gag lead to tubular budding. J Virol. 82:6788-6797.
90. Campbell S, Vogt VM. 1997. In vitro assembly of virus-like particles with

Rous sarcoma virus Gag deletion mutants: identification of the p10 domain as a morphological determinant in the formation of spherical particles. J Virol. 71:4425-4435.

91. Schur FKM, Dick RA, Hagen WJH, Vogt VM, Briggs JAG. 2015. The structure of immature virus-like Rous sarcoma virus Gag particles reveals a structural role for the p10 domain in assembly. J Virol. 89:10294-10302.
92. Datta SAK, Temeselew LG, Crist RM, Soheilian F, Kamata A, Mirro J, Harvin D, Nagashima K, Cachau RE, Rein A. 2011. On the role of the SP1 domain in HIV-1 particle assembly: a molecular switch? J Virol. 85:4111-4121.
93. Schur FKM, Hagen WJH, Rumlová M, Ruml T, Müller B, Kraüsslich HG, Briggs JAG. 2015. Structure of the immature HIV-1 capsid in intact virus particles at 8.8 Å resolution. Nature. 517:505-508.
94. Briggs JAG, Riches JD, Glass B, Bartonova V, Zanetti G, Krausslich H-G. 2009. Structure and assembly of immature HIV. Proc Natl Acad Sci. 106:11090-11095.
95. Pak AJ, Grime JMA, Sengupta P, Chen AK, Durumeric AEP, Srivastava A, Yeager M, Briggs JAG, Lippincott-Schwartz J, Voth GA. 2017. Immature HIV-1 lattice assembly dynamics are regulated by scaffolding from nucleic acid and the plasma membrane. Proc Natl Acad Sci. 114:E10056-E10065.
96. Mattei S, Schur FK, Briggs JA. 2016. Retrovirus maturation - an extraordinary structural transformation. Curr Opin Virol. 18:27-35.
97. Pornillos O, Ganser-Pornillos BK, Yeager M. 2011. Atomic-level modelling of the HIV capsid. Nature. 469:424-427.
98. Yeager M. 2011. Design of in vitro symmetric complexes and analysis by hybrid methods reveal mechanisms of HIV capsid assembly. J Mol Biol. 410:534-552.
99. Perilla JR, Gronenborn AM. 2016. Molecular architecture of the retroviral capsid. Trends Biochem Sci. 41:410-420.
100. Mattei S, Glass B, Hagen WJH, Kräusslich HG, Briggs JAG. 2016. The structure and flexibility of conical HIV-1 capsids determined within intact

virions. Science. 354:1434-1437.

101. Lanman J, Lam TKT, Emmett MR, Marshall AG, Sakalian M, Prevelige PE. 2004. Key interactions in HIV-1 maturation identified by hydrogen-deuterium exchange. Nat Struct Mol Biol. 11(7), 676-677.
102. Postler TS, Desrosiers RC. 2012. The tale of the long tail: the cytoplasmic domain of HIV-1 gp41. J Virol. 87:2-15.
103. Murakami T, Freed EO. 2002. The long cytoplasmic tail of gp41 is required in a cell type-dependent manner for HIV-1 envelope glycoprotein incorporation into virions. Proc Natl Acad Sci. 97:343-348.
104. Tedbury PR, Freed EO. 2014. The role of matrix in HIV-1 envelope glycoprotein incorporation. Trends Microbiol. 22:372-378.
105. Freed EO, Martin MA. 1996. Domains of the human immunodeficiency virus type 1 matrix and gp41 cytoplasmic tail required for envelope incorporation into virions. J Virol. 70:341-351.
106. Da Silva ES, Mulinge M, Bercoff DP. 2013. The frantic play of the concealed HIV envelope cytoplasmic tail. Retrovirology. 10:54.
107. Freed EO, Orenstein JM, Buckler-White AJ, Martin MA. 1994. Single amino acid changes in the human immunodeficiency virus type 1 matrix protein block virus particle production. J Virol. 68:5311-5320.
108. Ono A, Huang M, Freed EO. 1997. Characterization of human immunodeficiency virus type 1 matrix revertants: effects on virus assembly, Gag processing, and Env incorporation into virions. J Virol. 71:4409-4418.
109. Brandano L, Stevenson M. 2011. A highly conserved residue in the C-terminal helix of HIV-1 Matrix is required for envelope incorporation into virus particles. J Virol. 86:2347-2359.
110. Murakami T, Freed EO. 2002. Genetic evidence for an interaction between human immunodeficiency virus type 1 matrix and alpha -helix 2 of the gp41 cytoplasmic tail. J Virol. 74:3548-3554.
111. Freed EO, Martin MA. 1995. Virion incorporation of envelope glycoproteins with long but not short cytoplasmic tails is blocked by specific, single amino

acid substitutions in the human immunodeficiency virus type 1 matrix. J Virol. 69:1984-1989.

112. Mammano F, Kondo E, Sodroski J, Bukovsky A, Göttlinger HG. 1995. Rescue of human immunodeficiency virus type 1 matrix protein mutants by envelope glycoproteins with short cytoplasmic domains. J Virol. 69:3824-3830.
113. Tedbury PR, Novikova M, Ablan SD, Freed EO. 2015. Biochemical evidence of a role for matrix trimerization in HIV-1 envelope glycoprotein incorporation. Proc Natl Acad Sci. 113:E182-E190.
114. Alfadhli A, Huseby D, Kapit E, Colman D, Barklis E. 2006. Human immunodeficiency virus type 1 matrix protein assembles on membranes as a hexamer. J Virol. 81:1472-1478.
115. Alfadhli A, Barklis RL, Barklis E. 2009. HIV-1 matrix organizes as a hexamer of trimers on membranes containing phosphatidylinositol-(4,5)-bisphosphate. Virology 387:466-472.
116. Roy NH, Chan J, Lambele M, Thali M. 2013. Clustering and mobility of HIV-1 Env at viral assembly sites predict its propensity to induce cell-cell fusion. J Virol. 87:7516-7525.
117. Ono A, Orenstein JM, Freed EO. 2000. Role of the Gag matrix domain in targeting human immunodeficiency virus type 1 assembly. J Virol. 74:2855-2866.
118. Freed EO, Englund G, Martin MA. 1995. Role of the basic domain of human immunodeficiency virus type 1 matrix in macrophage infection. J Virol. 69:3949-3954.
119. Klopfenstein DR, Tomishige M, Stuurman N, Vale RD. 2002. Role of phosphatidylinositol(4,5)bisphosphate organization in membrane transport by the Unc104 kinesin motor. Cell. 109:347-358.
120. Zhou W, Parent LJ, Wills JW, Resh MD. 1994. Identification of a membrane-binding domain within the amino-terminal region of human immunodeficiency virus type 1 Gag protein which interacts with acidic phospholipids. J Virol. 68:2556-69.

121. Callahan EM, Wills JW. 2000. Repositioning basic residues in the M domain of the Rous sarcoma virus Gag protein. J Virol. 74:11222-11229.
122. Watanabe SM, Medina GN, Eastep GN, Ghanam RH, Vlach J, Saad JS, Carter CA. 2018. The matrix domain of the Gag protein from avian sarcoma virus contains a PI(4,5)P2-binding site that targets Gag to the cell periphery. J Biol Chem. 293:18841-18853.
123. Dalton AK, Murray PS, Murray D, Vogt M, Dalton AK, Murray PS, Murray D, Vogt VM. 2005. Biochemical characterization of Rous sarcoma virus MA protein interaction with membranes. J Virol. 79:6227-6238.
124. Chan J, Dick RA, Vogt VM. 2011. Rous sarcoma virus Gag has no specific requirement for phosphatidylinositol-(4,5)-bisphosphate for plasma membrane association in vivo or for liposome interaction in vitro. J Virol. 85:10851-10860.
125. Wen Y, Dick RA, Feigenson GW, Vogt VM. 2016. Effects of membrane charge and order on membrane binding of the retroviral structural protein Gag. J Virol. 90:9518-9532.
126. Doktorova M, Heberle FA, Kingston RL, Khelashvili G, Cuendet MA, Wen Y, Katsaras J, Feigenson GW, Vogt VM, Dick RA. 2017. Cholesterol promotes protein binding by affecting membrane electrostatics and solvation properties. Biophys J. 113:2004-2015.
127. Datta SAK, Zhao Z, Clark PK, Tarasov S, Alexandratos JN, Campbell SJ, Kvaratskhelia M, Lebowitz J, Rein A. 2007. Interactions between HIV-1 Gag molecules in solution: an inositol phosphate-mediated switch. J Mol Biol. 365:799-811.
128. Bryant M, Ratner L. 1990. Myristoylation-dependent replication and assembly of human immunodeficiency virus 1. Proc Natl Acad Sci. 87:523-527.
129. Gottlinger HG, Sodroski JG, Haseltine WA. 1989. Role of capsid precursor processing and myristoylation in morphogenesis and infectivity of human immunodeficiency virus type 1. Proc Natl Acad Sci. 86:5781-5785.
130. O'Carroll IP, Soheilian F, Kamata A, Nagashima K, Rein A. 2012. Elements in

HIV-1 Gag contributing to virus particle assembly. Virus Res. 171:341-345.

131. Borsetti A, Ohagen A, Gottlinger HG. 1998. The C-terminal half of the human immunodeficiency virus type 1 Gag precursor is sufficient for efficient particle assembly. J Virol. 72:9313-9317.

132. Reil H. 1998. Efficient HIV-1 replication can occur in the absence of the viral matrix protein. EMBO J. 17:2699-2708.

133. Barros M, Heinrich F, Datta SAK, Rein A, Karageorgos I, Nanda H, Lösche M. 2016. Membrane binding of HIV-1 Matrix protein: dependence on bilayer composition and protein lipidation. J Virol. 90:4544-4555.

134. Saad JS, Miller J, Tai J, Kim A, Ghanam RH, Summers MF. 2006. Structural basis for targeting HIV-1 Gag proteins to the plasma membrane for virus assembly. Proc Natl Acad Sci. 103:11364-11369.

135. Shkriabai N, Datta SAK, Zhao Z, Hess S, Rein A, Kvaratskhelia M. 2006. Interactions of HIV-1 Gag with assembly cofactors. Biochemistry. 45:4077-4083.

136. Chukkapalli V, Hogue IB, Boyko V, Hu W-S, Ono A, Hogue IB, Chukkapalli V, Hu W-S, Boyko V, Hogue IB, Boyko V, Hu W-S, Ono A. 2007. Interaction between the human immunodeficiency virus type 1 Gag Matrix domain and phosphatidylinositol-(4,5)-bisphosphate is essential for efficient Gag membrane binding. J Virol. 82:2405-2417.

137. Llewellyn GN, Grover JR, Olety B, Ono A. 2013. HIV-1 Gag associates with specific Uropod-directed microdomains in a manner dependent on its MA highly basic region. J Virol. 87:6441-6454.

138. Olety B, Ono A. 2014. Roles played by acidic lipids in HIV-1 Gag membrane binding. Virus Res. 93:108-115.

139. Nadaraia-Hoke S, Bann D V., Lochmann TL, Gudleski-O'Regan N, Parent LJ. 2013. Alterations in the MA and NC domains modulate phosphoinositide-dependent plasma membrane localization of the Rous sarcoma virus Gag protein. J Virol. 87:3609-3615.

140. Tang C, Loeliger E, Luncsford P, Kinde I, Beckett D, Summers MF. 2004.

Entropic switch regulates myristate exposure in the HIV-1 matrix protein. Proc Natl Acad Sci. 101:517-522.

141. Freed EO. 2006. HIV-1 Gag: Flipped out for PI(4,5)P2. Proc Natl Acad Sci. 103:11101-11102.
142. Mercredi PY, Bucca N, Loeliger B, Gaines CR, Mehta M, Bhargava P, Tedbury PR, Charlier L, Floquet N, Muriaux D, Favard C, Sanders CR, Freed EO, Marchant J, Summers MF. 2016. Structural and molecular determinants of membrane binding by the HIV-1 Matrix protein. J Mol Biol. 428:1637-1655.
143. Rulli SJ, Hibbert CS, Mirro J, Pederson T, Biswal S, Rein A. 2007. Selective and nonselective packaging of cellular RNAs in retrovirus particles. J Virol. 81:6623-6631.
144. Campbell S, Fisher RJ, Towler EM, Fox S, Issaq HJ, Wolfe T, Phillips LR, Rein A. 2001. Modulation of HIV-like particle assembly in vitro by inositol phosphates. Proc Natl Acad Sci. 98:10875-10879.
145. Campbell S, Rein A. 1999. In vitro assembly properties of human immunodeficiency virus type 1 Gag protein lacking the p6 domain. J Virol. 73:2270-2279.
146. Dick RA, Zadrozny KK, Xu C, Schur FKM, Lyddon TD, Ricana CL, Wagner JM, Perilla JR, Ganser-Pornillos BK, Johnson MC, Pornillos O, Vogt VM. 2018. Inositol phosphates are assembly co-factors for HIV-1. Nature, 560:509-512.
147. Dick RA, Mallery DL, Vogt VM, James LC. 2018. IP6 regulation of HIV capsid assembly, stability, and uncoating. Viruses. 10:640-651.
148. Yu F, Joshi SM, Ma YM, Kingston RL, Simon MN, Vogt VM. 2001. Characterization of Rous sarcoma virus Gag particles assembled in vitro. J Virol. 75:2753-2764.
149. Ott DE, Coren L V., Shatzer T. 2009. The nucleocapsid region of human immunodeficiency virus type 1 Gag assists in the coordination of assembly and Gag processing: role for RNA-Gag binding in the early stages of assembly. J Virol. 83:7718-7727.

150. Ott DE, Coren L V., Chertova EN, Gagliardi TD, Nagashima K, Sowder RC, Poon DTK, Gorelick RJ. 2003. Elimination of protease activity restores efficient virion production to a human immunodeficiency virus type 1 nucleocapsid deletion mutant. J Virol. 77:5547-5556.
151. Zhang Y, Qian H, Love Z, Barklis E. 1998. Analysis of the assembly function of the human immunodeficiency virus type 1 Gag protein nucleocapsid domain. J Virol. 72:1782-1789.
152. Accola MA, Strack B, Gottlinger HG. 2000. Efficient particle production by minimal Gag constructs which retain the carboxy-terminal domain of human immunodeficiency virus type 1 capsid-p2 and a late assembly domain. J Virol. 74:5395-5402.
153. Crist RM, Datta SAK, Stephen AG, Soheilian F, Mirro J, Fisher RJ, Nagashima K, Rein A. 2008. Assembly properties of human immunodeficiency virus type 1 Gag-leucine zipper chimeras: implications for retrovirus assembly. J Virol. 83:2216-2225.
154. Alfadhli A, Dhenub TC, Still A, Barklis E. 2005. Analysis of human immunodeficiency virus type 1 Gag dimerization-induced assembly. J Virol. 79:14498-14506.
155. Yang Y, Qu N, Tan J, Rushdi MN, Krueger CJ, Chen AK. 2018. Roles of Gag-RNA interactions in HIV-1 virus assembly deciphered by single-molecule localization microscopy. Proc Natl Acad Sci. 115:6721-6726.
156. Gamble TR, Yoo S, Vajdos FF, Von Schwedler UK, Worthylake DK, Wang H, McCutcheon JP, Sundquist WI, Hill CP. 1997. Structure of the carboxyl-terminal dimerization domain of the HIV-1 capsid protein. Science. 278:849-853.
157. Fogarty KH, Berk S, Grigsby IF, Chen Y, Mansky LM, Mueller JD. 2013. Interrelationship between cytoplasmic retroviral Gag concentration and Gag-membrane association. J Mol Biol. 426:1611-1624.
158. Kutluay SB, Bieniasz PD. 2010. Analysis of the initiating events in HIV-1 particle assembly and genome packaging. PLoS Pathog. 6:e1001200.

159. Fogarty KH, Chen Y, Grigsby IF, MacDonald PJ, Smith EM, Johnson JL, Rawson JM, Mansky LM, Mueller JD. 2011. Characterization of cytoplasmic Gag-Gag interactions by dual-color z-scan fluorescence fluctuation spectroscopy. Biophys J. 100:1587-1595.
160. Dalton AK, Ako-adjei D, Murray PS, Murray D, Vogt VM. 2007. Electrostatic interactions drive membrane association of the human immunodeficiency virus type 1 Gag MA domain. J Virol. 81:6434-6445.
161. Dick RA, Kamynina E, Vogt VM. 2013. Effect of multimerization on membrane association of rous sarcoma virus and HIV-1 matrix domain proteins. J Virol. 87:13598-13608.
162. O'Carroll IP, Crist RM, Mirro J, Harvin D, Soheilian F, Kamata A, Nagashima K, Rein A. 2012. Functional redundancy in HIV-1 viral particle assembly. J Virol. 86:12991-12996.
163. Accola MA, Höglund S, Göttlinger HG. 1998. A putative alpha-helical structure which overlaps the capsid-p2 boundary in the human immunodeficiency virus type 1 Gag precursor is crucial for viral particle assembly. J Virol. 72:2072-2078.
164. Guo X, Roldan A, Hu J, Wainberg MA, Liang C. 2005. Mutation of the SP1 sequence impairs both multimerization and membrane-binding activities of human immunodeficiency virus type 1 Gag. J Virol. 79:1803-1812.
165. Kräusslich HG, Fäcke M, Heuser AM, Konvalinka J, Zentgraf H. 1995. The spacer peptide between human immunodeficiency virus capsid and nucleocapsid proteins is essential for ordered assembly and viral infectivity. J Virol. 69:3407-3419.
166. Liang C, Hu J, Russell RS, Roldan A, Kleiman L, Wainberg MA. 2002. Characterization of a putative helix across the capsid-sp1 boundary that is critical for the multimerization of human immunodeficiency virus type 1 Gag. J Virol. 76:11729-11737.
167. Newman JL, Butcher EW, Patel DT, Mikhaylenko Y, Summers MF. 2004. Flexibility in the P2 domain of the HIV-1 Gag polyprotein. Protein Sci.

13:2101-2107.

168. Datta SAK, Clark PK, Fan L, Ma B, Harvin DP, Sowder RC, Nussinov R, Wang Y-X, Rein A. 2016. Dimerization of the SP1 region of HIV-1 Gag induces a helical conformation and association into helical bundles: implications for particle assembly. J Virol. 90:1773-1787.
169. Garbitt RA, Bone KR, Parent LJ. 2004. Insertion of a classical nuclear import signal into the matrix domain of the Rous sarcoma virus Gag protein interferes with virus replication. J Virol. 78:13534-13542.
170. Garbitt-Hirst R, Kenney SP, Parent LJ. 2009. Genetic evidence for a connection between rous sarcoma virus Gag nuclear trafficking and genomic RNA packaging. J Virol. 83:6790-6797.
171. Larson DR, Ma YM, Vogt VM, Webb WW. 2003. Direct measurement of Gag - Gag interaction during retrovirus assembly with FRET and fluorescence correlation spectroscopy. J Cell Bio. 162:1233-1244.
172. Bush DL, Monroe EB, Bedwell GJ, Prevelige PE, Phillips JM, Vogt VM. 2014. Higher-order structure of the Rous sarcoma virus SP assembly domain. J Virol. 88:5617-5629.
173. Dick RA, Barros M, Jin D, Lösche M, Vogt VM. 2015. Membrane binding of the Rous sarcoma virus Gag protein is cooperative and dependent on the spacer peptide assembly domain. J Virol. 90:2473-2485.
174. Quigley JP, Rifkin DB, Reich E. 1971. Phospholipid composition of Rous sarcoma virus, host cell membranes and other enveloped RNA viruses. Virology. 46:106-116.
175. Quigley JP, Rifkin DB, Reich E. 1972. Lipid studies of Rous sarcoma virus and host cell membranes. Virology 50:550-557.
176. Pessin JE, Glaser M. 1980. Budding of Rous sarcoma virus and vesicular stomatitis virus from localized lipid regions in the plasma membrane of chicken embryo fibroblasts. J Biol Chem. 255:9044-9050.
177. Aloia RC, Tian H, Jensen FC. 1993. Lipid composition and fluidity of the human immunodeficiency virus envelope and host cell plasma membranes.

Proc Natl Acad Sci. 90:5181-5.

178. Lorizate M, Sachsenheimer T, Glass B, Habermann A, Gerl MJ, Kräusslich H-GG, Brügger B. 2013. Comparative lipidomics analysis of HIV-1 particles and their producer cell membrane in different cell lines. Cell Microbiol. 15:292-304.
179. Simons K, Ikonen E. 1997. Functional rafts in cell membranes. Nature. 387:569-572.
180. Ono A, Freed EO. 2001. Plasma membrane rafts play a critical role in HIV-1 assembly and release. Proc Natl Acad Sci. 98:13925-13930.
181. Chan R, Uchil PD, Jin J, Shui G, Ott DE, Mothes W, Wenk MR. 2008. retroviruses human immunodeficiency virus and murine leukemia virus are enriched in phosphoinositides. J Virol. 82:11228-11238.
182. Brugger B, Glass B, Haberkant P, Leibrecht I, Wieland FT, Krausslich H-G. 2006. The HIV lipidome: A raft with an unusual composition. Proc Natl Acad Sci. 103:2641-2646.
183. Kaiser H-J, Lingwood D, Levental I, Sampaio JL, Kalvodova L, Rajendran L, Simons K. 2009. Order of lipid phases in model and plasma membranes. Proc Natl Acad Sci. 106:16645-16650.
184. Sonnino S, Prinetti A. 2012. Membrane domains and the “lipid raft”. Concept Curr Med Chem. 20:4-21.
185. Dick RA, Goh SL, Feigenson GW, Vogt VM. 2012. HIV-1 Gag protein can sense the cholesterol and acyl chain environment in model membranes. Proc Natl Acad Sci. 109:18761-18766.

CHAPTER 2

PI(4,5)P2 CLUSTERING AND ITS IMPACT ON BIOLOGICAL FUNCTIONS[1]

PHOSPHOINOSITIDES

Phosphoinositides (PIPs) are small molecules, all phosphorylated derivatives of phosphatidylinositol (PI). Since the discovery of PI and PIPs by Mable and Lowell Hokin in the 1950s (1), these lipids gained significant research interest as they profoundly affect hundreds of biochemical processes in eukaryotic cells. PI is synthesized primarily in the endoplasmic reticulum (ER), and is then transferred to other membranes either by vesicular transport or by non-vesicular lipid transport via PI transfer proteins (PITPs) (2). PITPs sequester PI from a membrane in their hydrophobic pockets and deliver it to specific membrane compartments for further phosphorylation by numerous lipid kinases, which makes PITPs critical regulators of phosphoinositide pathways (3-5). Reversible phosphorylation of the PI inositol ring at positions 3, 4 and 5 produces seven phosphoinositide species. Each phosphoinositide is predominantly found at a distinct subcellular localization, see Fig. 2.1. The spatial distribution, steady-state levels, and the conversion to other species

[1] This following chapter is written for an invited review article, which will be in Volume 90, Annu Rev Biochem.

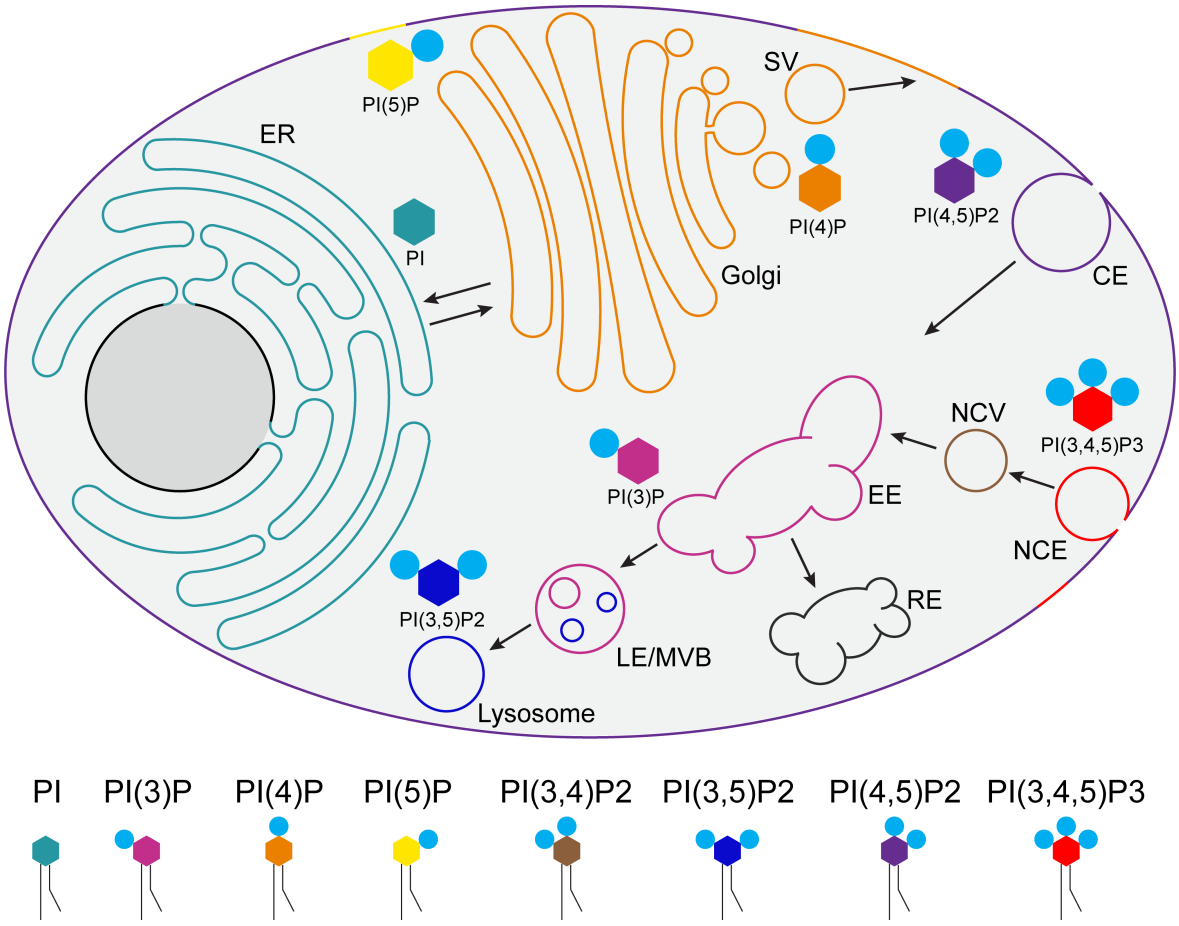

Fig 2.1 Subcellular distributions of phosphatidylinositol (PI) and phosphoinositides (PIPs). The headgroup of PIPs is simplified as an inositol ring with 1-3 phosphate groups at different positions. This depiction only illustrates the cellular location where a particular phosphoinositide species is prominently found. CE as clathrin-dependent endocytosis, NCE as clathrin-independent endocytosis, NCV as non-clathrin endocytic vesicles, EE as early endosomes, RE as recycling endosomes, MVB as multivesicular bodies, LE as late endosomes, L as lysosome, ER as endoplasmic reticulum, and SV as secretory vesicles. Black arrow indicates the progression of membrane trafficking pathways.

are primarily regulated by phosphoinositide kinases and phosphatases, whose localization and activation are also tightly controlled (6). Among PIPs, phosphatidylinositol 4,5-bisphosphate, abbreviated as PI(4,5)P2 or PIP2, the most abundant phosphoinositide found in mammalian cells, plays critical roles regarding cell life and death, and many aspects of PIP2 biology have been intensively reviewed (7-22). In vivo effects of PIP2 are complicated to work out because hundreds of proteins bind to it. In addition, PIP2 itself is an unusual phospholipid with unique properties that complicate its biochemistry, and these complexities likely affect its behavior in cells, independent of protein binding. This review focuses on illustrating the biochemical and biophysical properties of PIP2, and highlights the broad cellular impacts of this unique lipid.

PIP2 HEADGROUPS AND ACYL CHAINS

PIP2 is among the most highly charged anionic phospholipids and it exhibits rich physical chemistry. PIP2 contains two phosphomonoesters at the 4- and 5-position and one phosphodiester in the 1- position connecting the headgroup to the glycerol backbone **(**Fig. 2.2**)**. The ionization behavior of PIP2 has been studied extensively by the use of 31P- nuclear magnetic resonance (NMR) (23-29). In micelles and bilayers, the PIP2 charge was determined based on the phosphorus chemical shift at different pH (30, 31). To determine the contribution to the membrane charge from anionic lipids, such as PIPs, it is important to know their intrinsic pKa (32). The pKa of the 4-phosphate and 5-phosphate was found to be 6.7 and 7.7 respectively, resulting in an overall charge of approximately -4 at physiological pH of 7.2 (23). However,

PIP2 in bilayers has a net charge of about -3 at the physiological ionic strength of 100mM KCl at pH 7.0, according to electrophoretic mobility assays, which in large part is because the abundant phosphatidylserine (PS) in physiological membranes renders overall membrane surface charge negative, which makes less favorable the creation of additional negative charge from PIP2 headgroup ionizations (31, 33). Upon protein binding or during Ca^{2+} or Zn^{2+} transient influx, the proton bound to PIP2 might also be displaced; thus, the net charge of PIP2 could either be -3, -4 or -5. Different ionization properties of the phosphomonoesters make PIP2 capable of forming both intramolecular hydrogen bonds with adjacent hydroxyl groups, and intermolecular hydrogen bonding with neighboring PIP2 molecules (23, 24, 26-28, 34).

Natural PIP2 has a mixture of different acyl chains, with the predominant species being sn-1 stearoyl and sn-2 arachidonoyl (see Fig.2.2) (35, 36). The 2 acyl chains attached to the first and second carbons of the glycerol are denoted as sn-1 and sn-2, respectively. The saturated stearoyl chain is 18-carbons long, while the polyunsaturated arachidonoyl chain is 20-carbons long with 4 double bonds. This high-degree of unsaturation makes PIP2 prefer a disordered environment (37, 38). However, PIP2 has also been reported to be associated with the “raft” or “detergent-resistant membranes” (13, 22, 38-46), which are enriched in cholesterol and saturated phospholipids with higher degree of membrane order compared to other regions of membranes (22, 46-48). The association between PIP2 and the lipid “raft” is a puzzling observation, because rafts are a

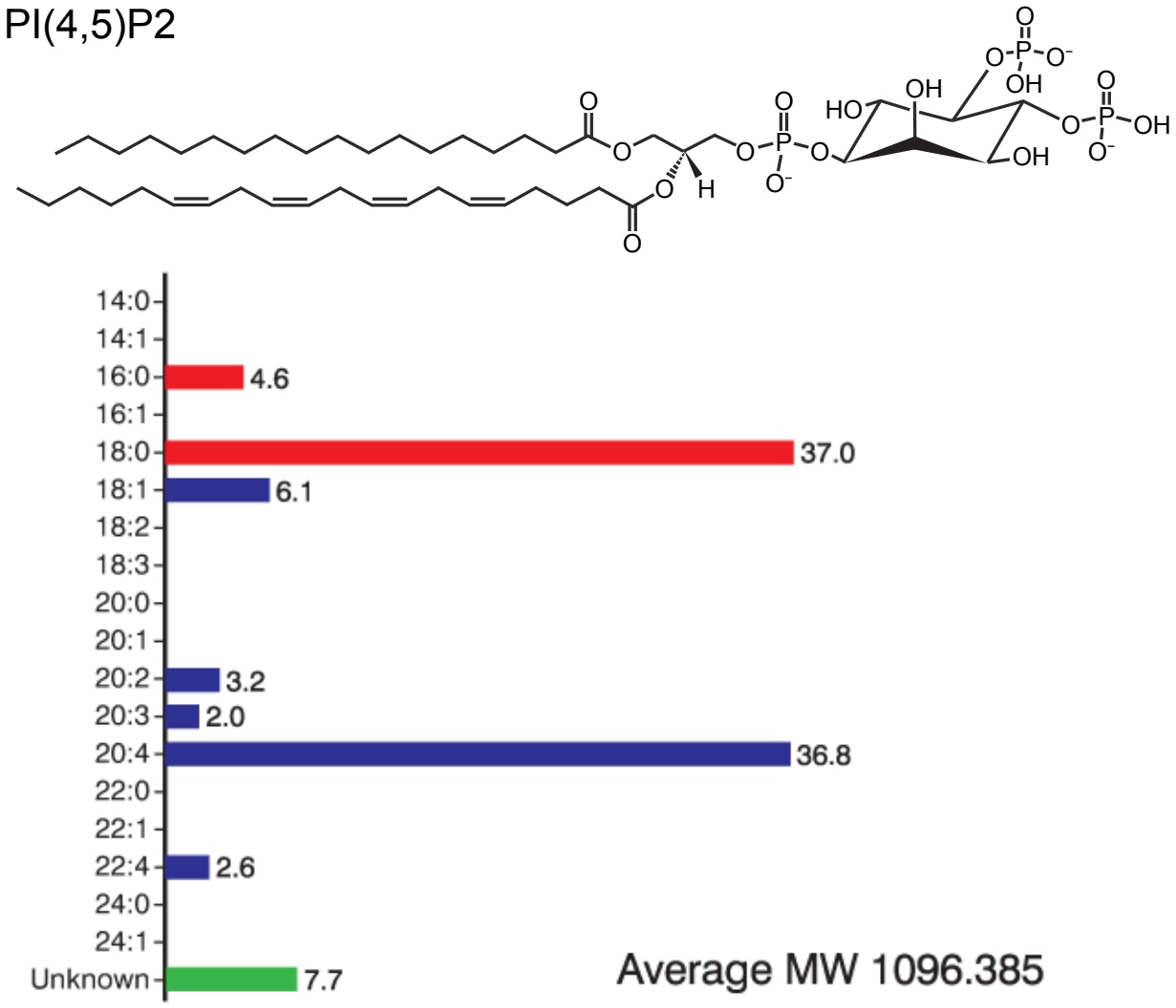

Fig 2.2 PI(4,5)P2 molecular structure and the acyl chain distribution of natural PI(4,5)P2. Top is the molecular structure of PI(4,5)P2. Bottom is the acyl chain distribution of PI(4,5)P2 extracted from swine brains (brain-PIP2, #840046). Images are adapted from Avanti Polar Lipids website.

property of the coexisting phases in the outer PM leaflet, whereas PIP2 is exclusively located at the inner PM leaflet. A plausible explanation, but one not yet supported by experiments, is that the PIP2 tends to locate across the PM from an outer leaflet "raft", leading to the PIP2 binding proteins being identified as "raft markers".

PIP2 FUNCTION IN CELLS

Located at the inner leaflet of the plasma membrane (PM), PIP2 comprises approximately 1-2 mol% of total PM lipids, and occupies in the range of 10,000–20,000 molecules/um^2 at the inner leaflet (49). With a crude model of all phospholipids being dissolved in the cytoplasm, an effective concentration of PIP2 in the cell is calculated to be approximately 10 μM (13). The synthesis of PIP2 (7) is primarily mediated by phosphoinositide kinases, PIP5K that phosphorylate PI(4)P, or to a lesser extent, by the PIP4K enzymes that phosphorylate PI(5)P. PIP2 is critically involved in different signal transduction pathways that regulate a broad spectrum of biological activities. PIP2 itself can act directly as a messenger (50) or serve as a precursor to generate the important secondary messengers inositol trisphosphate (IP3) and diacylglycerol (DAG), produced when PIP2 is hydrolyzed by phospholipase C (PLC) (51). Phosphatidylinositol 3,4,5-trisphosphate (PI(3,4,5)P3), which is involved in cell survival, growth, intracellular vesicle trafficking, cytoskeletal rearrangement, and cell metabolism is generated from PIP2 by class I phosphoinositide (3) kinases (PI(3) kinases) (52). PIP2 also plays central roles in a broad spectrum of cellular functions, including exocytosis/endocytosis (10, 53-57), ion channel and transporter regulation (58-60), actin cytoskeleton assembly (61-65), endosomal trafficking (7, 55,

66), membrane fusion (10, 54, 67, 68), cell polarization (6, 69), phagocytosis (55, 70, 71) and cell directional migration (72). PIP2 downstream signaling and PIP2-derived metabolites have been implicated in human diseases such as diabetes, bipolar disorder and cancer (12, 73-76).

With its turnover being spatially and temporally regulated, PIP2 is well suited to recruit diverse cellular proteins and to interact with various effector proteins. Typically, PIP2 binding proteins are classified under several major categories in regard to their functions, such as membrane transport and trafficking, actin cytoskeletal dynamics/organization, functional enzymes, PM binding, small GTPase GEF/GAP, protein kinases and phosphatases, and several minor categories, such as cell adhesion molecules, transcription/translation factors, and microtubule proteins (77).

A large group of PIP2 binding proteins are involved in membrane transport and trafficking. Endocytosis is regulated by PIP2 at several steps such as vesicle formation, maturation, and fission. Clathrin-mediated endocytosis (CME) is a well-studied form of endocytosis with numerous proteins interacting with PIP2 using different strategies (12, 56). The PH in Dynamin-1 and -2, ENTH (Epsin N-terminal homology) of Epsin1 and 2, Hip1/1R, and ANTH (AP180 N-terminal homology) of AP180, CALM interacts with PIP2 with a defined binding site. In contrast, α and μ2 subunits of AP-2, profilin, and the Wiskott-Aldrich Syndrome protein (WASP) family proteins (66, 78) bind to PIP2 via surface exposed basic patches. Other actin-associated proteins, such as Bin-Amphiphysin-Rvs (BAR) family proteins that deform membranes, inducing protrusions or invaginations, interact with PIP2 headgroup

electrostatically and cooperatively as they assemble, some even insert amphipathic α helices into the lipid bilayer. Some distinct proteins associate with PIP2 related to exocytosis, including Synaptotagmin-1, Syntaxin-1A, Munc13, Rabphillin, VAMP-2, and Granuphilin (12).

PIP2 is the best-characterized actin cytoskeleton regulator among all PIPs. PIP2 has been shown to facilitate actin cytoskeleton formation beneath the PM, and any change in PIP2 local concentrations affects actin dynamics. An increase of PIP2 levels activates proteins that induce actin filament assembly, such as ERM-family proteins, Talin, and WASP family proteins that activate Arp2/3 complex. An increase of PIP2 levels also inhibits proteins that promote actin filament disassembly, such as Gelsolin, heterodimeric capping protein, ADF/Cofilin, Profilin, and Twinfilin (63). Actin and cytoskeletal modulating proteins use either defined PIP2 binding domains such as FERM domains, or a cluster of positively charged and/or hydrophobic residues such as MARCKS (myristoylated alanine-richC kinase substrate), GAP43 (a growth associated protein), and CAP23 (a cytoskeleton-associated protein). Furthermore, a number of actin-associated proteins, such as BAR domain proteins, are capable of directly deforming phosphoinositide-rich membranes to induce plasma membrane protrusions or invaginations. A cluster of proteins targeted to the PM by PIP2 are classified as small GTPases or GTPase regulators, such as Rho, Arf, Ras and Rab families. These proteins usually harbor a polybasic patch and hydrophobic modifications such as palmitoyl, prenyl, and myristoyl. Rho and Arf6 families bind to PIP2 during cytoskeleton regulation.

PIP2 binds to a variety of structured protein modules such as Pleckstrin homology (PH) domains (Fig. 2.3) (79). PH domains, about 120-amino acid long, are best known for their ability to bind PIPs with high affinity and specificity, although less than 10% of all PH domains share this property (79-83). Most PH domains bind to PIP2 weakly and nonspecifically. Many PH domains share similar core structures, consisting of a pair of antiparallel β sheets with a C-terminal α-helix. There are primarily three types of PH domains in terms of the PIPs binding site: some contain the KXn(K/R)XR motif or a canonical PIP-binding site in the loop connecting strands β1 and β2, such as phospholipase Cδ1 PH domain (PH-PLCδ1) (84); some do not harbor the KXn(K/R)XR motif and instead have a non-canonical PIP-binding site, as found in the β-spectrin PH domain (85); others contain both canonical and non-canonical PIP-binding sites, such as ASAP1 PH domain (86, 87). PH-PLCδ1 is the best characterized of PIP2- specific binding proteins, and its fluorescent chimera versions have been used to study cellular PIP2 localization and function (88-91). Several basic residues in PH-PLCδ1 were predicted to bind to PIP2 (Fig. 2.3) (92). To test whether these basic residues are sufficient for specific PIP2 binding, a short peptide with amino acids corresponding to residues 30–43 of PH-PLCδ1 was synthesized. However, this peptide only binds to PIP2 weakly and exhibits little specificity, which suggests that the intact tertiary structure of the PH domain is required for high affinity PIP2-specific binding. The 4- and 5-phosphates forming hydrogen bonding networks with Lys30 and Lys57 in PH-PLCδ1 lock PIP2 inside of the binding pocket (84). PH-PLCδ1 binds to the PIP2 polar head group with a 1:1 stoichiometry, with a Kd of 2 μM in vitro (93). Additionally, PH-PLCδ1 also binds to

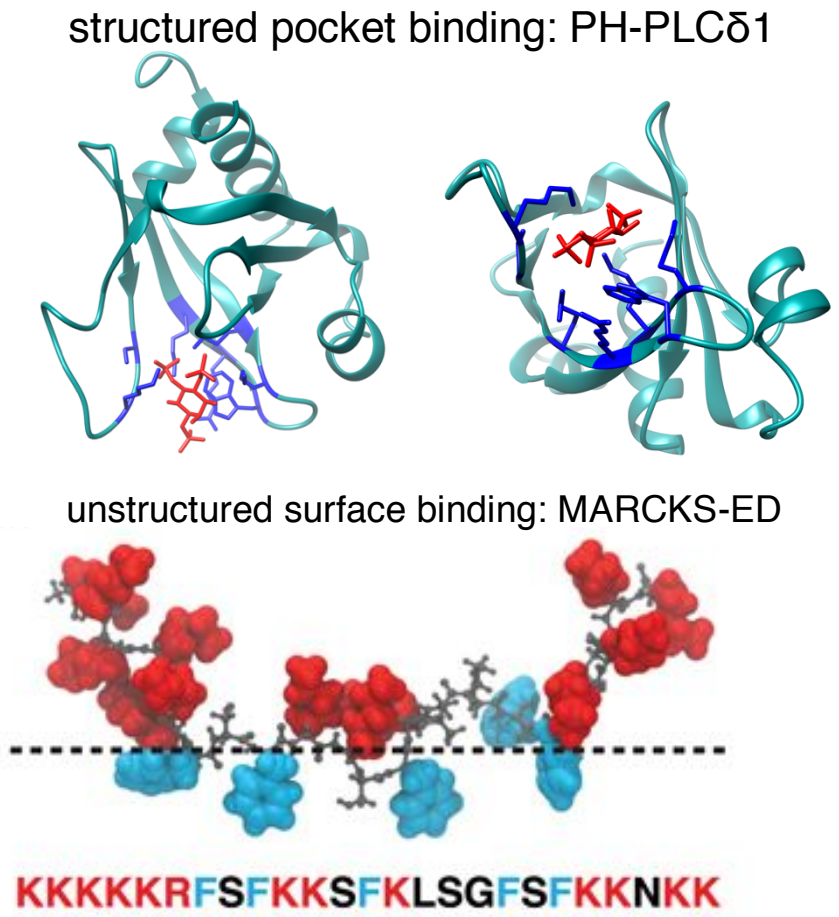

Fig 2.3 Examples of PI(4,5)P2 binding proteins. Top: the pleckstrin homology domain of phospholipase C-δ1 (PH-PLCδ1) is a representative PI(4,5)P2 binding protein with structured biding pocket. The top panel shows structures of PH-PLCδ1binding to Inositol 1,4,5-triphosphate (IP3) from different angles (PDB:1MAI). Residues in PH-PLCδ1 (cyan) interacting with IP3 (red) are colored in dark blue: Lys32, Trp34, Lys30, Arg38, Arg40, Ser55, and Lys57. Bottom: the effector domain (ED) of MARCKS (Myristoylated Alanine Rich Protein Kinase C Substrate) binding to membranes (151-175). The basic residues area colored in red, and hydrophobic residues are colored in blue. This image is adapted from Kastelowitz, N., Tamura, R., Onasoga, A., Stalker, T.J., White, O.R., Brown, P.N., Brodsky, G.L., Brass, L.F., Branchford, B.R., Di Paola, J. and Yin, H., 2017. Peptides derived from MARCKS block coagulation complex assembly on phosphatidylserine. *Sci Rep* 7.1: 4275. https://doi.org/10.1038/s41598-017-04494-y. This article is available under the terms of the Creative Commons Attribution License (CC BY). https://creativecommons.org/licenses/by/4.0/

the soluble d-myo-IP3 with even higher affinity, almost 8-fold compared to PIP2 (84, 93, 94). Excess IP3 can abolish the binding of the PH domain to PIP2 in vitro, which would interfere with the function of the PH domain as a PIP2 sensor in cells.

FERM domains, approximately 300 amino acids in length, were originally defined by their presence at the N-terminus of the erythrocyte band 4.1 protein (F) and the related cytoskeletal proteins Ezrin (E), Radixin (R), and Moesin (M) (95-97). These domains are also found in the cytoskeletal protein Talin, the tumor suppressor Merlin, and several tyrosine kinases (such as JAK, FAK) and phosphatases (such as PTPN3 and PTPN4) (68, 98). Upon binding to PIP2, the FERM domain of these proteins is released from its autoinhibitory status, allowing these proteins to serve as adaptors between the actin cytoskeleton and the PM (99). The FERM domain is composed of three subdomains A, B, and C. Subdomain C contains a fold resembling PH (100). However, the region responsible for PIP2 binding is a basic cleft between the subdomains A and C. Further mutagenesis studies imply that other regions of the FERM domain may also contribute to PIP2 binding. These residues involved in PIP2 binding are conserved, and the sequence homology suggests a potential PIP2 binding pocket.

Another PIP2 binding module is ENTH domain, which plays a critical role in CME (101). ENTH domains contain approximately 140 amino acids, and are found in Epsin1 and 2, and Hip1R. NMR studies determined that positively charged residues in a cleft of the Epsin ENTH domain contribute to PIP2 binding (102). ENTH binds to PIP2 much stronger than a related domain called ANTH. Another structured domains selectively binding to PIP2 is the PX domain of the CPK PI-3 kinase (103).

While many proteins have developed specific PIP2 binding pockets, other proteins use unstructured basic regions to bind to PIP2 via nonspecific electrostatic interactions. MARCKS protein is among the best-studied of those proteins (Fig. 2.3) (13, 104, 105). MARCKS protein binds to the negatively charged inner leaflet of the PM using two mechanisms: an N-terminal myristate inserts hydrophobically into the bilayer, and a conserved effector domain interacts with membrane with its 13 basic residues (residues 151–175: KKKKKRFSFKKSFKLSGFSFKKNKK). MARCKS effector domain binds to and sequesters 3 PIP2 molecules (13, 106). The 5 aromatic Phe residues in the effector domain are shown to be inserted into bilayers (104, 107-110). This insertion would pull the adjacent basic residues closer to the membrane surface where the electrostatic potential is stronger, thereby enhancing lateral PIP2 sequestration. Membrane-bound MARCKS can be dissociated from the PM by Ca^{2+}-loaded Calmodulin or by phosphorylation of the Ser residues of the effector domain by protein kinase C (13).

Treating these membrane-bound molecules as if they were water-soluble molecules within the volume of the cytosol, the physiological level of MARCKS is estimated to be ~2 μM in fibroblasts and ~10 μM in neuronal tissue, a similar range to that estimated for PIP2 concentration in cells (13). These levels indicate that MARCKS could potentially bind and sequester a significant fraction of the PIP2. MARCKS-sequestered PIP2 would be less susceptible to hydrolysis by PLCδ1 compared to exposed PIP2 when MARCKS is dissociated. In addition to MARCKS, PIP2 binds strongly to growth-associated protein of 43 kDa (GAP-43) and cortical-associated protein of 23 kDa (CAP-23) (13, 38, 107). These three motility-associated

proteins are termed GMC proteins, and they share important properties: They all contain a basic effector domain, are reported to localize in the cholesterol-enriched domains or “rafts”, and laterally sequester PIP2 (45, 107, 111). GAP-43 association with rafts was found to require dual palmitoylation of its N-terminus (112).

ROLE OF PIP2 IN VIRUS REPLICATION

Besides the numerous roles PIP2 plays to maintain normal cell functions, it is also indispensable during the lifecycle of many viruses, including human immunodeficiency virus 1 (HIV-1) and Ebola virus. Consistent with its roles in vesicle transport, trafficking, and actin cytoskeletal regulation, PIP2 also impacts viruses that hijack cellular machinery during various stages of infection.

The role of PIP2 begins as early as viral entry. Many enveloped viruses such as Influenza virus and Vesicular stomatitis virus (VSV) use PIP2-dependent CME for productive infection (113-118). Some non-enveloped viruses, such as Foot and-mouth disease virus (FMDV), use integrins as their receptor, are highly dependent on PIP2 for internalization (119). One study reported that PIP2 plays a role in HIV-1 entry (120).

PIP2 is essential for genome replication of some viruses, such as Hepatitis C virus (HCV). HCV, like other flaviviruses, replicates its RNA genome in close contact with invaginated membranous structures that might be derived from organelles such as ER, Golgi body, and endosome (121, 122). The N-terminal amphipathic helix (AH) of the non-structured protein NS5A binds to PIP2 through a pair of highly conserved basic amino acids, Lys 20 and Lys 26. This NS5A-PIP2 interaction induces a

conformational change that stabilizes the interaction between NS5A and TBC1D20, a GTPase- activating protein for Rab1, which is required for establishing efficient HCV replication (123, 124). Importantly, these Lys residues are highly conserved across all HCV isolates, and in NS4B protein of polioviruses and rhinoviruses.

The most studied role of PIP2 during the viral lifecycle is in viral assembly (125). Many cell studies have shown that PIP2 is critical in HIV-1 particle assembly (126, 127). Depleting PIP2 at the PM by overexpression of 5ptaseIV, which breaks down PIP2, significantly reduces both HIV-1 assembly at the PM and viral release from cells. Altering the PIP2 localization to endosomal compartments by expression of an Arf6 mutant Q67L also drastically reduces viral release from cells (126). A recent study observed less HIV-1 Gag assembly upon rapid PIP2 level disruption at the PM, and enhanced Gag assembly upon restoration of PM PIP2 levels in living cells (128). Consistently, several biochemical studies suggest that the membrane binding of HIV-1 Gag and Gag-related proteins is significantly enhanced in the presence of PIP2, shown by either liposome flotation assays or pelleting assays (127, 129-133). All of these results suggest that basic residues in MA interact directly with PIP2 (126). Specific HIV-1 MA interactions with PIP2 were detected by mass spectrometric protein footprinting (134). NMR studies also confirmed that the HIV-1 MA domain binds specifically to water soluble short-chain (C4 and C8) analogs of PIP2 (135). Lipidomic studies suggest that HIV-1 virions have an elevated PIP2 level compared with the host PM from where the virions bud (136). This PIP2 enrichment requires the HIV-1 MA domain, because a Gag mutant lacking the polybasic globular head of MA but still containing the N-terminal myristate incorporates significantly

less PIP2 than WT (136-138). HIV-1 viral membranes were also reported to have increased “raft” lipid components cholesterol and sphingomyelin (SM), as well as lipids from the cytosolic leaflet such as PIP2, phosphatidylserine (PS), and plasmalogen-phosphatidylethanolamine (pl-PE) (136, 137, 139, 140). It was therefore hypothesized that HIV-1 buds from PIP2-rich raft-like microdomains and that HIV-1 exploits MA–PIP2 interactions for efficient virus assembly and release.

MA interaction with PIP2 is also reported for other retroviruses, such as HIV-2, Mason-Pfizer monkey virus (M-PMV), equine infectious anemia virus (EIAV), and murine leukemia virus (MLV) (132, 136, 141). In contrast, human T-lymphotropic virus type 1 (HTLV-1) (142) and Rous Sarcoma virus (RSV) (143) are reported to be much less dependent on PIP2 for viral assembly and release than HIV-1 Gag. In addition to retroviruses, several studies show that PIP2 is required for stabilizing and/or inducing oligomerization of the Ebola virus (EBOV, a filovirus) structural protein VP40 at the PM. VP40 has been shown to be indispensable for viral particle formation (144). However, the VP40 of another Filovirus, Marburg virus (MARV), seems to lack specific interactions with PIP2, instead acting as a promiscuous anionic charge sensor (145). A recent study suggests that influenza hemagglutinin (HA) protein tightly colocalizes with PIP2 at the PM in infected cells, and PIP2 clustering and dynamics follow an HA-dependent potential gradient (146).

Other than transmission by release of viral particles into the extracellular space, viruses like HIV-1 can also be spread through cell-cell transmission by forming a virological synapse (VS)(147). A VS forms at the contact site of infected and uninfected T cells, mediated by Envelope interactions with receptor (CD4) and

coreceptors (CXCR4 and CCR5) (148). Synapse complex formation relies on efficient actin cytoskeleton remodeling in the target cells (149). Upon Env and Gag being recruited to the cell–cell contact sites, viral particles transfer across the VS into the uninfected cells. PIP2 is involved in this process, since it regulates actin-binding protein accumulation that triggers VS formation, thus ensuring efficient viral dissemination.

PIP2 MICELLE FORMATION

The amphipathic nature of PIP2 results in two possible major structures in the presence of water: micelles and membrane bilayers. The self-assembly of phospholipids is driven by increased water entropy when their nonpolar tails are removed from water, and is stabilized by electrostatic and hydrogen-bond interactions among hydrophilic heads and the aqueous environment. Other phospholipids with long acyl chains form bilayers, but without micelles being detected because of extreme insolubility. The strongly hydrophilic headgroup makes PIP2 capable of forming micelles in an aqueous environment (150-152), but in the presence of sufficient bilayer phase, PIP2 is more stable within the lipid bilayers.

A characteristic for any micelle-forming surfactant is the critical micelle concentration or CMC, defined as the minimal concentration above which surfactant monomers aggregate to form micelles. Beyond the CMC, any additional surfactant of the same type forms more micelles, leaving the monomer concentration almost constant. The shape and size of a micelle are dependent on the molecular structure and the aqueous conditions such as surfactant concentration, pH, ionic type and strength

and temperature. Common methods to determine CMC are light scattering, dye solubilization, and surface tension (153). Both light scattering and the solubility of a hydrophobic dye increase with increasing surfactant concentration above the CMC, whereas surface tension decreases with increasing surfactant monomer concentration, reaching a minimum value at the CMC. Few measurements of CMC values for PIP2 have been reported, for example, a CMC of 30−40 μM using light scattering (154), a CMC of 10 μM using the Coomassie blue dye method (155), and 12.5 μM using the dye DPH (156). Additionally, Palmer (157) observed that PIP2 CMC in the buffers 50 mM PIPES or 50mM Tris at pH 7.0 is 30 μM, whereas that in water is 200 μM.

The aggregation number of each PIP2 micelle has been determined by gel filtration chromatography with the PIP2 micelle in complex with PIP2 binding proteins, such as PKC or profilin (158, 159). These complexes form micelles of molecular weight 93,000 with an estimated aggregation number of 82, and a Stokes radius of 39 Å. Interestingly, Janmey and colleagues (160-163) showed that PIP2 exists as small micelles in the presence of buffer ions or/and monovalent cations, such as 100 mM NaCl and KCl, whereas the addition of millimolar concentrations of divalent cations such as Mg^{2+}, Ca^{2+}, or Ba^{2+} induces the formation of large, multilamellar PIP2 aggregates, visible by electron microscopy (EM). This PIP2 cluster formation with divalent cations is presumably through bridging of PIP2 headgroups. The addition of EDTA or EGTA disrupts these PIP2 aggregates, confirming that this process is reversible. In summary, PIP2 aqueous micelle formation can be seen as the form of PIP2 clustering behavior in the absence of other lipids. Even though this type

of clustering as micelles is not physiologically relevant, it does indicate how interactive PIP2 headgroups are despite multiple negative charges.

PIP2 CLUSTERING BEHAVIOR IN VIVO

Evidence suggests that PIP2 forms clusters at the cellular PM. The Fujimoto group (164) visualized concentrated PIP2 pools at the rim of caveolae as well as in the coated pit in cultured cells, using an EM technique without chemical fixation or artificial probes. Many studies report PIP2 clustering in intact cells or on membrane sheets derived from cells, and most of these studies detect PIP2 accumulation by fluorescently labeled PH-PLCδ1, acyl-chain labeled fluorescent PIP2, or by PIP2-specific antibodies. Many groups have employed super-resolution microscopy to visualize PIP2. Using direct stochastic optical reconstruction microscopy (dSTORM), PIP2 clusters were found to be in domains of about 65 nm in intact PC12 cells by use of PIP2-specific antibodies directly conjugated with AlexaFluor 647 (165). Three quarters of the observed PIP2 clusters are reported to be elongated and one quarter to be circular. Using stimulated-emission depletion microscopy (STED), a study suggests that PIP2 comprises ~ 80% of all the inner leaflet lipids within clusters, and that these PIP2 clusters are ~ 70 nm diameter with fluorescent PH-PLCδ1 or ~ 90 nm in diameter with a PIP2 antibody, which would indicate ~1000 PIP2 molecules in each cluster (166). Using fluorescence photoactivation localization microscopy (FPALM), a recent report observed larger PIP2 clusters in live cells, approximately 150 nm in diameter using acyl-chain labeled fluorescent PIP2 delivered across the PM by the carrier protein histone H1; even larger clusters are found in fixed cells, approximately

400 nm in diameter detected by fluorescent PH-PLCδ1. Of note, another group using confocal microscopy (167) reported that the size of the PIP2 cluster using a PIP2 secondary antibody was enhanced upon adding a tertiary antibody. Thus, the visualization of PIP2 clusters using antibodies needs to be carefully examined and interpreted.

Numerous cellular PIP2 binding proteins are also proposed to modulate PIP2 distribution and induce PIP2 cluster formation. For example, MARCKS, GAP43, CAP23 and Syntaxin 1 have been reported to laterally sequester PIP2 at the PM (111, 168). A large fraction of PIP2 at the inner leaflet is believed to be electrostatically sequestered or bound to and released by proteins containing a basic patch, such as MARCKS protein (107). Each MARCKS can bind 3 PIP2 molecules with a dissociation constant of 10^{-8} M (105). This bound PIP2 would be released only upon transient Ca^{2+} influx or upon phosphorylation of a key serine residue by protein kinase C. At the same time, other effector proteins could have access to these concentrated PIP2 platforms to activate downstream functions. Only a small fraction of PIP2 is believed to diffuse freely in the PM. The evidence for PIP2 being laterally sequestered by proteins comes from such cellular studies. In several cell types, MARCKS is not uniformly distributed at the PM, but is enriched in membrane ruffles or nascent phagosomes (169, 170). A similar PIP2 distribution pattern was later observed using fluorescent PH-PLCδ probes (70, 171). Importantly, Van Rheenen and colleagues, using advanced imaging methods to characterize the bumpy cell surface (172, 173), showed that the apparent enrichment of PIP2 detected by PH-PLCδ clustering was not due to PIP2 cluster formation, but instead was caused by an increased lipid content in

submicroscopic folds and ruffles, and thus was a visualization artifact. When MARCKS is disassociated from the PM into the cytosol by PKC phosphorylation, the free PIP2 level at the PM increased as membrane tension increased, due to PIP2-dependent cytoskeletal adhesion to the PM (174). Another study showed that PIP2 co-localized with GMC proteins MARCKS, GAP43 and CAPS23 in cholesterol-rich microdomains in many cell lines using antibody labeling. Overexpression of GMC increases the detectable PIP2 clusters; GMC lacking effector domains seems to reduce PIP2 accumulation. However, the characteristic patchy pattern of GMC and PIP2 microdomains was not detectable when macroscopic clusters of GPI-linked proteins were prevented by fixation with glutaraldehyde (111).

Other groups employed unfixed PC12 cell membrane sheets, derived from the PM by gentle sonication, to study PIP2 lateral organization (175). They reported (166, 168) that Syntaxin-1, a SNARE protein that catalyzes regulated exocytosis, forms clusters in the PM, mediated by electrostatic interactions with PIP2. Syntaxin-1 contains a polybasic region (basic residues KARRKK) juxtaposed to a transmembrane domain, sequestering PIP2 headgroups. Using STED, they found that the polybasic region is required for PIP2 co-clustering with Syntaxin 1, and such nanoscopic PIP2 clusters were also required for Syntaxin-1 sequestering. PIP2-Syntaxin clusters serve as recognition and association sites for vesicle docking during Ca^{2+}-stimulated membrane fusion (176). Another group reported Ca^{2+} to link smaller PIP2–Syntaxin-1 clusters into larger domains and that this clustering effect is reversible (177). Locally concentrated PIP2 - Ca^{2+} can recruit more downstream effector proteins such as CAPS, Munc13, and Synaptotagmin to facilitate assembly of the complete fusion

machinery at the site of release (168). Together, these studies suggest that PIP2 clustering may occur as a consequence of lateral sequestration by effector proteins upon physiological Ca^{2+} influx, and that these protein-PIP2 clusters regulate the accessibility of PIP2 to other effector proteins.

In addition to protein sequestration, upon activation of specific PIP kinases, PIP2 synthesis is localized to the inner leaflet of the PM (18). Type I phosphatidylinositol 4-phosphate 5-kinase (PIP5K) is mostly responsible for the generation of PIP2 from PI(4)P at the PM, since PI(4)P is the second most abundant PIP at the inner leaflet (178). Via distinct signaling pathways, PIP5K isoforms and splice variants have specific interactions with different proteins that allow PIP5K to target subcellular localizations such as the PM, focal adhesions, the Golgi, and the nucleus (179). PIP2 is also locally synthesized at sites of actin remodeling, giving rise to membrane ruffles, filopodia, lamellipodia, and phagosomes. PIP2 accumulation at phagosomes due to PIP5K has been detected (180). This accumulation is transient, as the DAG level significantly increases and the PIP2 level decreases upon PLC activation. Small GTPases such as Rho, Rac family, Arf6, specific proteins such as Talin, and phospholipids such as phosphatidic acid (PA) have been shown to activate and regulate PIP5K activity, and then modulate PIP2 localized synthesis (9, 11, 12, 22, 179). Targeted PIP2 production by PIP5K further regulates various PIP2 effector proteins during biological functions. Thus, it is likely that these separated PIP2 pools are spatially and temporally choreographed by a combination of enzymes, effector proteins, and probably other cytosolic factors. However, the mechanistic details of

how these separate pools of PIP2 form are unclear and in vitro studies could provide more information at a molecular level.

PIP2 CLUSTERING BEHAVIOR IN VITRO

Models of PIP2 accumulation in vitro are primarily based on mechanistic details of PIP2 cluster formation. Several models could explain PIP2 clustering in bilayers. PIP2 clustering is proposed to be induced by a combination of electrostatic bridging by multivalent metal ions such as Ca^{2+} and Mg^{2+} (see Fig. 2.4) (181-183), hydrogen bonding networks among PIP2 headgroups (24-28, 184), and protein basic patches (107). Molecular dynamics simulations (185, 186) indicate that clustered PIP2 affects protein binding, with protein binding further modulating PIP2 enrichment.

In the absence of multivalent cations or polybasic proteins, hydrogen bonding networks between PIP2 headgroups might induce PIP2 clustering, despite electrostatic repulsion between highly negatively charged PIP2. Support for this hypothesis is that demixing of PIP2 in fluid PC bilayers can occur at membrane concentration as low as 1% (23, 29). Using Förster resonance energy transfer (FRET), PIP2 segregation from PC was observed at high pH, probably stabilized by hydrogen bond networks formed between the hydroxyl groups and the phosphomonoester and phosphodiester groups of adjacent PIP2. An NMR study (28) reported that PIP2 exhibited a biphasic pH-dependent ionization behavior, which could be explained by intermolecular sharing of the last remaining proton between the vicinal phosphomonoester groups. Strikingly, two studies (24, 27) showed that 5–20 mol% PIP2 induced macroscopic phase

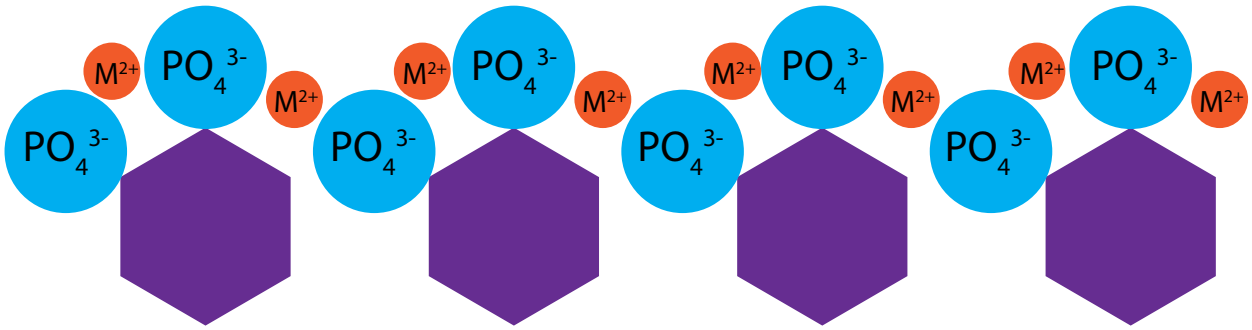

Fig 2.4 Molecular depiction of multivalent cation-bridged PI(4,5)P2 clusters. Multivalent cations are shown in orange circles. Each PI(4,5)P2 headgroup is shown as an purple inositol ring with two blue phosphate groups on 4- and 5-positions. PI(4,5)P2 clusters form via electrostatic interactions between positively charged cations and negatively charged phosphate groups.

separation in GUVs in the presence of 20 mol% PI or cholesterol, using multivalent cation-free buffers. PI was suggested to form a separate phase with PIP2, while Chol was observed to be present in both phases. Such extremely large fractions of PIP2 in membranes are not physiological, so this kind of macroscopic phase separation might not occur at physiological PIP2 levels. It is also reported (24) that cholesterol, but not cholesterol derivatives with the hydroxyl group modified, promoted and stabilized PIP2 domains. This result indicates that the cholesterol hydroxyl group might participate in intermolecular hydrogen bond formation, possibly with the cholesterol serving as a spacer between PIP2 molecules within domains. Other bulk lipid components such as PE could also influence PIP2 ionization properties, perhaps serving as hydrogen bond donors (27, 184). A different group (34) showed that the presence of chaotropic agents, such as monovalent salts, urea and temperature, specifically and significantly expanded the PIP2 molecular area in lipid monolayers. These results indicate that without multivalent cations, hydrogen bond networks might cluster PIP2 and reduce the area per PIP2, forming condensed PIP2 clusters. Taken together, hydrogen bonding networks might contribute to PIP2 cluster formation to some degree, charge bridging by multivalent cations and charge shielding by proteins seem to play dominant roles under physiological conditions (Fig. 2.4).

PIP2 binding to multivalent cations has been reported in both monolayers and bilayers. Early investigations found cation binding to PIP2 that is not membrane-bound. Ca^{2+} or Mg^{2+} dramatically affected the elution profile of PIP2 through an ion exchange column, probably by decreasing the effective charge of PIP2 when a stable chelate formed (187, 188). Ca^{2+} and Mg^{2+} binding to PIP2 induced large multilamellar

PIP2 aggregates (152, 188, 189). in both model membranes and red blood cell membranes, cation binding to PIP2 revealed that PIP2 has higher affinity for Ca^{2+} than for Mg^{2+} (190, 191). Studies of Langmuir monolayers (34, 192) showed that divalent cations bind to PIP2. In contrast to chaotropic agents such as monovalent salts which expanded the area per PIP2 molecule in monolayers, Ca^{2+} significantly condensed the area per PIP2 molecule. Surface pressure measurements showed this condensing effect to be reversible. The addition of Ca^{2+} decreased the surface pressure at constant monolayer area. The surface pressure recovered to the normal level upon adding an excess of EDTA to chelate all of the Ca^{2+}. Since Mg^{2+} showed minimal effect on surface pressure under the same conditions, a Ca^{2+} titration assay at different Mg2+ concentrations was performed (193). The estimated PIP2-cation apparent dissociation constant in these monolayers was similar, approximately 4.6 μM for Ca^{2+} and 7.7 μM for Mg^{2+}.

Additional studies on membrane bilayers provided more details of PIP2 and multivalent cation association. Based on electrophoretic mobility measurements (31), the intrinsic association constants of Ca^{2+} and Mg^{2+} for PIP2 were 500 M^{-1} and 100 M^{-1}, respectively. Another group (193) reported that the calculated intrinsic association constant for PIP2 in bilayers was 360 M^{-1} for Ca^{2+} and 220 M^{-1} for Mg^{2+}, based on surface potential measurements. Attenuated total reflection Fourier transform infrared (ATR-FTIR) measurements suggest that upon binding to PIP2 headgroups, partial water loss occurs from the hydration shell of Ca^{2+} but not Mg2+, presumably due to the tight binding of Mg^{2+} to water molecules. Collectively, these studies

provide evidence of Ca^{2+} and Mg^{2+} binding tightly to PIP2 headgroups, and indicate cluster- promotion upon binding.

Several groups have visualized divalent cation-induced PIP2 cluster formation on monolayers, bilayers, or cell membranes. By including fluorescently labeled PIP2, calcium-dependent PIP2 clusters were seen in monolayers using fluorescence microscopy at PIP2 concentrations between 8-50 mol% (192). Ellenbroek and coworkers (186) published PIP2 phase diagrams in monolayers with 1mM Ca^{2+}, based on atomic force microscopy (AFM) and fluorescence microscopy. They showed that divalent cation-induced PIP2 clusters were visible at as low as 2 mol% PIP2 at pH 7.4. Using supported lipid monolayers the same group later employed tapping mode AFM imaging and visualized sub-micrometer-sized PIP2 clusters with a radius of about 40 nm induced by micromolar Ca^{2+}, and smaller clusters induced by millimolar Mg^{2+} (193). A different group found that in the absence of divalent cations, giant unilamellar vesicles (GUVs) that contain 5 mol% total PIP2 and 0.1% fluorescent PIP2 looked uniform. Divalent cations induced PIP2 cluster formation in a concentration-dependent manner above 25 μM for Ca^{2+} and above 300 μM for Mg^{2+}. Furthermore, the presence of high concentrations of divalent cations (>300 μM for Ca^{2+} and >1 mM for Mg^{2+}) rendered the GUVs more fragile and caused vesicle rupture (167). However, a different group (194) did not observe PIP2 clusters in GUVs containing 1 mol% PIP2 with 100 μM Ca^{2+}. Their fluorescence depolarization data imply that an average cluster has about 15 PIP2 molecules.

PIP2 clusters on cell membrane sheets have been visualized primarily by PIP2-specific binding proteins with fluorescent tags, such as PH-PLCδ, or by PIP2

antibodies, by use of fluorescence microscopic methods. For example, one group (165) employed dSTORM to image PC12 cell membrane sheets with anti-PIP2 antibodies directly conjugated with Alexa Fluor 647. They estimated PIP2 cluster size to be ~65 nm. As mentioned in an earlier section, Honigmann and coworkers (168) employed STED microscopy to find that PIP2 clusters in PC12 cell membranes had an average diameter of ~70 nm by fluorescent PH-PLCδ, and an average diameter of ~90 nm detected by a monoclonal PIP2 antibody plus a secondary antibody labeled with Alexa Fluor 488.

In summary, these imaging studies on monolayers, GUVs, and cell membrane sheets indicate that PIP2-cation clusters are most likely to be submicroscopic by conventional confocal microscopy. The exact size of these nanoscopic PIP2 clusters could only be determined by super resolution microscopy with optimized labeling methods. Moreover, whether fluorescent protein probes like PH-PLCδ or fluorescent lipid antibody induce artifacts in cluster formation or size needs to be carefully investigated.

Determining lipid lateral diffusion is crucial to understand membrane spatial heterogeneity. Another way to confirm PIP2 clustering is to determine if the PIP2 molecular diffusion rate slows down in the membrane. Lipid diffusion has been studied in model membranes and intact cell membranes by methods (195) such as fluorescence correlation spectroscopy (FCS) and fluorescence recovery after photobleaching (FRAP). The Prieto group (194) detected Ca^{2+}-induced clustering of PIP2 by use of FCS. The diffusion coefficient of PIP2 decreased in the presence of 100 μM Ca^{2+}, while that of the control lipid POPS remained unchanged. This study

concluded that the high sensitivity of PIP2 diffusion to Ca^{2+} indicates that PIP2 cluster size must be larger than dimers. The Janmey group (193) also used FCS to detect cation-induced retardation of diffusion of PIP2 in GUVs. One millimolar Mg^{2+} slowed the diffusion of fluorescently labeled PIP2 by 4-fold, in agreement with nanoscopic PIP2 clusters being induced by Mg^{2+}. Compared to Mg^{2+} and Zn^{2+}, Ca^{2+} exhibited more pronounced retardation of PIP2 diffusion. The diffusion of PIP2 is slowed to 0.8 ± 0.4 μm2/s by 10 μM Ca^{2+}, which is similar to the diffusion coefficient of PIP2 on the inner leaflet of the PM. The McLaughlin group (196) studied PIP2 diffusion in the PM of fibroblasts and epithelial cells, as well as in model membranes like GUVs. They used fluorescent PIP2 to either label the outer leaflet by incubating GUVs with PIP2-containing micelles, or label the inner leaflet by microinjecting PIP2-containing micelles into GUVs. They reported the PIP2 diffusion coefficient to be about 0.8 $\mu m^2/s$ in the inner leaflet, 2–3 fold slower than in plasma membrane-derived blebs or in GUVs. Another paper from the McLaughlin group (106) reported that the diffusion of PIP2 is 10 times slower in the presence of micromolar Ca^{2+}. In the presence 1 mol% PIP2 in GUVs, the diffusion rate of membrane-associated fluorescently labeled polybasic peptide Lys13 is only about half of that in a PIP2-free membrane, indicating that the polybasic peptide diffuses together with the laterally sequestered PIP2. This result suggests that there can be two different PIP2 populations present in the PM. The lower diffusion coefficient of PIP2 in the inner leaflet is consistent with the hypothesis that about two thirds of the PIP2 is reversibly and electrostatically associated with multivalent cations and basic membrane proteins or cytoskeleton, while the rest of the PIP2 is free. Another study that employed FRAP on living cells showed that the

fluorescence from injected PIP2 fails to recover at the forming phagosome but recovers rapidly in other membrane regions. Slow diffusion would allow PIP2 within the forming phagosome to concentrate during phagocytosis. Together, these studies provide strong evidence that PIP2 diffusion rate slows down significantly when PIP2 cluster formation occurs as a result of multivalent cation bridging and cellular protein sequestration.

Since PIP2-cation clusters are most likely to be nanoscopic, sensitive biophysical methods such as FRET, fluorescence self-quenching, and fluorescence anisotropy are required to provide molecular details about these clusters. The Janmey group (193) used FRET to study divalent cation-induced PIP2 clustering in membrane bilayers and found that the trend in inducing PIP2 cluster formation follows the order of $Ca^{2+} >> Mg^{2+} > Zn^{2+}$ at a fixed 5 mol% PIP2. By the use of fluorescence anisotropy, the Prieto group (194) reported that Ca^{2+} at physiological concentrations up to 100 μM induces PIP2 clusters. At identical concentrations, Ca^{2+} is significantly more efficient than Mg^{2+} in promoting PIP2 clustering (197). 5 mM Mg^{2+} was able to drive PIP2 clustering more efficiently than 100 μM Ca^{2+}. The Prieto group (194) also employed fluorescence self-quenching to address the PIP2 lateral distribution in PC bilayers. The steady-state fluorescence intensity of TopFluor-PIP2 was measured at several concentrations. Self-quenching was observed as Ca^{2+} concentration increased, but no self-quenching was seen in the presence of 5 mM EDTA for up to 1 mol% total PIP2 (194). Most previous studies only focused on the effect of physiological cations such as Ca^{2+}, with Ca^{2+} - free condition as the negative control. However, without adding metal chelators EDTA or EGTA to buffers, or without using CHELEX-treated

buffers, other multivalent cations can still be present (198, 199). Discrepancies in the PIP2 literature might come from multivalent cation contamination in buffers, as we showed recently (181). Thus, careful sample and buffer preparation is necessary to study PIP2 behavior.

Although PIP2 clustering is supported by abundant evidence, most previous in vitro studies used non-physiological PIP2 concentrations > 5 mol%, and buffers containing uncharacterized multivalent cation contamination. A recent study (181) showed that buffers prepared with American Chemical Society grade chemicals with 99% purity, stored in borosilicate glass bottles, contained Ca^{2+} (60 μM), Al^{3+} (10 μM), Zn^{2+} (6 μM), and Fe^{3+} (0.1 μM) by measurement with inductively coupled plasma optical emission spectroscopy (ICP-OES).

Characterizing PIP2 behavior at high PIP2 concentrations misses the origin of PIP2-PIP2 association. Recently, we found a maximal solubility of free PIP2 in model membranes, above which PIP2 clustering occurs in the presence of multivalent cations. Both self-quenching and FRET were used to examine PIP2 self-aggregation behavior over a wide concentration range from 0.01 up to 2 mol% in model bilayers that mimic the inner leaflet lipid composition PE/PS/Chol and in buffers with known cation types and concentrations. PIP2 starts to self-associate at extremely low concentrations of 0.02–0.05 mol% of total lipids, with multivalent cations absolutely required for this type of PIP2 clustering. The maximal PIP2 solubility prior to clustering was termed the “critical PIP2 concentration” (CPC) by analogy with the CMC being the critical micelle concentration. This type of PIP2 association was described to be PIP2-cation clustering because EDTA eliminates the PIP2 clusters. For

both FRET and self-quenching, the linear increase with increasing PIP2 fraction above the CPC implies that all additional PIP2 forms more clusters that possess the same properties. This abrupt onset of PIP2 self-association is a characteristic of high-order aggregation, as in micelle formation or phase separation. PIP2-cation cluster formation is not dependent on a particular multivalent cation. Al^{3+} had the strongest effect on cluster formation, and Mg^{2+} the weakest, but a variety of cations promoted clustering, including Ca^{2+}, Zn^{2+}, and Fe^{3+}. As low as 1 μM of Al^{3+}, Ca^{2+}, Fe^{3+}, Zn^{2+}, or 50μM Mg^{2+} was enough to cause PIP2 clustering above the CPC in a buffer containing 100 mM KCl and 20 mM HEPES. Many previous studies did not consider the possible multivalent cation contaminants present in the micromolar range in salts and buffers. Moreover, metal ions are leached from glass over time, complicating interpretation of some previous reports on PIP2 behavior.

We pointed out that PIP2 clustering is a headgroup-specific behavior, not influenced by the PIP2 hydrophobic acyl chain types (181). Another important finding is that other PIP species can co-cluster with PIP2, but PI cannot. This result indicates that the phosphate groups on the 3, 4, or 5 positions of the inositol ring are required for the co-clustering, with positively charged multivalent cations bridging the negatively charged phosphomonoesters. Thus, pools of different PIPs could exist; for example, PI(4)P and PIP2 could co-exist within the same cluster at the inner leaflet of the PM. While multivalent cations are absolutely required for PIP2-cation cluster formation, the bulk membrane composition surrounding the PIP2 also influences PIP2 clustering. For example, self-quenching of fluorescent TopFluo-PIP2 in POPE/liver-PI/Chol is six-fold higher than in POPC alone. Cholesterol or PI promotes more clustering,

though the mechanism is unclear. Physiological levels of 0.5 mM Mg^{2+} that mimic the resting state are sufficient to induce physiological levels of 2 mol% PIP2 to cluster; an additional 100μM Ca^{2+}, mimicking transient cellular calcium influx, causes even stronger PIP2 clustering. In summary, this study sheds light on how PIP2 exists as "spatially separated pools" in cells, because it quantitatively pinpoints several experimental factors that affect clustering in vitro.

HOW PROTEINS RECOGNIZE AND RESPOND TO PIP2 CLUSTERS

In cytosol, the total concentration of PIP2 binding proteins far exceeds that of PIP2 at the inner leaflet, implying that PIP2 clustering could be highly regulated. In this review, we propose four properties of this unique lipid in cells that are key to its behavior (Fig. 2.5):

(i) PIP2 clusters can form and be modulated by multiple factors like composition and cations, independent of any binding protein. PIP2-cation clusters form at extremely low concentrations in model membranes, a new behavior of PIP2 that we propose also occurs in cells. In cells, it is most likely that free and clustered PIP2 co-exist (Fig. 2.5b). In vivo, local multivalent cations, local lipid composition, and many binding proteins could significantly influence PIP2 properties and be responsible in part for PIP2 being in "spatially separated pools". In turn, these spatially separated pools of free and clustered PIP2 could further regulate protein-binding events.

(ii) PIP2-cluster inducing binders such as multivalent cations, polyamines and proteins with basic patches regulate PIP2 properties, and further regulate other cellular factors

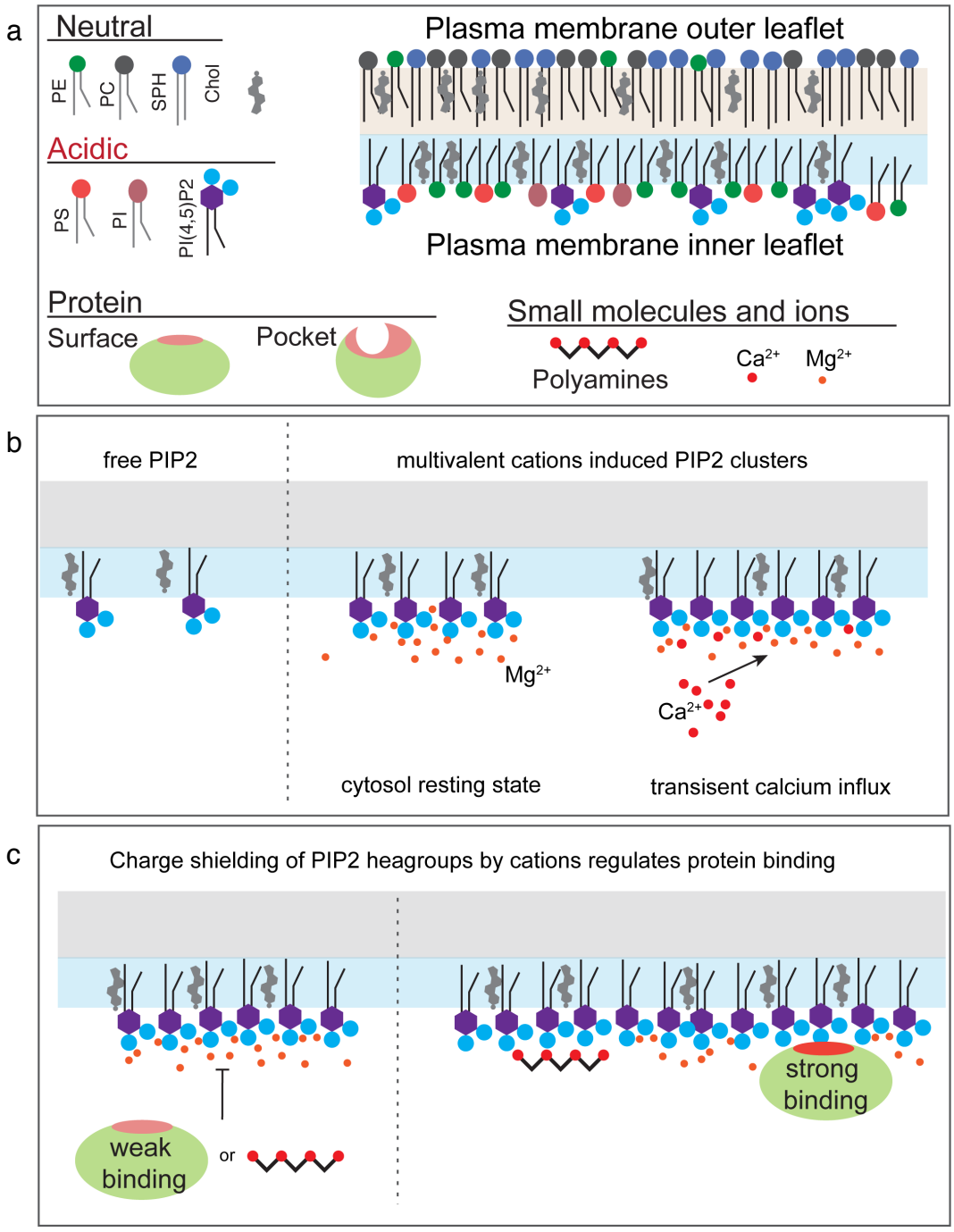

Fig 2.5 Different modes of protein responding to PI(4,5)P2 clusters. (a) The asymmetric lipid distribution across the PM. (b) PI(4,5)P2 clusters can form in the presence of physiological multivalent cations. Spatially separated pools of free and clustered PI(4,5)P2 co-exist at the inner leaflet of the PM. (c) Charge shielding and sequestering negatively charged PI(4,5)P2 headgroups by cations and polybasic small molecules regulates protein binding to PI(4,5)P2; (followed by the next page)

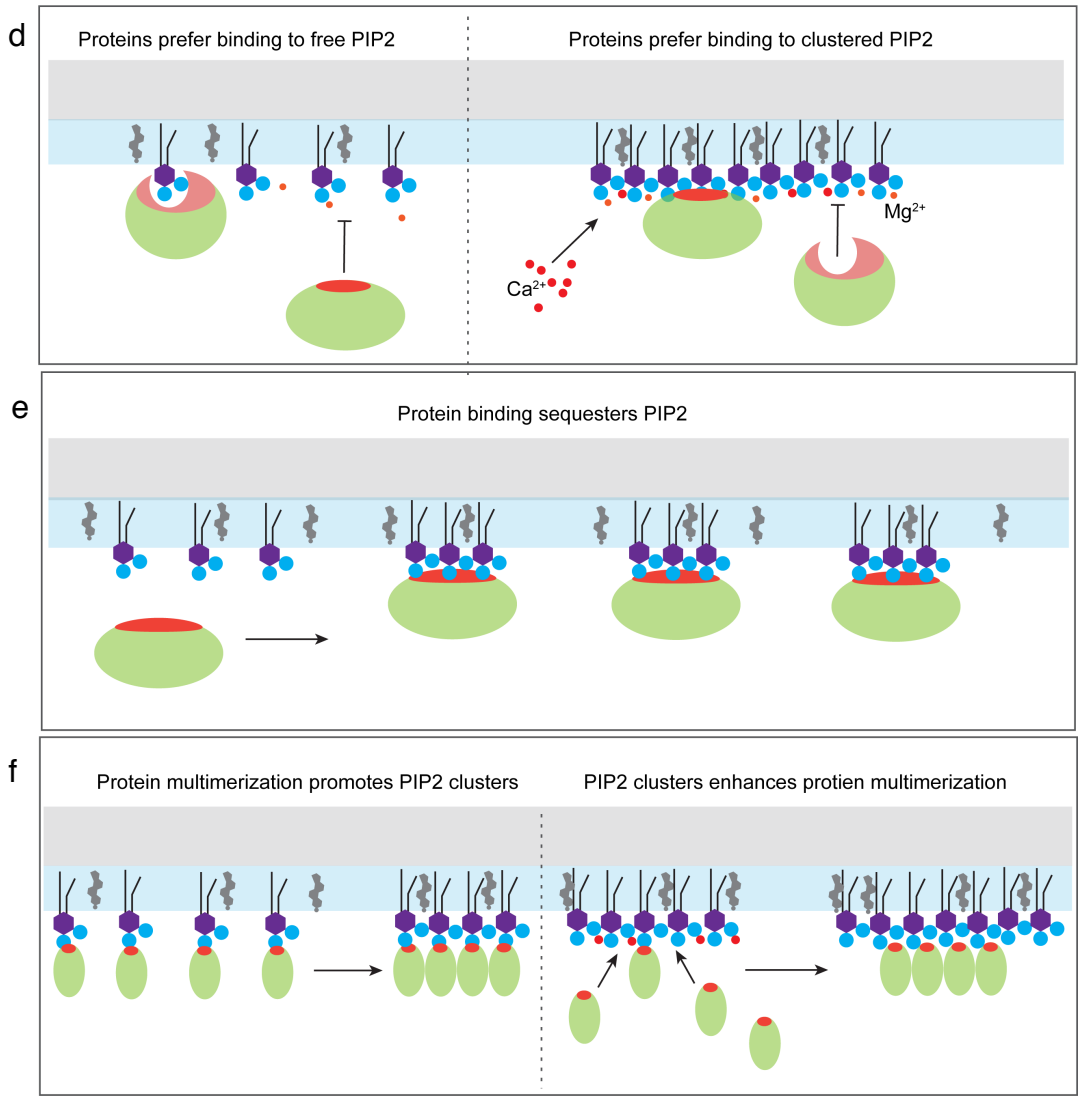

(d) Some proteins prefer to bind free PI(4,5)P2 while others bind PI(4,5)P2 in clusters. During transient calcium influx or any local cation changes, proteins targeting to free PI(4,5)P2 could have reduced binding; while proteins targeting to clustered PI(4,5)P2 could have enhanced binding. (e) Upon membrane binding, some proteins can sequester local PI(4,5)P2. (f) Some proteins induce PI(4,5)P2 cluster formation as they multimerize on membranes; in turn, multimerized proteins have enhanced membrane binding.

having access to PIP2 (Fig. 2.5c). Although the PIP2 concentration in the PM cytosolic leaflet is 1–2 mol%, a majority of this PIP2 must be sequestered by proteins or by multivalent cations. PIP2 lateral organization and function could undergo significant changes in the presence of physiologically relevant concentrations of multivalent cations, which influence PIP2-dependent cellular processes. One study (200) found that intracellular Mg^{2+} inhibits a PIP2-requiring ion channel called KCNQ2/3. Mg^{2+} reduces the current by electrostatically binding to PIP2, significantly reducing the free PIP2 available for interaction with these channels. This mechanism is likely to modulate many other PIP2-dependent ion channels and cellular processes. In another example, Mg^{2+} and polyamines electrostatically bind to PIP2, and could inhibit the activity of PLC by decreasing the amount of free PIP2 available for hydrolysis (201). The details of electrostatic charge shielding of PIP2 by multivalent cations, polyamines, and polybasic proteins would be different because of membrane charge density, ionic radius, dehydration energy of cations, and the manner of bringing together multiple charges. However, one final result could be similar: shielding and sequestering negatively charged PIP2 headgroups prevent PIP2 from interacting with certain binding molecules (Fig. 2.5c).

(iii) Some proteins prefer to bind free PIP2 while others bind PIP2 in clusters (Fig. 2.5d). Several, or even many, populations of PIP2 could co-exist depending on local multivalent cation concentration and local lipid concentration, and free PIP2 could be in equilibrium with clustered PIP2. The headgroup of free PIP2 is exposed, and thus proteins that preferentially bind to sparsely distributed free PIP2 would have immediate access. The headgroup of clustered PIP2 must be bound by cations or

proteins; those proteins that preferentially bind to clustered PIP2 would be competing against bound cations for access to PIP2 molecules. PIP2-cation clusters could form a two-dimensional array of the many PIP2 phosphate groups together with multivalent cations. The degree of PIP2-cation clustering would depend on the type and concentration of multivalent cations and on the surrounding lipid compositions. Local changes of multivalent cations and lipid surroundings will affect the free and clustered PIP2 concentration, thus further influencing PIP2 binding protein types, concentrations, and functions. For example, during transient calcium influx, more cation-bridged PIP2 clusters would form, and the proteins that target clustered PIP2 could experience enhanced function, while proteins that target free PIP2 could experience decreased function (Fig. 2.5d). Proteins such as PH-PLCδ1 might prefer free PIP2 for several reasons. First, PH-PLCδ1 contains a canonical PIP2 binding pocket PLCδ1-PH domain that is proposed to interact with the PI(4,5)P2 headgroup noncooperatively in 1:1 stoichiometry (84). Second, multivalent cations binding to PIP2 headgroups confine lipid headgroup tilt angle, inhibiting PLCδ1-PH domain recognition according to liposome assays and molecular dynamics simulations (202). However, whether PLCδ1-PH further clusters PIP2 upon membrane binding is not clear. Unlike PLCδ1-PH with its canonical PIP2 binding site, proteins with a polybasic region or patch, such as MARCKS and N-WASP bind to PIP2 in a multivalent manner. The activation of N-WASP has been shown to depend on PIP2 concentrations; once the PIP2 level is above a threshold, N-WASP will bind to PIP2 cooperatively with an apparent Hill coefficient of about 20. This sharp PIP2 sensitivity can be tuned by modulating the polybasic region (203).

(iv) Clustering of proteins bound to PIP2 could sequester PIP2 or even induce PIP2 clustering (Fig. 2.5e), especially if those proteins could multimerize on membranes (Fig. 2.5f). Clustered PIP2 could then recruit more proteins to achieve downstream functions. The behavior of Syntaxin 1 in PC12 cells (166) shows that clustering of membrane-bound proteins can lead to formation of PIP2 clusters by electrostatic interactions with juxta-membrane basic residues. Another example of protein multimerization inducing PIP2 clusters is BAR superfamily proteins. Both I-BAR, F-BAR and N-BAR domains from many mammalian proteins have been shown to induce PIP2 clustering (204-208). These BAR domains assemble into stable scaffolds to bend membranes, and restrict PIP2 lateral diffusion by generating stable PIP2-BAR domain clusters. Other than PIP2, BAR domains could also cluster PI(3,4,5)P3 and PI3P, indicating this clustering is through electrostatic sequestration. Several studies show that the PH domain of Dynamin-1 and -2 binds to PIP2 with low affinity, with a Kd value above 1 mM (209). However, oligomerization of dynamin can locally cluster PIP2 at coated pits. Concentrated PIP2 allows multiple PH domains to interact with membranes with higher affinity, promoting vesicle scission during CME (94, 210, 211). Perhaps similarly to clustering by cellular proteins, PIP2 is also sequestered by viral proteins. PIP2 enrichment in HIV-1 viral membranes and the efficient self-assembly of the Gag protein have led to competing hypotheses: First, these PIP2-rich domains pre-exist and are targeted by Gag; second, PIP2 clustering is only induced by Gag multimerization during assembly; third, PIP2 clusters pre-exist at the inner leaflet, while Gag multimerization further promotes this enrichment effect. Carefully designed

experiments with model membranes and purified proteins could elucidate this mechanism.

CONCLUSIONS AND OUTSTANDING QUESTIONS

The rich physical chemistry of PIP2 contributes to its being an interesting and important phospholipid in cells. Despite electrostatic repulsion, PIP2 can form clusters by two major attractive interactions, hydrogen bonding and multivalent cation bridging, with the latter having perhaps a predominant role in cells. Spatially separated pools of PIP2 could arise from localized PIP2 aggregation due to local differences in multivalent cations and lipid compositions, as well as localized PIP2 synthesis and breakdown. PIP2 clustering changes the orientation and accessibility of the headgroups, which would have many implications for the biological function of this phospholipid. A given protein is likely to preferentially bind to either free PIP2 or clustered PIP2 (Fig. 2.5d); PIP2-bound proteins are also likely to either promote or disrupt pre-existing PIP2 clusters. Tight control of local synthesis and turnover of PIP2, together with well-regulated cluster formation and recruitment of selected proteins to specific sites at the inner leaflet of the PM, create a broad spectrum of PIP2-dependent cellular functions.

PIP2 clusters likely exist in all cells and are recognized and utilized by hundreds of cellular proteins, so understanding the nature of PIP2 behavior is fundamental to cell biology. It is of great importance to investigate the biophysical properties of PIP2-cation or PIP2-protein clusters in vitro, especially upon cellular protein binding and transient calcium influx or zinc spark, a fertilization activation

induced release of billions of zinc ions in an exocytotic event (212). Only when we have a better understanding of this unique lipid, could we seek answers for more complicated questions. In the future, it would be critical to elucidate the mechanisms of how PIP2, an inner leaflet lipid, is mysteriously found associated with "rafts" in the PM outer leaflet microdomains. Other than HIV-1, it is likely that many other enveloped viruses also rely on PIP2 clusters to assemble progeny viral particles and then bud from infected cells; perhaps this specific PIP2-dependence could be these viruses' Achille's heel.

REFERENCES

1. Hokin M, Hokin L. 1953. Enzyme secretion and into phospholipides. J Biol Chem. 203:967-77.
2. Wiedemann C, Cockcroft S. 1998. The role of phosphatidylinositol transfer proteins (PITPs) in intracellular signalling. Trends Endocrinol Metab. 9:324-328.
3. Cockcroft S. 2012. The diverse functions of phosphatidylinositol transfer proteins. Springer. 185-208.
4. Rizzieri KE, Vincent P, Bankaitis VA, Phillips SE, Gaucher EA, Schaaf G. 2006. The diverse biological functions of phosphatidylinositol transfer proteins in eukaryotes. Crit Rev Biochem Mol Biol 41:21–49.
5. Cunningham E, Thomas GMH, Ball A, Hiles I, Cockcroft S. 1995. Phosphatidylinositol transfer protein dictates the rate of inositol trisphosphate production by promoting the synthesis of PIP2. Curr Biol. 5:775–783.
6. Shewan A, Eastburn DJ, Mostov K. 2011. Phosphoinositides in cell architecture. Cold Spring Harb Perspect Biol. 3:1–17.
7. Toker A. 1998. The synthesis and cellular roles of phosphatidylinositol 4,5-bisphosphate. Curr Opin Cell Biol. 10:254–261.
8. Czech MP. 2000. PIP2 and PIP3. Cell 100:603–606.
9. Choi S, Thapa N, Tan X, Hedman AC, Anderson RA. 2015. PIP kinases define PI(4,5)P2 signaling specificity by association with effectors. Biochim Biophys Acta - Mol Cell Biol Lipids. 1851:711–723.
10. Martin TFJ. 2001. PI(4,5)P2 regulation of surface membrane traffic. Curr Opin Cell Biol. 13:493–499.
11. Di Paolo G, De Camilli P. 2006. Phosphoinositides in cell regulation and membrane dynamics. Nature. 443:651–657.
12. Balla T. 2013. Phosphoinositides: tiny lipids with giant impact on cell regulation. Physiol Rev. 93:1019–1137.
13. McLaughlin S, Wang J, Gambhir A, Murray D. 2002. PIP_2 and proteins: interactions, organization, and information flow. Annu Rev Biophys Biomol

Struct 31:151–175.

14. Sun Y, Thapa N, Hedman AC, Anderson RA. 2013. Phosphatidylinositol 4,5-bisphosphate: Targeted production and signaling. BioEssays. 35:513–522.
15. Carlton JG, Cullen PJ. 2005. Coincidence detection in phosphoinositide signaling. Trends Cell Biol. 15:540–547.
16. Rocha-Perugini V, Gordon-Alonso M, Sánchez-Madrid F. 2014. PIP2: Choreographer of actin-adaptor proteins in the HIV-1 dance. Trends Microbiol. 22:379–388.
17. Tan X, Thapa N, Choi S, Anderson RA. 2015. Emerging roles of PtdIns(4,5)P2 - beyond the plasma membrane. J Cell Sci. 128:4047–4056.
18. Doughman RL, Firestone AJ, Anderson RA. 2003. Phosphatidylinositol phosphate kinases put PI(4,5)P2 in its place. J Membr Biol. 194:77–89.
19. Hilgemann DW. 2007. Local PIP2 signals: When, where, and how? Pflugers Arch Eur J Physiol. 455:55–67.
20. Brown DA. 2015. PIP2 Clustering: From model membranes to cells. Chem Phys Lipids. 192:33–40.
21. Loew LM. 2007. Where does all the PIP2 come from? J Physiol. 582:945–951.
22. Kwiatkowska K. 2010. One lipid, multiple functions: How various pools of PI(4,5)P2 are created in the plasma membrane. Cell Mol Life Sci. 67:3927–3946.
23. Redfern DA, Gericke A. 2004. Domain formation in phosphatidylinositol monophosphate/phosphatidylcholine mixed vesicles. Biophys J. 86:2980–2992.
24. Jiang Z, Redfern RE, Isler Y, Ross AH, Gericke A. 2014. Cholesterol stabilizes fluid phosphoinositide domains. Chem Phys Lipids. 182:52–61.
25. Kooijman EE, Gericke A. 2014. Physical chemistry and biophysics of polyphosphoinositide mediated lipid signaling. Chem Phys Lipids. 182:1–2.
26. Graber ZT, Gericke A, Kooijman EE. 2014. Phosphatidylinositol-4,5-bisphosphate ionization in the presence of cholesterol, calcium or magnesium ions. Chem Phys Lipids. 182:62–72.
27. Graber ZT, Jiang Z, Gericke A, Kooijman EE. 2012. Phosphatidylinositol-4,5-

bisphosphate ionization and domain formation in the presence of lipids with hydrogen bond donor capabilities. Chem Phys Lipids. 165:696–704.

28. Kooijman EE, King KE, Gangoda M, Gericke A. 2009. Ionization properties of phosphatidylinositol polyphosphates in mixed model membranes. Biochemistry. 48:9360–9371.
29. Redfern DA, Gericke A. 2005. pH-dependent domain formation in phosphatidylinositol polyphosphate/phosphatidylcholine mixed vesicles. J Lipid Res. 46:504–515.
30. van Paridon PA, de Kruijff B, Ouwerkerk R, Wirtz KWA. 1986. Polyphosphoinositides undergo charge neutralization in the physiological pH range: a 31P-NMR study. Biochim Biophys Acta (BBA)/Lipids Lipid Metab. 877:216–219.
31. Toner M, Vaio G, McLaughlin A, McLaughlin S. 1988. Adsorption of cations to phosphatidylinositol 4,5-bisphosphate. Biochemistry. 27:7435–7443.
32. Moncelli MR, Becucci L, Guidelli R. 1994. The intrinsic pKa values for phosphatidylcholine, phosphatidylethanolamine, and phosphatidylserine in monolayers deposited on mercury electrodes. Biophys J. 66:1969–1980.
33. Tsui FC, Ojcius DM, Hubbell WL. 1986. The intrinsic pKa values for phosphatidylserine and phosphatidylethanolamine in phosphatidylcholine host bilayers. Biophys J. 49:459–468.
34. Levental I, Cebers A, Janmey PA. 2008. Combined electrostatics and hydrogen bonding determine PIP2 intermolecular interactions. J Am Chem Soc. 130:9025–9030.
35. Holub BJ, Kuksis A. 1971. Differential distribution of orthophosphate- 32 P and glycerol- 14 C among molecular species of phosphatidylinositols of rat liver in vivo. J Lipid Res. 12:699–705.
36. Traynor-Kaplan A, Kruse M, Dickson EJ, Dai G, Vivas O, Yu H, Whittington D, Hille B. 2017. Fatty-acyl chain profiles of cellular phosphoinositides. Biochim Biophys Acta - Mol Cell Biol Lipids. 1862:513–522.
37. Liu AP, Fletcher DA. 2006. Actin polymerization serves as a membrane

domain switch in model lipid bilayers. Biophys J. 91:4064–4070.

38. Tong J, Nguyen L, Vidal A, Simon SA, Skene JHP, McIntosh TJ. 2008. Role of GAP-43 in sequestering phosphatidylinositol 4,5-bisphosphate to raft bilayers. Biophys J. 94:125–133.
39. Brown DA. 2006. Lipid rafts, detergent-resistant membranes, and raft targeting signals. Physiology. 21:430–439.
40. Simons K, Sampaio JL. 2011. Membrane organization and lipid rafts. Cold Spring Harb Perspect Biol. 3:a004697–a004697.
41. Simons K, Ikonen E. 1997. Functional rafts in cell membranes. Nature. 387:569–572.
42. Hong Z, Staiculescu MC, Hampel P, Levitan I, Forgacs G. 2012. How cholesterol regulates endothelial biomechanics. Front Physiol. 3, 426.
43. Laux T, Fukami K, Thelen M, Golub T, Frey D, Caroni P. 2000. GAP43, MARCKS, and CAP23 modulate PI (4, 5) P2 at plasmalemmal rafts, and regulate cell cortex actin dynamics through a common mechanism. J Cell Biol. 149(7), 1455-1472.
44. Takenawa T, Itoh T. 2006. Membrane targeting and remodeling through phosphoinositide-binding domains. IUBMB Life. 58:296–303.
45. Lanier LM, Gertler FB. 2000. Actin cytoskeleton: Thinking globally, actin' locally. Curr Biol. 10:655–657.
46. Rozelle AL, Machesky LM, Yamamoto M, Driessens MHE, Insall RH, Roth MG, Luby-Phelps K, Marriott G, Hall A, Yin HL. 2000. Phosphatidylinositol 4,5-bisphosphate induces actin-based movement of raft-enriched vesicles through WASP-Arp2/3. Curr Biol. 10:311–320.
47. Hammond GR V. 2016. Does PtdIns(4,5)P2 concentrate so it can multi-task? Biochem Soc Trans. 44:228–233.
48. Johnson CM, Chichili GR, Rodgers W. 2008. Compartmentalization of phosphatidylinositol 4,5-bisphosphate signaling evidenced using targeted phosphatases. J Biol Chem. 283:29920–29928.
49. Falkenburger BH, Jensen JB, Dickson EJ, Suh BC, Hille B. 2010.

Phosphoinositides: Lipid regulators of membrane proteins. J Physiol. 588:3179–3185.

50. Hinchliffe K. 2000. Intracellular signalling: Is PIP2 a messenger too? Curr Biol. 10:104–105.
51. Berridge MJ, Irvine RF. 1984. Inositol triphosophate, a novel second messenger in cellular transduction. Nature. 312:315–321.
52. Stephens, L.R., Hughes, K.T. and Irvine, R.F., 1991. Pathway of phosphatidylinositol (3, 4, 5)-trisphosphate synthesis in activated neutrophils. Nature, 351:33-39.
53. Koch M, Holt M. 2012. Coupling exo- and endocytosis: An essential role for PIP2 at the synapse. Biochim Biophys Acta - Mol Cell Biol Lipids. 1821:1114–1132.
54. Martin TFJ. 2012. Phosphoinositides II: the diverse biological functions 59:111–130.
55. Simonsen A, Wurmser AE, Emr SD, Stenmark H. 2001. The role of phosphoinositides in membrane transport. Curr Opin Cell Biol 13:485–492.
56. Jost M, Simpson F, Kavran JM, Lemmon MA, Schmid SL. 1998. Phosphatidylinositol-4,5-bisphosphate is required for endocytic coated vesicle formation. Curr Biol. 8:1399–1404.
57. Zoncu R, Perera RM, Sebastian R, Nakatsu F, Chen H, Balla T, Ayala G, Toomre D, De Camilli P V. 2007. Loss of endocytic clathrin-coated pits upon acute depletion of phosphatidylinositol 4,5-bisphosphate. Proc Natl Acad Sci. 104:3793–3798.
58. Hilgemann DW, Feng S, Nasuhoglu C. 2003. the complex and intriguing lives of PIP2 with ion channels and transporters. Sci Signal 2001:re19-re19.
59. Suh BC, Hille B. 2005. Regulation of ion channels by phosphatidylinositol 4,5-bisphosphate. Curr Opin Neurobiol. 15:370–378.
60. Robertson B. 2007. Regulation of ion channels and transporters by phosphatidylinositol 4,5-bisphosphate. J Physiol. 582:901–902.
61. Bucki R, Wang Y-H, Yang C, Kandy SK, Fatunmbi O, Bradley R, Pogoda K,

Svitkina T, Radhakrishnan R, Janmey PA. 2019. Lateral distribution of phosphatidylinositol 4,5-bisphosphate in membranes regulates formin and ARP2/3 -mediated actin nucleation. J Biol Chem. 294:4704-4722.

62. Fukami K, Furuhashit K, Inagakit M. 1992. Requirement of phosphatidylinositol 4 , S . bisphosphate for a-actinin function 359:150–152.
63. Saarikangas J, Zhao H, Lappalainen P. 2010. Regulation of the actin cytoskeleton-plasma membrane interplay by phosphoinositides. Physiol Rev. 90:259–289.
64. Yin HL, Janmey PA. 2003. Phosphoinositide regulation of the actin cytoskeleton. Annu Rev Physiol. 65:761–789.
65. Janmey PA, Stossel TP. 1987. Modulation of gelsolin function by phosphatidylinositol 4,5-bisphosphate. Nature. 325:362–364.
66. Cullen PJ, Cozier GE, Banting G, Mellor H. 2001. Modular phosphoinositide-binding domains - Their role in signalling and membrane trafficking. Curr Biol. 11:882–893.
67. James DJ, Khodthong C, Kowalchyk JA, Martin TFJ. 2008. Phosphatidylinositol 4,5-bisphosphate regulates SNARE-dependent membrane fusion. J Cell Biol. 182:355–366.
68. Mani T, Hennigan RF, Foster LA, Conrady DG, Herr AB, Ip W. 2011. FERM domain phosphoinositide binding targets merlin to the membrane and is essential for its growth-suppressive function. Mol Cell Biol. 31:1983–1996.
69. Krahn MP, Wodarz A. 2012. Phosphoinositide lipids and cell polarity: linking the plasma membrane to the cytocortex. Essays Biochem. 53:15–27.
70. Meyer T, Wells A, Teruel M, Grinstein S, Anderson R, York JD, Botelho RJ, Dierckman R, Teruel M, Dierckman R, Anderson R, Wells A, York JD, Meyer T, Grinstein S. 2002. Localized biphasic changes in phosphatidylinositol-4,5-bisphosphate at sites of phagocytosis. J Cell Biol. 151:1353–1368.
71. Scott CC, Dobson W, Botelho RJ, Coady-Osberg N, Chavrier P, Knecht DA, Heath C, Stahl P, Grinstein S. 2005. Phosphatidylinositol-4, 5-bisphosphate hydrolysis directs actin remodeling during phagocytosis. J Cell Biol. 169:139–

149.

72. Schill NJ, Sun Y, Anderson RA, Wagoner MP, Ling K. 2006. Movin' on up: the role of PtdIns(4,5)P2 in cell migration. Trends Cell Biol. 16:276–284.
73. Skwarek LC, Boulianne GL. 2009. Great expectations for PIP: phosphoinositides as regulators of signaling during development and disease. Dev Cell. 16:12–20.
74. Liu Y, Bankaitis VA. 2010. Phosphoinositide phosphatases in cell biology and disease. Prog Lipid Res. 49:201–217.
75. Pendaries C, Tronchère H, Plantavid M, Payrastre B. 2003. Phosphoinositide signaling disorders in human diseases. FEBS Lett. 546:25–31.
76. Waugh MG. 2015. PIPs in neurological diseases. Biochim Biophys Acta - Mol Cell Biol Lipids. 1851:1066–1082.
77. Catimel B, Schieber C, Condron M, Patsiouras H, Connolly L, Catimel J, Nice EC, Burgess AW, Holmes AB. 2008. The PI(3,5)P2 and PI(4,5)P2 Interactomes research articles. J Proteome Res. 7:5295–5313.
78. Rohatgi R, Ho HH, Kirschner MW. 2010. Mechanism of N-WASP activation by CDC42 and phosphatidylinositol. Cell. 150:1299–1309.
79. Rebecchi MJ, Scarlata S. 1998. Pleckstrin homology domains: a common fold with diverse functions. Annu Rev Biophys Biomol Struct. 27:503–28.
80. Harlan JE, Hajduk PJ, Yoon HS, Fesik SW. 1994. Pleckstrin homology domains bind to PIP2. Nature. 371:168-170.
81. Lemmon MA. 2008. Membrane recognition by phospholipid-binding domains. Nat Rev Mol Cell Biol. 9:99–111.
82. Klopfenstein DR, Tomishige M, Stuurman N, Vale RD. 2002. Role of Phosphatidylinositol(4,5)bisphosphate organization in membrane transport by the Unc104 kinesin motor. Cell. 109:347-358.
83. Lemmon MA. 2003. Phosphoinositide recognition domains. Traffic. 4:201-213.
84. Ferguson KM, Lemmon MA, Schlessinger J, Sigler PB. 1995. Structure of the high affinity complex of inositol trisphosphate with a phospholipase C pleckstrin homology domain. Proc Natl Acad Sci. 92:10472-10476.

85. Wilmanns M, Nilges M, Oschkinat H, Saraste M, Macias MJ, Hyvönen M. 2018. Structure of the binding site for inositol phosphates in a PH domain. EMBO J. 14:4676–4685.
86. Jian X, Tang W-K, Zhai P, Roy NS, Luo R, Gruschus JM, Yohe ME, Chen P-W, Li Y, Byrd RA, Xia D, Randazzo PA. 2015. Molecular basis for cooperative binding of anionic phospholipids to the PH Domain of the Arf GAP ASAP1. Structure. 23:1977–1988.
87. Yamamoto E, Kalli AC, Yasuoka K, Sansom MSP. 2016. Interactions of pleckstrin homology domains with membranes: adding back the bilayer via high-throughput molecular dynamics. Structure. 24:1421–1431.
88. Szentpetery Z, Balla A, Kim YJ, Lemmon MA, Balla T. 2009. Live cell imaging with protein domains capable of recognizing phosphatidylinositol 4,5-bisphosphate; a comparative study. BMC Cell Biol. 10:67.
89. Várnai P, Balla T. 1998. Visualization of phosphoinositides that bind pleckstrin homology domains: Calcium- and agonist-induced dynamic changes and relationship to myo-[3H]inositol-labeled phosphoinositide pools. J Cell Biol. 143:501–510.
90. Balla T, Varnai P. 2003. Visualizing Cellular Phosphoinositide Pools with GFP-Fused Protein-Modules. Sci Signal. 2002:pl3-pl3.
91. Watt SA, Kular G, Fleming IN, Downes CP, Lucocq JM. 2002. Subcellular localization of phosphatidylinositol 4,5-bisphosphate using the pleckstrin homology domain of phospholipase C δ1. Biochem J. 363:657–666.
92. Garcia P, Gupta R, Shah S, Morris AJ, Rudge SA, Scarlata S, Petrova V, McLaughlin S, Rebecchi MJ. 1995. The pleckstrin homology domain of phospholipase C-.delta.1 binds with high affinity to phosphatidylinositol 4,5-bisphosphate in bilayer membranes. Biochemistry. 34:16228–16234.
93. Lemmon MA, Fergusonti KM, O'brient R, Sigler PB, Schlessinger J. 1995. Specific and high-affinity binding of inositol phosphates to an isolated pleckstrin homology domai. Biochemistry. 92:10472–10476.
94. Lemmon MA, Ferguson KM. 2000. Signal-dependent membrane targeting by

pleckstrin homology (PH) domains. Biochem J. 350:1-18.

95. Niggli V, Andréoli C, Roy C, Mangeat P. 1995. Identification of a phosphatidylinositol-4,5-bisphosphate-binding domain in the N-terminal region of ezrin. FEBS Lett. 376:172–176.
96. Tsukita S, Yonemura S. 1999. Cortical actin organization : lessons from ERM. J Biol Chem. 274:34507–34510.
97. Chishti A, Kim A, Hoover KB. 1998. The FERM domain : a unique module involved in. Trends in Biochem Sci. 23:281-282.
98. Frame MC, Patel H, Serrels B, Lietha D, Eck MJ. 2010. The FERM domain: Organizing the structure and function of FAK. Nat Rev Mol Cell Biol. 11:802–814.
99. Fehon RG, McClatchey AI, Bretscher A. 2010. Organizing the cell cortex: The role of ERM proteins. Nat Rev Mol Cell Biol. 11:276–287.
100. Hamada K. 2002. Structural basis of the membrane-targeting and unmasking mechanisms of the radixin FERM domain. EMBO J. 19:4449–4462.
101. Legendre-Guillemin V. 2003. ENTH/ANTH proteins and clathrin-mediated membrane budding. J Cell Sci. 117:9–18.
102. Itoh T, Koshiba S, Kigawa T, Kikuchi A, Yokoyama S, Takenawa T. 2001. Role of the ENTH domain in phosphatidylinositol-4,5-bisphosphate binding and endocytosis. Science. 291(5506), 1047-1051.
103. Czech MP, Xu W, Song X, Zhang A, Zhou GW, Huang G, Virbasius J V., Liang X. 2002. Phox homology domains specifically bind phosphatidylinositol phosphates. Biochemistry. 40:8940–8944.
104. Arbuzova A, Murray D, McLaughlin S. 1998. MARCKS, membranes, and calmodulin: Kinetics of their interaction. Biochim Biophys Acta - Rev Biomembr. 1376:369–379.
105. Wang J, Arbuzova A, Hangyas-Mihalyne G, McLaughlin S. 2001. The effector domain of myristoylated alanine-rich C kinase substrate binds strongly to phosphatidylinositol 4,5-bisphosphate. J Biol Chem. 276:5012–5019.
106. Golebiewska U, Gambhir A, Hangyás-Mihályné G, Zaitseva I, Rädler J,

McLaughlin S. 2006. Membrane-bound basic peptides sequester multivalent (PIP2), but not monovalent (PS), acidic lipids. Biophys J. 91:588–599.

107. Wang J, Gambhir A, Hangyás-Mihályné G, Murray D, Golebiewska U, McLaughlin S. 2002. Lateral sequestration of phosphatidylinositol 4,5-bisphosphate by the basic effector domain of myristoylated alanine-rich C kinase substrate is due to nonspecific electrostatic interactions. J Biol Chem. 277:34401–34412.
108. Gambhir A, Hangyas-Mihalyne G, Zaitseva I, Cafiso DS, Wang J, Murray D, Pentyala SN, Smith SO, McLaughlin S, Gambhir A, Pentyala SN, Smith SO, McLaughlin S. 2004. Electrostatic sequestration of PIP2 on phospholipid membranes by basic/aromatic regions of proteins. Biophys J. 86:2188–2207.
109. Rauch ME, Ferguson CG, Prestwich GD, Cafiso DS. 2002. Myristoylated alanine-rich C kinase substrate (MARCKS) sequesters spin-labeled phosphatidylinositol 4,5-bisphosphate in lipid bilayers. J Biol Chem. 277:14068–14076.
110. Denisov G, Wanaski S, Luan P, Glaser M, McLaughlin S. 1998. Binding of basic peptides to membranes produces lateral domains enriched in the acidic lipids phosphatidylserine and phosphatidylinositol 4,5- bisphosphate: An electrostatic model and experimental results. Biophys J. 74:731–744.
111. Laux T, Fukami K, Thelen M, Golub T, Frey D, Caroni P. 2000. GAP43, MARCKS, and CAP23 Modulate PI(4,5)P2 at plasmalemmal rafts, and regulate cell cortex actin dynamics through a common mechanism. J Cell Biol. 149:1455–1472.
112. Arni S, Keilbaugh SA, Ostermeyer AG, Brown DA. 1998. Association of GAP-43 with detergent-resistant membranes requires two palmitoylated cysteine residues. J Biol Chem. 273:28478–28485.
113. Matlin KS, Reggio H, Helenius A, Simons K. 1982. Pathway of vesicular stomatitis virus entry leading to infection. J Mol Biol. 156:609–631.
114. Cossart P, Helenius A. 2014. Endocytosis of viruses and bacteria. Cold Spring Harb Perspect Biol. 6:a016972.

115. Sun E, He J, Zhuang X. 2013. Live cell imaging of viral entry. Curr Opin Virol. 3:34–43.
116. DeTulleo L. 2002. The clathrin endocytic pathway in viral infection. EMBO J. 17:4585–4593.
117. Lakadamyali M, Rust MJ, Zhuang X. 2004. Endocytosis of influenza viruses. Microbes Infect. 6:929–936.
118. Blanchard E, Belouzard S, Goueslain L, Wychowski C, Dubuisson J, Wakita T, Rouille Y. 2006. Hepatitis C virus entry depends on clathrin-mediated endocytosis. J Virol. 80:6964–6972.
119. Vázquez-Calvo Á, Sobrino F, Martín-Acebes MA. 2012. Plasma membrane phosphatidylinositol 4,5 bisphosphate is required for internalization of foot-and-mouth disease virus and vesicular stomatitis virus. PLoS One. 7:e45172.
120. Barrero-Villar M, Barroso-Gonzalez J, Cabrero JR, Gordon-Alonso M, Alvarez-Losada S, Munoz-Fernandez MA, Sanchez-Madrid F, Valenzuela-Fernandez A. 2008. PI4P5-Kinase I is required for efficient hiv-1 entry and infection of T cells. J Immunol. 181:6882–6888.
121. Egger D, Bienz K, Gosert R, Moradpour D, Bianchi L, Wolk B, Blum HE. 2002. Expression of Hepatitis C virus proteins induces distinct membrane alterations including a candidate viral replication complex. J Virol. 76:5974–5984.
122. Harboring H-C, Replicons S, Gosert R, Egger D, Lohmann V, Bartenschlager R, Blum HE, Bienz K, Moradpour D. 2003. Identification of the Hepatitis C virus RNA replication complex in. J Virol. 77:5487–5492.
123. Winters M, Sklan EH, Staschke K, Aroeti B, Oakes TM, Elazar M, Danieli T, Glenn JS. 2007. A Rab-GAP TBC domain protein binds Hepatitis C virus NS5A and mediates viral replication. J Virol. 81:11096–11105.
124. Pfeffer SR, Sklan EH, Lambright DG, Serrano RL, Einav S, Glenn JS. 2007. TBC1D20 Is a Rab1 GTPase-activating protein that mediates Hepatitis C virus replication. J Biol Chem. 282:36354–36361.
125. Waheed AA, Freed EO. 2018. the role of lipids in retroviral replication.

retrovirus-cell interactions. Elsevier Inc. (pp. 353-399). Academic Press.

126. Ono A, Ablan SD, Lockett SJ, Nagashima K, Freed EO. 2004. Phosphatidylinositol (4,5) bisphosphate regulates HIV-1 Gag targeting to the plasma membrane. Proc Natl Acad Sci. 101:14889–14894.
127. Chukkapalli V, Hogue IB, Boyko V, Hu W-S, Ono A, Hogue IB, Chukkapalli V, Hu W-S, Boyko V, Hogue IB, Boyko V, Hu W-S, Ono A. 2007. Interaction between the human immunodeficiency virus type 1 Gag Matrix domain and phosphatidylinositol-(4,5)-bisphosphate is essential for efficient Gag membrane binding. J Virol. 82:2405–2417.
128. Mücksch F, Laketa V, Müller B, Schultz C, Kräusslich H-G. 2017. Synchronized HIV assembly by tunable PIP2 changes reveals PIP2 requirement for stable Gag anchoring. Elife. 6:e25287.
129. Dick RA, Goh SL, Feigenson GW, Vogt VM. 2012. HIV-1 Gag protein can sense the cholesterol and acyl chain environment in model membranes. Proc Natl Acad Sci. 109:18761–18766.
130. Olety B, Ono A. 2014. Roles played by acidic lipids in HIV-1 Gag membrane binding. Virus Res. 193:108–115.
131. Mercredi PY, Bucca N, Loeliger B, Gaines CR, Mehta M, Bhargava P, Tedbury PR, Charlier L, Floquet N, Muriaux D, Favard C, Sanders CR, Freed EO, Marchant J, Summers MF. 2016. Structural and molecular determinants of membrane binding by the HIV-1 Matrix protein. J Mol Biol. 428:1637–1655.
132. Hamard-Peron E, Juillard F, Saad JS, Roy C, Roingeard P, Summers MF, Darlix J-L, Picart C, Muriaux D. 2010. Targeting of murine leukemia virus Gag to the plasma membrane is mediated by PI(4,5)P2/PS and a polybasic region in the matrix. J Virol. 84:503–515.
133. Inlora J, Collins DR, Trubin ME, Chung JYJ, Ono A. 2014. Membrane binding and subcellular localization of retroviral Gag proteins are differentially regulated by MA interactions with phosphatidylinositol-(4,5)-bisphosphate and RNA. MBio. 5:1–13.
134. Shkriabai N, Datta SAK, Zhao Z, Hess S, Rein A, Kvaratskhelia M. 2006.

Interactions of HIV-1 Gag with assembly cofactors. Biochemistry. 45:4077–4083.

135. Saad JS, Miller J, Tai J, Kim A, Ghanam RH, Summers MF. 2006. Structural basis for targeting HIV-1 Gag proteins to the plasma membrane for virus assembly. Proc Natl Acad Sci. 103:11364–11369.
136. Chan R, Uchil PD, Jin J, Shui G, Ott DE, Mothes W, Wenk MR. 2008. Retroviruses human immunodeficiency virus and murine leukemia virus are enriched in phosphoinositides. J Virol. 82:11228–11238.
137. Brugger B, Glass B, Haberkant P, Leibrecht I, Wieland FT, Krausslich H-G. 2006. The HIV lipidome: A raft with an unusual composition. Proc Natl Acad Sci. 103:2641–2646.
138. Lorizate M, Sachsenheimer T, Glass B, Habermann A, Gerl MJ, Kräusslich H-G, Brügger B. 2013. Comparative lipidomics analysis of HIV-1 particles and their producer cell membrane in different cell lines. Cell Microbiol. 15:292–304.
139. Lorizate M, Brügger B, Akiyama H, Glass B, Müller B, Anderluh G, Wieland FT, Kräusslich H-G. 2009. Probing HIV-1 membrane liquid order by laurdan staining reveals producer cell-dependent differences. J Biol Chem. 284:22238–22247.
140. Gordon, L. M., Jensen, F. C., Curtain, C. C., Mobley, P. W., & Aloia, R. C. (1988). Thermotropic lipid phase separation in the human immunodeficiency virus. Biochimica et Biophysica Acta (BBA)-Biomembranes, 943(2), 331-342.
141. Stansell E, Apkarian R, Haubova S, Diehl WE, Tytler EM, Hunter E. 2007. Basic residues in the Mason-Pfizer monkey virus Gag matrix domain regulate intracellular trafficking and capsid-membrane interactions. J Virol. 81:8977–8988.
142. Inlora J, Chukkapalli V, Derse D, Ono A. 2011. Gag localization and virus-like particle release mediated by the matrix domain of human T-lymphotropic virus type 1 Gag are less dependent on phosphatidylinositol-(4,5)-bisphosphate than those mediated by the matrix domain of HIV-1 Gag. J Virol. 85:3802–3810.

143. Chan J, Dick RA, Vogt VM. 2011. Rous sarcoma virus gag has no specific requirement for phosphatidylinositol-(4,5)-bisphosphate for plasma membrane association in vivo or for liposome interaction in vitro. J Virol. 85:10851–10860.
144. Johnson KA, Taghon GJF, Scott JL, Stahelin R V. 2016. The Ebola Virus matrix protein, VP40, requires phosphatidylinositol 4,5-bisphosphate (PI(4,5)P 2) for extensive oligomerization at the plasma membrane and viral egress. Sci Rep. 6:1–14.
145. Wijesinghe KJ, Stahelin R V. 2015. Investigation of the lipid binding properties of the Marburg virus matrix protein VP40. J Virol. 90:3074–3085.
146. Wallace J, Mlodzianoski MJ, Maginnis MS, Lilieholm J, Mehmood K, Busse B, Curthoys NM, Parent M, Waters H, Butler MB, Zimmerberg J, Raut P, Hess ST. 2019. Influenza hemagglutinin modulates , phosphatidylinositol (4,5) bisphosphate membrane clustering. Biophys J. 116:893–909.
147. Alvarez RA, Barría MI, Chen BK. 2014. unique features of HIV-1 spread through t cell virological synapses. PLoS Pathog. 10:e1004513.
148. Clapham PR, Weiss RA. 1997. Spoilt for choice of co-receptors. Nature. 388:230–231.
149. Jolly C, Kashefi K, Hollinshead M, Sattentau QJ. 2004. HIV-1 cell to cell transfer across an Env-induced, actin-dependent synapse. J Exp Med. 199:283–293.
150. Hirai M, Takizawa T, Yabuki S, Hirai T, Hayashi K. 1995. Thermotropic phase transition of phosphatidylinositol 4,5-bisphosphate aggregates in aqueous solution. J Phys Chem. 99:17456–17460.
151. Hendrickson, H.S., 1970. Physical properties and interactions of phosphoinositides. Annu NY Acad Sci, 165:668-676.
152. Hirai M, Takizawa T, Yabuki S, Nakata Y, Hirai T, Hayashi K. 1996. Salt-dependent phase behaviour of the phosphatidylinositol 4,5-diphosphate-water system. J Chem Soc - Faraday Trans. 92:1493–1498.
153. Bhairi SM, Mohan C. 2001. A Guide to the properties and uses of detergents in

biology and biochemistry. Calbiochem-Novabiochem Corporation. 1-41.

154. Moens PDJ, Bagatolli LA. 2007. Profilin binding to sub-micellar concentrations of phosphatidylinositol (4,5) bisphosphate and phosphatidylinositol (3,4,5) trisphosphate. Biochim Biophys Acta – Biomembr. 1768:439–449.

155. Huang F, Huang K. 1991. Interaction of protein kinase c isozymes with phosphatidylinositol 4,5-bisphosphate. J Biol Chem. 40:4437–4445.

156. Lee E-NN, Lee S-YY, Lee D, Kim J, Paik SR. 2003. Lipid interaction of α-synuclein during the metal-catalyzed oxidation in the presence of Cu^{2+} and H2O2. J Neurochem. 84:1128–1142.

157. Palmer FB. 1981. The phosphatidyl-myo-inositol-4,5-biphosphate phosphatase from Crithidia fasciculata. Can J Biochem. 59:469–76.

158. Sugiura Y. 1981. Structure of molecular aggregates of 1-(3-sn-phosphatidyl)-l-myo-inositol 3,4-bis(phosphate) in water. BBA - Biomembr 641:148–159.

159. Stewart Hendrickson H, Reinertsen JL. 1969. Comparison of metal-binding properties of trans-1,2-cyclohexanediol diphosphate and deacylated phosphoinositides. Biochemistry. 8:4855–4858.

160. Janmey, P.A. and Stossel, T.P. 1989. Gelsolin-polyphosphoinositide interaction. J Biol Chem. 264:4825-4831.

161. Liepiņa I, Czaplewski C, Janmey P, Liwo A. 2003. Molecular dynamics study of a gelsolin-derived peptide binding to a lipid bilayer containing phosphatidylinositol 4,5-bisphosphate. Biopolym - Pept Sci Sect. 71:49–70.

162. Jammey PA, Iida K, Yin HL, Stossel TP. 1987. Polyphosphoinositide micelles and polyphosphoinositide-containing vesicles dissociate endogenous gelsolin-actin complexes and promote actin assembly from the fast-growing end of actin filaments blocked by gelsolin. J Biol Chem. 262:12228–12236.

163. Flanagan LA, Cunningham CC, Chen J, Prestwich GD, Kosik KS, Janmey PA. 1997. The structure of divalent cation-induced aggregates of PIP2 and their alteration by gelsolin and tau. Biophys J. 73:1440–1447.

164. Fujita A, Cheng J, Tauchi-Sato K, Takenawa T, Fujimoto T. 2009. A distinct pool of phosphatidylinositol 4,5-bisphosphate in caveolae revealed by a

nanoscale labeling technique. Proc Natl Acad Sci. 106:9256–9261.

165. Wang J, Richards DA. 2012. Segregation of PIP2 and PIP3 into distinct nanoscale regions within the plasma membrane. Biol Open. 1:857–862.

166. Van Den Bogaart G, Meyenberg K, Risselada HJ, Amin H, Willig KI, Hubrich BE, Dier M, Hell SW, Grubmüller H, Diederichsen U, Jahn R. 2011. Membrane protein sequestering by ionic protein-lipid interactions. Nature. 479:552–555.

167. Carvalho K, Ramos L, Roy C, Picart C. 2008. Giant unilamellar vesicles containing phosphatidylinositol(4,5) bisphosphate: Characterization and functionality. Biophys J. 95:4348–4360.

168. Honigmann A, Van Den Bogaart G, Iraheta E, Risselada HJ, Milovanovic D, Mueller V, Müllar S, Diederichsen U, Fasshauer D, Grubmüller H, Hell SW, Eggeling C, Kühnel K, Jahn R. 2013. Phosphatidylinositol 4,5-bisphosphate clusters act as molecular beacons for vesicle recruitment. Nat Struct Mol Biol. 20:679–686.

169. Myat MM, Anderson S, Allen L-AH, Aderem A. 2004. MARCKS regulates membrane ruffling and cell spreading. Curr Biol. 7:611–614.

170. Allen LH. 1995. A role for MARCKS, the alpha isozyme of protein kinase C and myosin I in zymosan phagocytosis by macrophages. J Exp Med. 182:829-840.

171. Tall EG, Spector I, Pentyala SN, Bitter I, Rebecchi MJ. 2000. Dynamics of phosphatidylinositol 4,5-bisphosphate in actin-rich structures. Curr Biol. 10:743-746.

172. Van Rheenen J, Achame EM, Janssen H, Calafat J, Jalink K. 2005. PIP2 signaling in lipid domains: A critical re-evaluation. EMBO J. 24:1664-1673.

173. Rheenen J van, Jalink K. 2002. Agonist-induced PIP2 hydrolysis inhibits cortical actin dynamics: regulation at a global but not at a micrometer scale. Mol Biol Cell. 13:3257-3267.

174. Sheetz MP, Sable JE, Döbereiner H-G. 2006. Continuous membrane-cytoskeleton adhesion requires continuous accommodation to lipid and cytoskeleton dynamics. Annu Rev Biophys Biomol Struct. 35:417-434.

175. Lang T, Bruns D, Wenzel D, Riedel D, Holroyd P, Thiele C, Jahn R. 2001. SNAREs are concentrated in cholesterol-dependent clusters that define docking and fusion sites for exocytosis. EMBO J. 20:2202-2213.
176. Martin TFJ. 2015. PI(4,5)P2-binding effector proteins for vesicle exocytosis. Biochim Biophys Acta - Mol Cell Biol Lipids. 1851:785-793.
177. Milovanovic D, Platen M, Junius M, Diederichsen U, Schaap IATT, Honigmann A, Jahn R, van den Bogaart G, Milovanovic D, Platen M, Jahn R, Junius M, Diederichsen U, van den Bogaart G. 2016. Calcium promotes the formation of Syntaxin 1 mesoscale domains through phosphatidylinositol 4,5-bisphosphate. J Biol Chem. 291:7868-7876.
178. Loijens JC, Boronenkov I V., Parker GJ, Anderson RA. 1996. The phosphatidylinositol 4-phosphate 5-kinase family. Adv Enzyme Regul. 36:115-140.
179. van den Bout I, Divecha N. 2009. PIP5K-driven PtdIns(4,5)P2 synthesis: regulation and cellular functions. J Cell Sci. 122:3837-3850.
180. Coppolino MG, Dierckman R, Loijens J, Collins RF, Pouladi M, Jongstra-Bilen J, Schreiber AD, Trimble WS, Anderson R, Grinstein S. 2002. Inhibition of phosphatidylinositol-4-phosphate 5-kinase Iα impairs localized actin remodeling and suppresses phagocytosis. J Biol Chem. 277:43849-43857.
181. Wen Y, Vogt VM, Feigenson GW. 2018. Multivalent cation-bridged PI(4,5)P2 clusters form at very low concentrations. Biophys J. 114:2630-2639.
182. Slochower DR, Wang YH, Tourdot RW, Radhakrishnan R, Janmey PA. 2014. Counterion-mediated pattern formation in membranes containing anionic lipids. Adv Colloid Interface Sci. 208:177-188.
183. Wang YH, Slochower DR, Janmey PA. 2014. Counterion-mediated cluster formation by polyphosphoinositides. Chem Phys Lipids. 182:38-51.
184. Graber ZT, Wang W, Singh G, Kuzmenko I, Vaknin D, Kooijman EE. 2015. Competitive cation binding to phosphatidylinositol-4,5-bisphosphate domains revealed by X-ray fluorescence. RSC Adv. 5:106536-106542.
185. Slochower DR, Huwe PJ, Radhakrishnan R, Janmey PA. 2013. Quantum and

all-atom molecular dynamics simulations of protonation and divalent ion binding to phosphatidylinositol 4,5-bisphosphate (PIP2). J Phys Chem B. 117:8322-8329.

186. Ellenbroek WG, Wang YH, Christian DA, Discher DE, Janmey PA, Liu AJ. 2011. Divalent cation-dependent formation of electrostatic PIP2 clusters in lipid monolayers. Biophys J. 101:2178-2184.
187. Hendrickson H, Ballou C. 1964. Ion exchange chromatography of intact brain phosphoinositides on diethylaminoethyl cellulose by gradient salt elution in a mixed solvent system. J Biol Chem. 239:1369-1373.
188. Hendrickson HS, Fullington JG. 1965. Stabilities of metal complexes of phospholipids: Ca(II), Mg(II), and Ni(II) complexes of phosphatidylserine and triphosphoinositide. Biochemistry. 4:1599-1605.
189. Fullisgton JG, Hendrickson HS, Division D. 1966. Phospholipid-metal complexes. 4098-4101.
190. Hauser H, Dawson RMC. 1967. The binding of calcium at lipid-water interfaces. Eur J Biochem. 1:61-69.
191. Buckley JT, Hawthorne JN. 1972. Erythrocyte membrane polyphosphoinositide metabolism and the regulation of calcium binding. J Biol Chem. 247:7218-7223.
192. Levental I, Christian DA, Wang Y-H, Madara JJ, Discher DE, Janmey PA. 2009. Calcium-dependent lateral organization in phosphatidylinositol 4,5-bisphosphate (PIP2)- and Cholesterol-containing monolayers. Biochemistry. 48:8241-8248.
193. Wang YH, Collins A, Guo L, Smith-Dupont KB, Gai F, Svitkina T, Janmey PA. 2012. Divalent cation-induced cluster formation by polyphosphoinositides in model membranes. J Am Chem Soc. 134:3387-3395.
194. Sarmento MJ, Coutinho A, Fedorov A, Prieto M, Fernandes F. 2014. Ca^{2+} induces PI(4,5)P2 clusters on lipid bilayers at physiological PI(4,5)P2and Ca^{2+}concentrations. Biochim Biophys Acta - Biomembr. 1838:822-830.
195. Lagerholm BC, Weinreb GE, Jacobson K, Thompson NL. 2004. Detecting

microdomains in intact cell membranes. Annu Rev Phys Chem. 56:309-336.

196. Golebiewska U, Nyako M, Woturski W, Zaitseva I, McLaughlin S. 2008. Diffusion coefficient of fluorescent phosphatidylinositol 4,5-bisphosphate in the plasma membrane of cells. Mol Biol Cell. 19:1663-1669.
197. Sarmento MJ, Coutinho A, Fedorov A, Prieto M, Fernandes F. 2017. Membrane order is a key regulator of divalent cation-induced clustering of PI(3,5)P2 and PI(4,5)P2. Langmuir. 33:12463-12477.
198. Sternweis PC. 1982. Aluminum: a requirement for activation of the regulatory component of adenylate cyclase by fluoride. Proc Natl Acad Sci. 79:4888-4891.
199. Rodushkin I, Engström E, Baxter DC. 2010. Sources of contamination and remedial strategies in the multi-elemental trace analysis laboratory. Anal Bioanal Chem. 396:365-377.
200. Suh B-C, Hille B. 2007. Electrostatic interaction of internal Mg^{2+} with membrane PIP_2 Seen with KCNQ K^+ channels. J Gen Physiol. 130:241-256.
201. Seo JB, Jung SR, Huang W, Zhang Q, Koh DS. 2015. Charge shielding of PIP2 by cations regulates enzyme activity of phospholipase C. PLoS One. 10:1-22.
202. Bilkova E, Pleskot R, Rissanen S, Sun S, Czogalla A, Cwiklik L, Róg T, Vattulainen I, Cremer PS, Jungwirth P, Coskun Ü. 2017. Calcium directly regulates phosphatidylinositol 4,5-bisphosphate headgroup conformation and recognition. J Am Chem Soc. 139:4019-4024.
203. Papayannopoulos V, Co C, Prehoda KE, Snapper S, Taunton J, Lim WA. 2005. A polybasic motif allows N-WASP to act as a sensor of PIP2 density. Mol Cell. 17:181-191.
204. Lappalainen P, Koskela EV V., Tkach V, Drubin DGG, Michelot A, Stamou D, Zhao H, Michelot A, Koskela EV V., Tkach V, Stamou D, Drubin DGG, Lappalainen P. 2013. Membrane-sculpting BARd Generate stable lipid microdomains. Cell Rep 4:1213-1223.
205. Saarikangas J, Zhao H, Pykäläinen A, Laurinmäki P, Mattila PK, Kinnunen PKJ, Butcher SJ, Lappalainen P. 2009. Molecular mechanisms of membrane deformation by I-BAR domain proteins. Curr Biol. 19:95-107.

206. Liu J, Sun Y, Drubin DG, Oster GF. 2009. The mechanochemistry of endocytosis. PLoS Biol. 7: e1000204.
207. Picas L, Viaud J, Schauer K, Vanni S, Hnia K, Fraisier V, Roux A, Bassereau P, Gaits-Iacovoni F, Payrastre B, Laporte J, Manneville JB, Goud B. 2014. BIN1/M-Amphiphysin2 induces clustering of phosphoinositides to recruit its downstream partner dynamin. Nat Commun. 5, 5647.
208. Stanishneva-Konovalova TB, Derkacheva NI, Polevova S V., Sokolova OS. 2016. The role of BAR domain proteins in the regulation of membrane dynamics. Acta Naturae. 8:60-69.
209. Zheng J, Cahill SM, Lemmon MA, Fushman D, Schlessinger J, Cowburn D. 1996. Identification of the binding site for acidic phospholipids on the PH domain of dynamin: Implications for stimulation of GTPase activity. J Mol Biol. 255:14-21.
210. Bethoney KA, King MC, Lemmon MA, Ostap EM, Hinshaw JE. 2009. A possible effector role for the pleckstrin homology (PH) domain of dynamin. Proc Natl Acad Sci. 106:13359-13364.
211. Lemmon MA, Frank DW, Lee A, Klein DE, Marks MS. 2002. The pleckstrin homology domains of dynamin isoforms require oligomerization for high affinity phosphoinositide binding. J Biol Chem. 273:27725-27733.
212. Que EL, Bleher R, Duncan FE, Kong BY, Gleber SC, Vogt S, Chen S, Garwin SA, Bayer AR, Dravid VP, Woodruff TK, O'Halloran T V. 2015. Quantitative mapping of zinc fluxes in the mammalian egg reveals the origin of fertilization-induced zinc sparks. Nat Chem. 7:130-139.

CHAPTER 3

EFFECTS OF MEMBRANE CHARGE AND ORDER ON MEMBRANE BINDING OF THE RETROVIRAL STRUCTURAL PROTEIN GAG[2]

ABSTRACT

The retroviral structural protein Gag binds to the inner leaflet of the plasma membrane (PM), and many cellular proteins do so as well. We used Rous sarcoma virus (RSV) Gag together with membrane sensors to study the principles governing peripheral protein membrane binding, including electrostatics, specific recognition of phospholipid headgroups, sensitivity to phospholipid acyl chain compositions, preference for membrane order, and protein multimerization. We used an in vitro liposome-pelleting assay to test protein membrane binding properties of Gag, the well-characterized MARCKS peptide, a series of fluorescent electrostatic sensor proteins (mNG-KRn), and the specific phosphatidylserine (PS) binding protein Evectin2. RSV Gag and mNG-KRn bound well to membranes with saturated and unsaturated acyl chains, whereas the MARCKS peptide and Evectin2 preferentially bound to membranes with unsaturated acyl chains. To further discriminate whether the primary

[2] The following chapter is reproduced from: Wen, Y., Dick, R. A., Feigenson, G. W., & Vogt, V. M. (2016). Effects of membrane charge and order on membrane binding of the retroviral structural protein Gag. *J Virol. 90*: 9518-9532.

driving force for Gag membrane binding is electrostatic interactions or preference for membrane order, we measured protein binding to giant unilamellar vesicles (GUVs) containing the same PS concentration in both disordered (Ld) and ordered (Lo) phases. RSV Gag and mNG-KRn membrane association followed membrane charge, independent of membrane order. Consistent with pelleting data, the MARCKS peptide showed preference for the Ld domain. Surprisingly, the PS sensor Evectin2 bound to the PS-rich Ld domain with 10-fold greater affinity than to the PS-rich Lo domain. In summary, we found that RSV Gag shows no preference for membrane order, while proteins with reported membrane-penetrating domains show preference for disordered membranes.

IMPORTANCE

Retroviral particles assemble on the PM and bud from infected cells. Our understanding of how Gag interacts with the PM and how different membrane properties contribute to overall Gag assembly is incomplete. This study examined how membrane charge and membrane order influence Gag membrane association. Consistent with previous work on RSV Gag, we report here that electrostatic interactions provide the primary driving force for RSV Gag membrane association. Using phase-separated GUVs with known lipid composition of the Ld and Lo phases, we demonstrate for the first time that RSV Gag is sensitive to membrane charge but not membrane order. In contrast, the cellular protein domain MARCKS and the PS sensor Evectin2 show preference for disordered membranes. We also demonstrate how

to define GUV phase composition, which could serve as a tool in future studies of protein membrane interactions.

INTRODUCTION

The retroviral structural protein Gag provides the primary driving force for virus assembly at the inner leaflet of the plasma membrane (PM), and Gag alone is sufficient to assemble into virus-like particles (VLPs) in cells (1) and also in vitro (2). Gag is synthesized in the cytosol and then is targeted to the PM by the N-terminal domain, MA. How Gag interacts with the inner leaflet of the PM and how the biophysical properties of the PM contribute to Gag assembly are not fully understood. Gag exploits one or more mechanisms governing binding of peripheral proteins to membranes, which include electrostatic interactions, hydrophobic interaction, recognition of specific lipid headgroups, protein multimerization, sensitivity to phospholipid acyl chain compositions, and preference for membrane order (3).

Prior work in the field has provided a number of important clues to how Gag binds to membranes. First, most retroviral Gag proteins have a cluster of basic residues in MA that interact with acidic lipids in the inner leaflet (4). Mutating these residues results in reduction of Gag membrane association and of virus release (5-7). In vitro, the negatively charged lipids phosphatidylserine (PS) or phosphatidylinositol 4,5-bisphosphate [PI(4,5)P2] are crucial for Gag or MA membrane association (8-13). Second, the Gag proteins of most retroviruses, like HIV-1, are modified by addition of the 14-carbon fatty acid myristate at the N-terminal glycine residue. Mutating this residue blocks myristoylation and also membrane binding and virus budding (14-16).

A few Gag proteins, like that of Rous sarcoma virus (RSV), are not fatty acylated. Third, in at least some retroviruses, like HIV-1, MA has a specific binding pocket for the PI(4,5)P2 headgroup (17, 18), and both Gag-PM binding and virus budding are reduced in PI(4,5)P2-depleted cells (8, 17). However, similar experiments for RSV Gag showed inconsistent results (12, 19, 20). For the PI(4,5)P2 effect, the relative roles of electrostatic attraction and specific headgroup binding are uncertain. Fourth, Gag binds to membranes in a cooperative fashion, with multimerization enhancing this interaction (21). RSV and HIV-1 MA dimers (21-23) and RSV MA hexamers (21) bind to membranes much more avidly than monomeric MA, both in vivo (for HIV-1) and in vitro (RSV and HIV-1). Finally, HIV-1 Gag associates preferentially with membranes containing unsaturated acyl chains compared with saturated chains and also preferentially associates with membranes containing cholesterol (Chol) (24). The mechanisms underlying these effects are unknown.

The PM comprises less than 10% of all cellular membranes and exhibits complex compositional and biophysical properties (25). Lipids are distributed asymmetrically, with the outer leaflet composed primarily of sphingomyelin (SM), phosphatidylcholine (PC), and Chol and the inner leaflet rich in phosphatidylethanolamine (PE), PS, phosphatidylinositol (PI), and cholesterol (25, 26). Based on indirect evidence, it is sometimes said that retroviruses assemble and bud from PM microdomains called “rafts” (27-29). For example, several lipidomic studies report that the retroviral membrane is enriched in the outer leaflet lipid SM compared with the PM from which the virus buds (30-33). Some lipidomic studies (34) have reported an enrichment of cholesterol in virions compared to total cellular

membranes. One previous study found a nonphysiological enrichment of cholesterol in virions compared to the cellular plasma membrane (33); however, a more thorough study found no significant enrichment in cholesterol (35). Additionally, in model membranes with coexisting raft and non-raft domains at a physiological cholesterol mole fraction of 0.35 to 0.4, cholesterol is present at similar levels in the coexisting domains (36-39). Also, under some conditions Gag is found in cold detergent-resistant membranes (DRMs) along with raft markers (40-43). However, DRMs are not a true reflection of proposed rafts in the PM, since detergent type, detergent concentration, temperature, and time affect the degree to which proteins and lipids are isolated in DRMs (44). Moreover, the difficulty in isolating pure PM limits our understanding of lipid and membrane behavior and of the contribution of membranes to retroviral assembly.

Possible phase separation must be taken into account in studies of protein binding to membranes, since lipid components will sort differently into any coexisting phases. In vitro, liquid-liquid phase separation can be observed with lipid-only mixtures of as few as three components (45, 46). Understanding biological membrane phases is facilitated by lipid compositional phase diagrams (36, 37, 47-50). Each lipid phase has well-defined and uniform properties, such as order and density, throughout the whole domain (25, 51). The liquid-ordered phase (Lo) is characterized by fast translational diffusion and high lipid acyl chain order, and it contains a large fraction of saturated acyl chains. The Lo phase has many of the properties attributed to lipid rafts in the PM (52). The liquid disordered phase (Ld) is characterized by fast translational diffusion but low lipid acyl chain order and a high concentration of

unsaturated acyl chains. The solid or gel phase (Lβ) is characterized by lipid diffusion thousands of times slower than that in Ld or Lo and by tightly packed saturated acyl chains. Of great biological relevance is the compositional region in which Ld and Lo phases coexist, which might reflect the phase behavior of the outer leaflet in the PM (45). In this study, we used two sizes of lipid-only model membranes to study the membrane binding of Gag and other peripheral proteins: large unilamellar vesicles (LUVs) and giant unilamellar vesicles (GUVs). The LUVs we use are 100 nm in size, and LUVbound protein can be quantitated by flotation in a density gradient (21) or centrifugation to a pellet (liposome pelleting) (53). GUVs we use are cell sized (10 m) and thus easily visualized by fluorescence microscopy when the membrane lipid phases or a protein are marked with a fluorescent dye (54, 55). Both kinds of vesicles are prepared with defined lipid composition. In GUVs with compositions giving rise to Lo and Ld coexistence, the separate domains can be visualized directly by dyes that preferentially partition into Lo or Ld (56). The challenge for interpreting protein binding in phase-separated GUVs is that the composition of each phase can be inferred only if the phase diagram is known. Such diagrams have been developed only for a few compositions (36- 39, 48, 57), and none are available for ternary mixtures that include PS in addition to PC-Chol.

A few studies with GUVs have provided insight into the membrane binding properties of HIV-1 Gag and MA (58-60). For example, purified ESCRT proteins were used to infer the assembly order of ESCRT proteins at HIV-1 Gag budding sites (58). In another study, in vitro-translated HIV-1 Gag from a wheat germ extract was used to demonstrate that saturated and unsaturated PI(4,5)P2 species affect the

membrane binding of HIV-1 Gag differently (59). In a different study, multimerized MA bound the Ld phase preferentially in two-phase GUVs (60). However, in those experiments the phase diagram was not known, hence the concentrations of negatively charged lipids in each phase were also unknown, making it difficult to ascribe the observed binding to phase preference as opposed to composition and charge preference.

It remains unclear how membrane order and membrane charge influence association of Gag with membranes. We previously reported that HIV-1 Gag binding to membranes is stimulated by high levels of cholesterol, which has the effect of ordering membranes, but also is stimulated by unsaturated lipids, which has the effect of disordering membranes (24). In a limited set of experiments in a follow-up study, we detected no significant sensitivity of purified RSV Gag to acyl chain saturation and membrane order (10). In the present study, in order to systematically probe the effect of membrane order and charge on RSV Gag membrane binding, we prepared a set of purified fluorescent electrostatic sensor proteins as well as phospholipid headgroup-specific binding proteins. Membrane binding of these control proteins in parallel with binding of RSV Gag and MA was assessed using two phase GUVs with defined PS distribution, together with liposome-pelleting assays. The work described here represents the first systematic study of the effect of charge, phase, and lipid order on a purified retroviral Gag protein in two-phase GUVs with known PS concentrations in each phase.

MATERIALS AND METHODS

DNA vectors, protein purification, and tissue culture

Purified proteins used in this study are pictured in Fig. 3.1. All DNA constructs used for protein purification were cloned into pSUMO (61) vector using standard subcloning techniques as previously described (53). Monomeric neon green (mNG) (62) was amplified from pHisII 6H-mNG, digested with BamHI and EagI, and ligated into pSUMO. pSUMO-mNG served as the vector to generate all other N-terminally tagged mNG proteins (Fig. 3.1). SUMO-mNG-KRn (n=4 [RKKR], n=8 [RKKRKKRK], or n=12 [RKKRKKRKKRKK]) and SUMO-mNG-MARCKS (KKKKKRFSCKKSFKLSGFSFKKNKK) (63, 64) were made by inserting annealed primers into SUMO-mNG using EagI and XhoI. The linker sequence between the tandem Evectin2 domains is VDGT (65). All SUMO-tagged proteins were purified using standard bacterial expression and affinity column techniques (10, 53). In brief, Escherichia coli BL21 cultures were grown at 37°C to an optical density at 600 nm of 0.6. Isopropyl -D-1-thiogalactopyranoside (IPTG) was added to a final concentration of 0.5 mM, and induced cells were harvested 5 to 6 h postinduction. Pelleted cells were resuspended in lysis buffer [20 mM Tris, pH 8, 500 mM NaCl, 2 mM tris(2-carboxyethyl)-phosphine (TCEP), and 2 mM phenylmethylsulfonyl fluoride (PMSF)] and lysed by sonication. After ultracentrifugation in a TLA-110 Beckman rotor at 90,000 rpm for 45 min, the supernatant was collected. RSV SUMO-MA-(mNG), SUMO-Gag-(mNG), SUMO-MASP+5 -mNG, SUMO-mNG-KR12, and SUMO-mNG-MARCKS supernatants were treated with polyethyleneimine (PEI) and spun at 10,000 rpm in a Sorvall 600 rotor at 4°C to remove nucleic acid. To the supernatant,

ammonium sulfate was added to 20% to precipitate the protein of interest, followed by centrifugation. The pellet was resuspended in binding buffer (20 mM Tris-HCl, pH 8, 50 mM NaCl, and 2 mM TCEP) and further purified by cation exchange chromatography (HiTrap SP FF; GE Healthcare) and Ni^{2+} affinity chromatography. SUMO-mNG, SUMO-mNG-KR4, SUMO-mNG-(Ev2)2, and SUMO-mNG-PH were only subjected to Ni^{2+} affinity chromatography (HisTrap HP; GE Healthcare). Following the first round of Ni^{2+} chromatography, eluted proteins were dialyzed against buffer (20 mM Tris-HCl, pH 8, 500 mM NaCl, and 1 mM TCEP) in the presence of ULP1 protease (66) to cleave off the SUMO tag. The ULP1 protease and SUMO tag were removed by Ni^{2+} affinity chromatography. Purified protein at 2 to 10 mg/ml was flash frozen in aliquots and stored at -80°C. The final protein preparation had an A260/A280 ratio of 0.58 to 0.59, indicating the absence of nucleic acid. Gag-mNG formed regular virus-like particles under standard in vitro assembly conditions screened by negative stain electron microscopy (10). All proteins had a purity of approximately 90% after affinity column purification, as judged from stained gels. A subset of constructs (Gag, KR4, KR8, KR12, and MARCKS) was cloned into a tissue culture plasmid for expression of mNG fusion proteins in avian cells. Cells were maintained, transfected, and prepared for imaging as previously described (53). Gag-mNG was localized in puncta at the PM, consistent with reports for Gag-green fluorescent protein (GFP) (21, 53). KR4 was mostly cytoplasmic and KR8 was in the nucleus, while KR12 and MARCKS were mostly in endosome-like vesicles (data not shown).

Phospholipids and fluorescent probes

Phospholipids (Table 3.1) were purchased from Avanti Polar Lipids (Alabaster, AL). Cholesterol was obtained from Nu-Chek Prep (Elysian, MN). Cholesterol stock solution was prepared by standard gravimetric procedures to ~ 0.2% error (67). The working stocks of the fluorescent lipid analogs dehydroergosterol (DHE; Sigma-Aldrich, St. Louis, MO), 3,3'-dilinoleyloxacarbocyanine perchlorate (Fast DiO; ThermoFisher, NY), naphtho[2,3-a]pyrene (naphthopyrene; Sigma-Aldrich, MO), and lissamine rhodamine 18:1,18:1-PE (LR-DOPE; Avanti, AL) were prepared in methanol. Probe concentrations were determined in methanol by absorption spectroscopy using an HP 8452A spectrophotometer (Hewlett-Packard, Palo Alto, CA). Fluorescent probe extinction coefficients were obtained from lot certificates of analysis: 12,900 M^{-1} cm^{-1} at 324 nm for DHE, 138,000 M^{-1} cm^{-1} at 499 nm for Fast DiO, 23,700 M^{-1} cm^{-1} at 460 nm for naphthopyrene, and 75,000 M^{-1} cm^{-1} at 560 nm for LR-DOPE. Concentrations of phospholipid stocks were determined to <1% error by inorganic phosphate assay (67). Purity of 99.5% was confirmed by thin-layer chromatography (TLC) on washed, activated silica gel plates (Alltech, Deerfield, IL), developed with chloroform-methanol-water (65:25:4) for all phospholipids, petroleum ether-diethyl ether-chloroform (7:3:3) for cholesterol, DHE, and naphthopyrene, chloroform-methanol (2:1) for Fast DiO, and chloroformmethanol (9:2) for LR-DOPE. TLC plates for brain PI(4,5)P2 were activated with K2 oxalate and developed with 1-propanol-2 M acetic acid (65:35).

LUV preparation and liposome-pelleting assay

LUVs with diameters of 100 nm in 20 mM Tris-HCl, pH 8.0, were prepared by rapid solvent exchange (RSE) as described by Buboltz and Feigenson (68), followed by extrusion through polycarbonate filters 31 times. In the liposome-pelleting assay (53), 15 g of purified protein and 50 g of LUVs were added to binding buffer (20 mM Tris-HCl, pH 8, with varied salt concentrations) to a final volume of 200 l binding reaction mixture at a final NaCl concentration of 50 mM, 150 mM, or 300 mM. The mixture was incubated at room temperature for 10 min. Tubes were ultracentrifuged at 90,000 rpm in a TLA-100 (Beckman) rotor for 45 min at 4°C. Supernatant was removed and the pellet was resuspended and subjected to SDS-PAGE analysis. Gels were Coomassie blue stained overnight and destained, and band intensity was determined by densitometry analysis using ImageQuant software 5.2.

ESR

Multilamellar vesicles (MLVs) were prepared as described previously (69) in buffer (20 mM Tris-HCl, pH 8, 150 mM NaCl). Each sample contained 2 mol lipid and 0.2 mol% of the spin label probe 16-DOXYL-stearic acid (Sigma-Aldrich). MLVs were centrifuged, excess buffer removed, and samples placed in thin glass capillary tubes. Electron spin resonance (ESR) spectra were collected for all samples on a 9.4-GHz Bruker continuous wave (cw)-ESR spectrometer (EMS) at room temperature (22°C). At least five scans were averaged for each sample. The maximum and minimum values of tensor A (A_{max} and A_{min}) were determined from each spectrum, and the order parameter was calculated according to Schorn and Marsh (70) using the hyperfine tensor (A_{xx}, A_{yy}, A_{zz}) =(5, 5, 32.8 G).

FRET

The phase boundaries at the ends of the tieline for composition DSPC/DOPC/Chol (30/45/25) [1,2-distearoyl-sn-glycero-3-phosphocholine-1,2-dioleoyl-sn-glycero-3-phosphocholine- cholesterol (30/45/ 25)] were determined by fluorescence resonance energy transfer (FRET) as previously described (36, 48). FRET samples were prepared at 2% compositional increments except near the phase boundary, where 1% increments were used (37, 48). DHE and Fast DiO were chosen as a FRET pair, at 1/100 and 1/700 fractions in total lipid. Light scattering and fluorescence background were controlled as described previously (71, 72). Lipids were mixed in chloroform to 120 nmol, and the organic solvent was replaced by buffer using RSE (68) and then sealed under argon. Equilibration was achieved by first heating samples to 55°C for 2 h followed by gradually cooling to 23°C at a rate of 2°C/h and then incubation at 23°C for 48 h. A 1.8-ml volume of buffer [200 mM KCl, 5 mM piperazine-N,N=-bis(2-ethanesulfonic acid), 1 mM EDTA, pH 7] was added to 0.2 ml of RSE sample to yield approximately 30 M lipid vesicles in the cuvette. Data were collected on a Hitachi F-7000 FL spectrofluorimeter (Hitachi High Technologies America, Inc., Schaumburg, IL) at 23°C. Using 5-nm bandpasses for excitation and emission slits and a 10-s integration time, intensity was measured in 4 channels (excitation/emission): DHE (327/393 nm), Fast DiO sensitized emission (327/503 nm), Fast DiO direct fluorescence (477/503 nm), and light scattering (440/420 nm). Briefly, corrections account for non-FRET contributions of direct fluorescence emission from donor and acceptor and scattering of excitation light by the vesicle suspension (71). Phase

boundaries were determined from FRET trajectories as the intersection of two straight lines drawn on either side of the boundary, as described in the relevant figure legends. Analysis of unsmoothed data gave similar boundary locations but with slightly larger uncertainties.

GUV preparation, imaging, and protein binding

The lipid compositions of each phase on the three types of GUVs used are shown in the figures. The same starting composition was chosen, DSPC/DOPC/Chol (30/45/25), marked by a black arrow in the figures. For GUVs having PS enriched in Ld, 33% of DOPC was replaced with 1,2-dioleoyl-sn-glycero3-phospho-L-serine (DOPS), and the resulting lipid mixture, DSPC/ DOPC/DOPS/Chol (30/30/15/25), contains approximately 24 mol% PS in Ld and 2 mol% PS in Lo. For GUVs having PS enriched in Lo, 41% of the DSPC was replaced with 1,2-dihexadecanoyl-sn-glycero-3-phosphoL-serine (DPPS), and the resulting lipid mixture, DSPC/DPPS/DOPC/ Chol (18/12/45/25), contains approximately 24 mol% PS in Lo and 2 mol% PS in Ld. The lipid composition of each phase of GUVs corresponds to that of the LUV Ld or Lo phase with 24 mol% PS in purple or red, as well as the LUV Ld or Lo phase with 2 mol% PS in blue or green used in the liposome-pelleting assay. The third type of GUV has PS in both Ld and Lo phases, with 33% of DOPC replaced with DOPS and 41 mol% of DSPC replaced with DPPS, yielding the lipid mixture DSPC/DPPS/DOPC/ DOPS/Chol (18/12/30/15/25), containing approximately 24 mol% PS in Ld and 24 mol% PS in Lo. GUV samples described here were prepared by gentle hydration (38, 73). A total of 300 nmol total lipid containing 0.02 mol% LR-DOPE was mixed in

chloroform, partially dried to a thin film in a culture tube using a rotary evaporator, and then dried with heating at 55°C under high vacuum for 1.5 h. The thin dry film was then hydrated with wet N2 gas at 55°C for 30 min. Lipid films were further hydrated with prewarmed sucrose buffer (125 mM sucrose, pH 8) and incubated at 55°C for 30 min. GUVs formed as the sample was cooled over 10 h to room temperature (23°C). GUVs were harvested into buffer (50 mM NaCl, 20 mM Tris, pH 8). All buffers were osmotically balanced, confirmed by measurements using an osmometer (Precision Systems Inc., Natick, MA). GUVs were imaged on a Nikon Eclipse Ti microscope (Nikon Instruments, Melville, NY) at 23°C, using a 60 , 1.2-numeric-aperture water immersion objective. Images were taken with an Andor Zyla VSC-01037 camera (Oxford Instruments, South Windsor, CT). Imaging used a low exposure time of 50 ms to minimize light-induced artifacts (74). LR-DOPE was excited at 555 nm, and emission was collected at 600 to 675 nm; naphthopyrene was excited at 430 nm, and emission was collected at 460 to 500 nm. When performing protein-membrane assays, only LR-DOPE was added as an Ld marker in GUVs. Protein was added to a final concentration of 1 M to preformed GUVs and incubated for 30 s before imaging. mNG was excited at 470 nm, and emission was collected at 495 to 525 nm. GUV images containing multiple colors were color merged using NIS software: mNG is green, LR-DOPE is red, and naphthopyrene is blue. The contrast of entire images was enhanced with NIS Elements Basic Research Software (MVI, Inc.). Quantification of fluorescence signals in microscopy images was determined using the line scan function of NIS Elements Basic Research Software. For the two-phase GUVs, line scans were performed on no fewer than 80 GUVs for each protein.

Quantification of Ld/Lo-bound protein was performed on GUVs with PS in Ld and Lo. On the merged GUV images, the background fluorescence intensity of unbound protein was subtracted from that of GUV-bound proteins. The Ld/Lo protein binding ratio was determined and expressed as a box plot, where the bottom, middle, and top lines of the box represent the first, second (median), and third quartiles, whiskers are the minimum and maximum values, and circles are outliers. For PI(4,5)P2 containing GUVs, two line scans per GUV and no fewer than 30 GUVs were measured. The relative fluorescence intensity of protein binding above background is shown as (membrane-bound fluorescence - background)/background, expressed as a percentage.

RESULTS

While electrostatic interaction is known to play a role in Gag-membrane binding, there have been no systematic studies using purified proteins. While at least some retroviruses have raft-like lipid compositions, no controlled experiments have probed the possible role of lipid-phase properties in membrane interactions. We address both of these topics for RSV Gag. We built and purified a series of fluorescent proteins that act as charge sensors, based on mNG with an added C-terminal tail of 4, 8, and 12 alternating lysine and arginine residues (Fig. 3.1). To bridge this study to other cellular proteins, mNG-MARCKS was included, since the MARCKS protein contains a well-characterized, 26-residue peripheral membrane interacting peptide (63, 64, 75, 76). This peptide has a cluster of 13 basic amino acids but also includes 5 hydrophobic residues that can contribute to membrane interaction. As further controls we created fusions of mNG with two lipid headgroup-binding proteins, Evectin2 and

Table 3.1: Lipids used to form unilamellar vesicles

Lipid name	Abbreviation	Acyl chains	Head group charge
1-palmitoyl,2-oleoyl-sn-glycero-3-phosphocholine	POPC	16:0/18:1	0
1,2-dioleoyl-sn-glycero-3-phosphocholine	DOPC	18:1/18:1	0
1,2-distearoyl-sn-glycero-3-phosphocholine	DSPC	18:0/18:0	0
1-palmitoyl-2-oleoyl-sn-glycero-3-phospho-L-serine	POPS	16:0/18:1	-1
1,2-dioleoyl-sn-glycero-3-phospho-L-serine	DOPS	18:1/18:1	-1
1,2-dihexadecanoyl-sn-glycero-3-phospho-L-serine	DPPS	16:0/16:0	-1
Brain L-α-phosphatidylinositol-4,5-bisphosphate	$PI(4,5)P_2$	18:0/20:4*	-3 to -4

*Predominant species

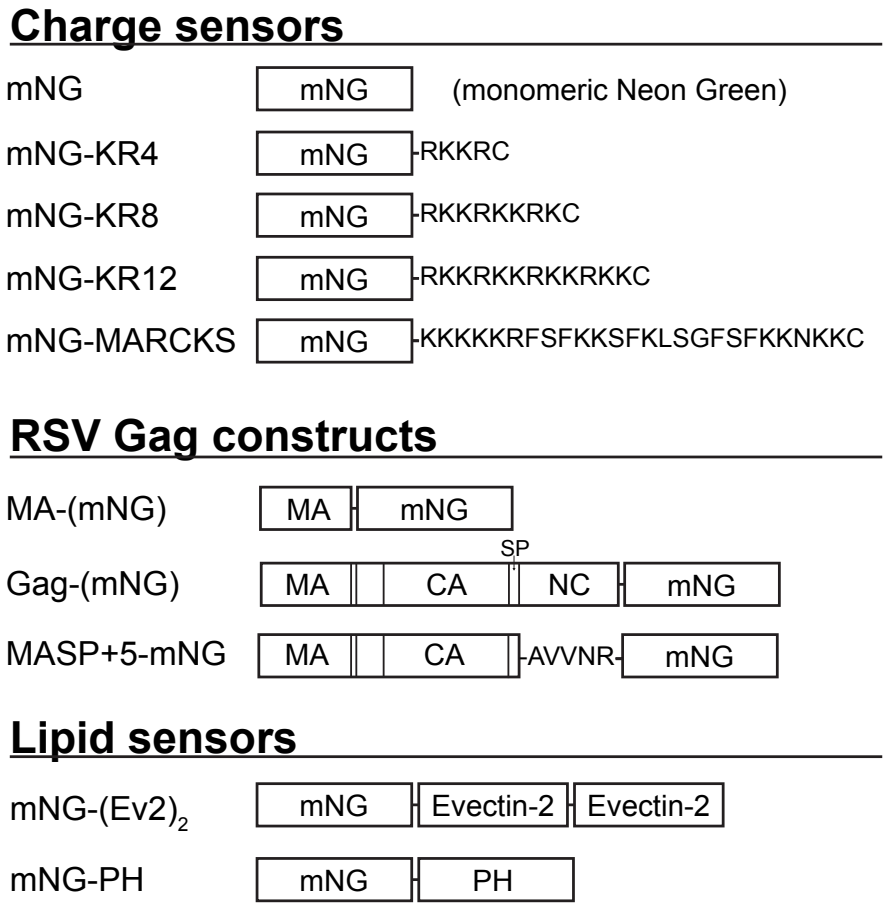

Fig 3.1 Schematic representation of purified proteins. All charge sensors (top) were N-terminally tagged with the monomeric Neon Green (mNG) fluorescent protein; mNG-MARCKS contains the 26-residue effector domain of MARCKS. RSV Gag constructs (middle) are C-terminally mNG tagged. A nontagged version of RSV MA and Gag was also purified. MASP^{+5}-mNG contains MA, CA, and SP plus the first 5 residues of the NC domain (53). Lipid sensors (bottom) are N-terminally tagged with mNG. The PS sensor mNG-(Ev2)2 contains two tandem PH domains of human Evectin2. The PI(4,5)P2 sensor mNG-PH contains the PH domain from human PLC 1.

the PH domain of phospholipase C 1. Evectin2, which we used as a tandem duplication (65), interacts specifically with PS (77), while the PH domain interacts specifically with PI(4,5)P2 (78).

Membrane surface potential is strongly affected by ions, which shield the negatively charged lipid headgroups and positively charged amino acid side chains and thus reduce electrostatic attraction to basic residues on proteins (22). Previous studies based on liposome flotation reported that RSV MA membrane binding decreases markedly with increasing NaCl concentration (22). To confirm and extend these observations, we used a centrifugation assay to determine how ionic strength influences interaction of viral and control proteins with LUVs. The percentage of purified protein in a membrane pellet was quantified at 50, 150, and 300 mM NaCl (Fig. 3.2A, lanes 1 to 3), with centrifugation in the absence of LUVs serving as the background control (background, lanes 4 to 6). mNG itself did not detectably pellet with LUVs at any NaCl concentration (Fig. 3.2B), confirming the expected lack of contribution of the mNG moiety to membrane binding. As predicted, the charge sensors were very sensitive to increasing salt, with a longer stretch of basic residues leading to more extensive LUV binding at a fixed NaCl concentration (79). mNG-MARCKS behaved similarly to mNG-KR12. For the viral proteins, approximately 70% of MA-(mNG) and Gag-(mNG) bound to LUVs at 50 mM, almost 10-fold more than at 300 mM (Fig. 3.2B), consistent with an electrostatic mode of membrane interaction (22). On the other hand, compared with the retroviral proteins and the charge sensors, the PS sensor mNG-(Ev2)2 was much less sensitive to ionic strength, showing a less than 2-fold change when NaCl was decreased from 300 mM to 50 mM.

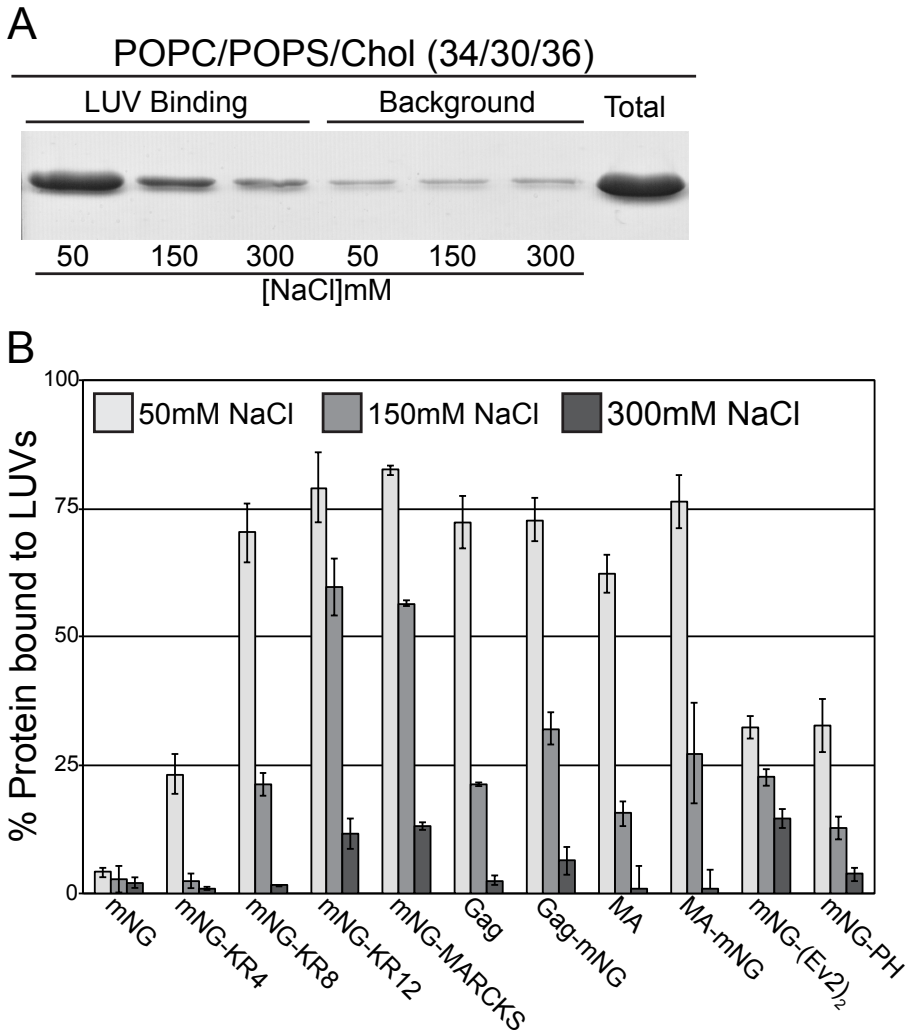

Fig 3.2 Effects of sodium chloride on protein-membrane binding. (A) LUVs were composed of POPC/POPS/Chol (34/30/36). A stained SDS gel of RSV MA is shown as an example of the liposome-pelleting assay at 50, 150, and 300 mM NaCl. Gel bands represent the amount of protein associated with pelleted LUVs at the three NaCl concentrations; background bands represent the protein pelleted in the absence of LUVs at the corresponding NaCl concentrations. Total is the total amount of protein used in each binding reaction. (B) White, light gray, and dark gray bars represent the average percentage of no fewer than three independent pelleting reactions at 50, 150, and 300 mM NaCl. Error bars represent standard deviations from the means.

The PI(4,5)P2 sensor mNG-PH was somewhat sensitive to ionic strength, pelleting with LUVs 8-fold less at 300 mM than at 50 mM. While PH is accepted to be specific for the PI(4,5)P2 headgroup (78, 80), we found that mNG-PH showed significant membrane binding at 50 mM NaCl even in the absence of PI(4,5)P2. This interaction may be mediated by several basic residues in the 1/2 loop of the PH domain, which also form part of the specific binding pocket for PI(4,5)P2 (81).

We also examined whether elevating PS concentration in membranes enhances protein binding (Fig. 3.3). As expected, RSV MA, mNG-KR8, mNG-KR12, and mNG-MARCKS had almost undetectable membrane binding at 0 mol% PS, with their LUV binding increasing as the PS concentration was raised from 10 to 50 mol%. Note that because of the absence of cholesterol, the membrane binding was weaker in this set of experiments than in those in Fig. 3.2. Overall, the results shown in Fig. 3.2 and 3.3 are evidence that electrostatic attraction is the driving force for membrane association of RSV MA and Gag, as it is for the charge sensors.

RSV Gag prefers membranes with mixed acyl chain compositions

Previously, we showed that HIV-1 Gag binds more strongly to membranes with unsaturated lipids than to membranes with saturated lipids (24). HIV-1 Gag may also be sensitive to the acyl chain content of PI(4,5)P2 in membranes (59). Sensitivity to acyl chain type is specific for the charged lipid [PS or PI(4,5)P2], whereas the acyl chains on PC have little influence on binding (10). In contrast to HIV-1 Gag, in previous studies RSV Gag did not respond to the level of unsaturation, either of PS or PC (10). Here, we systematically tested RSV Gag binding to five types of LUVs at the

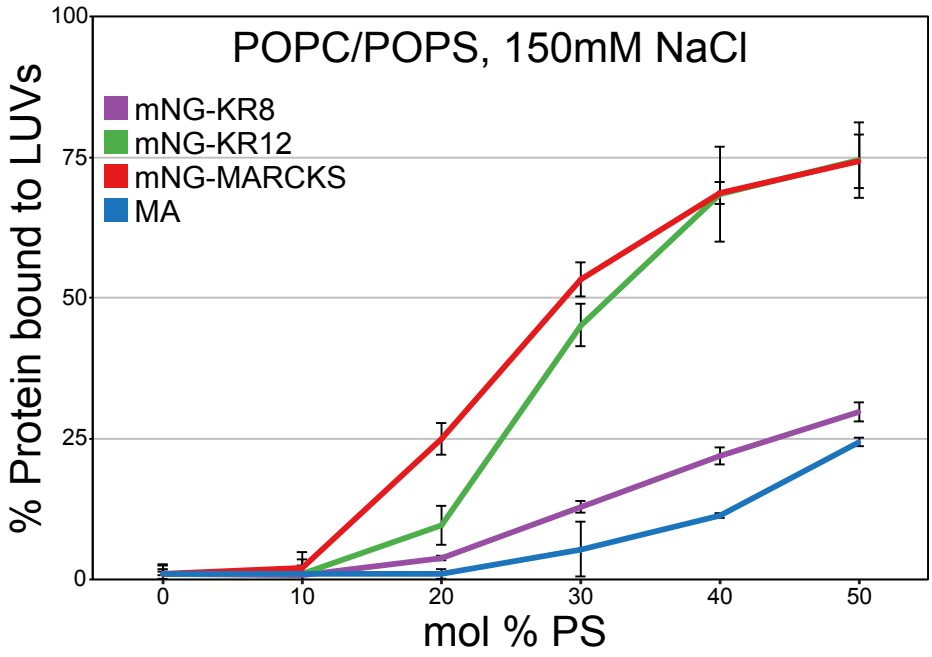

Fig 3.3 Protein binding to POPC/POPS LUVs with increasing PS concentration. LUVs were prepared with POPC-POPS, with 10 mol% POPS incremental increases from 0 to 50 mol%. The curves show the percentage of protein bound to LUVs at the six POPS concentrations. Binding levels of mNG-KR8, mNGKR-12, mNG-MARCKS, and RSV MA are shown in purple, green, red, and blue, respectively. All data points represent the averages from no fewer than three independent liposome-pelleting assays at 150 mM NaCl; error bars represent standard deviations from the means.

physiologically relevant concentration of 36 mol% cholesterol. The fluorescent protein charge sensors and lipid headgroup sensors were tested in parallel. Membrane lipid compositions were confirmed by GUV imaging analysis to be uniform, not phase separated (data not shown).

RSV Gag, RSV MA, and mNG-KR8 shared the same membrane-binding patterns (Fig. 3.4). More specifically, the two types of LUVs having one phospholipid with two unsaturated acyl chains (18:1, 18:1) and the other phospholipid with two saturated acyl chains (16:0, 16:0 or 18:0, 18:0) consistently supported approximately 15% more binding than the other three types of LUVs in which all of the acyl chains in both phospholipids were either saturated or unsaturated. The origin of this difference is unclear, but it is known that in PC-PS membranes where each lipid has different acyl chains, the lipid mixing is nonideal (82) and the PS has a higher thermodynamic activity (83).

In contrast, mNG-MARCKS and mNG-(Ev2)2 had different membrane binding properties than RSV MA, Gag, and mNG-KR8 (Fig. 3.4). Both mNG-MARCKS and mNG-(Ev2)2 showed the strongest binding to LUVs with unsaturated PS (for example, DOPC/DOPS/Chol), regardless of the acyl chain saturation of PC, and had the weakest binding to LUVs with both PC and PS having saturated chains (DSPC/DPPS/Chol). In addition, for the two types of LUVs with different saturated and unsaturated lipids, the one with unsaturated PS and saturated PC (DSPC/DOPS/Chol) supported higher binding than the one with saturated PS and unsaturated PC (DOPC/DPPS/Chol). One model to account for these results holds that mNG-MARCKS and mNG-(Ev2)2 prefer unsaturated PS, which may be more

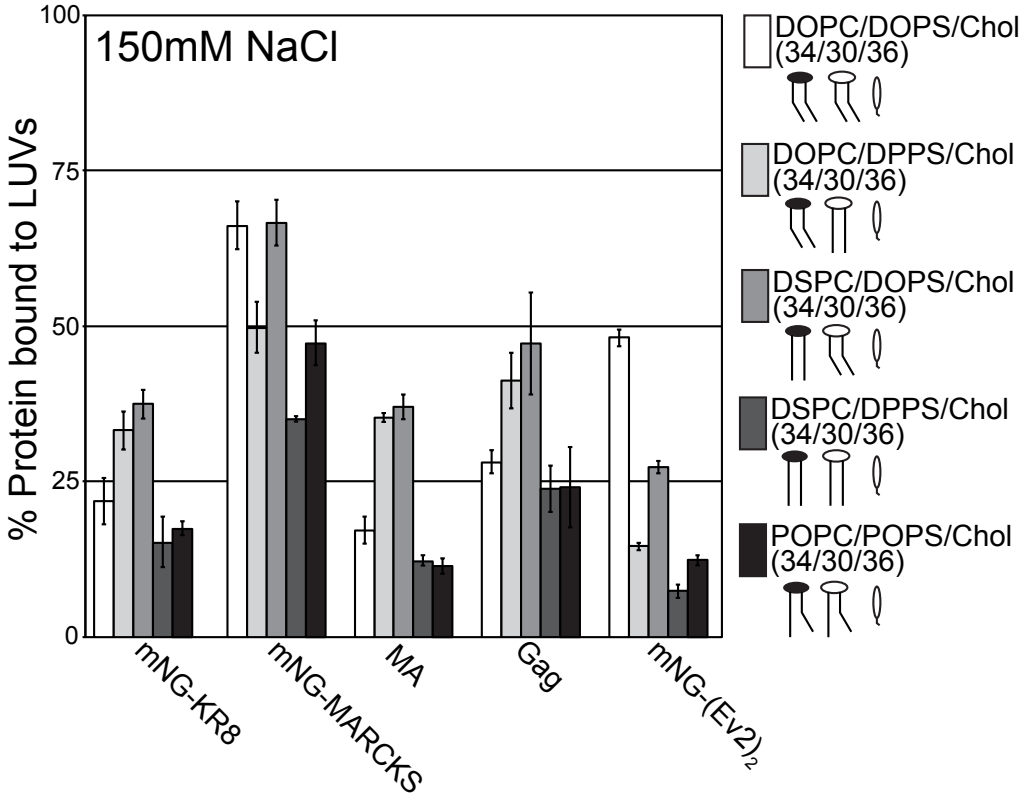

Fig 3.4 Effects of saturated and unsaturated lipid acyl chains on protein membrane association. The five LUV compositions are shown on the right side. Cartoons represent different types of lipid acyl chains and headgroups. Black and white ovals represent PC and PS, respectively. Straight lines represent saturated acyl chains, and kinked lines represent unsaturated acyl chains. The oval symbol represents cholesterol. All graphs show the percentage of total protein associated with LUVs at 150 mM NaCl. Bars represent the averages from no fewer than three independent liposome-pelleting assays; error bars represent standard deviations from the means.

favorable for protein hydrophobic amino acid side chain insertion. A similar effect of the HIV-1 Gag myristate modification might explain why this Gag protein strongly prefers to bind to membranes with unsaturated PS (24). To further test the effects of PS acyl chain saturation, we prepared two series of four-component LUVs, systematically varying the PS concentrations (Fig. 3.5A). Starting with LUVs rich in unsaturated PC [DSPC/DOPC/Chol (8/56/36)], DOPC was replaced with unsaturated DOPS in increments of 10 mol%. Similarly, starting with LUVs rich in saturated PC [DSPC/DOPC/Chol (56/8/36)], DSPC was replaced with the saturated DPPS in increments of 10 mol%. As expected, in both cases for all proteins tested, higher concentrations of PS led to increased binding (Fig. 3.5B). For MA, mNG-KR12, and mNG-MARCKS, the LUVs with unsaturated PS (0 to 50% DOPS) and LUVs with saturated PS (0 to 50% DPPS) supported protein binding to a similar level at the same PS concentration. However, mNG-(Ev2)2 had a very strong preference for LUVs with unsaturated PS, consistent with the results shown in Fig. 3.4. In summary, RSV MA and Gag do not show a strong preference for membranes with either saturated or unsaturated lipids, while Evectin2 and possibly MARCKS show preference for membranes with unsaturated PS.

Gag binding follows membrane charge while Evectin2 binding follows membrane order

At certain concentrations, mixing high-melting-temperature (Tm) lipids, low Tm lipids, and cholesterol results in phase separation (45, 51). Numerous FRET and/or ESR measurements and GUV imaging studies are needed to create phase diagrams to

A

DOPC	DSPC	**DOPS**	Chol	DOPC	DSPC	**DPPS**	Chol
56	8	**0**	36	8	56	**0**	36
46	8	**10**	36	8	46	**10**	36
36	8	**20**	36	8	36	**20**	36
26	8	**30**	36	8	26	**30**	36
16	8	**40**	36	8	16	**40**	36
6	8	**50**	36	8	6	**50**	36

B

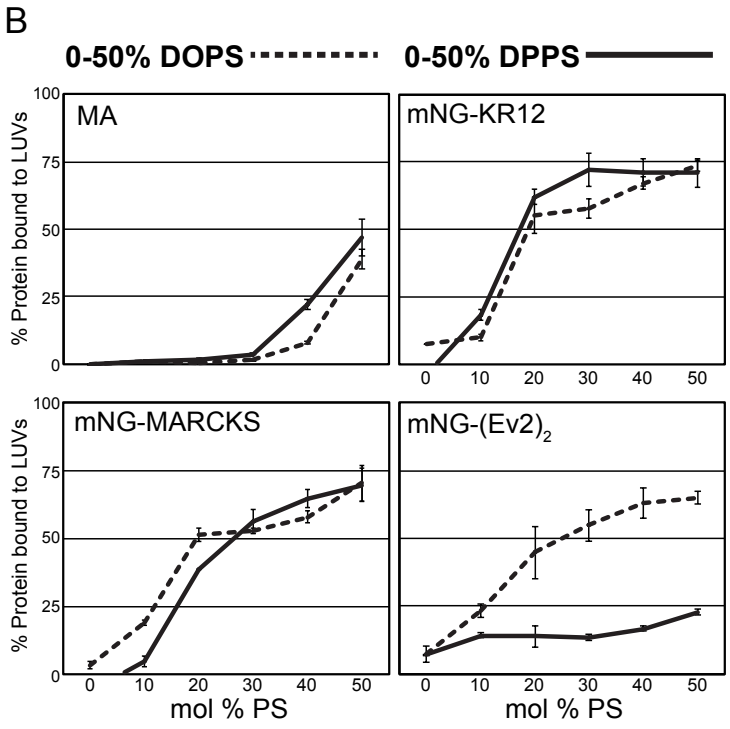

Fig 3.5 Effect of increasing PS concentration of Ld and Lo membranes on protein membrane association. (A) Compositions of LUVs studied. The left side shows LUVs composed of DOPC/DSPC/DOPS/Chol (Ld) with fixed DSPC and Chol mol% but increasing DOPS (in boldface) and decreasing DOPC mol%. The right side shows LUVs composed of DOPC-DSPC-DPPSChol (Lo) with fixed DOPC and Chol mol% but increasing DPPS (in boldface) and decreasing DSPC mol%. All LUVs are single phase (uniform), confirmed by GUV image analysis (data not shown). (B) Dashed lines represent protein binding to Ld LUVs composed of DOPC/DSPC/DOPS/Chol (DOPS 0 to 50 mol%); solid lines represent protein binding with Lo LUVs composed of DOPC/DSPC/DPPS/Chol (DPPS 0 to 50 mol%). All data points represent averages from no fewer than three independent liposome-pelleting assays at 150 mM NaCl; error bars represent standard deviations from the means.

represent the lipid compositions of such membranes (49, 84). On a ternary phase diagram, the phase boundaries and samples prepared along a tieline enable calculating the exact lipid compositions of each phase in the membrane. On any point of total sample composition within the Ld+Lo coexistence region, the tieline through this point (dashed line in Fig. 3.6B) intercepts the phase boundaries, connecting the compositions of the two coexisting phases that are in equilibrium (46). Along a tieline the fraction of each coexisting phase is known. Currently, the majority of published phase diagrams describe neutral lipid mixtures (36-39, 48). No published data are available with ternary phase diagrams containing PC/PS/Chol. To allow accurate calculations of lipid compositions that include PS and to determine phase boundaries, we employed FRET assays (72) using the two fluorescent dyes DHE and Fast DiO to measure 75 lipid mixtures prepared along a tieline. DHE preferentially partitions into the Lo phase (48), and Fast DiO preferentially partitions into the Ld phase (56). The stimulated acceptor emission was measured as a FRET signal along the tieline on the phase diagram (Fig. 3.6A and B). First, we measured the FRET signal of the 75 samples composed of DSPC/DOPC/Chol without any PS replacement (Fig. 3.6A, middle). Consistent with the published phase diagram (36, 48), the original phase boundaries are at DSPC of 0.05 (Ld) and DSPC of 0.58 (Lo). We next measured two sets of 75 samples with partial PS replacement. In each set PC was replaced with PS that contained the same acyl chain type, so that the percentage of high Tm and low Tm lipids remained the same. In the first set of experiments, 33% of the total DOPC was replaced with DOPS for all samples along the tieline (Fig. 3.6A, top). This replacement shifted the Ld phase boundary to DSPC of 0.09, i.e., 0.04 to the right

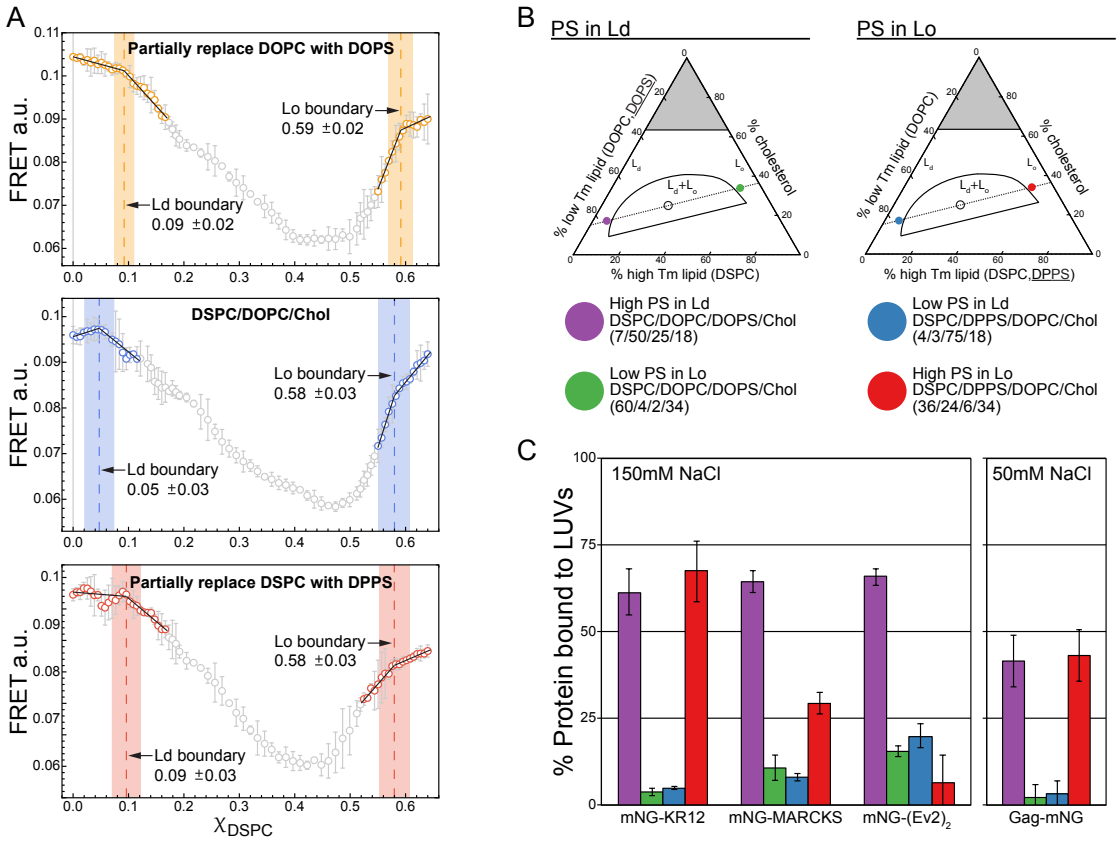
A
Partially replace DOPC with DOPS
Lo boundary
0.59 ±0.02
Ld boundary
0.09 ±0.02
DSPC/DOPC/Chol
Lo boundary
0.58 ±0.03
Ld boundary
0.05 ±0.03
Partially replace DSPC with DPPS
Lo boundary
0.58 ±0.03
Ld boundary
0.09 ±0.03
FRET a.u.
X DSPC
B
PS in Ld
PS in Lo
% low Tm lipid (DOPC,DOPS)
% high Tm lipid (DSPC)
% cholesterol
% low Tm lipid (DOPC)
% high Tm lipid (DSPC,DPPS)
High PS in Ld
DSPC/DOPC/DOPS/Chol
(7/50/25/18)
Low PS in Lo
DSPC/DOPC/DOPS/Chol
(60/4/2/34)
Low PS in Ld
DSPC/DPPS/DOPC/Chol
(4/3/75/18)
High PS in Lo
DSPC/DPPS/DOPC/Chol
(36/24/6/34)
C
150mM NaCl
50mM NaCl
% Protein bound to LUVs
mNG-KR12
mNG-MARCKS
mNG-(Ev2)2
Gag-mNG

Fig 3.6 Protein binding to LUVs with PS in Ld or Lo phases. (A) The effect on phase boundaries of adding PS to DSPC/DOPC/Chol. Shown is stimulated acceptor emission (FRET; arbitrary units) versus DSPC mole fraction (DSPC) for three compositional trajectories, measured along straight lines as shown in panel B. Each trajectory passes through the mixture composition DSPC/DOPC/Chol (30/45/25) (black circle) in the phase diagrams in panel B. The top graph in panel A shows the measured FRET along a single trajectory in which 33% DOPC has been replaced with DOPS. The middle graph shows the FRET trajectory of membranes of DSPC/DOPC/Chol, with no PS replacement. The bottom graph shows the FRET trajectory of membranes in which 41% of the DSPC is replaced with DPPS. Each trajectory contains 75 data points. Data were locally smoothed, and phase boundaries were determined by fitting a subset of data near the boundary (colored open circles) to a piecewise linear function. Vertical dashed lines indicate the left and right phase boundaries, and vertical colored bars indicate the confidence intervals. (B, left) Phase diagram of DSPC/DOPC/Chol with 33% of total DOPC replaced with DOPS. (Right) Phase diagram of DSPC/DOPC/ Chol with 41% of total DSPC replaced with DPPS. The locations of the four LUV compositions studied are marked on the corresponding phase diagram. Colors correspond to LUV compositions just below the phase diagrams, and their representative levels of protein binding are pictured in the charts. High PS means 24 mol% PS, and low PS means 2 mol% PS. (C) The amount of protein binding to the four types of LUVs shown in panel B. Liposome-pelleting assays for mNG-KR12, mNG-MARCKS, and mNG-(EV2)2 at 150 mM NaCl are shown on the left; the liposome binding for Gag-mNG at 50 mM NaCl is shown on the right. All bars represent the averages from no fewer than three independent liposome-pelleting assays; error bars represent standard deviations from the means. The order parameter, S, determined by ESR (not shown) of each membrane composition was 0.14 for Ld (purple and blue) and 0.31 for Lo (green and red).

compared with the original boundary along the tieline. The Lo phase boundary remained close to DSPC of 0.59. In the second set of experiments, 41% of the total DSPC was replaced with DPPS for all samples along the tieline (Fig. 3.6A, bottom). We found the Ld phase boundary shifted to DSPC of 0.09 along the tieline, while the Lo phase boundary stayed at DSPC of 0.58. In summary, these results imply that replacing up to 41% of PC with PS in the membrane changes the phase boundaries along the chosen tieline only slightly. Importantly for our experiments, replacing 33% of the total DOPC with DOPS, or replacing 41% of the total DSPC with DPPS, resulted in the same PS concentration in the Ld and Lo phases, respectively, at our chosen two-phase GUV compositions.

The previous figures show that Gag has no preference for membranes composed either of fully saturated lipids (DSPC/ DPPS/Chol) or fully unsaturated lipids (DOPC/DOPS/Chol) (Fig. 3.4). To directly test the hypothesis that Gag does not recognize membrane order, we compared membrane binding using two sets of LUVs having the same PS concentration but with different membrane orders (Fig. 3.6B). In the case of partially replacing DOPC with DOPS (Fig. 3.6B, left), the two points at the phase boundaries correspond to compositions of the coexisting Ld (purple circle) and Lo (green circle) phases. The corresponding Ld composition contains 24 mol% PS, while Lo composition contains 2 mol% PS. In the case of partially replacing DSPC with DPPS (Fig. 3.6B, right), the two points at the phase boundaries correspond to compositions of the coexisting Ld (blue circle) and Lo (red circle) phases. The corresponding Ld composition has 2 mol% PS, while the Lo composition has 24 mol% PS. In liposome pelleting assays shown in Fig. 3.6C, Gag-mNG and mNG-

KR12 behaved similarly, with binding correlated only with PS concentration, independent of membrane order. Both proteins bound to high-PS LUVs strongly and to low-PS LUVs weakly. In contrast, mNG-MARCKS and mNG-(Ev2)2 bound more strongly to LUVs with high PS in Ld, showing a 2-fold and 10-fold preference, respectively.

We next sought to confirm the liposome-pelleting results with a GUV assay that enables direct visualization of protein binding to membranes of controlled lipid composition. An advantage of GUVs having coexisting phases is that they allow competition for binding to portions of the membrane with distinct properties, such as membrane order. Three types of GUVs were prepared with lipid compositions similar to those for the LUVs shown in Fig. 3.6. The first type (PS in Ld; Fig. 3.7A, top) contained 24 mol% PS in Ld and 2 mol% PS in Lo. The second type (PS in Lo; Fig. 3.7A, middle) contained 2 mol% PS in Ld and 24 mol% PS in Lo. The third type of GUV (PS in Ld+Lo; Fig. 3.7A, bottom), contained 24 mol% PS in both Ld and Lo phases. LR-DOPE, a red fluorescent marker for the Ld phase, was added for all three types of GUVs (56) (see Materials and Methods for details).

In protein binding assays with GUVs, both mNG-KR12 and Gag-mNG bound similarly to the phase with high PS (24 mol%), whether it was Ld or Lo (Fig. 3.7C). For GUVs with high PS in both Ld and Lo, the ratio of protein bound to Ld compared with Lo was approximately 1, as quantified for over 80 GUVs (Fig. 3.7B). mNG-MARCKS also bound to GUVs with high PS in Ld and to GUVs with high PS in Lo. However, for the GUVs with high PS in both phases, the fluorescence intensity of mNG-MARCKS in the Ld phase was twice that of the Lo phase (Fig. 3.7B). Thus,

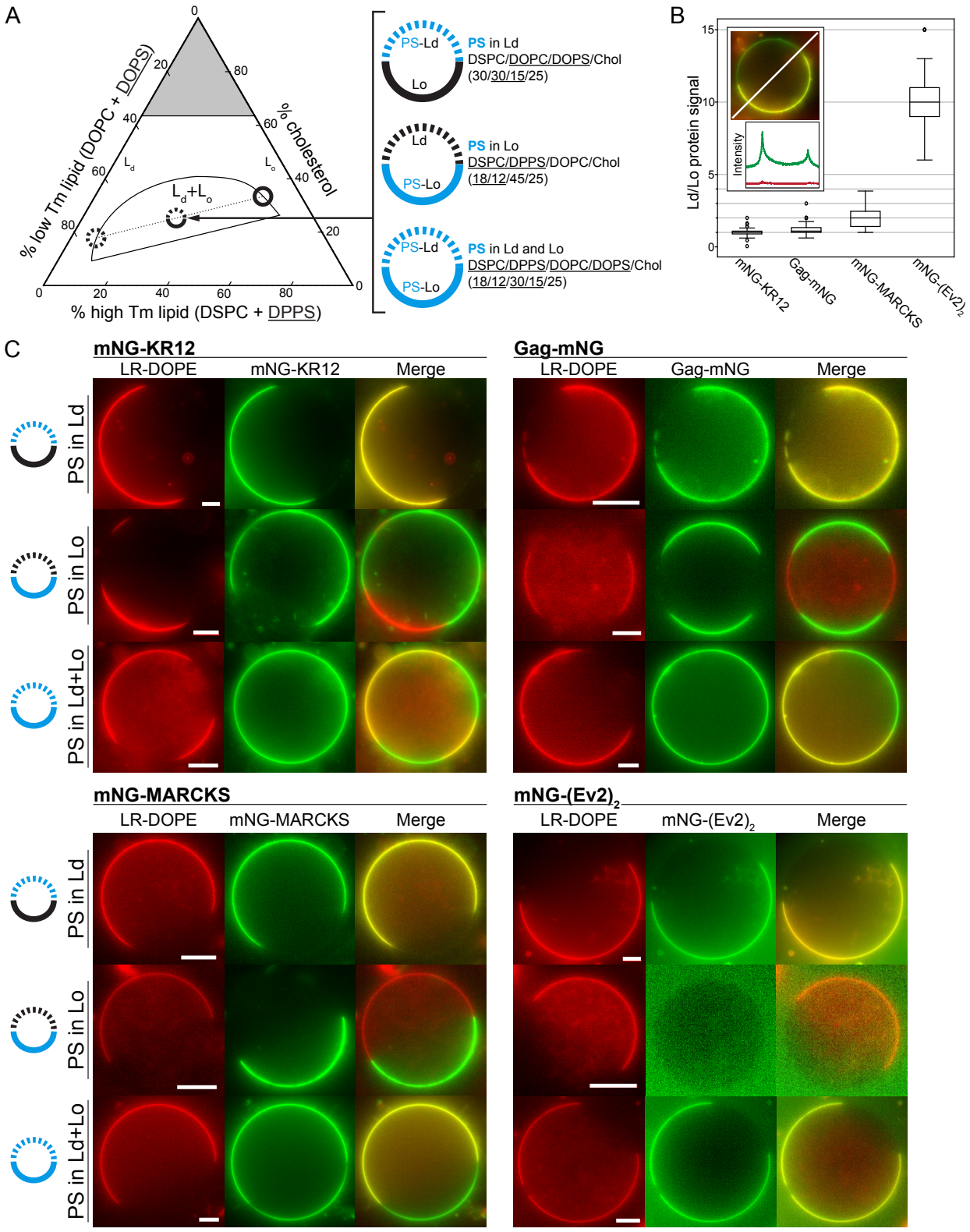
A
% low Tm lipid (DOPC + DOPS)
% high Tm lipid (DSPC + DPPS)
% cholesterol
L_d
L_o
L_d+L_o
PS-Ld
Lo
PS in Ld
DSPC/DOPC/DOPS/Chol
(30/30/15/25)
Ld
PS-Lo
PS in Lo
DSPC/DPPS/DOPC/Chol
(18/12/45/25)
PS-Ld
PS-Lo
PS in Ld and Lo
DSPC/DPPS/DOPC/DOPS/Chol
(18/12/30/15/25)
B
Ld/Lo protein signal
Intensity
mNG-KR12
Gag-mNG
mNG-MARCKS
mNG-(Ev2)2
C
mNG-KR12
LR-DOPE
mNG-KR12
Merge
Gag-mNG
LR-DOPE
Gag-mNG
Merge
mNG-MARCKS
LR-DOPE
mNG-MARCKS
Merge
mNG-(Ev2)2
LR-DOPE
mNG-(Ev2)2
Merge
PS in Ld
PS in Lo
PS in Ld+Lo

Fig 3.7 Protein binding to Ld+Lo GUVs. (A) DSPC/DOPC/Chol phase diagram. The dotted line drawn between the dashed circle (Ld) and solid circle (Lo) is the tieline that connects the compositions of the Ld and Lo phases that coexist. The circle at the center of the two-phase region of the phase diagram represents the overall composition that has split into the two coexisting phases. GUV lipid compositions are shown on the right, and the diagram depicts the location of PS enrichment in blue: top, PS in the Ld phase; middle, PS in the Lo phase; bottom, PS in both Ld and Lo phases. (B) Box plot shows the ratio of protein fluorescence in Ld phase to that in Lo phase when PS is in both phases. (Inset) Example of line-scan and intensity plot for mNG signal (green) and LR-DOPE (Ld phase marker; red). Box plots represent no fewer than 80 individual GUVs quantified for each protein-GUV binding assay at 50 mM NaCl, as described in Materials and Methods. (C) Representative fluorescence from wide-field microscopy images of protein (final concentration, ~1 μM) binding to phase-separated GUVs at 50 mM NaCl. GUV binding assays were performed on the three GUV compositions depicted in panel A. For each panel, the first column is LR-DOPE labeling of Ld phase (red channel), the middle column is mNG-tagged protein (green channel), and the right column shows LR-DOPE and mNG merged channels. Scale bar, 20 μm.

consistent with experiments using liposome pelleting, mNG-MARCKS has a modest preference for disordered membranes at the same PS concentration. Remarkably, the fluorescent PS sensor mNG-(Ev2)2 showed an even stronger preference for the Ld phase. It bound detectably only to the GUVs with a PS-rich Ld phase; in GUVs with the same high PS in both phases, it bound 10-fold more strongly to Ld than to Lo. In summary, the results both from liposome pelleting and GUVs demonstrate that RSV Gag-mNG behaves like the charge sensor mNG-KR12, independent of the membrane order. In contrast, mNG-(Ev2)2 and, to a lesser extent, mNG-MARCKS also recognize membrane order, preferring the disordered phase.

Effects of PI(4,5)P2, cholesterol, and multimerization on membrane binding

PI(4,5)P2 comprises approximately 2 mol% of total inner leaflet lipid (85) and contributes to the negative charge of the PM. This phosphoinositide is found at higher levels in viral membranes of HIV-1 and murine leukemia virus (MuLV) than in the PM (33), suggesting a role in retroviral assembly and budding (8). While HIV-1 MA has a specific PI(4,5)P2 binding pocket (3, 17), RSV MA has no known PI(4,5)P2 binding pocket. When PI(4,5)P2 was depleted in HIV-1 Gag-expressing cells by cotransfecting 5-phosphatase, most Gag was no longer PM localized and virus budding was reduced (8). In parallel experiments with RSV Gag and HIV-1 Gag, depleting PI(4,5)P2 affected PM association and viral budding much less for RSV than for HIV-1 (19). However, other researchers observed reduced RSV Gag PM localization and viral release in PI(4,5)P2-depleted cells but without a parallel assay

with HIV-1 Gag (20). Thus, the nature of the interactions in vivo between RSV Gag and PI(4,5)P2 remains unclear.

To further explore whether RSV Gag binds to PI(4,5)P2 through a specific lipid headgroup pocket or through electrostatic interactions, we compared RSV Gag with mNG-PH, which has a structured PI(4,5)P2 binding pocket (78, 80), and also with the mNG-based charge sensors, which have only unstructured basic tails (Fig. 3.8). Membrane binding was tested for mNG-KR8, Gag-mNG, and mNG-PH at 30 mol% PS and for mNG-KR12 and mNG-MARCKS at 20 mol% PS. The membrane binding of mNGKR12 and mNG-MARCKS at 30 mol% PS without Chol and without PI(4,5)P2 was already high and thus masked the Chol and PI(4,5)P2 effect. Therefore, we performed the assay at 20 mol% PS. At these PS concentrations the effects of cholesterol and PI(4,5)P2 were most pronounced (Fig. 3.8B). The additional PI(4,5)P2 increased membrane binding of mNG-KR8 slightly, and as expected it enhanced mNG-PH binding very strongly. Membrane association of mNG-KR12, mNG-MARCKS, and RSV Gag-mNG was significantly increased (Fig. 3.8), which implies that a protein being highly responsive to PI(4,5)P2 does not require a PI(4,5)P2 binding pocket. A similar inference was made previously in studies of the MARCKS peptide (63, 76).

Cholesterol increases HIV-1 Gag and RSV Gag binding to LUVs (10, 24). To address if this is a general effect for all peripheral membrane binding proteins, we tested Gag-mNG and, in parallel, the charge and lipid headgroup sensors (Fig. 3.8). Cholesterol added to 36 mol% increased the membrane binding of Gag-mNG and mNG-KR12 significantly, mNG-MARCKS mildly, but mNG-KR8 and mNG-PH not

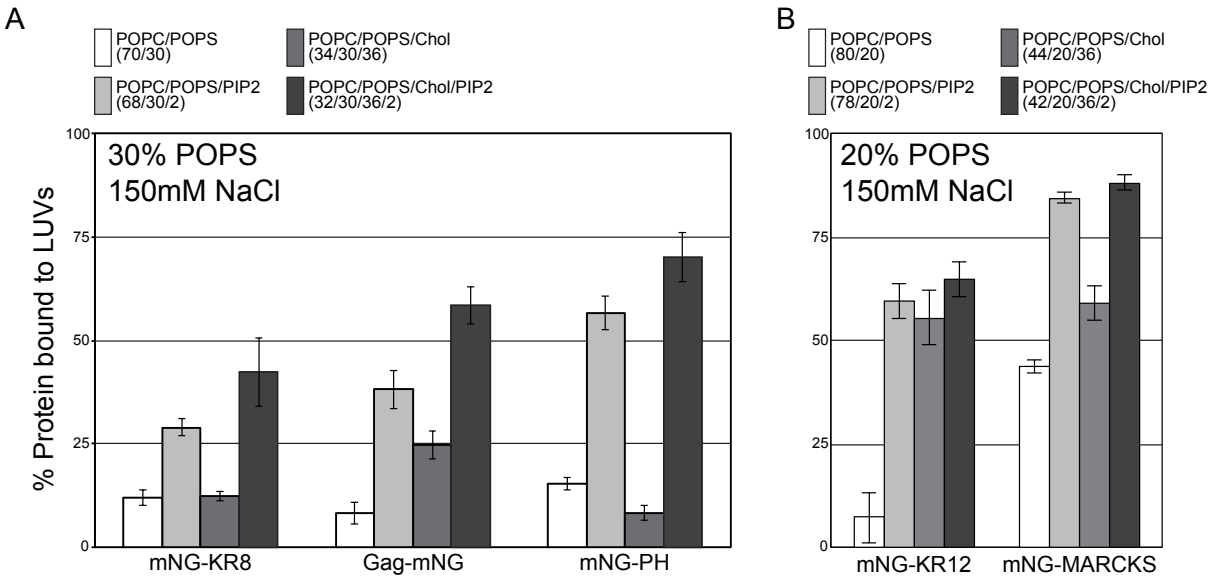

Fig 3.8 Effects of cholesterol and PI(4,5)P2 on protein-membrane binding. (A and B) Compositions of LUVs are shown at the top. PIP2 is short for PI(4,5)P2. (A) LUVs contained 30 mol% POPS; liposome-pelleting assays were at 150 mM NaCl. (B) LUVs contained 20 mol% POPS; liposome-pelleting assays were at 150 mM NaCl. Data are averages from no fewer than three independent liposome-pelleting assays; error bars represent standard deviations from the means.

at all. These data suggest that cholesterol enhances membrane interactions only for strong membrane binders such as RSV Gag-mNG and mNG-KR12 but has little effect on weak binders such as mNG-KR8.

To build upon the liposome-pelleting results, we used GUVs that did not have Ld+Lo phase separation to examine the effects of PI(4,5)P2 on membrane binding of RSV MA-mNG, Gag-mNG, and the charge sensors. GUVs were prepared with POPC/POPS/ Chol in the presence or absence of 2 mol% PI(4,5)P2. All of the proteins tested bound to GUVs uniformly but with different intensities (Fig. 3.9A). Protein-membrane binding was semiquantified by performing line scan analysis on at least 30 GUVs for each fluorescent protein, with subtraction of background fluorescence measured as far as possible from the GUV itself (Fig. 3.9B). Of note, all of the GUV binding assays were performed at 50 mM NaCl, which is lower than the level in the liposome-pelleting assays. As expected, mNG-PH bound weakly to GUVs with no PI(4,5)P2, similarly to mNG-KR4, while it bound 16-fold more strongly to GUVs with 2 mol% PI(4,5)P2 (Fig. 3.9B, far right column). PI(4,5)P2 increased GUV binding of mNG-KR12 about 3-fold above background and increased Gag-mNG binding by about 50%. These results are qualitatively consistent with those based on liposome pelleting (Fig. 3.8). In summary, these results show that PI(4,5)P2 stimulates membrane binding significantly not only for mNG-PH, which has a structured PI(4,5)P2 binding pocket, but also for the charge sensors. Thus, robust responses to PI(4,5)P2 can be entirely electrostatic.

Previous experiments suggested that the stronger membrane interaction of RSV Gag compared to that of MA is due to the capacity of Gag to multimerize (21)

A

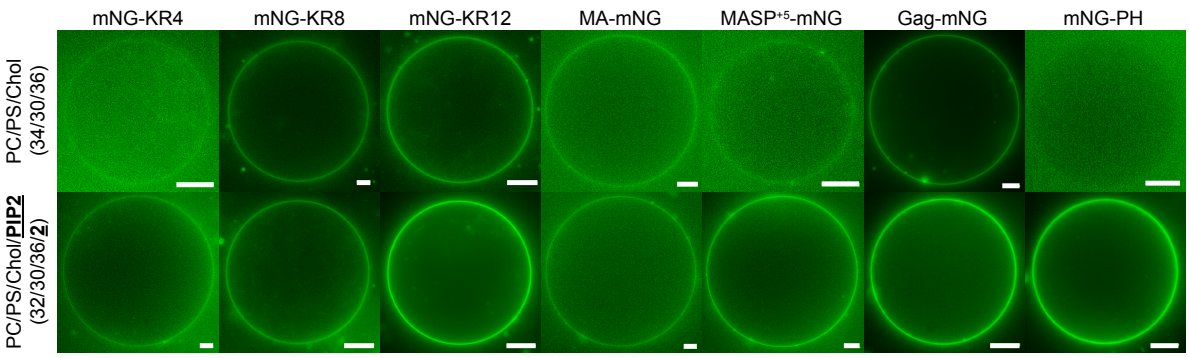

B Relative fluorescence intensity of membrane bound protein above background (%)

Protein	mNG-KR4	mNG-KR8	mNG-KR12	MA-mNG	MASP+5-mNG	Gag-mNG	mNG-PH
no PIP2	10% ± 1%	40% ± 3%	90% ± 22%	10% ± 3%	10% ± 2%	110% ± 15%	10% ± 3%
+2% PIP2	20% ± 4%	60% ± 12%	270% ± 33%	30% ± 3%	60% ± 5%	160% ± 8%	160% ± 13%

Fig 3.9 PI(4,5)P2 enhances binding of proteins to uniform POPC/POPS/Chol GUVs. (A) Representative images of GUV protein binding assays at 50 mM NaCl. For each protein a GUV binding assay was performed at least three times independently. Top row, POPC/POPS/Chol (34/30/36); bottom row, POPC/POPS/Chol/PI(4,5)P2 (32/30/36/2). All samples were imaged using the same microscope settings. Brightness and contrast for each image were not adjusted. The fluorescence that appears to be inside the GUVs is due to out-of-focus light. Scale bar, 20 μm. (B) Relative fluorescence intensity of membrane-bound protein above background. At least 30 individual GUVs and 2 line scans per GUV were quantified for each protein, as described in Materials and Methods. The relative percentage of protein binding above background is shown. The averages from at least 60 measurements are displayed ± standard deviations.

and not to the presence of the basic NC domain, which also has the capacity to interact with anionic lipids (86). At least in part, multimerization is induced by the formation of a six-helix bundle comprising the SP segment and short adjoining sequences of six Gag molecules (2, 87). Using the GUV assay, we tested the effects of PI(4,5)P2 on binding of a Gag protein missing NC but including the entire SP domain, MASP+5 -mNG (21). In the absence of PI(4,5)P2, MASP+5 -mNG bound to GUVs weakly, similar to MA-mNG. However, in the presence of PI(4,5)P2, the binding of MASP+5 -mNG was almost double that of MA-mNG, although it was lower than that of Gag-mNG, possibly due to a lack of positively charged NC domain. These results are consistent with the model in which membrane interaction of proteins lacking a specific binding pocket is stimulated by PI(4,5)P2 only for proteins that bind tightly (e.g., can multimerize).

DISCUSSION

The mechanism by which the retroviral Gag protein is targeted to the inner leaflet of the PM is complex and incompletely defined. At least for some retroviruses, the viral lipid composition differs from the composition of the plasma membrane, including an enrichment of the outer leaflet lipid SM and the inner leaflet lipids PS and plasmalogen-PE (30-32, 34, 35, 88). Both because high SM content is considered a characteristic of lipid rafts (27) and because, under some conditions, the viral Gag and Env proteins fractionate with raft markers in lysed cells (89, 90), retroviruses sometimes have been said to “bud from rafts” (27-29, 89). However, since rafts in living cells are poorly defined and nanoscopic (3) and since lipid mixtures like that

found in the inner leaflet do not form an Lo phase, the meaning of a putative raft association is unclear. The mechanism of Gag-membrane association probably is simplest for RSV, since this protein is unusual in not carrying a critical hydrophobic N-terminal myristate modification. From in vitro experiments, the isolated RSV MA domain previously was shown to interact with membranes electrostatically (22). A similar conclusion was reached for RSV Gag in vivo based on mutational analyses and quantitative budding assays (5). However, systematic analyses of the effect of lipid composition on the membrane binding properties of any purified Gag protein have not been reported previously. Lipid composition is known to dramatically influence HIV-1 Gag-membrane interaction in vitro, but the mechanism remains to be clarified (24).

In this study, we examined how membrane charge, acyl chain type, and membrane order influence the membrane binding of purified RSV Gag. Key to interpretation of the results were comparisons with purified nonviral control proteins. The latter included fluorescent proteins with added stretches of 4, 8, or 12 basic residues (charge sensors) or with added domains known to bind to specific lipid headgroups (lipid sensors). Membrane binding for all of the proteins was quantified both by pelleting assay with LUVs and by fluorescence assay with GUVs. Overall, the data showed that membrane interaction of RSV MA, Gag, and the charge sensors was sensitive to ionic strength, to PS concentration, and, for the charge sensors, also to the number of basic residues (5). Gag bound more strongly to acidic membranes than did MA, as shown previously (21, 53), presumably due to its ability to multimerize. Overall, these results confirm that electrostatics provides the primary driving force for RSV Gag membrane association. We also found that Gag binding was enhanced by

cholesterol. Gag preferred membranes with phospholipids containing different acyl chain saturations, possibly due to nonideal mixing (e.g., DSPC/DOPS/Chol or DOPC/DPPS/Chol). In contrast, the control proteins carrying the MARCKS peptide (mNG-MARCKS) or the PS headgroup-specific binding domain [mNG-(Ev2)2] preferred membranes with unsaturated lipids. Finally, Gag and the charge sensors showed no preference for liquid-ordered (Lo, i.e., raft-like) versus liquid-disordered (Ld) phases when these phases had the same PS composition, in striking contrast to mNG-(Ev2)2, for which Ld binding was at least 10-fold higher than for Lo.

Specially constructed fluorescent protein charge sensors have been used previously for in vivo and in vitro studies of PM binding proteins (79, 91). The mNG-KR4, mNG-KR8, and mNG-KR12 proteins obviously differ from MA or Gag in that the basic residues are sequential in the primary amino acid sequence and thus presumably are unstructured. In contrast, the basic residues in the membrane interacting face of MA domains of retroviruses are largely fixed and mostly not contiguous. Thus, detailed comparisons of the behavior of MA and the charge sensors may not be warranted. Nevertheless, of the three charge sensors that we constructed, the one with eight basic residues, mNG-KR8, in most assays behaved most similarly to MA-(mNG), consistent with the presence of up to 6 membrane-interacting lysine residues on the surface that is inferred to interact with the bilayer (5) (M. Doktorava, personal communication). For the purposes of this study, our first-order assumption was that K and R residues would be functionally similar. However, in fact the two proteins with lysine or arginine homopolymeric basic residues, mNG-K8 and mNG-R8, were not identical in their binding properties, with mNG-R8 interacting more

tightly with LUVs (data not shown). The mechanism underlying these differences is unclear.

Previous studies that sought to compare retroviral protein binding to Lo and Ld phases did not take into account the possibly different PS concentrations in each phase (60). For proteins with basic patches that bind to acidic lipids like PS, it is not possible to interpret preference for one phase over another without knowing how much PS is in each phase. It is not trivial to establish conditions in which Lo and Ld have the same PS concentration. In our studies, we started with a published phase diagram without PS (36, 48) and then performed FRET measurements to determine the new phase boundaries when PC was partially replaced with PS along a chosen tieline. The resulting phase boundaries then were used to find lipid compositions in which the PS concentration was identical in Ld and Lo. To our knowledge, this is the first study to systematically and rigorously compare the roles of membrane charge and membrane order on the interaction of a purified retroviral Gag protein with membranes.

Why does mNG-(Ev2)2 strongly prefer Ld over Lo phases, even when the concentration of the PS headgroups to which the protein binds is the same? From the crystal structure of Ev2 bound to PS (77), we speculate that hydrophobic residues in Ev2 that are close to the membrane become inserted in a shallow manner into the inner core of the bilayer, and that this insertion is disfavored in the Lo phase. Alternatively, perhaps the headgroups of PS in Ld have a slightly different conformation than those in Lo, for example, with different conformation around the glycerol backbone, which somehow disfavors binding. The former model seems more plausible, since mNG-MARCKS also shows preference for Ld, although this preference is less extreme. The

MARCKS peptide comprises not only 13 basic residues, which presumably are unstructured, but also 5 phenylalanine residues that might insert into the membrane (63, 85, 92). Mutational studies could address the mechanism of Ld preference for these two proteins.

The effects of cholesterol and acyl chains on binding of RSV Gag and the control proteins are difficult to interpret in a simple mechanistic way. While no detailed model fully accounts for the distinctive acyl chain preferences of Gag and the control proteins, we do have such a model for the cholesterol effect on MA binding, based on all-atom molecular dynamics simulations of membrane with bound protein and on calculations of surface potentials (M. Doktorova, personal communication). Cholesterol condenses the phospholipids in a bilayer, leading to an increase in charge density in the plane of the headgroups, thereby increasing negative surface potential.

Consistent with previous reports that PI(4,5)P2 enhanced HIV-1 Gag membrane binding (24), PI(4,5)P2 also enhanced the membrane binding of all proteins tested. There is a known PI(4,5)P2 binding pocket in HIV-1 Gag but no known PI(4,5)P2 binding pocket in RSV Gag. Here, we found that 2 mol% PI(4,5)P2 not only enhanced the membrane binding of the PI(4,5)P2 sensor PH that has a specific binding pocket but also enhanced the membrane binding of the charge sensors, such as mNG-KR12 and mNG-MARCKS, which have no structured binding pocket. The finding for MARCKS is also consistent with the previous finding that the MARCKS peptide itself responds to PI(4,5)P2 significantly (63, 75, 76, 85, 93). PI(4,5)P2 has 3 to 4 negative charges, which creates higher local charge density than PS. PI(4,5)P2 can enhance protein membrane binding through electrostatic interactions or through specific

binding pockets. Even though it is still not clear whether RSV Gag has a PI(4,5)P2 binding pocket, we showed that a specific binding pocket is not required for a protein to be highly responsive to the presence of PI(4,5)P2. We also observed that MA-mNG and MASP+5 -mNG bound to membranes to a similar level in the absence of PI(4,5)P2, whereas MASP+5 -mNG and hexameric MA showed higher membrane binding than monomeric MA in the presence of PI(4,5)P2, suggesting multimerization enhances membrane binding or PI(4,5)P2 enhances multimerization. In our study, we used both pelleting assays with LUVs and fluorescence assay with GUVs to study protein membrane interactions. The majority of both results were comparable. For example, when examining whether protein binding follows membrane charge or membrane order, we tested protein binding using Ld and Lo coexisting GUVs and uniform LUVs that mimic each phase. Both assays gave the same readout of a high PS Ld/high PS Lo protein-bound ratio. We also employed both assays for probing the effect of PI(4,5)P2, in which PI(4,5)P2 was shown to increase membrane binding of all tested proteins. The similarity in results between GUVs and LUVs implies that membrane curvature is not a major factor affecting protein binding. However, the two assays also have a few minor discrepancies. Most liposome pelleting assays were done at 150 mM NaCl, whereas for technical reasons all of the protein GUV binding assays were done at 50 mM NaCl. This difference in ionic strength probably explains why PI(4,5)P2 enhanced Gag-mNG to different levels. The two membrane binding assays complement each other. On the one hand, LUV pelleting has the advantage of being more efficient, flexible, and rapid at testing various protein-membrane combinations. LUVs also are less likely to have composition variation, since LUVs are prepared

through RSE, which is designed to bypass the dry lipid film state to avoid lipid demixing (68, 94). On the other hand, GUV image analysis not only enables direct visualization of protein membrane binding but also enables quantification of simultaneous and competitive protein binding.

In summary, we employed biochemical and biophysical approaches to elucidate that membrane charges provide RSV Gag the primary driving force for associating with membranes, while membrane order barely affects RSV membrane binding. However, membrane order clearly does influence the membrane association of the cellular protein domain MARCKS and the PS sensor Evectin2. The results shown here for RSV will serve as a platform for further studies with other retroviral proteins like HIV-1 Gag, as well as cellular proteins that interact with the inner leaflet of the PM.

ACKNOWLEDGMENTS

Frederick A. Herberle helped with FRET data analysis and plotting, and David G. Ackerman generated boxplots for GUV analysis. We thank the National Biomedical Center for Advanced ESR Technology at Cornell University and Siddarth Chandrasekaran and Milka Doktorova for help with ESR data collection and analysis.

REFERENCES

1. Sundquist WI, Krausslich HG. 2012. HIV-1 assembly, budding, and maturation. Cold Spring Harb Perspect Med. 2:a006924.
2. Bush DL, Vogt VM. 2014. In vitro assembly of retroviruses. Annu Rev Virol. 1:561-580.
3. Dick RA, Vogt VM. 2014. Membrane interaction of retroviral Gag proteins. Front Microbiol. 5:187.
4. Murray PS, Li Z, Wang J, Tang CL, Honig B, Murray D. 2005. Retroviral matrix domains share electrostatic homology: models for membrane binding function throughout the viral life cycle. Structure. 13:1521-1531.
5. Callahan EM, Wills JW. 2000. Repositioning basic residues in the M domain of the Rous sarcoma virus Gag protein. J Virol. 74:11222-11229.
6. Nelle TD, Wills JW. 1996. A large region within the Rous sarcoma virus matrix protein is dispensable for budding and infectivity. J Virol. 70:2269-2276.
7. Wills JW, Craven RC, Weldon RJ, Nelle TD, Erdie CR. 1991. Suppression of retroviral MA deletions by the amino-terminal membrane-binding domain of p60src. J Virol. 65:3804-3812.
8. Ono A, Ablan SD, Lockett SJ, Nagashima K, Freed EO. 2004. Phosphatidylinositol (4,5) bisphosphate regulates HIV-1 Gag targeting to the plasma membrane. Proc Natl Acad Sci.101:14889-14894.
9. Prchal J, Srb P, Hunter E, Ruml T, Hrabal R. 2012. The structure of myristoylated Mason-Pfizer monkey virus matrix protein and the role of phosphatidylinositol-(4,5)-bisphosphate in its membrane binding. J Mol Biol. 423:427-438.
10. Dick RA, Datta SAK, Nanda H, Fang X, Wen Y, Barros M, Wang Y-X, Rein A, Vogt VM. 2015. Hydrodynamic and membrane binding properties of purified Rous sarcoma virus Gag protein. J Virol. 89:10371-10382.
11. Saad JS, Ablan SD, Ghanam RH, Kim A, Andrews K, Nagashima K, Soheilian F, Freed EO, Summers MF. 2008. Structure of the myristylated human immunodeficiency virus type 2 matrix protein and the role of phosphatidylinositol-(4,5)-bisphosphate in membrane targeting. J Mol Biol. 382:434-447.

12. Inlora J, Collins DR, Trubin ME, Chung JY, Ono A. 2014. Membrane binding and subcellular localization of retroviral Gag proteins are differentially regulated by MA interactions with phosphatidylinositol-(4,5)-bisphosphate and RNA. mBio. 5:e02202.
13. Chukkapalli V, Hogue IB, Boyko V, Hu W-S, Ono A. 2008. Interaction between the human immunodeficiency virus type 1 Gag matrix domain and phosphatidylinositol-(4,5)-bisphosphate is essential for efficient Gag membrane binding. J Virol. 82:2405-2417.
14. Rein A, McClure MR, Rice NR, Luftig RB, Schultz AM. 1986. Myristylation site in Pr65gag is essential for virus particle formation by Moloney murine leukemia virus. Proc Natl Acad Sci. 83:7246-7250.
15. Bryant M, Ratner L. 1990. Myristoylation-dependent replication and assembly of human immunodeficiency virus 1. Proc Natl Acad Sci. 87:523-527.
16. Gottlinger HG, Sodroski JG, Haseltine WA. 1989. Role of capsid precursor processing and myristoylation in morphogenesis and infectivity of human immunodeficiency virus type 1. Proc Natl Acad Sci. 86:5781-5785.
17. Saad JS, Miller J, Tai J, Kim A, Ghanam RH, Summers MF. 2006. Structural basis for targeting HIV-1 Gag proteins to the plasma membrane for virus assembly. Proc Natl Acad Sci. 103:11364-11369.
18. Shkriabai N, Datta SA, Zhao Z, Hess S, Rein A, Kvaratskhelia M. 2006. Interactions of HIV-1 Gag with assembly cofactors. Biochemistry. 45:4077-4083.
19. Chan J, Dick RA, Vogt VM. 2011. Rous sarcoma virus Gag has no specific requirement for phosphatidylinositol-(4,5)-bisphosphate for plasma membrane association in vivo or for liposome interaction in vitro. J Virol. 85:10851-10860.
20. Nadaraia-Hoke S, Bann DV, Lochmann TL, Gudleski-O'Regan N, Parent LJ. 2013. Alterations in the MA and NC domains modulate phosphoinositide-dependent plasma membrane localization of the Rous sarcoma virus Gag protein. J Virol. 87:3609-3615.

21. Dick RA, Kamynina E, Vogt VM. 2013. Effect of multimerization on membrane association of Rous sarcoma virus and HIV-1 matrix domain proteins. J Virol. 87:13598-13608.
22. Dalton AK, Murray PS, Murray D, Vogt VM. 2005. Biochemical characterization of rous sarcoma virus MA protein interaction with membranes. J Virol. 79:6227-6238.
23. Dalton AK, Ako-Adjei D, Murray PS, Murray D, Vogt VM. 2007. Electrostatic interactions drive membrane association of the human immunodeficiency virus type 1 Gag MA domain. J Virol. 81:6434-6445.
24. Dick RA, Goh SL, Feigenson GW, Vogt VM. 2012. HIV-1 Gag protein can sense the cholesterol and acyl chain environment in model membranes. Proc Natl Acad Sci. 109:18761-18766.
25. van Meer G, Voelker DR, Feigenson GW. 2008. Membrane lipids: where they are and how they behave. Nat Rev Mol Cell Biol. 9:112-124.
26. Verkleij AJ, Zwaal RFA, Roelofsen B, Comfurius P, Kastelijn D, Van Deenen LLM. 1973. The asymmetric distribution of phospholipids in the human red cell membrane. A combined study using phospholipases and freeze-etch electron microscopy. Biochimica et Biophysica Acta (BBA) - Biomembrans. 323:178-193.
27. Simons K, Ikonen E. 1997. Functional rafts in cell membranes. Nature. 387:569-572.
28. Mañes S, del Real G, Martínez-A C. 2003. Pathogens: raft hijackers. Nat Rev Immunology 3:557-568.
29. Knipe DM, Howley PM. 2007. Fields Virology. Lippincott Williams & Wilkins. Fifth Edition, Section 1, General Virol. 194.
30. Quigley JP, Rifkin DB, Reich E. 1971. Phospholipid composition of Rous sarcoma virus, host cell membranes and other enveloped RNA viruses. Virology. 46:106-116.
31. Quigley JP, Rifkin DB, Reich E. 1972. Lipid studies of Rous sarcoma virus and host cell membranes. Virology. 50:550-557.

32. Aloia RC, Tian H, Jensen FC. 1993. Lipid composition and fluidity of the human immunodeficiency virus envelope and host cell plasma membranes. Proc Natl Acad Sci. 90:5181-5185.
33. Chan R, Uchil PD, Jin J, Shui G, Ott DE, Mothes W, Wenk MR. 2008. Retroviruses human immunodeficiency virus and murine leukemia virus are enriched in phosphoinositides. J Virol. 82:11228-11238.
34. Brugger B, Glass B, Haberkant P, Leibrecht I, Wieland FT, Krausslich HG. 2006. The HIV lipidome: a raft with an unusual composition. Proc Natl Acad Sci. 103:2641-2646.
35. Lorizate M, Sachsenheimer T, Glass B, Habermann A, Gerl MJ, Kräusslich H-G, Brügger B. 2013. Comparative lipidomics analysis of HIV-1 particles and their producer cell membrane in different cell lines. Cellular microbiol 15:292-304.
36. Zhao J, Wu J, Heberle FA, Mills TT, Klawitter P, Huang G, Costanza G, Feigenson GW. 2007. Phase studies of model biomembranes: complex behavior of DSPC/DOPC/cholesterol. Biochimica et Biophysica Acta. 1768:2764-2776.
37. Petruzielo RS, Heberle FA, Drazba P, Katsaras J, Feigenson GW. 2013. Phase behavior and domain size in sphingomyelin-containing lipid bilayers. Biochimica et Biophysica Acta (BBA) - Biomembranes 1828:1302-1313.
38. Konyakhina TM, Feigenson GW. 2016. Phase diagram of a polyunsaturated lipid mixture: Brain sphingomyelin/1-stearoyl-2-docosahexaenoyl-sn-glycero-3-phosphocholine/cholesterol. Biochimica et Biophysica Acta (BBA) - Biomembranes 1858:153-161.
39. Feigenson GW, Buboltz JT. 2001. Ternary phase diagram of dipalmitoyl-pc/dilauroyl-pc/cholesterol: nanoscopic domain formation driven by cholesterol. Biophys J. 80:2775-2788.
40. Nguyen DH, Hildreth JEK. 2000. Evidence for budding of human immunodeficiency virus type 1 selectively from glycolipid-enriched membrane lipid rafts. J Virol. 74:3264-3272.

41. Ding L, Derdowski A, Wang JJ, Spearman P. 2003. Independent segregation of human immunodeficiency virus type 1 Gag protein complexes and lipid rafts. J Virol. 77:1916-1926.
42. Halwani R, Khorchid A, Cen S, Kleiman L. 2003. Rapid localization of Gag/GagPol complexes to detergent-resistant membrane during the assembly of human immunodeficiency virus type 1. J Virol. 77:3973-3984.
43. Holm K, Weclewicz K, Hewson R, Suomalainen M. 2003. Human immunodeficiency virus type 1 assembly and lipid rafts: Pr55(Gag) associates with membrane domains that are largely resistant to Brij98 but sensitive to Triton X-100. J Virol. 77:4805-4817.
44. Brown DA. 2006. Lipid rafts, detergent-resistant membranes, and raft targeting signals. Physiology. 21:430-439.
45. Feigenson GW. 2006. Phase behavior of lipid mixtures. Nat Chem Biol. 2:560-563.
46. Heberle FA, Feigenson GW. 2011. Phase separation in lipid membranes. Cold Spring Harb Perspect Biol. 3:a004630-a004630.
47. Feigenson GW. 2009. Phase diagrams and lipid domains in multicomponent lipid bilayer mixtures. Biochimica et Biophysica Acta (BBA) - Biomembranes 1788:47-52.
48. Konyakhina TM, Wu J, Mastroianni JD, Heberle FA, Feigenson GW. 2013. Phase diagram of a 4-component lipid mixture: DSPC/DOPC/POPC/chol. Biochimica et Biophysica Acta 1828:2204-2214.
49. Goh SL, Amazon JJ, Feigenson GW. 2013. Toward a better raft model: modulated phases in the four-component bilayer, DSPC/DOPC/POPC/Chol. Biophys J. 104:853-862.
50. Veatch SL, Keller SL. 2005. Miscibility phase diagrams of giant vesicles containing sphingomyelin. Phys Rev Lett. 94:148101.
51. Feigenson GW. 2007. Phase boundaries and biological membranes. Annu Rev Biophys Biomol Struc. 36:63-77.

52. Lingwood D, Simons K. 2010. lipid rafts as a membrane-organizing principle. Science. 327:46-50.
53. Dick RA, Barros M, Jin D, Lösche M, Vogt VM. 2015. Membrane binding of the Rous sarcoma virus Gag protein is cooperative and dependent on the SPA domain. J Virol. 90:2473-2485.
54. Wesołowska O, Michalak K, Maniewska J. 2009. Giant unilamellar vesicles—a perfect tool to visualize phase separation and lipid rafts in model systems. Acta Biochim Pol. 56:33-39.
55. Pott T, Bouvrais H, Méléard P. 2008. Giant unilamellar vesicle formation under physiologically relevant conditions. Chem and Phys of Lipids 154:115-119.
56. Baumgart T, Hunt G, Farkas ER, Webb WW, Feigenson GW. 2007. Fluorescence probe partitioning between Lo/Ld phases in lipid membranes. Biochimica et Biophysica Acta (BBA) - Biomembranes 1768:2182-2194.
57. Chiang Y-W, Costa-Filho AJ, Freed JH. 2007. Dynamic molecular structure and phase diagram of DPPC−Cholesterol binary mixtures: A 2D-ELDOR Study. J Phys Chem B. 111:11260-11270.
58. Carlson LA, Hurley JH. 2012. In vitro reconstitution of the ordered assembly of the endosomal sorting complex required for transport at membrane-bound HIV-1 Gag clusters. Proc Natl Acad Sci.109:16928-16933.
59. Olety B, Veatch SL, Ono A. 2015. PI(4,5)P2 acyl chains differentiate membrane binding of HIV-1 Gag from that of the phospholipase Cδ1 PH domain. J Virol. 89:7861-7873.
60. Keller H, Krausslich HG, Schwille P. 2013. Multimerizable HIV Gag derivative binds to the liquid-disordered phase in model membranes. Cellular Microbiol. 15:237-247.
61. Malakhov MP, Mattern MR, Malakhova OA, Drinker M, Weeks SD, Butt TR. 2004. SUMO fusions and SUMO-specific protease for efficient expression and purification of proteins. J Struc and Func Genomics 5:75-86.
62. Shaner NC, Lambert GG, Chammas A, Ni Y, Cranfill PJ, Baird MA, Sell BR, Allen JR, Day RN, Israelsson M, Davidson MW, Wang J. 2013. A bright

monomeric green fluorescent protein derived from Branchiostoma lanceolatum. Nat Methods 10:407-409.

63. Gambhir A, Hangyás-Mihályné G, Zaitseva I, Cafiso DS, Wang J, Murray D, Pentyala SN, Smith SO, McLaughlin S. 2004. Electrostatic sequestration of PIP2 on phospholipid membranes by basic/aromatic regions of proteins. Biophys J. 86:2188-2207.
64. Murray D, Ben-Tal N, Honig B, McLaughlin S. 1997. Electrostatic interaction of myristoylated proteins with membranes: simple physics, complicated biology. Structure. 5:985-989.
65. Uchida Y, Hasegawa J, Chinnapen D, Inoue T, Okazaki S, Kato R, Wakatsuki S, Misaki R, Koike M, Uchiyama Y, Iemura S, Natsume T, Kuwahara R, Nakagawa T, Nishikawa K, Mukai K, Miyoshi E, Taniguchi N, Sheff D, Lencer WI, Taguchi T, Arai H. 2011. Intracellular phosphatidylserine is essential for retrograde membrane traffic through endosomes. Proc Natl Acad Sci. 108:15846-15851.
66. Marblestone JG, Edavettal SC, Lim Y, Lim P, Zuo X, Butt TR. 2006. Comparison of SUMO fusion technology with traditional gene fusion systems: Enhanced expression and solubility with SUMO. Protein Science. 15:182-189.
67. Kingsley PB, Feigenson GW. 1979. Synthesis of a perdeuterated phospholipid - 1,2-dimyristoyl-sn-glycero-3-phosphocholine-d72. Chem Phys Lipids. 24:135-147.
68. Buboltz JT, Feigenson GW. 1999. A novel strategy for the preparation of liposomes: rapid solvent exchange. Biochimica et Biophysica Acta (BBA) - Biomembranes 1417:232-245.
69. Kaasgaard T, Mouritsen OG, Jørgensen K. 2003. Freeze/thaw effects on lipid-bilayer vesicles investigated by differential scanning calorimetry. Biochimica et Biophysica Acta (BBA) - Biomembranes. 1615:77-83.
70. Schorn K, Marsh D. 1997. Lipid mixing in dimyristoyl phosphatidylcholine-dimyristoyl glycerol dispersions: spin label ESR studies. Biochimica et Biophysica Acta (BBA) - Biomembranes. 1323:57-64.

71. Heberle FA, Buboltz JT, Stringer D, Feigenson GW. 2005. Fluorescence methods to detect phase boundaries in lipid bilayer mixtures. Biochimica et Biophysica Acta (BBA) - Mol Cell Res. 1746:186-192.
72. Buboltz JT. 2007. Steady-state probe-partitioning fluorescence resonance energy transfer: a simple and robust tool for the study of membrane phase behavior. Phys Rev E. 76:021903.
73. Jiang Z, Redfern RE, Isler Y, Ross AH, Gericke A. 2014. Cholesterol stabilizes fluid phosphoinositide domains. Chem and Phys of Lipids. 182:52-61.
74. Morales-Penningston NF, Wu J, Farkas ER, Goh SL, Konyakhina TM, Zheng JY, Webb WW, Feigenson GW. 2010. GUV preparation and imaging: Minimizing artifacts. Biochimica et Biophysica Acta (BBA) - Biomembranes 1798:1324-1332.
75. Glaser M, Wanaski S, Buser CA, Boguslavsky V, Rashidzada W, Morris A, Rebecchi M, Scarlata SF, Runnels LW, Prestwich GD, Chen J, Aderem A, Ahn J, McLaughlin S. 1996. Myristoylated alanine-rich c kinase substrate (MARCKS) produces reversible inhibition of phospholipase C by sequestering phosphatidylinositol 4,5-bisphosphate in lateral domains. J. Biol Chem. 271:26187-26193.
76. Golebiewska U, Gambhir A, Hangyás-Mihályné G, Zaitseva I, Rädler J, McLaughlin S. 2006. Membrane-bound basic peptides sequester multivalent (PIP2), but not monovalent (PS), acidic lipids. Biophys J. 91:588-599.
77. Okazaki S, Kato R, Uchida Y, Taguchi T. 2012. Structural basis of the strict phospholipid binding specificity of the pleckstrin homology domain of human evectin-2. Acta Crystallographica Section D: Biological Crystallography, 68:117-123.
78. Harlan JE, Hajduk PJ, Yoon HS, Fesik SW. 1994. Pleckstrin homology domains bind to phosphatidylinositol-4, 5-bisphosphate. Nature. 371:168-170.
79. Yeung T, Gilbert GE, Shi J, Silvius J, Kapus A, Grinstein S. 2008. Membrane phosphatidylserine regulates surface charge and protein localization. Science. 319:210-213.

80. Garcia P, Gupta R, Shah S, Morris AJ, Rudge SA, Scarlata S, Petrova V, McLaughlin S, Rebecchi MJ. 2002. The pleckstrin homology domain of phospholipase C-delta1 binds with high affinity to phosphatidylinositol 4,5-bisphosphate in bilayer membranes. Biochemistry. 34:16228-16234.
81. Singh SM, Murray D. 2003. Molecular modeling of the membrane targeting of phospholipase C pleckstrin homology domains. Protein Sci. 12:1934-1953.
82. Huang J, Swanson JE, Dibble AR, Hinderliter AK, Feigenson GW. 1993. Nonideal mixing of phosphatidylserine and phosphatidylcholine in the fluid lamellar phase. Biophys J. 64:413-425.
83. Swanson JE, Feigenson GW. 1990. Thermodynamics of mixing of phosphatidylserine/phosphatidylcholine from measurements of high-affinity calcium binding. Biochemistry. 29:8291-8297.
84. Heberle FA, Wu J, Goh SL, Petruzielo RS, Feigenson GW. 2010. Comparison of three ternary lipid bilayer mixtures: FRET and ESR reveal nanodomains. Biophys J. 99:3309-3318.
85. McLaughlin S, Murray D. 2005. Plasma membrane phosphoinositide organization by protein electrostatics. Nature. 438:605-611.
86. Datta SA, Heinrich F, Raghunandan S, Krueger S, Curtis JE, Rein A, Nanda H. 2011. HIV-1 Gag extension: conformational changes require simultaneous interaction with membrane and nucleic acid. J Mol Biol. 406:205-214.
87. Bush DL, Monroe EB, Bedwell GJ, Prevelige PE, Phillips JM, Vogt VM. 2014. Higher-order structure of the Rous sarcoma virus SP assembly domain. J Virol. 88:5617-5629.
88. Quigley JP, Rifkin DB, Reich E. 1971. Phospholipid composition of Rous sarcoma virus, host cell membranes and other enveloped RNA viruses. Virology. 46:106-116.
89. Pessin JE, Glaser M. 1980. Budding of Rous sarcoma virus and vesicular stomatitis virus from localized lipid regions in the plasma membrane of chicken embryo fibroblasts. J. Biol Chem. 255:9044-9050.

90. Leung K, Kim J-O, Ganesh L, Kabat J, Schwartz O, Nabel GJ. 2008. HIV-1 assembly: viral glycoproteins segregate quantally to lipid rafts that associate individually with HIV-1 capsids and virions. Cell Host & Microbe. 3:285-292.
91. Ono A. 2010. Relationships between plasma membrane microdomains and HIV-1 assembly. Biol Cell. 102:335-350.
92. Yeung T, Terebiznik M, Yu L, Silvius J, Abidi WM, Philips M, Levine T, Kapus A, Grinstein S. 2006. Receptor activation alters inner surface potential during phagocytosis. Science. 313:347-351.
93. Zhang W, Crocker E, McLaughlin S, Smith SO. 2003. Binding of peptides with basic and aromatic residues to bilayer membranes: phenylalanine in the myristoylated alanine-rich C kinase substrate effector domain penetrates into the hydrophobic core of the bilayer. J. Biol Chem. 278:21459- 21466.
94. McLaughlin S, Wang J, Gambhir A, Murray D. 2002. PIP2 and proteins: interactions, organization, and information flow. Annu Rev Biophys Biomol Struc. 31:151-175.
95. Buboltz JT. 2009. A more efficient device for preparing model-membrane liposomes by the rapid solvent exchange method. Rev Sci Instrum. 80:124301-124305.

CHAPTER 4

MULTIVALENT CATION-BRIDGED PI(4,5)P_2 CLUSTERS FORM AT VERY LOW CONCENTRATIONS[3]

ABSTRACT

Phosphatidylinositol 4,5-bisphosphate (PI(4,5)P_2 or PIP2), is a key component of the inner leaflet of the plasma membrane in eukaryotic cells. In model membranes, PIP2 has been reported to form clusters, but whether these locally different conditions could give rise to distinct pools of unclustered and clustered PIP2 is unclear. By use of both fluorescence self-quenching and Förster resonance energy transfer assays, we have discovered that PIP2 self-associates at remarkably low concentrations starting below 0.05 mol% of total lipids. Formation of these clusters was dependent on physiological divalent metal ions, such as Ca^{2+}, Mg^{2+}, Zn^{2+}, or trivalent ions Fe^{3+} and Al^{3+}. Formation of PIP2 clusters was also headgroup-specific, being largely independent of the type of acyl chain. The similarly labeled phospholipids phosphatidylcholine, phosphatidylethanolamine, phosphatidylserine, and phosphatidylinositol exhibited no such clustering. However, six phosphoinositide species co-clustered with PIP2. The

[3] The following chapter is reproduced from: Wen, Yi, Volker M. Vogt, and Gerald W. Feigenson. 2018. Multivalent cation-bridged PI (4, 5) P2 clusters form at very low concentrations. *Biophy J.* 114: 2630-2639.

degree of PIP2 cation clustering was significantly influenced by the composition of the surrounding lipids, with cholesterol and phosphatidylinositol enhancing this behavior. We propose that PIP2 cation-bridged cluster formation, which might be similar to micelle formation, can be used as a physical model for what could be distinct pools of PIP2 in biological membranes. To our knowledge, this study provides the first evidence of PIP2 forming clusters at such low concentrations. The property of PIP2 to form such clusters at such extremely low concentrations in model membranes reveals, to our knowledge, a new behavior of PIP2 proposed to occur in cells, in which local multivalent metal ions, lipid compositions, and various binding proteins could greatly influence PIP2 properties. In turn, these different pools of PIP2 could further regulate cellular events.

INTRODUCTION

Phosphatidylinositol 4,5-bisphosphate, or PI(4,5)P2 (PIP2), is the major phosphoinositide phosphate species in mammalian cells. Located mainly at the plasma membrane (PM) inner leaflet at 1-2 mol% (1,2), PIP2 is a key player in numerous cellular signaling pathways (3). For example, PIP2 hydrolysis is catalyzed by phospholipase C to generate two second messengers: diacylglycerol and inositol 1,4,5-triphosphate (4,5). PIP2 is also the precursor of another important lipid second messenger, Phosphatidylinositol (3,4,5)-trisphosphate [PI(3,4,5)P3] (6). PIP2 is known to interact with hundreds of different proteins, playing important roles in a broad spectrum of cellular functions, including exocytosis/endocytosis (7), endosomal trafficking (8,9), cytoskeleton assembly (10), cell polarization, cell migration (3), and

ion channel control (11). PIP2 also facilitates assembly of viruses such as human immunodeficiency virus 1 (12-14). What seem to be local membrane enrichments of PIP2 have led to the hypothesis that distinct pools of PIP2 exist in cells (8,9,15).

Although PIP2 appears to form clusters in vitro (16), an understanding of this process has remained elusive, in part because the physical basis of this molecular aggregation is unclear. Many previous studies were based on non-physiological conditions, for example, PIP2 concentrations much greater than the 1-2 mol% in the PM or else bulk lipid compositions, e.g., only phosphatidylcholine (PC) not reflecting the PM inner leaflet where most PIP2 is found in cells (17-19). One type of PIP2 cluster involves hydrogen-bonding networks revealed by nuclear magnetic resonance studies (20-22). A different type of PIP2 cluster is based on divalent metal ions Ca^{2+} or Mg^{2+} bridging headgroup phosphates (18,19,23-27). Complementing these experimental approaches, molecular dynamics simulations also showed that Ca^{2+} altered PIP2 properties and induced PIP2 cluster formation (28,29).

Some evidence suggests that PIP2 cluster formation also occurs in cells or in unfixed (30,31) or rapidly frozen (32) membrane sheets prepared from cells. PIP2 microdomains have been visualized indirectly primarily by PIP2-specific binding proteins with fluorescent tags, e.g., the pleckstrin homology domain of phospholipase C δ1 or by PIP2 antibodies (31,33). Most PIP2 studies in cells have focused on PIP2 association driven by cellular PIP2-binding proteins (16,34,35), such as myristoylated alanine-rich C-kinase substrate, which appears to modulate the PIP2 distribution at the inner leaflet during various cellular events (2,16,36,37). But whether PIP2 forms clusters in cells without the influence of binding proteins or antibodies is unexplored.

No direct experimental data have been reported that show maximal solubility of free PIP2 in model membranes, above which clustering occurs. Such high-order aggregation is well known for micelle formation (38). As we show, characterizing PIP2 behavior starting at concentrations of >0.1 mol% misses the origin of PIP2-PIP2 association. Here, we used a traditional approach of surface and colloid chemistry to study micelle formation or phase separation (39). We started with a very low PIP2 concentration and examined its self-aggregation behavior over a wide concentration range from 0.01 up to 2 mol%, exploiting the sensitive assays of self-quenching and Förster resonance energy transfer (FRET). Self-association showed a distinct starting concentration that we term the ‘‘critical PIP2 concentration’’ (CPC). The CPC was remarkably low, i.e., 0.02-0.05 mol% of total lipids, in well-defined, chemically simplified model lipid bilayer mixtures that mimic the inner leaflet lipid composition. Multivalent metal ions were absolutely required for this type of PIP2- PIP2 association. Without special precautions, such metal ions typically contaminate buffers and are leached from glass, complicating interpretations of previous reports on PIP2 behavior.

MATERIALS AND METHODS

Phospholipids and fluorescent probes

1-palmitoyl-2-oleoyl-sn-glycero-3-phosphoethanolamine (POPE), 1-palmitoyl-2-oleoyl-sn-glycero-3-phospho-L-serine (POPS), 1-palmitoyl-2-oleoylsn-glycero-3-phosphocholine (POPC), L-a-phosphatidylinositol (bovine liver PI), L-a-phosphatidylinositol-4,5-bisphosphate (bovine brain-PI(4,5) P2), brain-PI4P,

18:1/18:1 PI3P, PI4P, PI5P, PI(3,4)P2, PI(3,5)P2, PI(4,5)P2, PI(3,4,5)P3, 18:0/20:4 PI(4,5)P2, and fluorescently labeled TopFluor (TF)- PI(4,5)P2 (1-oleoyl-2-{6-[4-(dipyrromethene boron difluoride)butanoyl] amino}hexanoyl-sn-glycero-3-phosphoinositol-4,5-bisphosphate), TMR-PI (4,5)P2 (1-oleoyl-2-(6-((4,4-difluoro-1,3-dimethyl-5-(4-methoxyphenyl)-4- bora-3a,4a-diaza-s-indacene-2-propionyl)amino)hexanoyl)-sn-glycero-3- phosphoinositol-4.5-bisphosphate; see Fig. 4.1 for both chemical structures), and similarly chain-labeled TF- and TMR-labeled phosphatidylethanolamine (PE), phosphatidylserine (PS), PC, and phosphatidylinositol (PI) were purchased from Avanti Polar Lipids (Alabaster, AL). 16:0/16:0 PI(4,5)P2 was purchased from Echelon Biosciences (Salt Lake City, UT). Cholesterol was purchased from Nu-Chek Prep (Elysian, MN). Cholesterol stock solution was prepared by standard gravimetric procedures to 0.2% error. Concentrations of all phospholipid stocks were determined to 1% error by inorganic phosphate assay (40). The working stocks of TF- and TMR-labeled PE, PS, and PC were prepared in chloroform; working stocks of TF- and TMR-labeled PI and PIP2 were prepared in chloroform:methanol:H_2O=20:9:1. Fluorescent probe extinction coefficients were obtained from lot certificates of analysis: 97,000 M^{-1} cm^{-1} at 496 nm for TF and 56,000 M^{-1} cm^{-1} at 544 nm for TMR. Probe concentrations were determined in methanol by absorption spectroscopy using an HP 8452A spectrophotometer (Hewlett-Packard, Palo Alto, CA). Lipid purity of R99.5% was confirmed by thin-layer chromatography (TLC). TLC was performed on washed, activated silica gel plates (Alltech, Deerfield, IL) developed with chloroform:methanol:water=65:25:4 for most phospholipids and for cholesterol with

petroleum ether:diethyl ether:chloroform=7:3:3. Especially useful, TLC plates for PIPs were pre-run with 10% K2C2O4+2 mM EDTA and then activated at 100 °C for 30 min before use. TLC plates for PIPs were developed with chloroform:methanol:4 N NH4OH= 45:35:10 (41,42).

Liposome preparation

A total of 250 nmol lipid mixtures, including an amount of PIP2 or other PIP for each experiment, were dispensed into each borosilicate culture tube using glass syringes (Hamilton, Reno, NC). Liposomes were prepared using rapid solvent exchange to directly transfer lipid mixtures from organic solvent to aqueous buffer without drying during preparation (43). Samples were sealed under argon at a final lipid concentration of 0.5 mM. Liposomes were then incubated at 55°C for 30 min and then slowly cooled to 23°C overnight with a temperature process controller (Love Controls, series 16A; Dwyer Instruments, Michigan City, IN). Samples were measured the next day. All liposome samples used, except in Fig. 4.13, were composed of the inner leaflet model POPE/POPS/Chol= 34/30/36.

Buffer preparation and metal ion measurement

All buffers used were based on 100 mM KCl, 20 mM HEPES (pH=7.2). ‘‘Standard buffers’’ were prepared with KCl (99%; Sigma-Aldrich, St. Louis, MO), HEPES (99%; Fisher Scientific, Hampton, NH), stored in borosilicate glass bottles, and used in the experiments shown in Figs. 4.2-4.7. What we refer to as ‘‘pure buffers’’ were prepared with KCl (99.999%; Sigma-Aldrich or ACROS (Geel, Belgium)), HEPES

(99.5%; Sigma-Aldrich), and stored in Teflon fluorinated ethylene propylene bottles (Nalgene). Water was purified to 18.2 MU by passage through a Barnstead MicroPure system (Thermo Fisher, Waltham, MA). Buffers used in the experiments shown in Figs. 4.7-4.14 were ‘‘pure buffers.’’ Micromolar levels of Al^{3+}, Ca^{2+}, Fe^{3+}, Zn^{2+}, and Mg^{2+} were prepared from 100 mM stock solutions stored at pH = 2-3. These stocks were made with aluminum chloride (99.999%), calcium chloride (99%), iron (III) chloride (99.9%), zinc chloride (99.995%) and magnesium chloride hexahydrate (99%), all from Sigma-Aldrich. Disodium EDTA (99%; Sigma-Aldrich) was prepared and stored as a 500 mM stock solution at pH = 7.2. Ion concentrations and purities of all stocks and freshly prepared buffers were confirmed by inductively coupled plasma optical emission spectroscopy (ICP-OES) at the Cornell Nutrient Analysis Laboratory using Spectro Arcos ICP-OES (44). The sample size was small enough that no digestion was necessary.

Self-quenching and FRET

A 1.8 mL volume of buffer was added to 0.2 mL of a 0.5 mM liposome sample to yield 50 mM total lipid in the cuvette. Fluorescence was collected on a Hitachi F-7000 FL spectrofluorimeter (Hitachi High Technologies America, Schaumburg, IL) at 23°C. Wavelengths used for self-quenching studies were (ex/em) as follows: TF (485/515 nm), TMR (544/569 nm), and light scattering (440/420 nm). For FRET studies, corrections were made for the non-FRET contributions of direct excitation of TMR acceptors and donor TF fluorescence bleedthrough as well as light scattering by the vesicle suspension. Data were collected with slits for ex/em = 5/5 nm and a 10 s

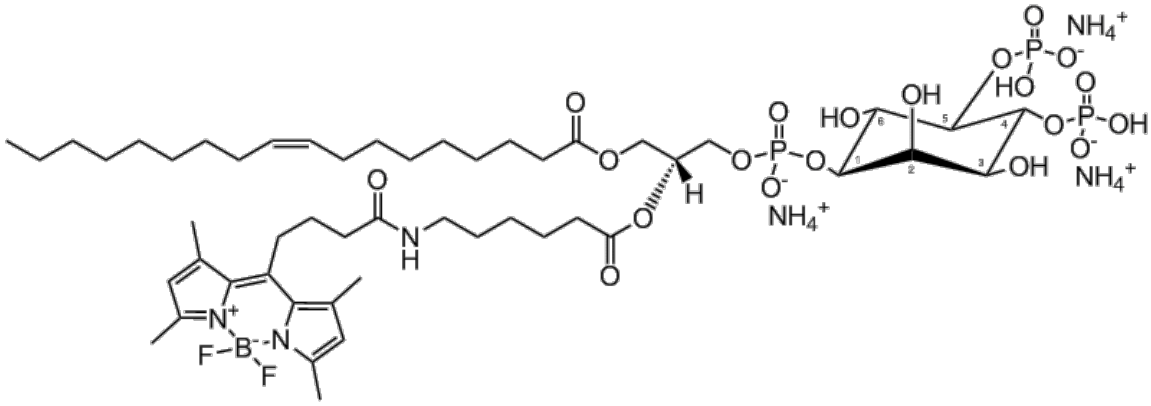

TF-PIP2

1-oleoyl-2-{6-[4-(dipyrrometheneboron difluoride)butanoyl]amino}hexanoyl-*sn*-glycero-3-phosphoinositol-4,5-bisphosphate (ammonium salt)

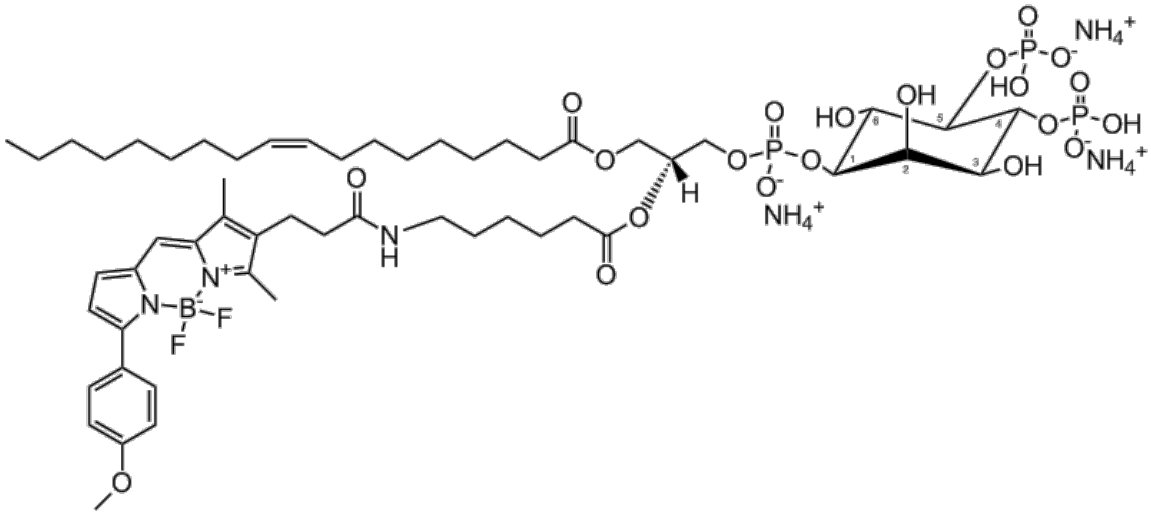

TMR-PIP2

1-oleoyl-2-(6-((4,4-difluoro-1,3-dimethyl-5-(4-methoxyphenyl)-4-bora-3a,4a-diaza-s-indacene-2-propionyl)amino)hexanoyl)-*sn*-glycero-3-phosphoinositol-4.5-bisphosphate (ammonium salt)

Fig 4.1 Chemical structures of acyl chain labeled PIP2 used. TF-PIP2 (top) and TMR-PIP2 (bottom)

integration time, except for 10/10 nm slits for experiments shown in Fig. 4.11 and 5/10 nm for experiments shown in Fig. 4.14, A and B.

RESULTS

PIP2 cluster formation is driven by multivalent metal ions

We exploited fluorescence self-quenching to detect PIP2 cluster formation with inner leaflet lipid model composition using POPE/POPS/Chol (34/30/36). We used the synthetic fluorescent PIP2 analog TF-PIP2 (see Fig. 4.1 for chemical structure) to examine PIP2 distribution in membranes. As shown by (19), self-quenching of TF-PIP2 can reveal PIP2-PIP2 association. In our standard buffer, increasing the concentration of TF-PIP2 led to a linear increase of fluorescence only up to 0.02 mol% of total lipids (Fig. 4.2). From 0.03 to 0.04 mol%, fluorescence increased weakly, implying fluorescence quenching via fluorophore-fluorophore interactions, and above 0.1% fluorescence increased by a little, apparently because of strong self-quenching. We interpret these results to reflect formation of tightly packed PIP2 in clusters. In stark contrast, the presence of 1 mM EDTA caused TF-PIP2 self-quenching to disappear completely, even up to 0.3 mol%, with only a linear increase in fluorescence being observed as the TF-PIP2 fraction increased. This EDTA effect implies that multivalent metal ions are present in the standard buffer and are required to induce such PIP2 cluster formation.

To confirm that cluster formation is specific to PIP2, we examined the self-quenching profiles of TF-labeled PE, PS, PC, and PI in the same standard buffer (Fig. 4.3). Increasing the concentrations of these labeled lipids from 0 to 0.5 mol% resulted in a

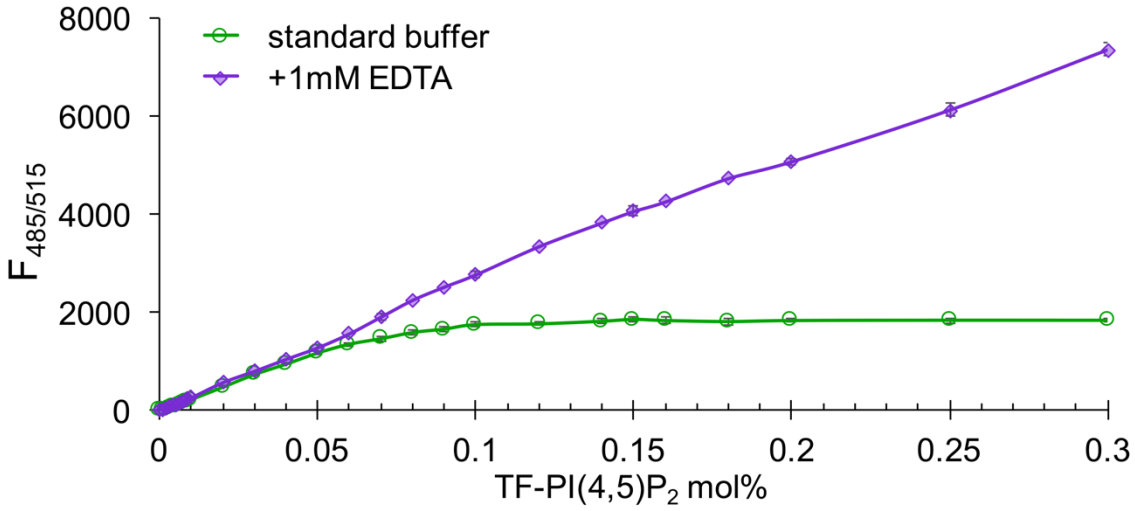

Fig 4.2 PIP2 clusters form at very low concentrations, but only in the presence of multivalent cations. Self-quenching occurs when a fluorescent TF-PIP2 concentration reaches CPC. Inner leaflet model membranes were POPE/POPS/Chol (34/30/36). Fluorescence was measured in standard buffer (green) or the same buffer plus 1 mM EDTA (purple) at 23°C. Assays were performed in triplicate with error bars of SDs from the means. Ex/Em slits were 5/5 nm in all experiments except as noted.

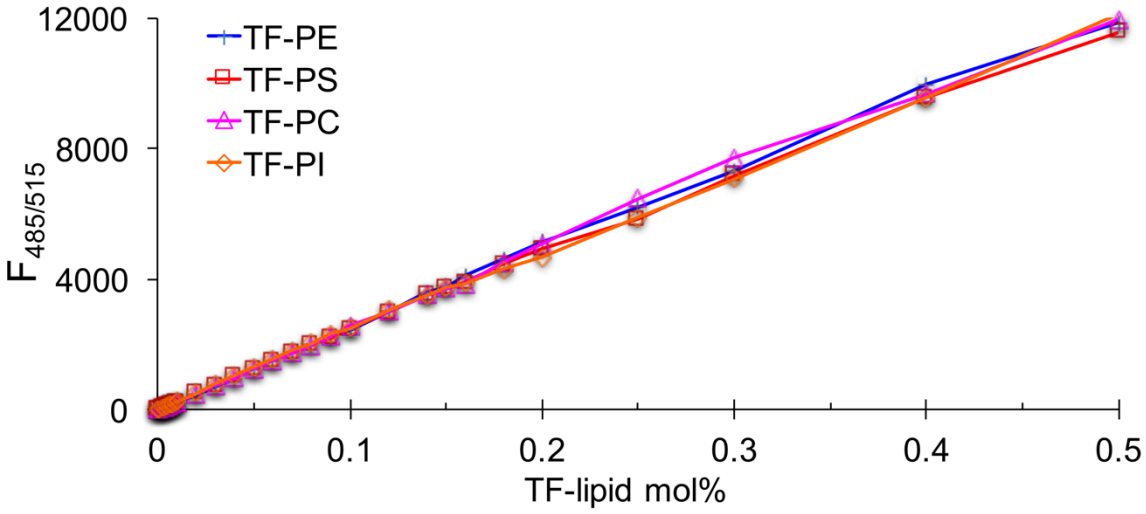

Fig 4.3 Other TF-labeled phospholipids do not form multivalent cation-dependent clusters. Fluorophore-labeled lipids were incorporated into inner leaflet model membranes with conditions as in Fig. 4.2. TF-PE (blue), TF-PS (red), TF-PC (magenta), TF-PI (orange) are shown.

linear increase of fluorescence, i.e., a lack of self-quenching and thus no cluster formation in this concentration range. EDTA only eliminated the self-quenching of TF-PIP2, but has a negligible effect on the fluorescence profile of other lipids such as TF-PC at these concentrations (Fig. 4.4). This behavior of TF-labeled lipids other than PIP2 means that the appearance of TF-PIP2 self-quenching in Fig. 4.2 at low concentrations is specific to PIP2 and not caused by the acyl chain fluorophore. TF-PC did undergo self-quenching above 2-3 mol% (Fig. 4.5). To examine whether unlabeled PIP2 exhibits similar cation-bridged clustering, we diluted TF-PIP2 twofold with brain-PIP2 or with 18:/18:1- or 18:0/20:4-PIP2 (Fig. 4.6). TF-PIP2 still showed a CPC at 0.02-0.03 mol%, which was consistent with unlabeled PIP2 forming clusters just like TF-labeled PIP2. As further confirmation, TMR-PIP2 (see Fig. 4.1 for chemical structure), which carries a slightly different acyl chain fluorescent label, also exhibited strong self-quenching at the same concentration as TF-PIP2, whereas again other TMR-labeled lipids did not self-quench (Fig. 4.7). These results clearly demonstrate that cluster formation is an intrinsic property of PIP2 rather than an artifact due to the TF or TMR moiety.

The striking effect of EDTA to eliminate PIP2 self-quenching shows that multivalent metal ions are crucial to PIP2 cluster formation. To examine which metal ions were present in the standard buffer prepared with reagent-grade chemicals, we used ICP-OES (44) to identify and quantitate these metal ions. The primary multivalent metal ions in the standard buffer were Ca^{2+} (57 mM), Al^{3+} (10 mM), Zn^{2+} (6 mM), and Fe^{3+} (0.1 mM), shown in Table 4.1. We then examined the effects of these four candidate metal ions on PIP2 cluster formation, individually and in combination. These

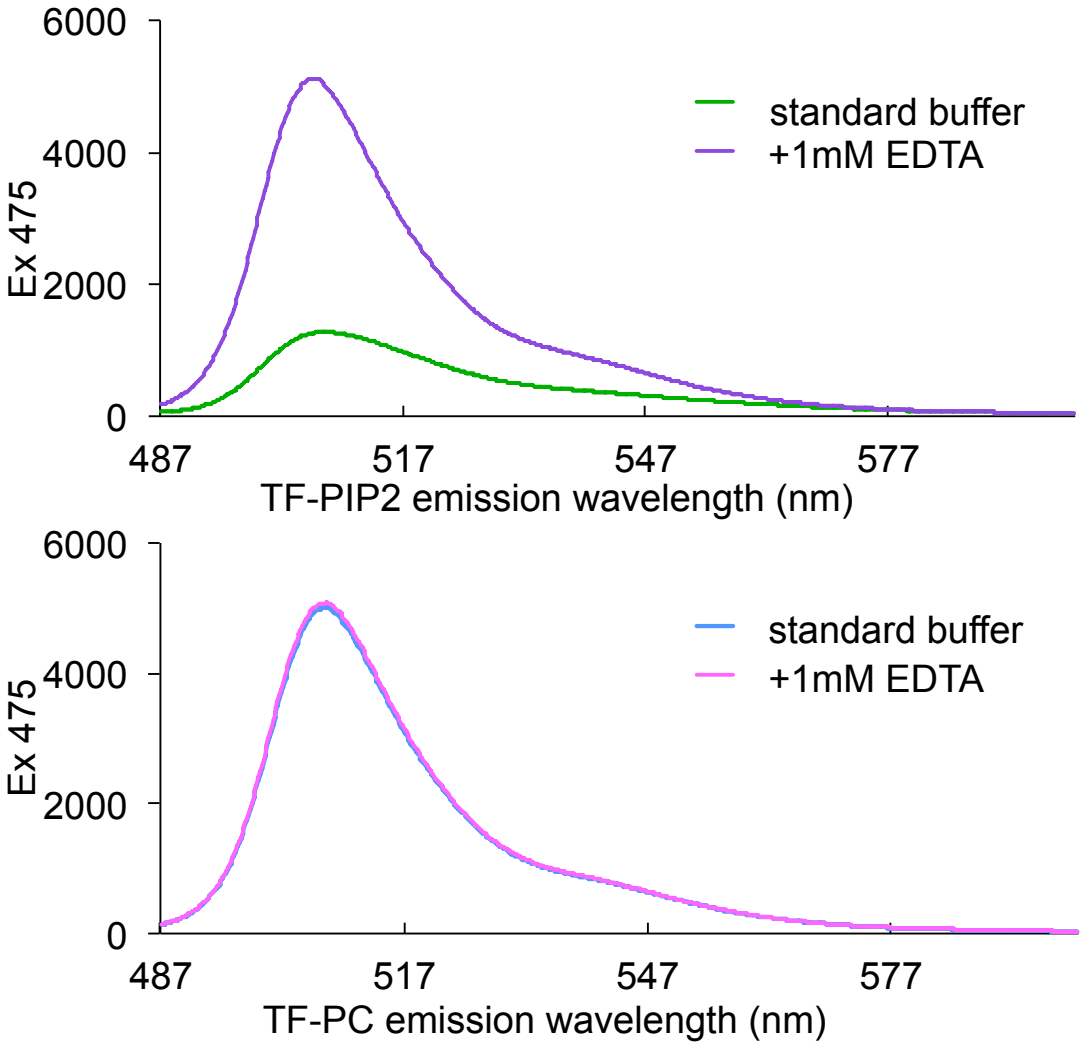

Fig 4.4 EDTA eliminates self-quenching of TF-PIP2, but has no effect on TF-PC in POPE/POPS/CHol (34/30/36). The emission spectrum of 0.3 mol% TF-PIP2 (top) and TF-PC (bottom) in inner leaflet model membranes was collected in standard buffer and in 1 mM EDTA.

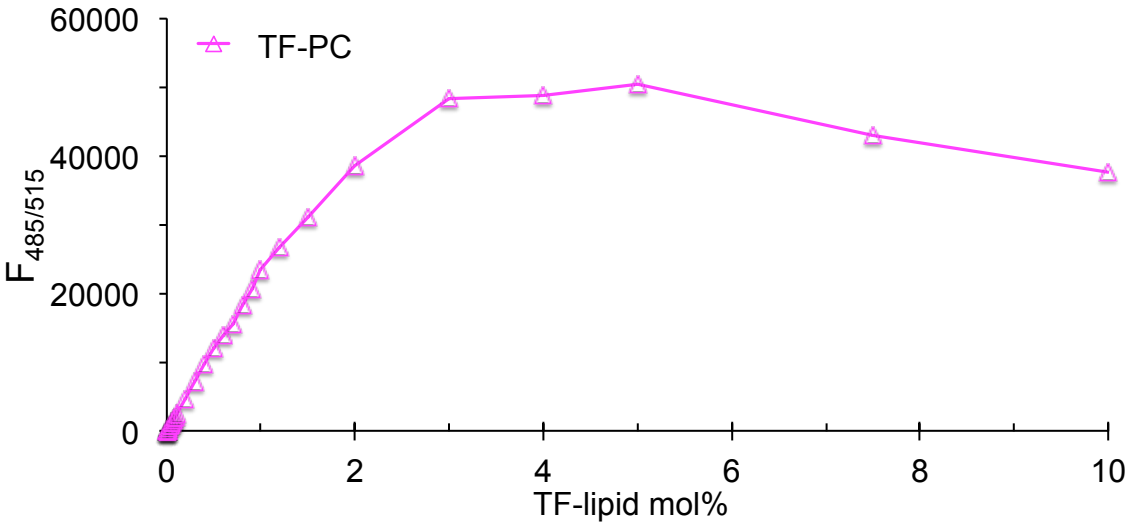

Fig 4.5 Self-quenching of TF-PC occurs only above ~2% of total lipids, at least 50-fold higher than for TF-PIP2. Inner leaflet model membranes were POPE/POPS/Chol (34/30/36). Fluorescence was measured in standard buffer (green) or the same buffer plus 1 mM EDTA (purple) at 23°C. Assays were performed in triplicate with error bars of SDs from the means.

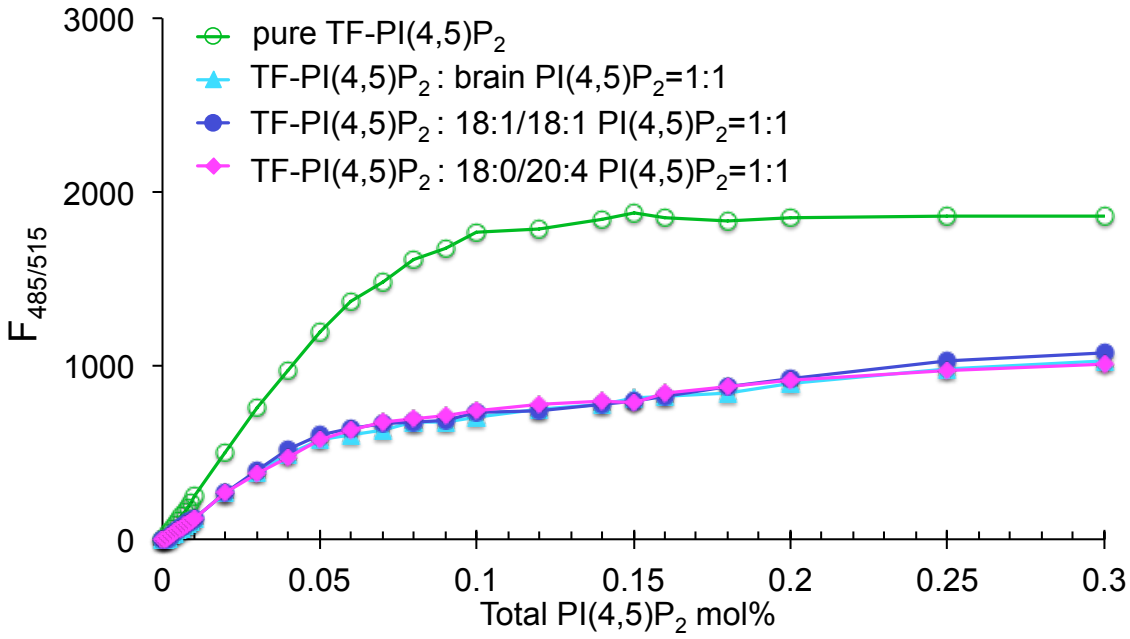

Fig 4.6 Unlabeled PIP2 incorporates into TF-PIP2 clusters. Self-quenching assays were carried out in POPE/POPS/Chol (34/30/36) as in Fig. 4.2. Pure TF-labeled PIP2 (green) is diluted 1:1 with unlabeled PIP2, either brain-PIP2 (cyan), 18:1/18:1-PIP2 (blue), or 18:0/20:4-PIP2 (magenta).

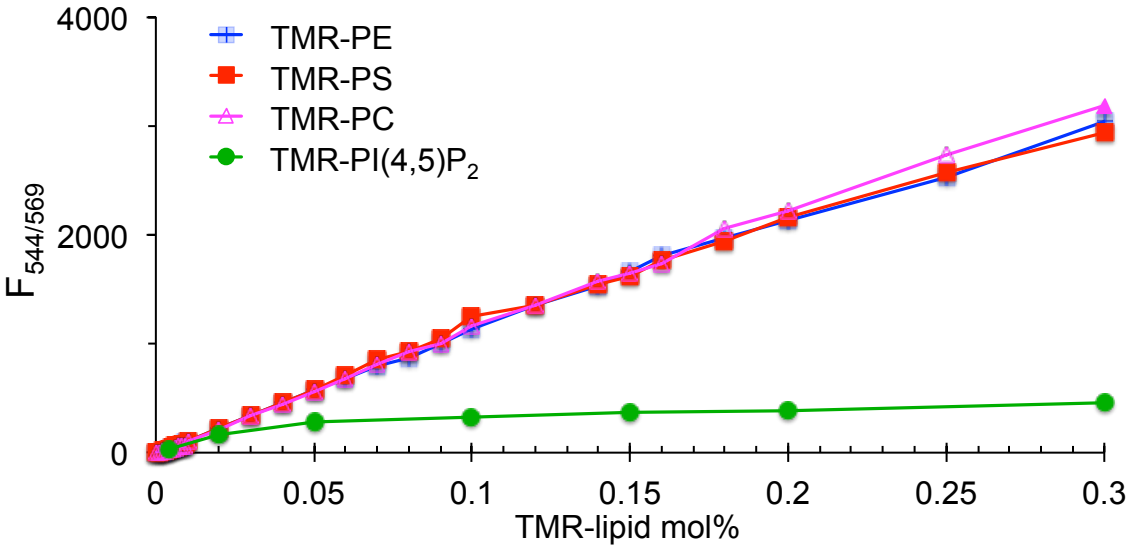

Fig 4.7 TMR-PIP2 forms cation-bridged clusters, but other TMR-labeled phospholipids do not. Self-quenching occurs when a fluorescent TMR-PIP2 concentration reaches CPC. Inner leaflet model membranes were POPE/POPS/Chol (34/30/36). Fluorescence was measured in standard buffer at 23°C. Assays were performed in triplicate with error bars of SDs from the means. TMR-PE (blue), TMR-PS (red), TMR-PC (magenta) and TMR-PIP2 (green).

experiments required buffers free of multivalent metal ions down to the sub-micromolar level, so we prepared a ‘‘pure buffer’’ from ultrapure chemicals, storing this in Teflon bottles to avoid leaching of metal ions from glass (45). ICP-OES analysis showed that contaminating metal ions in pure buffer stored in Teflon bottles was <0.1 mM (Table 4.1). This pure buffer was used in experiments shown in Figs. 4.8-4.14 with or without the addition of multivalent metal ions or EDTA.

We tested 1, 3, 5, 10, and 100 mM of Al^{3+}, Ca^{2+}, Fe^{3+}, and Zn^{2+} added to pure buffer. Because the cytosol contains 0.5 mM free Mg^{2+} in many cell types (46), we also tested this Mg^{2+} concentration. Based on the self-quenching experiment shown in Fig. 4.2 for TF-PIP2, we chose a defined PIP2 concentration of 0.3 mol% at which to compare each metal ion for PIP2 cluster formation (Fig. 4.8). We interpret a reduced fluorescence relative to the maximal fluorescence of the EDTA control to reflect PIP2 cluster formation. In this assay, 0.3 mol% TF-PIP2 in pure buffer exhibited 84% of the fluorescence observed in the EDTA control, which was consistent with the sub-micromolar concentrations of multivalent metal ions still present in this buffer. Fig. 4.8 shows that as little as an additional 1 mM of either Al^{3+}, Ca^{2+}, Fe^{3+}, or Zn^{2+} caused significant further self-quenching. Among the four candidate multivalent metal ions tested, Al^{3+} at 5 mM promoted PIP2 cluster formation most strongly, giving the lowest fluorescence. Combining 3 mM each of Al^{3+}, Ca^{2+}, Fe^{3+}, and Zn^{2+} yielded similar PIP2 cluster formation compared with that of 3 mM Al^{3+} alone. With 0.5 mM Mg^{2+} as the only multivalent cation, TFPIP2 exhibited 67% of the maximal fluorescence, implying that physiological levels of Mg^{2+} cause PIP2 to form loose clusters. We also tested the effect of Mg^{2+} from 0.05 to 0.5 mM in the presence of 0.5 mM EGTA to

Table 4.1 Multivalent metal ion analysis by ICP-OES

Metal ion [µM]	Al^{3+}	Ca^{2+}	Fe^{3+}	Mg^{2+}	Zn^{2+}
MQ H_2O	-	-	-	-	-
standard buffer (in glass)	10	57	0.1	-	6
pure buffer (in glass)	0.2	7	-	16	0.2
pure buffer (in Teflon)	-	0.1	-	-	0.1
pure buffer+ 0.5mM Mg^{2+} / 3µM each of Al^{3+}, Ca^{2+}, Fe^{3+} and Zn^{2+} (in Teflon)	3	3	3	490	3
0.5mM Mg^{2+}	-	-	-	500	-
1mM Al^{3+}	1050	0.1	-	-	0.1
1mM Ca^{2+}	-	980	-	-	0.1
1mM Fe^{3+}	0.5	0.5	1020	-	0.1
1mM Zn^{2+}	-	0.1	1	-	1010
5µM TF-PI(4,5)P_2 (in MQ H_2O)	-	-	-	-	-
5µM TMR-PI(4,5)P_2 (in MQ H_2O)	0.4	0.2	-	-	0.1
10µM Brain-PI(4,5)P_2 (in MQ H_2O)	0.2	0.5	-	-	0.1
6.3µM POPS (in MQ H_2O)	0.2	0.5	-	0.2	0.4
63µM POPS (in MQ H_2O)	0.2	0.2	-	-	-

Note: "-" means undetectable (< 0.1 µM). Standard buffer was prepared with 99% KCl, 99% HEPES; pure buffer was prepared with 99.999% KCl, 99.5% HEPES. Multivalent metal ions are diluted from 100mM stocks.

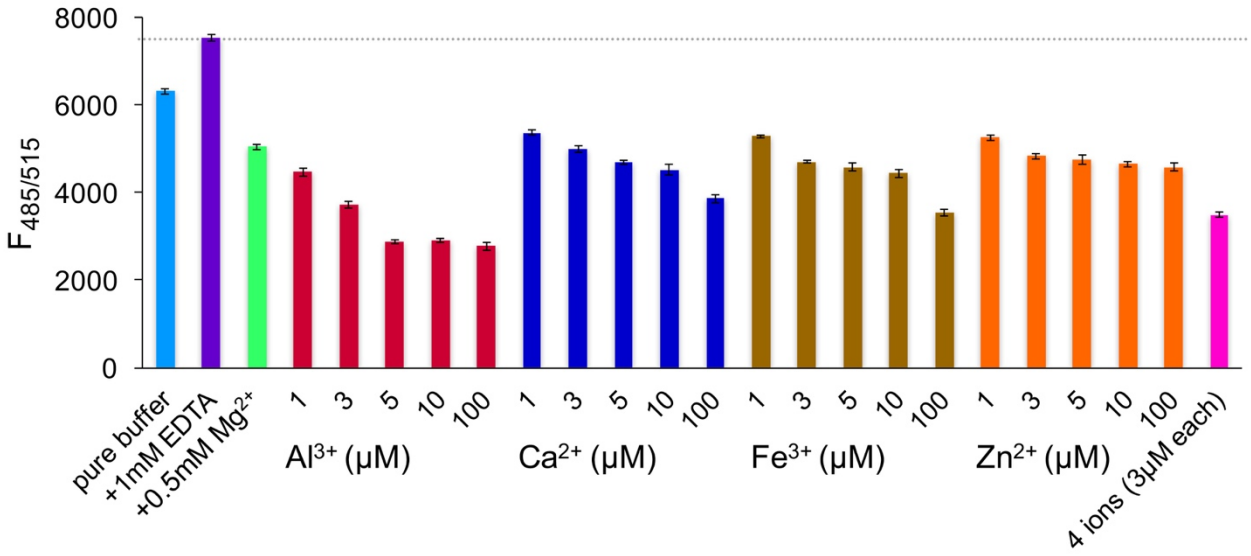

Figure 4.8 Various multivalent metal ions drive TF-PIP2 to form clusters. Each bar shows fluorescence from a fixed 0.3 mol% of TF-PIP2 in inner leaflet model membranes as in Fig. 1 except for differences in ionic conditions. See Materials and Methods for a description of highly purified "pure buffer." Pure buffer, or pure buffer plus the following was used: 1 mM EDTA; 0.5 mM Mg^{2+}; 1, 3, 5, 10, or 100 mM each of Al^{3+}, Ca^{2+}, Fe^{3+}, and Zn^{2+}; or a combination of 3 mM each of Al^{3+}, Ca^{2+}, Fe^{3+}, and Zn^{2+}. Error bars show SDs from the mean from at least three independent measurements.

eliminate all other multivalent metal ions. TF-PIP2 cluster promotion by Mg^{2+} was found to be concentration dependent, i.e., the higher the [Mg^{2+}], the greater the TF-PIP2 self-quenching observed (Fig. 4.9).

Switching to pure buffer containing known amounts of multivalent metal ions, we found TF-PIP2 self-quenching profile was similar to that shown in Fig. 4.2, which was carried out in the standard buffer. We tested the combination of 0.5 mM Mg^{2+} with 3 mM each of Al^{3+}, Ca^{2+}, Fe^{3+}, and Zn^{2+}. With this mixture, TF-PIP2 exhibited strong self-quenching starting at 0.02 mol%. Although Al^{3+} is not a cytosolic ion of interest, we examined it here because of its strong promotion of PIP2 clustering. We also tested a more physiological buffer containing 0.5 mM Mg^{2+} together with 100 mM Ca^{2+}, which mimics the transient calcium influx environment near the inner leaflet of the PM (Fig. 4.10). Physiological levels of Ca^{2+} and Mg^{2+} are sufficient to cause strong TF-PIP2 quenching, confirming that the PIP2 clustering we are observing here is biologically relevant. Considering that the buffer containing 0.5 mM Mg^{2+} and 3 mM each of Al^{3+}, Ca^{2+}, Fe^{3+}, and Zn^{2+} still causes the strongest PIP2 clustering, we used this mixed ion buffer for experiments shown in Figs. 4.11-4.14 to maximize the self-quenching and FRET signals.

High-resolution examination of PIP2 cluster formation

A simple model to describe cluster formation posits that at very low concentrations, PIP2 exists essentially as individual molecules freely diffusing in the membrane. At the CPC, these PIP2 self-associate, analogous to micelle or phase formation. To test this model, we developed a dilution experiment based on reversible fluorescence self-

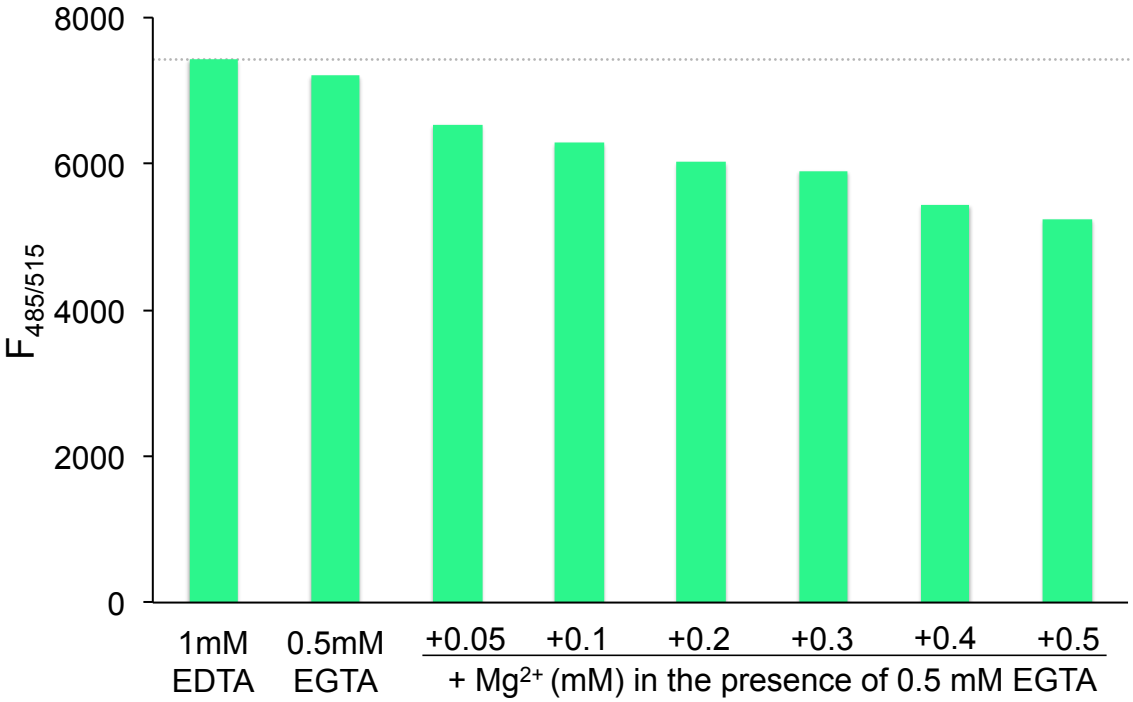

Fig 4.9 Mg^{2+} drives PIP2 clustering. Bars represent the fluorescence from a fixed 0.3 mol% TF-PIP2 in POPE/POPS/Chol (34/30/36) with the following additions: 1mM EDTA, 0.5 mM EGTA, or increasing concentrations of Mg^{2+} from 0.05 mM up to 0.5 mM in the presence of 0.5mM EGTA.

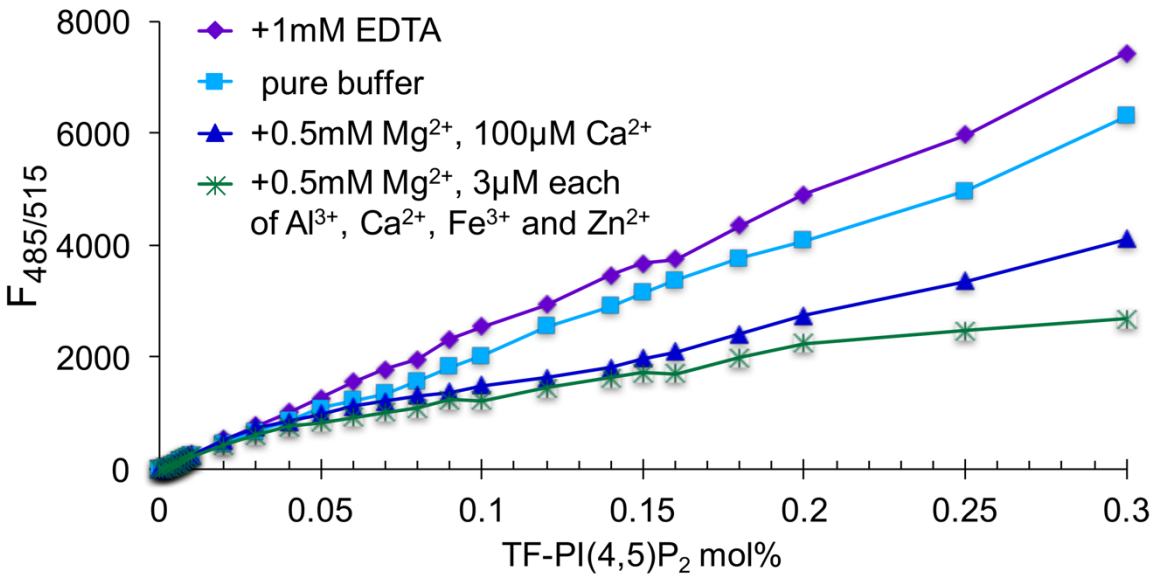

Figure 4.10 Physiological metal ion conditions can also cause strong PIP2 clustering. Analysis as in Fig. 1 measured in three buffer conditions is shown: pure buffer +1 mM EDTA (purple, diamond), pure buffer (light blue, square), pure buffer + 0.5 mM Mg^{2+} and 100 mM Ca^{2+} (dark blue, triangle), and pure buffer + 0.5 mM Mg^{2+} and 3 mM each of Al^{3+}, Ca^{2+}, Fe^{3+}, and Zn^{2+} (green, asterisk).

quenching. We reasoned that if unlabeled PIP2 behaves just like TF-PIP2, then gradually increasing the concentration of unlabeled PIP2 in the presence of a constant TF-PIP2 concentration would have these effects. 1) First, the unlabeled PIP2 would dilute the unclustered TF-PIP2 without changing the fluorescence when total PIP2 is still below the CPC, i.e., a perfectly horizontal line of fluorescence versus total PIP2 concentration. 2) Then, upon reaching the CPC, the unlabeled PIP2 would drive self-association, abruptly reducing fluorescence. 3) Finally, at higher concentrations, the unlabeled PIP2 would dilute the fluorescent PIP2 molecules that are in the clusters, relieving self-quenching and therefore leading to an increase in fluorescence. In the experiment shown in Fig. 4.11, each of the 68 points represents a liposome sample with a fixed 0.01 mol% of TF-PIP2, together with increasing concentrations of brain-PIP2, from 0 to 1.0 mol%. The initial 0.01 mol% TF-PIP2 was not in clusters, still being dispersed in the membranes (Fig. 4.10). As unlabeled brain PIP2 was added, up to a total PIP2 concentration of 0.02 mol% (Fig. 4.11, shaded region in inset), TF-PIP2 fluorescence was constant, still at its maximal unquenched level, as shown pictorially by the dispersed green dots in the cartoon. When total PIP2 exceeded that concentration, TF-PIP2 self-quenching began, as evidenced by decreasing fluorescence, implying cluster formation (Fig. 4.11, circle of green and black dots in cartoon). Between 0.02 and 0.13 mol%, TF fluorescence continuously decreased, indicating significant self-quenching even with the ratio of labeled to unlabeled PIP2 within the cluster being in the range of 0.1. When the concentration of total PIP2 reached 0.13 mol%, additional brain PIP2 diluted the TF-PIP2 in each cluster enough that fluorescence again increased. Eventually the fluorescence fully recovered to

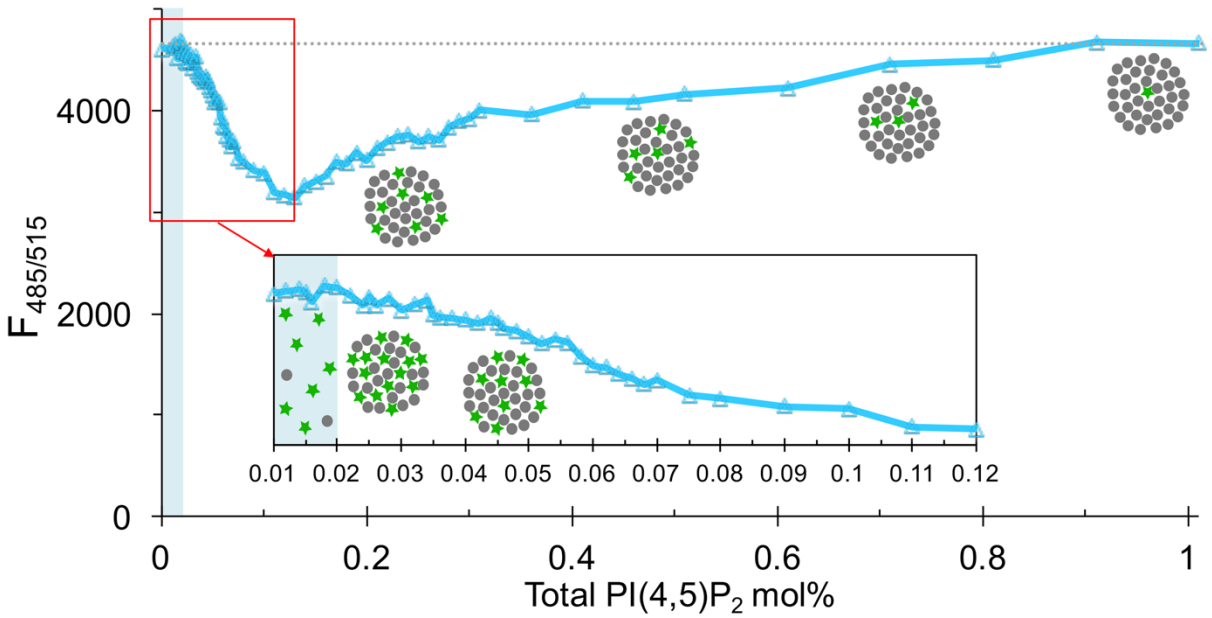

Fig 4.11 PIP2 cluster formation starts at a low, well-defined PIP2 concentration. Each point is the fluorescence from a fixed 0.01 mol% TF-PIP2 in POPE/POPS/Chol (34/30/36) with additional unlabeled brain-PIP2 from 0.002 to 1 mol%. The X axis indicates total PIP2 from 0.01 up to 1.01 mol %. All samples are in pure buffer with 0.5 mM Mg^{2+} and 3 mM of each Al^{3+}, Ca^{2+}, Fe^{3+}, and Zn^{2+}. The inset shows expansion of the 0.01– 0.12 mol% data. Schematic illustrations show that PIP2 stays dispersed at very low concentrations and then forms clusters just above 0.02 mol%. At that point, most of the fluorescence is from the free TF-PIP2, and fluorescence from clusters is significantly quenched. As more brain-PIP2 (black circles) is added, TF-PIP2 (green stars) is diluted, leading to dequenching in each cluster. The assay was repeated three times independently with similar results.

exactly its initial unquenched value. This unique self-quenching profile supports the conclusion that PIP2 self-associates, forming cation-bridged clusters.

Self-association of PIP2 is headgroup-specific

To study whether acyl chain types affect PIP2 cluster formation, we compared four PIP2 species differing in acyl chain length and saturation: 18:1/18:1, 18:0/20:4, 16:0/16:0, and the natural brain-PIP2, which contains a mixture of acyl chains (Fig. 4.12A). We made use of the finding shown in Fig. 4.2 and Fig. 4.10 that at 0.2 mol%, TF-PIP2 is highly quenched in the presence of multivalent metal ions. Each point in Fig. 4.12A represents an individual liposome sample that contained 0.2 mol% of TF-PIP2 together with additional unlabeled PIP2 species, ranging in concentration from 0.25 to 4 mol% of total lipids. If the unlabeled PIP2 were to co-cluster with TF-PIP2, then TF-PIP2 would be diluted in each cluster by the unlabeled PIP2. All four unlabeled PIP2 species diluted the highly quenched TF-PIP2 in exactly the same way. These results imply that the clustering behavior is not influenced by the hydrophobic portion of the PIP2 molecule.

We also tested whether other PIP species can co-cluster with PIP2 (Fig. 4.12B). PI phosphate (PI3P, PI4P, PI5P), PI bisphosphate (PI(3,4)P2, PI(3,5)P2, PI(4,5)P2), and PI trisphosphate (PI(3,4,5)P3) were studied using the same dilution assay as in Fig. 4.12A, with a fixed 0.2 mol% of TF-PIP2 and varying concentrations of PI or the seven PIP species. PI did not dilute the TF-PIP2 signal and thus did not co-cluster with PIP2. In contrast, all PIP species co-clustered with PIP2 to similar degrees. We found these small differences to be reproducible in independent

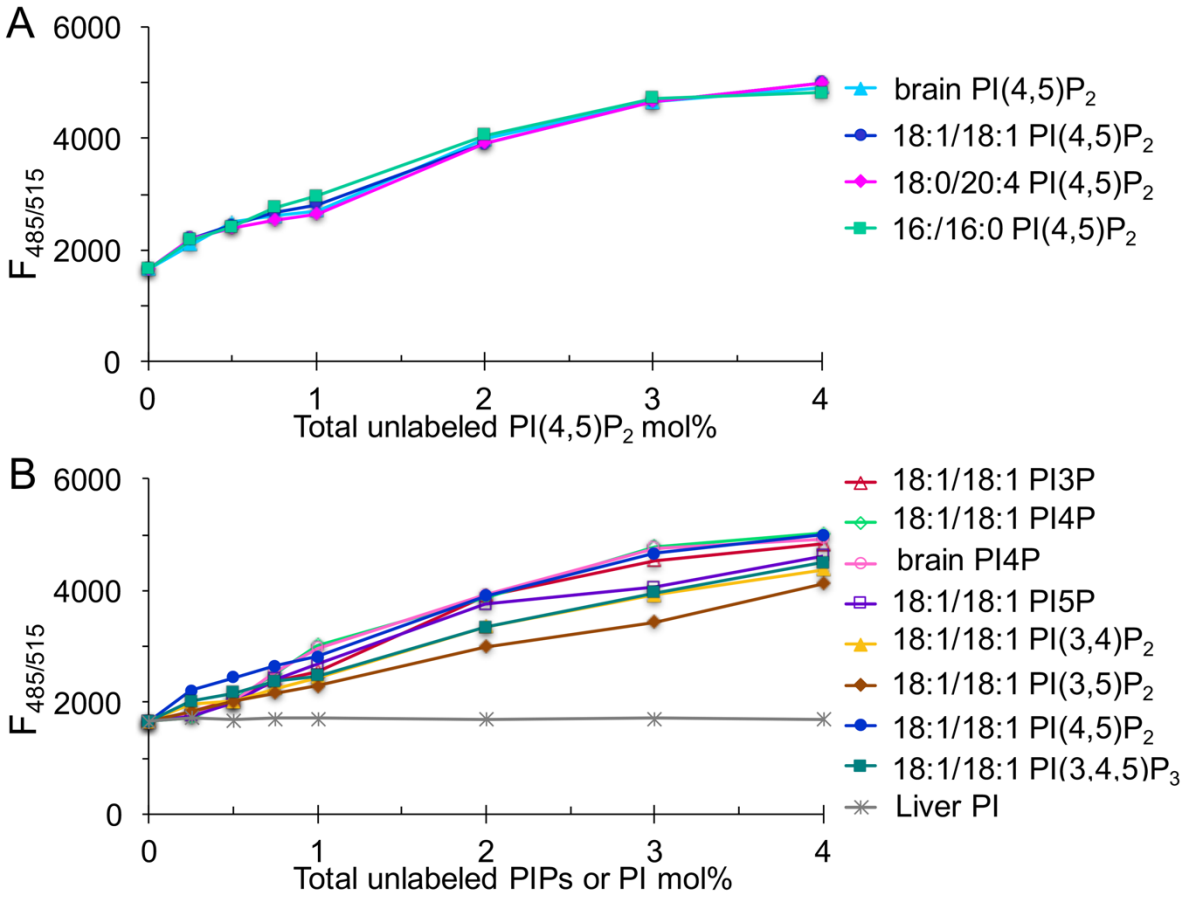

Fig 4.12 Effects of acyl chain type and PIP headgroup on co-clustering with PIP2. (A) Acyl chains do not influence PIP2 incorporation into clusters. Each line corresponds to a fixed 0.2 mol% TF-PIP2 in POPE/POPS/ Chol (34/30/36), with increasing amounts of unlabeled PIP2 in pure buffer plus 0.5 mM Mg^{2+} and 3 mM each of Al^{3+}, Ca^{2+}, Fe^{3+}, and Zn^{2+}, brain-PI(4,5)P2 (cyan), 18:1-PI(4,5)P2 (blue), 18:0/20:4-PI(4,5)P2 (magenta), and 16:0-PI(4,5)P2 (green). (B) Other PIP species enter PIP2 clusters, but PI does not. Assay as in (A) but with additional unlabeled PI or PIPs is shown; liver PI (gray), brain-PI4P (pink), or the 18:1/18:1 species PI3P (red), PI4P (lime), PI5P (purple), PI(3,4)P2 (yellow), PI(3,5)P2 (brown), PI(4,5)P2 (blue), and PI(3,4,5)P3 (green) are shown. Small differences in PIPs co-clustering were reproducible in independent measurements.

measurements. That PI phosphate can co-cluster but PI cannot shows that one additional phosphate group on the inositol ring is sufficient for cation-bridged clustering to occur. In summary, co-clustering with PIP2 requires only PIP headgroups and is insensitive to acyl chains.

Membrane composition affects PIP2 cation cluster formation

To explore the PIP2 mixing behavior in different lipid environments, we examined PIP2 cluster formation in mixtures besides POPE/POPS/Chol. We compared the self-quenching of 0.3 mol% PIP2 in different model membranes in pure buffer containing 0.5 mM Mg^{2+} together with 3 mM each of Ca^{2+}, Al^{3+}, Fe^{3+}, and Zn^{2+} (Fig. 4.13). Similar to the experiments shown in Fig. 4.8, the lower the fluorescence at this fixed mol% of TF-PIP2 compared to the maximal fluorescence in the EDTA control, the stronger the PIP2 cluster formation. The results showed that PIP2 cation cluster formation was indeed dependent on bulk lipid composition. We found notable promotion of PIP2 cation clustering by cholesterol and by PI: 1) the presence of 36 mol% cholesterol in mixtures with POPC and POPC/POPS favored cluster formation. That cholesterol strongly enhances cluster formation implies either of two quite different mechanisms: 1) cholesterol does not enter the PIP2 cation clusters but instead promotes immiscibility of PIP2 by increasing its chemical potential, decreasing the fraction of free, unquenched TF-PIP2; or 2) cholesterol does enter and condense PIP2 cation clusters, promoting fluorescence quenching. The latter is less likely, given the poly-unsaturation of brain-PIP2 and the mono-unsaturation of all other lipids except for liver-PI in this experiment and the known preference of cholesterol to be

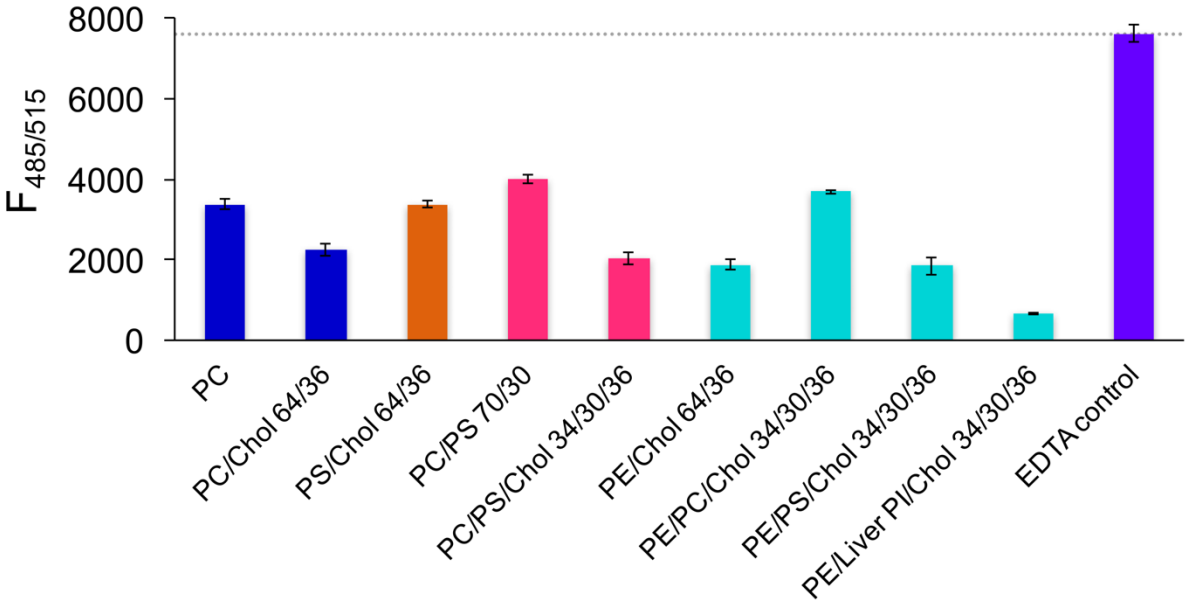

Fig 4.13 Lipid composition strongly affects PIP2-cation cluster formation. Bars show fluorescence from a fixed 0.3 mol% TF-PIP2 in model membranes with different lipid compositions. Phospholipid chains were 16:0/18:1 (PO), except for liver PI. Samples were prepared in pure buffer þ 0.5 mM Mg^{2+} and 3 mM each of Al^{3+}, Ca^{2+}, Fe^{3+}, and Zn^{2+}, except for the 1 mM EDTA control. Means and SDs from at least three independent measurements are shown. An EDTA control was measured for every membrane composition; the right-side purple bar shows the average fluorescence of all EDTA controls.

surrounded by saturated acyl chains. We note that studies in the absence of multivalent cations favor the interpretation that cholesterol binds to and stabilizes multivalent cation-free PIP2 clusters (20); in POPE/X/Chol (34/30/36), the strongest self-quenching was observed when X = liver-PI with a value of 9% maximal fluorescence. We interpret this result to imply an especially low PIP2 solubility in the presence of PI, which is a known major component of the PM cytosolic leaflet. Compared with the simple PC composition used by many researchers, the six-fold greater quenching of TF-PIP2 fluorescence in POPE/liver-PI/Chol shows that bulk membrane composition is a major factor in the formation of PIP2 cation clusters.

PIP2 self-association is detected with high sensitivity by FRET

We used an independent experimental method, FRET, to study PIP2 cation-bridged cluster formation (47). This technique is sufficiently sensitive to detect PIP2 at the low concentrations below the CPC. The FRET assay has several advantages. First, most of the PIP2 is unlabeled brain-PIP2, with the donor fluorophore TF-PIP2 and the acceptor fluorophore TMR-PIP2 each comprising only 1% of the total PIP2. Second, the form of the FRET signal enables a more precise identification of the CPC where PIP2 self-association abruptly starts. Liposome samples were prepared with varying fractions of total PIP2, each with a constant ratio of 98/1/1 = brain-PIP2/TF-PIP2/TMR-PIP2. At these low fluorophore fractions, the donor TF-PIP2 and the acceptor TMR-PIP2 showed no self-quenching (data not shown). Eight different ionic conditions were studied (Fig. 4.14A). We observed modest but clear PIP2 cluster formation by 0.5 mM Mg^{2+} with a CPC of 0.04 mol%. This effect of Mg^{2+} is

consistent with that observed by self-quenching (Fig. 4.8). Adding an additional 3 mM of any of the multivalent metal ions to the 0.5 mM Mg^{2+} resulted in a stronger FRET signal and lower CPC, which was again consistent with the self-quenching data (Fig. 4.14B). With 3 mM Al^{3+} and 0.5 mM Mg^{2+}, the strongest FRET signals were observed, and the lowest CPC = 0.02 mol% of total lipids. Combining 3 mM each of Al^{3+}, Ca^{2+}, Fe^{3+}, and Zn^{2+} with 0.5 mM Mg^{2+} did not further increase the FRET or lower the CPC. These FRET results reveal two different kinds of evidence of PIP2 cation interactions. First, the magnitude of the FRET signal at 2 mol% of total PIP2 is different for the different multivalent metal ions (Fig. 4.14A), with the largest FRET signals found in the presence of Al^{3+} and 100 mM Ca^{2+} and a far smaller FRET signal from Mg^{2+}. A greater FRET signal might indicate closer packing of PIP2 fluorophores within a tight cation-bridged cluster compared to a looser cluster. Second, the remarkably low PIP2 CPC of 0.02-0.04 mol% indicates high-affinity interaction of the PIP2 with the cation. Consistently, Al^{3+} showed the highest affinity for PIP2. At the physiological level of 2 mol% total PIP2, we also measured FRET between TF-PIP2 and TMR-PIP2 in the physiological buffer that contains 0.5 mM Mg^{2+} + 10 mM Ca^{2+} (in Fig. 4.14C, note that narrower slits were used than in Fig. 4.14, A and B). This FRET signal is 3-fold greater than that in the 1 mM EDTA control buffer, slightly lower than the maximal FRET signal in 0.5 mM Mg^{2+} + 3 mM each of the four other ions. Under these near-physiological conditions, FRET is in agreement with the self-quenching results shown in Fig. 4.10 for PIP2-forming clusters. As a control FRET experiment in which clustering is not expected, TF-PI and TMR-PI replaced the two similarly labeled PIP2 species in each buffer condition. The PI FRET pair showed the

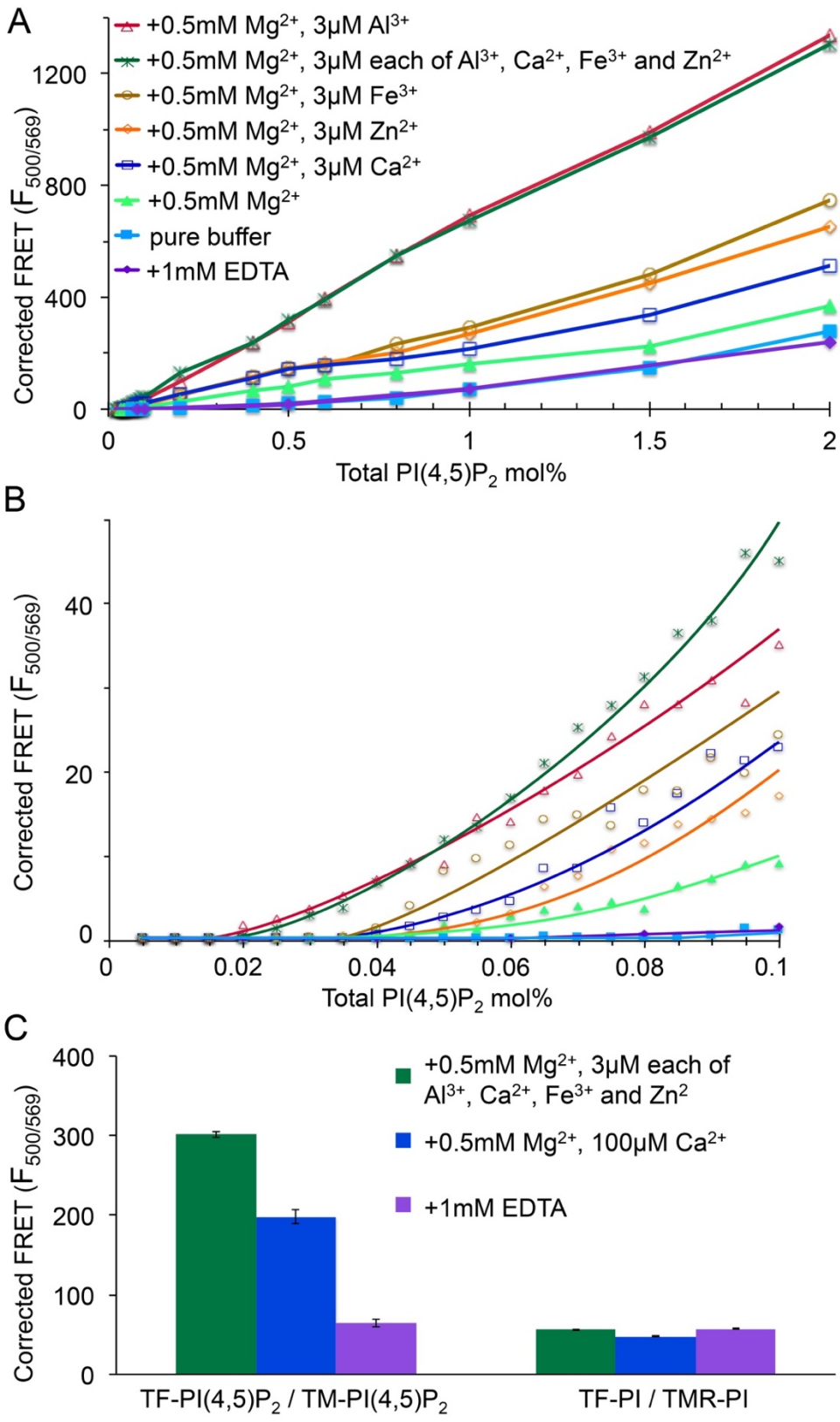
A
+0.5mM Mg2+, 3μM Al3+
+0.5mM Mg2+, 3μM each of Al3+, Ca2+, Fe3+ and Zn2+
+0.5mM Mg2+, 3μM Fe3+
+0.5mM Mg2+, 3μM Zn2+
+0.5mM Mg2+, 3μM Ca2+
+0.5mM Mg2+
pure buffer
+1mM EDTA
Corrected FRET (F500/569)
Total PI(4,5)P2 mol%
B
Corrected FRET (F500/569)
Total PI(4,5)P2 mol%
C
+0.5mM Mg2+, 3μM each of Al3+, Ca2+, Fe3+ and Zn2
+0.5mM Mg2+, 100μM Ca2+
+1mM EDTA
Corrected FRET (F500/569)
TF-PI(4,5)P2 / TM-PI(4,5)P2
TF-PI / TMR-PI

Fig 4.14 FRET detects cation dependence of PIP2 cluster formation. (A) Corrected FRET is shown (see Materials and Methods) as a function of PIP2 concentration in POPE/POPS/Chol (34/30/36). PIP2 mixtures were 98% brain-PIP2 + 1% of the donor TF-PIP2 and 1% of the acceptor TMR-PIP2. Ex/Em slits were 5/10 nm with a temperature of 23°C. (B) Expansion is shown of the low concentration region of (A) with PIP2 from 0.005 to 0.1 mol%. (C) Physiological levels of Ca^{2+} and Mg^{2+} lead to strong clustering of 2 mol% PIP2 but not PI. Corrected FRET signals for 2 mol% total PIP2 measured as in (A), in parallel with 2% total PIP2 and PI, of which 98% was brain-PIP2 and 1% each was TF-PI and TMR-PI. Buffer conditions were 0.5 mM Mg^{2+} and 3 mM each of Al^{3+}, Ca^{2+}, Fe^{3+}, and Zn^{2+} (green), 0.5 mM Mg^{2+} and 100 mM Ca^{2+} (blue), and 1 mM EDTA (purple). Ex/Em slits were 5/5 nm. Bars represent averages from at least three independent measurements; error bars represent SDs from the mean.

same background FRET signals in all three buffers, i.e., no effect of EDTA or metal ion, confirming that PI does not form clusters, which was consistent with the self-quenching results of Fig. 4.4. We emphasize that the background FRET signals with EDTA we observed here (above 0.5 mol% total PIP2) might arise from loose clusters formed by hydrogen-bonding networks, as suggested by previous studies (20-22). In summary, the quantitative agreement of the self-quenching and FRET assays indicates that they are reporting on the same phenomenon of cation-bridged cluster formation.

DISCUSSION

We have discovered a fundamental feature of PIP2 behavior that occurs in a wide range of model lipid bilayers and that is likely to be important for understanding PIP2 function in cells: in the presence of micromolar concentrations of multivalent cations or of a physiological 0.5 mM Mg^{2+} concentration, PIP2 molecules freely diffuse in the bilayer only up to 0.02-0.05 mol% of total lipid. Starting at this low CPC, additional PIP2 molecules form clusters bridged by multivalent metal ions, in equilibrium with free PIP2 in the bilayer.

An abrupt onset of PIP2-PIP2 contacts at the same PIP2 concentration appears in both the self-quenching experiment of Fig. 4.11 and the FRET experiment of Fig. 4.14. This sudden start of self-association is a characteristic of high-order aggregation, as in micelle formation or phase separation (39). However, with the data obtained so far, we cannot distinguish whether PIP2 self-association represents a phase within the bilayer or else a high-order aggregation, as with micelles. PIP2 cluster formation does not depend on acyl chain species and excludes the phospholipids PE, PC, PS, and PI,

which themselves show little or no clustering. In contrast, the six other known phosphoinositide species co-cluster with the cation-bridged PIP2 clusters. An abrupt onset of FRET signals implies that some type of cluster has formed distinct from the bulk lipid and into which the previously very dilute dyes have become concentrated. Although the clusters form abruptly at low PIP2 concentrations of 0.02-0.05 mol%, the incremental FRET increase with added PIP2 gradually reaches a linear increase at > 0.1 mol% up to the physiological range of 1-2 mol%. A similar result is found for self-quenching. For both FRET and self-quenching, the linear increase with increasing PIP2 mol% above the CPC implies that all additional PIP2 has the same properties, with larger or more numerous clusters but of the same material.

Thus, although the PIP2 concentration in the PM cytosolic leaflet is reported to be 1-2 mol%, if our model membranes reflect the behavior of cell membranes in the presence of multivalent cations, a majority of this PIP2 could be tied up in PIP2 cation clusters. The chemical potential of PIP2 in this cluster would be low. That is, the PIP2 tendency to bind or react should be equal to that of the free PIP2, which is at a concentration of only 2-5 molecules per 10,000 lipids, almost two orders of magnitude lower than might be expected based on its fraction within the PM cytosolic leaflet. Or, from another point of view, a change in the local concentration of multivalent cations such as Ca^{2+}, from sub-micromolar to perhaps tens of micromolar, can be viewed in two ways. 1) In that region of the PM where PIP2 cation clusters form, the thermodynamic activity of PIP2 drops significantly, e.g., 25- to 50-fold from 1 to 0.04 or 0.02 mol%. (2) In that same region of the PM, cation-bridged clusters form, on which some proteins assemble, for example, viral Gag proteins. In other words, some

kinds of PIP2-controlled behavior would decrease significantly, but other kinds could increase when PIP2 forms clusters.

For several reasons, previous studies with model membranes were not able to uncover the remarkable PIP2 behavior described here. First, those studies focused on membranes containing PIP2 at, or in many cases above, the 1-2 mol% present in the PM cytosolic leaflet. According to our findings, PIP2 at greater than 0.1 mol% of total lipids in the presence of multivalent metal ions would exist in these PIP2 cation clusters. Only very sensitive techniques, such as those based on fluorescence, are able to report on PIP2 behavior in the range of concentrations where we have shown PIP2 self-association to begin. Second, many other studies did not account for the effects of multivalent metal ions, which typically are present as contaminants in the micromolar range and which we now know to be critical in promoting clustering. Some published experiments, especially those in the presence of EDTA, studied what one might refer to as ‘‘free PIP2.’’ Such PIP2 could still be hydrogen bonded in a network but would be expected to be less tightly associated than the PIP2 cation clusters that we describe here.

PIP2 self-association is robust in the sense of not being dependent on a particular multivalent cation. Al^{3+} had the strongest influence on cluster formation, and Mg^{2+} had the weakest, but the variety of cations that promote cluster formation, which include Ca^{2+}, Zn^{2+}, and Fe^{3+}, implies that the two-dimensional array of the many PIP2 phosphate groups creates a strong cation-binding matrix. Physiological levels of 100 mM Ca^{2+} and 0.5 mM Mg^{2+} are sufficient to cause strong PIP2 clustering, which implies that PIP2 is most likely to be clustered during transient cellular calcium influx.

We do not yet have a molecular model to explain the mechanism by which multivalent metal ions promote clustering, with some ions such as Al^{3+} being more effective than others such as Mg^{2+}. One possibility is that the quantitatively lesser self-quenching and FRET promoted by Mg^{2+}, compared with some other multivalent ions, might reflect more loosely packed PIP2, with other lipid molecules in the cluster hindering direct contact between PIP2 molecules. Another possibility is that the cluster size differs depending on the ion. Fluorescent PIP2 molecules at the periphery of a cluster presumably would be less quenched, and the fraction of molecules at the periphery would be larger for clusters with dimensions of a few nanometers than for ones with micron size. However, it is important to note that the critical concentration at which clustering begins is similar for all of the ions tested, i.e, in the range of 0.02-0.05 mol% of total lipid. In forming a stable cation-bridged cluster, PIP2 cation behavior is like the well-known inorganic chemical behavior of the strong association of multivalent cations with phosphate itself (48). It is noteworthy that even with the repulsive effect of the approximately four negative charges under physiological conditions (21,49,50), PIP2 molecules still strongly attract each other by multivalent metal ion bridging of headgroup phosphates. This attraction would affect PIP2 physical chemical properties and spatial distribution in membranes.

Much previous research was based on especially simple lipid compositions. Our finding that bulk lipid composition affects clustering has consequences for the behavior of PIP2 in cells. That PIP2 cation clustering depends on the type and concentration of multivalent cations and on the composition of the surrounding lipids has an interesting implication. The concentration at which clusters form is also the

concentration of free PIP2 in the bilayer in equilibrium with clustered PIP2. If compositionally distinct regions occur in the cytosolic leaflet of the PM and if multivalent metal ion type or concentration is spatially localized, for example as in transient Ca^{2+} or Zn^{2+} influx at certain sites (51,52), different local concentrations of free PIP2 would result. Consistent with this idea, the original suggestion of ‘‘membrane rafts’’ was based on experimental findings of distinct compositional regions, apical and basolateral, in intestinal epithelial cell PMs (53).

Understanding how PIP2 exists as ‘‘spatially separated pools’’ in cellular membranes will be an important underpinning of analysis of function. A large number of cellular proteins interact with PIP2. The proteins that bind to free PIP2 would experience decreased function when PIP2 cation-bridged clusters form, whereas those that bind preferentially to such clusters would experience enhanced function. Carefully designed experiments with model membranes and purified proteins could define such preferences for individual proteins. Elucidating the status of the PIP2 molecules in the PM is critical to understanding the cell biological behavior resulting from protein binding. The methods that we report here can be used to examine even better and more complex models of the PM, including PIP2 within a membrane model with additional components, such as PE/PS/PI/PC/Chol, and including the polyunsaturated acyl chains abundant in natural PE and PS.

ACKNOWLEDGEMENTS

We thank the Cornell Nutrient Analysis Laboratory and Michael A. Rutzke and Tatyana Dokuchayeva for help with ICP-OES data collection and analysis. We thank

Robert A. Dick for providing helpful advice. This work was supported by National Institutes of Health grants 2R01GM107013 (V.M.V.) and R01GM105684 (G.W.F.).

REFERENCES

1. Ferrell, J.E., and W.H. Huestis. 1984. Phosphoinositide metabolism and the morphology of human erythrocytes. J Cell Biol. 98:1992-1998.
2. McLaughlin, S., J. Wang, A. Gambhir, and D. Murray. 2002. PIP2 and proteins: interactions, organization, and information flow. Annu Rev Biophys Biomol Struc. 31:151-175.
3. Balla, T. 2013. Phosphoinositides: tiny lipids with giant impact on cell regulation. Physiol Rev. 93:1019-1137.
4. Rhee, S.G. 2001. Regulation of phosphoinositide-specific phospholipase C. Annu Rev Biochem. 70:281-312.
5. Berridge, M.J., and R.F. Irvine. 1984. Inositol trisphosphate, a novel second messenger in cellular signal transduction. Nature. 312:315-321.
6. Cantley, L.C. 2002. The phosphoinositide 3-kinase pathway. Science. 296:1655-1657.
7. Martin, T.F.J. 2015. PI(4,5)P2-binding effector proteins for vesicle exocytosis. BBA - Mol Cell Biol of Lipids. 1851:785-793.
8. Simonsen, A., A.E. Wurmser, S.D. Emr, and H. Stenmark. 2001. The role of phosphoinositides in membrane transport. Curr Opin Cell Biol. 13:485-492.
9. Martin, T.F. 2001. PI(4,5)P2 regulation of surface membrane traffic. Curr Opin Cell Biol. 13:493-499.
10. Raucher, D., T. Stauffer, W. Chen, K. Shen, S. Guo, J.D. York, M.P. Sheetz, and T. Meyer. 2000. Phosphatidylinositol 4,5-Bisphosphate Functions as a Second Messenger that Regulates Cytoskeleton-Plasma Membrane Adhesion. Cell. 100:221-228.
11. Suh, B.-C., and B. Hille. 2005. Regulation of ion channels by phosphatidylinositol 4,5-bisphosphate. Curr Opin in Neurobiol. 15:370-378.
12. Ono, A., S.D. Ablan, S.J. Lockett, K. Nagashima, and E.O. Freed. 2004. Phosphatidylinositol (4,5) bisphosphate regulates HIV-1 Gag targeting to the plasma membrane. Proc Natl Acad Sci. 101:14889-14894.

13. Saad, J.S., and D.M. Muriaux. 2015. Editorial: Role of lipids in virus assembly. Front. Microbiol. 6410.
14. Mücksch, F., V. Laketa, B. Müller, C. Schultz, and H.-G. Kräusslich. 2017. Synchronized HIV assembly by tunable PIP2 changes reveals PIP2 requirement for stable Gag anchoring. Elife. 6: e25287.
15. Hinchliffe, K.A., A. Ciruela, and R.F. Irvine. 1998. PIPkins1, their substrates and their products: new functions for old enzymes. Biochimica et Biophysica Acta. 143687-104.
16. Brown, D.A. 2015. PIP2 Clustering: From model membranes to cells. Chem Phys Lipids. 192:33-40.
17. Redfern, D.A., and A. Gericke. 2005. pH-dependent domain formation in phosphatidylinositol polyphosphate/phosphatidylcholine mixed vesicles. J. Lipid Res. 46504-515.
18. Levental, I., D.A. Christian, Y.-H. Wang, J.J. Madara, D.E. Discher, and P.A. Janmey. 2009. Calcium-dependent lateral organization in phosphatidylinositol 4,5-bisphosphate (PIP2)- and cholesterol-containing monolayers. Biochemistry. 48:8241-8248.
19. Sarmento, M.J., A. Coutinho, A. Fedorov, M. Prieto, and F. Fernandes. 2014. Ca^{2+} induces PI(4,5)P2 clusters on lipid bilayers at physiological PI(4,5)P2 and Ca^{2+} concentrations. Biochimica et Biophysica Acta (BBA) - Biomembranes. 1838:822-830.
20. Jiang, Z., R.E. Redfern, Y. Isler, A.H. Ross, and A. Gericke. 2014. Cholesterol stabilizes fluid phosphoinositide domains. Chem Phys of Lipids. 182: 52-61.
21. Kooijman, E.E., K.E. King, M. Gangoda, and A. Gericke. 2009. Ionization properties of phosphatidylinositol polyphosphates in mixed model membranes. Biochemistry. 48:9360-9371.
22. Graber, Z.T., Z. Jiang, A. Gericke, and E.E. Kooijman. 2012. Phosphatidylinositol-4,5-bisphosphate ionization and domain formation in the presence of lipids with hydrogen bond donor capabilities. Chem Phys Lipids. 165:696-704.

23. Wang, Y.H., A. Collins, L. Guo, K.B. Smith-Dupont, F. Gai, T. Svitkina, and P.A. Janmey. 2012. Divalent cation-induced cluster formation by polyphosphoinositides in model membranes. J. Am. Chem. Soc. 134:3387-3395.
24. Slochower, D.R., Y.-H. Wang, R.W. Tourdot, R. Radhakrishnan, and P.A. Janmey. 2014. Counterion-mediated pattern formation in membranes containing anionic lipids. Advances in Colloid and Interface Science. 208:177-188.
25. Wang, Y.-H., D.R. Slochower, and P.A. Janmey. 2014. Counterion-mediated cluster formation by polyphosphoinositides. Chem Phys Lipids. 182:38-51.
26. Levental, I., A. Cēbers, and P.A. Janmey. 2008. Combined electrostatics and hydrogen bonding determine intermolecular interactions between polyphosphoinositides. J. Am. Chem Soc. 130:9025-9030.
27. Carvalho, K., L. Ramos, C. Roy, and C. Picart. 2008. Giant unilamellar vesicles containing phosphatidylinositol (4,5) bisphosphate: characterization and functionality. Biophys J. 95:4348-4360.
28. Slochower, D.R., P.J. Huwe, R. Radhakrishnan, and P.A. Janmey. 2013. Quantum and all-atom molecular dynamics simulations of protonation and divalent ion binding to phosphatidylinositol 4,5-bisphosphate (PIP2). J Phys Chem. B. 117:8322-8329.
29. Ellenbroek, W.G., Y.-H. Wang, D.A. Christian, D.E. Discher, P.A. Janmey, and A.J. Liu. 2011. Divalent cation-dependent formation of electrostatic PIP2 clusters in lipid monolayers. Biophys J. 1012178-2184.
30. Honigmann, A., G. van den Bogaart, E. Iraheta, H.J. Risselada, D. Milovanovic, V. Mueller, S. Müllar, U. Diederichsen, D. Fasshauer, H. Grubmüller, S.W. Hell, C. Eggeling, K. Kühnel, and R. Jahn. 2013. Phosphatidylinositol 4,5-bisphosphate clusters act as molecular beacons for vesicle recruitment. Nat Struct Mol Biol. 20:679-686.
31. van den Bogaart, G., K. Meyenberg, H.J. Risselada, H. Amin, K.I. Willig, B.E. Hubrich, M. Dier, S.W. Hell, H. Grubmüller, U. Diederichsen, and R. Jahn. 2011. Membrane protein sequestering by ionic protein- lipid interactions. Nature. 479552-555.

32. Fujita, A., J. Cheng, K. Tauchi-Sato, T. Takenawa, and T. Fujimoto. 2009. A distinct pool of phosphatidylinositol 4,5-bisphosphate in caveolae revealed by a nanoscale labeling technique. Proc Natl Acad Sci. 1069256-9261.
33. Varnai, P., and T. Balla. 1998. Visualization of phosphoinositides that bind pleckstrin homology domains: calcium- and agonist-induced dynamic changes and relationship to myo-[3H]inositol-labeled phosphoinositide pools. J Cell Biol. 143:501-510.
34. Laux, T., K. Fukami, M. Thelen, T. Golub, D. Frey, and P. Caroni. 2000. GAP43, MARCKS, and CAP23 modulate PI(4,5)P2 at plasmalemmal rafts, and regulate cell cortex actin dynamics through a common mechanism. J Cell Biol. 149:1455-1472.
35. McLaughlin, S., and D. Murray. 2005. Plasma membrane phosphoinositide organization by protein electrostatics. Nature. 438:605-611.
36. Glaser, M., S. Wanaski, C.A. Buser, V. Boguslavsky, W. Rashidzada, A. Morris, M. Rebecchi, S.F. Scarlata, L.W. Runnels, G.D. Prestwich, J. Chen, A. Aderem, J. Ahn, and S. McLaughlin. 1996. Myristoylated alanine-rich C kinase substrate (MARCKS) produces reversible inhibition of phospholipase c by sequestering phosphatidylinositol 4,5-bisphosphate in lateral domains. J. Biol Chem. 271:26187-26193.
37. Gambhir, A., G. Hangyás-Mihályné, I. Zaitseva, D.S. Cafiso, J. Wang, D. Murray, S.N. Pentyala, S.O. Smith, and S. McLaughlin. 2004. Electrostatic sequestration of PIP2 on phospholipid membranes by basic/aromatic regions of proteins. Biophys J. 862188-2207.
38. Davis, B.M., J.L. Richens, and P. O'Shea. 2011. Label-free critical micelle concentration determination of bacterial quorum sensing molecules. Biophys J. 101:245-254.
39. Israelachvili, J.N., 2011. Intermolecular and surface forces. Academic press.
40. Kingsley, P.B., and G.W. Feigenson. 1979. Synthesis of a perdeuterated phospholipid - 1,2-dimyristoyl-sn-glycero-3-phosphocholine-d72. Chem Phys Lipids. 24:135-147.

41. Gonzalez-Sastre, F., & Folch-Pi, J. 1968. Thin-layer chromatography of the phosphoinositides. J Lipid Res, 9:532-533.
42. Andrews, W. V., & Conn, P. M. 1987. Measurement of inositol phospholipid metabolites by one-dimensional thin-layer chromatography. Methods in enzymology, 141:156-168.
43. Buboltz, J.T., and G.W. Feigenson. 1999. A novel strategy for the preparation of liposomes: rapid solvent exchange. Biochimica et Biophysica Acta (BBA) - Biomembranes. 1417:232-245.
44. Rutzke, M.A. 2017. Atomic absorption, inductively coupled plasma optical emission spectroscopy, and infrared spectroscopy. 2nd Ed. Springer International Publishing. 1-8.
45. Jang, H.K., Y.D. Chung, S.W. Whangbo, I.W. Lyo, C.N. Whang, S.J. Lee, and S. Lee. 2000. Effects of chemical etching with hydrochloric acid on a glass surface. J. Vac. Sci. Technol. A. 18:2563-6.
46. Romani, A. 2007. Regulation of magnesium homeostasis and transport in mammalian cells. Archives of Biochemistry and Biophysics. 458:90-102.
47. Loura, L.M.S., and M. Prieto. 2011. FRET in membrane biophysics: an overview. Front Physiol. 2:82.
48. Rashchi, F. and Finch, J.A., 2000. Polyphosphates: a review their chemistry and application with particular reference to mineral processing. Minerals Engineering, 13:1019-1035.
49. Toner, M., G. Vaio, A. McLaughlin, and S. McLaughlin. 1988. Adsorption of cations to phosphatidylinositol 4,5-bisphosphate. Biochemistry. 27:7435-7443.
50. van Paridon, P.A., B. De Kruijff, R. Ouwerkerk, and K.W. Wirtz. 1986. Polyphosphoinositides undergo charge neutralization in the physiological pH range: a 31P-NMR study. Biochimica et Biophysica Acta. 877:216-219.
51. Que, E.L., R. Bleher, F.E. Duncan, B.Y. Kong, S.C. Gleber, S. Vogt, S. Chen, S.A. Garwin, A.R. Bayer, V.P. Dravid, T.K. Woodruff, and T.V. O'Halloran. 2014. Quantitative mapping of zinc fluxes in the mammalian egg reveals the origin of fertilization-induced zinc sparks. Nat Chem. 7:130-139.

52. Parekh, A.B. and Penner, R., 1997. Store depletion and calcium influx. Physiol Rev, 77:901-930.
53. Simons, K., and G. van Meer. 1988. Lipid sorting in epithelial cells. Biochemistry. 27:6197-6202.

CHAPTER 5

MULTIMERIZATION OF THE HIV-1 STRUCTURAL PROTEIN GAG PROMOTES PI(4,5)P_2 CLUSTERING DURING RETROVIRAL ASSEMBLY

ABSTRACT

Located at the inner leaflet of the plasma membrane (PM), phosphatidylinositol 4,5-bisphosphate [PI(4,5)P_2, here PIP2] has been proposed to exist in distinct pools or microdomains. Multiple cellular factors can contribute to such spatially separated PIP2 clusters. The two most important factors are multivalent cation bridging and protein sequestration. PIP2 is critically involved not only in many cellular processes, but also in HIV-1 virus assembly and release. For example, in vitro at a physiological level of 2 mol%, PIP2 is sufficient to significantly enhance membrane binding of the viral structural protein Gag. In vivo, depletion of PIP2 from the PM results in a significant decrease in HIV budding. Furthermore, the HIV-1 viral membrane is enriched in PIP2 compared with the host PM. These results led to a hypothesis that HIV-1 assembles at, and buds from, PIP2-rich clusters of the PM. However, key details of this model remain elusive. Under physiological ionic strength, and cation and pH conditions, PIP2 is reported to exist in both free and clustered states in vitro. Using purified Gag derivative proteins and model membranes with PM inner leaflet lipid compositions, I aimed to answer two questions: (1) Does HIV-1 Gag

recognize and target PIP2 clusters? I observed that in giant unilamellar vesicle (GUVs) assays, fluorescently labeled, myristoylated HIV-1 MA, the membrane-binding domain of Gag, prefers binding to membranes containing PIP2 in clusters compared with membranes with free PIP2. By contrast, fluorescent charge sensor proteins hardly sense any difference between membranes containing free and clustered PIP2. I thus hypothesize that the HIV-1 structural protein Gag exploits PIP2 clusters as sites of viral assembly. (2) Does membrane association and multimerization cause PIP2 clustering? HIV-1 MA can form trimers on PIP2-containing membranes. The longer HIV-1 Gag protein MASP, which harbors the intact spacer peptide, is able to form hexamers. I found that free PIP2 can be induced to form clusters upon HIV-1 MA and MASP membrane association, revealed by self-quenching of acyl chain-labeled fluorescent PIP2 in large unilamellar vesicle (LUVs). In addition, under resting conditions with 0.5mM Mg^{2+}, pre-existing PIP2 clusters induced by Mg^{2+} are further promoted by HIV-1 MA trimerization and MASP hexamerization. However, MA and MASP multimerization defective mutants fail to reorganize PIP2 lateral distributions. My study provides the first evidence that HIV-1 Gag selectively targets PIP2 clusters for viral assembly and that Gag binding and multimerization can further enrich PIP2 at assembly sites.

INTRODUCTION

Assembly of retroviruses, such as human immunodeficiency type 1 (HIV-1), is driven by the structural polyprotein Gag. All retroviral Gag proteins have three major

domains: the matrix domain (MA), which interacts with the inner leaflet of the plasma membrane (PM); the capsid domain (CA), which mediates Gag-Gag oglimerization; and the nucleocapsid domain (NC), which packages two copies of viral genomic RNAs into a ribonucleoprotein (RNP) complex. In addition, HIV-1 Gag also contains three small peptide fragments: a short spacer peptide between CA and NC termed SP1 and two peptides downstream of NC, called SP2 and p6. Approximately 2000 copies of Gag assemble at the PM to form an immature virion, with the N-terminal MA domain associating with the inner leaflet of the PM, the central CA domain forming a hexameric lattice arranged as an incomplete sphere, and the C-terminal end of Gag bound to viral genomic RNA (1, 2). During or immediately after budding, the virus undergoes major rearrangements triggered by cleavage of Gag by the viral protease (PR) resulting in the formation of a mature virion. The rate of proteolytic cleavage varies for the different PR sites within Gag, with the fastest at SP1-NC, followed by SP2-p6, MA-CA, NC-SP2, and finally, CA-SP1 (3). The liberated CA domains condense to form a conical core that encapsulates the RNA-NC ribonucleoprotein complex, which is the hallmark of an infectious mature HIV-1 viral particle (4, 5). Liberated MA domains remain associated with the viral membrane.

The MA domain of HIV-1 serves several functions during retroviral assembly (6). Gag is synthesized in cytosol, and then the MA domain directs Gag to the negatively charged inner leaflet of the PM through a bipartite signal: the N-terminal 14-carbon myristate and a patch of basic residues (7). The insertion of myristate into membranes provides approximately 8 kcal/mol in free energy to the protein-lipid interaction, which alone is not sufficient for MA membrane binding (8). Mutation of

the glycine at position 2 to alanine blocks myristoylation of HIV-1 MA (9). The non-myristoylated version of HIV-1 Gag and MA exhibit reduced membrane binding compared to wild type myristoylated proteins (10-12). According to surface plasmon resonance (SPR) and liposome flotation assays, MA myristoylation increases the membrane binding affinity by a factor of 10 (10). The basic patch of residues on the globular head of MA, including the highly basic region (HBR) which spans residues 15-31, is critical for efficient membrane binding. Mutations in the MA HBR redirect Gag to intracellular compartments and reduce PM-localized Gag (13). Structural and mutagenesis studies demonstrate that amino acids in the HBR are exposed on the surface of the MA domain (13-14). These amino acids interact with negatively charged lipids the inner leaflet, phosphatidylserine (PS) and phosphatidylinositol (4,5) bisphosphate (15-18). Both the electrostatic interactions between the basic patch of the globular head and negatively charged lipids at the inner leaflet, and the hydrophobic interaction between the N-terminal myristate and the membrane bilayer core, are required for correct PM targeting (6, 19, 20). However, the relative contributions from electrostatic interactions and hydrophobic interactions are difficult to decipher.

HIV-1 MA is reported to contain a specific binding pocket for the headgroup of PIP2 (21). PIP2 increases HIV-1 MA membrane binding in liposome pelleting and flotation assays (15). Based on SPR measurements, specific interactions with PIP2 enhance MA membrane affinity at a level similar to that of MA myristoylation (10). HIV-1 Gag binding to PIP2 is mediated by the basic amino acids in MA, especially K29 and K31. Myristoylated Gag with these amino acids mutated has an almost 3-fold decrease in binding to PIP2-containing liposomes compared to wild type Gag (15, 22).

Interestingly, a Gag mutant with all lysines and arginines switched in the HBR (HBR/RK switch) exhibits almost no binding to PIP2-containing liposomes, which indicates that not only the overall charge but also the specific amino acid sequence within HBR is critical for HIV-1 Gag interaction with PIP2 (18, 23). In addition, the PIP2-binding site overlaps with an RNA-binding site in MA. RNA bound to the MA HBR blocks interactions with PS membranes, but not with PIP2 containing membranes, which indicates that MA-binding RNA might serve as a regulator to ensure that Gag targets PIP2-rich sites at the PM, instead of intracellular membranes (24, 25). Overexpression of polyphosphoinositide 5-phosphatase IV (5ptaseIV), which depletes PIP2 at the PM, abrogates HIV-1 virus particle release and redirects Gag to intracellular compartments (26). According to several lipidomics studies, HIV-1 viral membranes are enriched in PIP2 compared to the host PM in an MA-dependent manner (27-29). Altogether, these results demonstrate that the specific interaction between HIV-1 MA and PIP2 is essential for correct PM targeting and retroviral assembly.

In addition to directing HIV-1 Gag to the PM for, MA is also involved in incorporation of envelope (Env) proteins into virus particles (30, 31). While the mechanism of Env localization to assembly sites remains unclear, many studies provide evidence of a direct interaction of HIV-1 MA and the cytoplasmic tail (CT) of Env during viral assembly (32-44). Assembly-competent MA mutants that fail to incorporate Env can be rescued by large C-terminal truncations of the CT of Env or compensatory mutations in MA (39). Similarly, Env mutant with small deletions in the CT that lead to Env-deficient particles can be rescued by mutations in MA (39).

Studies show that Gag reduces Env mobility at assembly sites, and this is dependent on Gag multimerization (45). These results indicate that MA interacts with and retains Env at virus assembly sites.

MA has been shown to form trimers in solution and in the crystals, and the three-dimensional structures (see Fig. 5.1) have been solved by several groups (46-48). A similar MA trimer was also observed in the crystal structure of another lentivirus, simian immunodeficiency virus (SIV) (49). The HIV-1 MA structures determined by NMR and X-ray crystallography are similar (48). MA consists of a large N-terminal globular head and a flexible C-terminal tail. An individual MA is composed of five α-helices, a short 3_{10} helical stretch, and three β-sheet strands. Helixes H1, H2, H3 and the 3_{10} helix pack around H4 to form a compact globular domain, while helix H5 is projected away from the β-sheet strands, which makes the C-terminal region distinct from its globular N-terminal. However, a major structural difference is a 6 Å displacement of a short 3_{10} helix positioned at the trimer interface (48). Further analysis showed that conserved residues P66 and G71 function as hinges that allow the 3_{10} helix to undergo a structural reorientation on trimerization. Thus, the flexibility of 3_{10} helix might play a role in viral assembly and disassembly.

MA is reported to be trimeric in both mature and immature particles indicating that in MA trimerization occurs in the context of the Gag lattice. Both myristoylated MA and MACA exhibit similar patterns hexamers of HIV-1 trimers on PIP2-containing membranes (50-52). Structure of the MA trimer shows the interface at

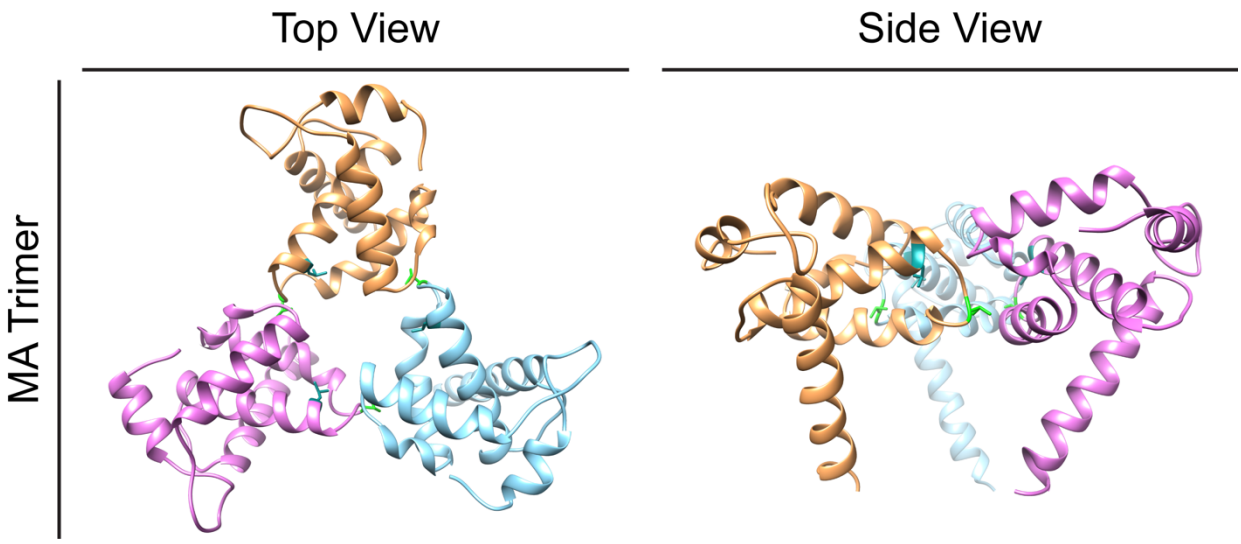

Fig 5.1 The crystal structure of HIV-1 MA trimers (PDB:1HW). Individual MA is shown in pink, orange, and blue. Mutations of T69 (green), L74 (cyan) lead to trimer-defective HIV-1 MA.

residues 42-77. Trimerized MA associates with the membranes, with the HBR of each MA molecule oriented towards the membrane.

MA trimerization is proposed to accommodate, or form around, the CT of HIV-1 Env (30). A cross-linking study found several mutations at the MA trimer interface that impair Env incorporation, such as 69TR, 69TD, and 74LE (see Fig. 5.1) (53). Env seems to be sterically excluded from trimer-defective viral particles. Interestingly, Env with a truncated CT is incorporated into these MA trimerization-defective particles. MA mutants that impose a steric hinderance with CT block Env incorporation and therefore viral infectivity. A 2d-crystallography study showed that HIV-1 MA assembles into hexamers of trimers on membranes containing PIP2 and that MA-CT interactions occur at the hexamer interface formed by six trimers (50, 54, 55). Recent investigations show that the mutation 62QR, located at the MA trimer interface, affects HIV-1 Env incorporation (41, 56). This 62QR mutation suppresses Env incorporation defects of other MA or CT mutations. Moreover, HIV-1 MA 62QR exhibits an enhanced trimerization capacity, but has a similar organization pattern on membranes, compared with the wildtype MA. The 62QR mutant also binds to HIV-1 CT with higher affinity than wildtype MA, which suggests that multivalent binding of MA and CT leads to efficient Env incorporation into assembling particles.

HIV-1 Gag contains a short conserved region called SP1, which is indispensable for viral assembly. Positioned between CA and NC, SP1 and seven residues upstream fold into a six-helix bundle (see Fig. 5.2), which helps form and stabilize the immature Gag hexamer (57-59). Insertion of a glycine or a proline into SP1, or mutations within SP1, such as H358, K359, A360, L363, A366, and

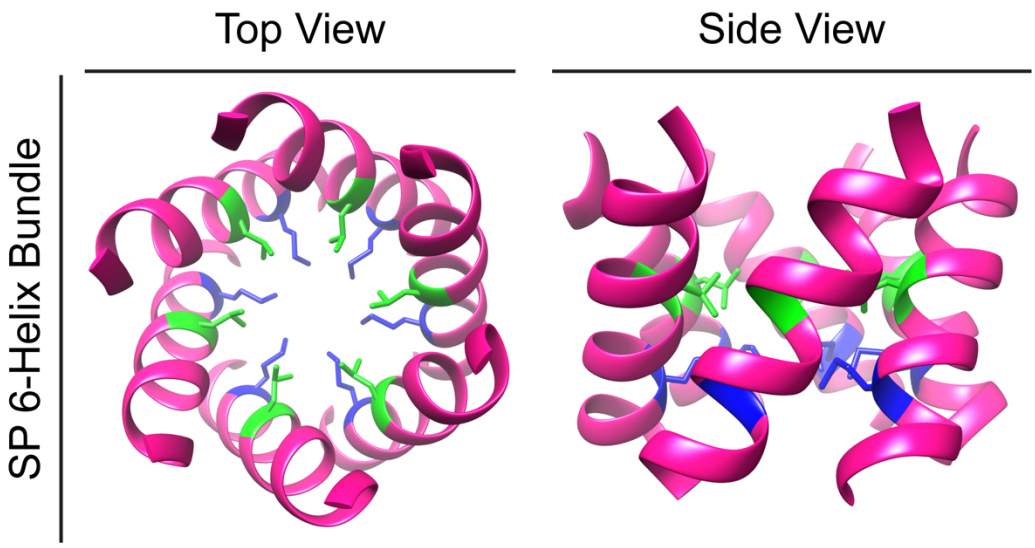

Fig 5.2 The structure of HIV-1 six-helix-bundle (6HB) (PDB:5L93). Mutations of 363L (green) or 367M (blue) destabilize 6HB formation.

M367, abrogate viral production, indicating that proper formation of the six-helix bundle is essential (60). Gag mutants with either 363LA or 367MA mutations exhibit a severely diminished ability for PM-association and virus production (61, 62). Studies report that the majority of membrane-bound Gag mutants are small oligomers, which implies that the significantly decreased membrane affinity of these mutants is due its defect in multimerization (61). Moreover, purified recombinant Gag mutant proteins also form lower amounts of high-molecular-weight complexes. These results suggest that mutations that block Gag multimerization inhibit Gag-membrane association. Interestingly, even though single mutation 363LA and 367MA restricts Gag binding to membranes, a double mutation 363LA/ 367MA restores this defect (62). Within SP1, hydrophobic residues L363 and M367, positioned on the same side of the helix (see Fig. 5.2), are able to mediate hydrophobic interactions between Gag molecules in a synergistic manner (63).

In addition to SP1, CA is required for Gag multimerization (64, 65). Like all retroviral CA proteins, HIV-1 CA is composed of two distinct folded sub-domains, the N-terminal domain (NTD) and the C-terminal domain (CTD). The NTD is composed of an N-terminal β-hairpin and 7 α-helices and; the CTD domain is composed of 4 α-helices and a 3_{10} helix (66). The assembly-defective mutations in CA are clustered in 3 regions: a surface composed of helices H4 to H6 in NTD, the CA dimer interface in CTD, and the loop preceding H8 at the base of the CTD (67, 68). Evidence suggests that HIV-1 CA CTD dimerizes in solution and crystallizes as a dimer, and that the CTD dimer interface is important for particle assembly, maturation, and infectivity (65, 69-71). The CTD dimer interface is formed by parallel packing between H9 of

adjacent CA proteins resulting in a hydrophobic core interface including amino acids 313V, 316W, 317M, and 321L. Located in the hydrophobic interface of the CA dimer, both 316WA and 317MA mutations block CA dimerization in vitro, and severely impair immature particle production in vivo (72). Taken together, these results show that the CA dimer interface is critical for efficient intermolecular Gag-Gag interaction, and ultimately, immature viral particle assembly.

Recently, PIP2 was shown to be able to form clusters at extremely low concentrations in model membranes (73). This clustering is dependent on the presence of multivalent cations, and is influenced by the surrounding lipid environment. HIV-1 has been suggested to assemble and bud from PIP2-rich domains. In this study, I aimed to understand whether HIV-1 Gag targets PIP2 clusters as assembly sites. Some cellular proteins have been reported to induce PIP2 to cluster in cellular membranes or in model membranes. I also wanted to elucidate whether Gag multimerization can cause PIP2 clustering. Here, using purified HIV-1 Gag derivatives and mutants, and employing model membranes with the inner leaflet lipid composition, I studied the interplay of PIP2-PIP2, Gag-PIP2, and Gag-Gag interactions that may take place during HIV-1 assembly.

MATERIALS AND METHODS

DNA cloning and protein purification

Purified proteins used in this study are pictured in Fig. 5.3. DNA constructs used for non-labeled protein purification were cloned straight into pSUMO or pET3xc vector using Integrated Device Technology gene block techniques. For fluorescently labeled

proteins, monomeric neon green (mNG) was amplified from pHisII 6H-mNG, and ligated into pSUMO or pET3xc vectors. All proteins were purified using standard bacterial expression and affinity column techniques. In brief, Escherichia coli BL21 cultures were grown at 37°C to an optical density at 600 nm of 0.6. For myristoylated proteins, DNA constructs in pET plasmid and another plasmid that expresses yeast N-terminal myristoyl transferase (yNMT) were co-transformed into BL21. For myristoylated proteins, myristic acid (10 mg/liter, Sigma) was added to BL21 cultures 1 h before induction (74). Isopropyl -D-1-thiogalactopyranoside (IPTG) was added to a final concentration of 0.5 mM for induction. Induced cells were harvested 6 h post-induction. Pelleted cells were resuspended in lysis buffer [20 mM Tris, pH 8, 500 mM NaCl, 2 mM tris(2-carboxyethyl)-phosphine (TCEP), and 2 mM phenylmethylsulfonyl fluoride (PMSF)] and lysed by sonication. After ultracentrifugation in a TLA-110 Beckman rotor at 90,000 rpm for 45 min, the supernatant was collected. Then, supernatants were treated with polyethyleneimine (PEI) and spun at 10,000 rpm in a Sorvall 600 rotor at 4°C to remove nucleic acid. To the supernatant, ammonium sulfate was added till precipitants of protein of interest form, usually in the range of 20-30%, followed by centrifugation. The pellet was resuspended in binding buffer (20 mM Tris-HCl, pH 8, 100 mM NaCl, and 2 mM TCEP) and further purified by desalting chromatography (HiTrap SP FF; GE Healthcare) and Ni^{2+} affinity chromatography. Following the first round of Ni^{2+} chromatography, eluted proteins were dialyzed against buffer (20 mM Tris-HCl, pH 8, 500 mM NaCl, and 1 mM TCEP). For proteins expressed in pSUMO vectors, the dialysis was performed in the presence of approximately 300 μg of ULP1 protease to cleave off the SUMO tag. The

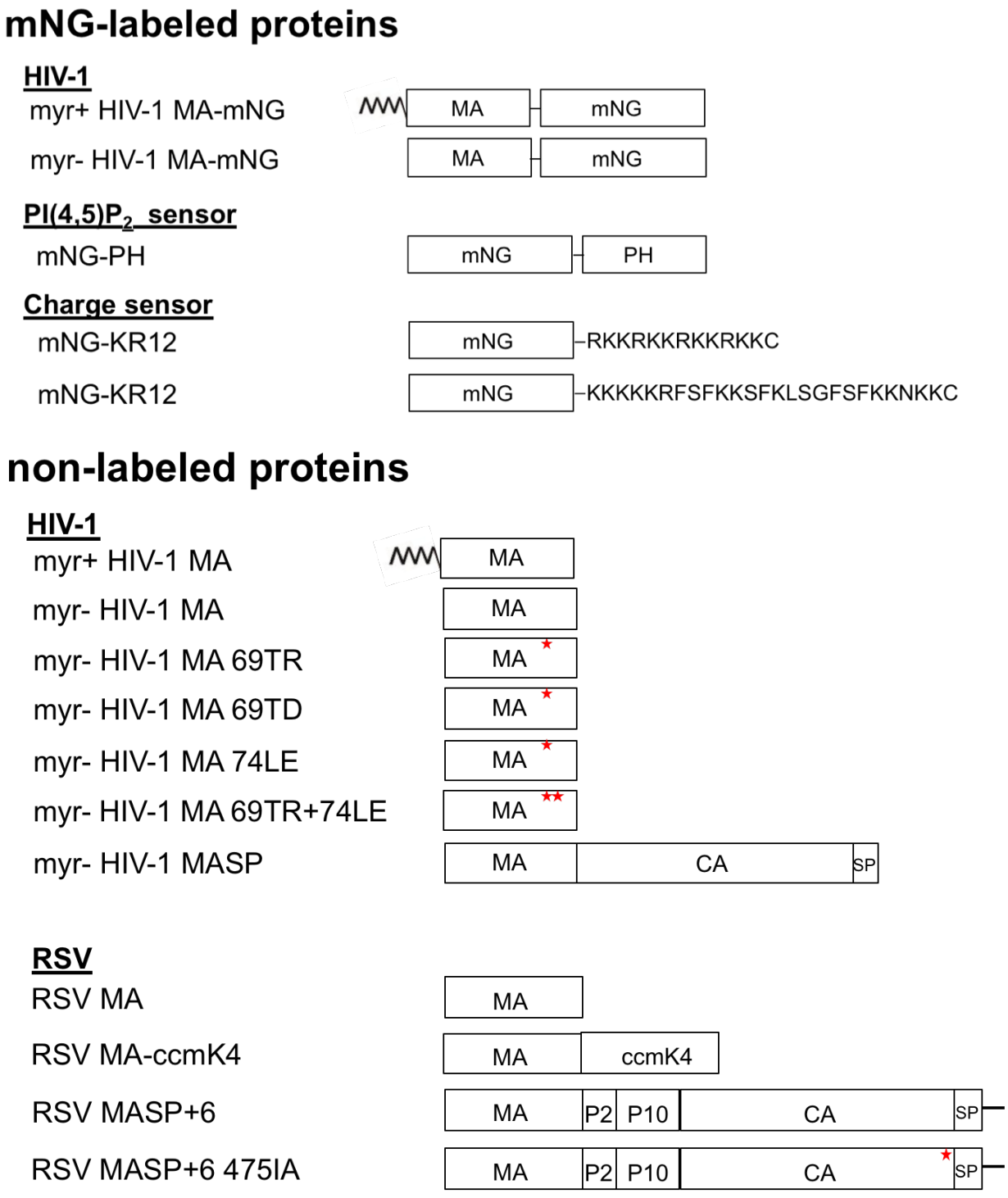

Fig 5.3 Schematic representation of proteins purified.

ULP1 protease and SUMO tag were removed by a second around of Ni^{2+} affinity chromatography (75). Purified protein at 2 to 10 mg/ml was flash frozen in aliquots and stored at -80°C. The final protein preparation had an A260/A280 ratio of 0.58 to 0.59, indicating the absence of nucleic acid. All proteins had a purity of approximately 90% after affinity column purification, as judged from stained gels.

Phospholipids and fluorescent probes

1-palmitoyl-2-oleoyl-sn-glycero-3-phosphoethanolamine (POPE), 1-palmitoyl-2-oleoyl-sn-glycero-3-phospho-L-serine (POPS), L-a-phosphatidylinositol-4,5-bisphosphate (bovine brain-PI(4,5) P2), and fluorescently labeled TopFluor (TF)-PI(4,5)P2 (1-oleoyl-2-{6-[4-(dipyrromethene boron difluoride)butanoyl] amino}hexanoyl-sn-glycero-3-phosphoinositol-4,5-bisphosphate), TMR-PI (4,5)P2 (1-oleoyl-2-(6-((4,4-difluoro-1,3-dimethyl-5-(4-methoxyphenyl)-4- bora-3a,4a-diaza-s-indacene-2-propionyl)amino)hexanoyl)-sn-glycero-3- phosphoinositol-4.5-bisphosphate were purchased from Avanti Polar Lipids (Alabaster, AL). Cholesterol was purchased from Nu-Chek Prep (Elysian, MN). Cholesterol stock solution was prepared by standard gravimetric procedures to 0.2% error. Concentrations of all phospholipid stocks were determined to 1% error by inorganic phosphate assay (76). The working stocks of TF- and TMR-labeled PIP2 were prepared in chloroform:methanol:H_2O=20:9:1. Fluorescent probe extinction coefficients were obtained from lot certificates of analysis: 97,000 M^{-1} cm^{-1} at 496 nm for TF and 56,000 M^{-1} cm^{-1} at 544 nm for TMR. Probe concentrations were determined in methanol by absorption spectroscopy using an HP 8452A spectrophotometer (Hewlett-

Packard, Palo Alto, CA). Lipid purity of R99.5% was confirmed by thin-layer chromatography (TLC). TLC was performed on washed, activated silica gel plates (Alltech, Deerfield, IL) developed with chloroform:methanol:water=65:25:4 for most phospholipids and for cholesterol with petroleum ether:diethyl ether:chloroform=7:3:3. TLC plates for PIP2 were pre-run with 10% K2C2O4+2 mM EDTA and then activated at 100 °C for 30 min before use. TLC plates for PIP2 were developed with chloroform:methanol:4 N NH4OH= 45:35:10 (73).

Buffer preparation and metal ion measurement

All buffers used were based on 100 mM KCl, 20 mM HEPES (pH=7.2). "Pure buffers" were prepared with KCl (99.999%; Sigma-Aldrich or ACROS (Geel, Belgium)), HEPES (99.5%; Sigma-Aldrich), and stored in Teflon fluorinated ethylene propylene bottles (Nalgene). Water was purified to 18.2 MΩ by passage through a Barnstead MicroPure system (Thermo Fisher, Waltham, MA). Micromolar levels of Al^{3+}, Ca^{2+}, Fe^{3+}, Zn^{2+}, and Mg^{2+} were prepared from 100 mM stock solutions stored at pH = 2-3. These stocks were made with aluminum chloride (99.999%), calcium chloride (99%), and magnesium chloride hexahydrate (99%), all from Sigma-Aldrich. Disodium EDTA (99%; Sigma-Aldrich) was prepared and stored as a 500 mM stock solution at pH = 7.2. Ion concentrations and purities of all stocks and freshly prepared buffers were confirmed by inductively coupled plasma optical emission spectroscopy (ICP-OES) (77) at the Cornell Nutrient Analysis Laboratory using Spectro Arcos ICP-OES.

LUV preparation

A total of 250 nmol lipid mixtures were dispensed into each borosilicate culture tube using glass syringes (Hamilton, Reno, NC). Large unilamellar vesicles (LUVs) were prepared using rapid solvent exchange (RSE), followed by extrusion through polycarbonate filters 31 times (78). Samples were sealed under argon at a final lipid concentration of 0.5 mM.

Self-quenching

Purified proteins were subject to buffer exchange and concentrating using spin columns. The final protein was in buffers matching the corresponding LUV buffers, in 100 mM KCl, 20 mM HEPES (pH=7.2), with or without additional EDTA or multivalent cations. A volume of 160 μl of 0.5mM LUVs and 40 μl of purified protein were mixed in the microcuvette to reach a total volume of 200 μl at room temperature. The final protein-membrane mixture was 400 μM lipids and 20 μM proteins. If PIP2 was 2 mol% of total lipids, a calculated 4 μM PIP2 was exposed to proteins on the outer leaflet. Fluorescence was collected on a Hitachi F-7000 FL spectrofluorimeter (Hitachi High Technologies America, Schaumburg, IL) at 23°C. Wavelengths used for self-quenching studies were (ex/em) as follows: TF (485/515 nm) and light scattering (440/420 nm). Data were collected with slits for ex/em=2.5/2.5 nm and a 10 s integration time.

Liposome pelleting assay

After self-quenching and FRET measurements, protein-LUV mixtures were ultracentrifuged at 90,000 rpm in a TLA-100 (Beckman) rotor for 45 min at 4°C. Supernatant was removed and the pellet was resuspended and subjected to SDS-PAGE analysis (79). Gels were Coomassie blue stained overnight and destained, and band intensity was determined by densitometry analysis using ImageQuant software 5.2 (80).

GUV preparation and confocal imaging

A total of 250 nmol total lipid containing 0.02 mol% LR-DOPE was mixed in chloroform, partially dried to a thin film in a culture tube using a rotary evaporator, and then dried with heating at 55°C under high vacuum for 1.5 h. The thin dry film was then hydrated with wet N2 gas at 55°C for 30 min. Lipid films were further hydrated with prewarmed ~225 mM sucrose buffer (Fisher Scientific) and incubated at 55°C for 30 min. GUVs formed as the sample was cooled over 10 h to room temperature (23°C) (80). GUVs were harvested into pure buffer 100 mM KCl, 20 mM HEPES (pH=7.2), with or without additional EDTA or multivalent cations. All buffers were osmotically balanced, confirmed by measurements using an osmometer (model No. 5004; Precision Systems, Natick, MA). an Eclipse C2+ Confocal Microscope (Nikon Instruments) with a 60×/1.2 NA water immersion objective, was used for GUV imaging at 23°C. Sample chambers for observation consisted of a No. 1.5 coverslip and traditional microscope slide separated with a silicone spacer (Sigma-Aldrich) of 0.25 mm thickness. Fluorescence signals were quantified in Fiji using the plot profile function. Line scan analysis was performed across the perimeter of each GUV to get

an average fluorescence intensity on the membrane, with background fluorescence subtracted. Two line scans per GUV and no fewer than 30 GUVs were analyzed for each protein under each buffer condition (see Fig. 5.4).

RESULTS

Myristoylated HIV-1 MA prefers binding to clustered PIP2 over free PIP2

PIP2 is hypothesized to exist as "spatially separated pools" at the inner leaflet of the PM (81). PIP2 clusters can form in the presence of multivalent cations (73). Under physiologically conditions in vitro, PIP2 can co-exist in free and clustered states. How HIV-1 MA might take advantage of PIP2 at assembly sites is unclear. Here, I purified fluorescent mNG-fusion proteins, and prepared giant unilamellar vesicles (GUVs) with the inner leaflet lipid composition POPE/POPS/Chol/PIP2 (32/30/36/2), for confocal visualization. I was able to modulate PIP2 lateral organization by controlling multivalent cation presence, types and concentrations. I tested three different cation conditions in 100mM KCl, 20mM HEPES (pH=7.2): 2mM EDTA in which PIP2 is free (unclustered), 0.5mM Mg^{2+} and 100μM Ca^{2+} to give moderate PIP2 clustering, and 0.5mM Mg^{2+} and 3μM Al^{3+} to give strong PIP2 clustering. In the absence of PIP2, the membrane binding of each protein was very similarly under these three buffer conditions (Fig. 5.5), suggesting that the bulk lipid environment POPE/POPS/Chol did not contribute to any difference in protein-membrane interactions in the presence of additional multivalent cations or EDTA.

I observed that HIV-1 MA membrane binding affinity is sensitive to PIP2 lateral organization. In GUVs with 2mol% PIP2, myristoylated HIV-1 MA had the

Protein-membrane binding = F(membrane bound) - F(background)

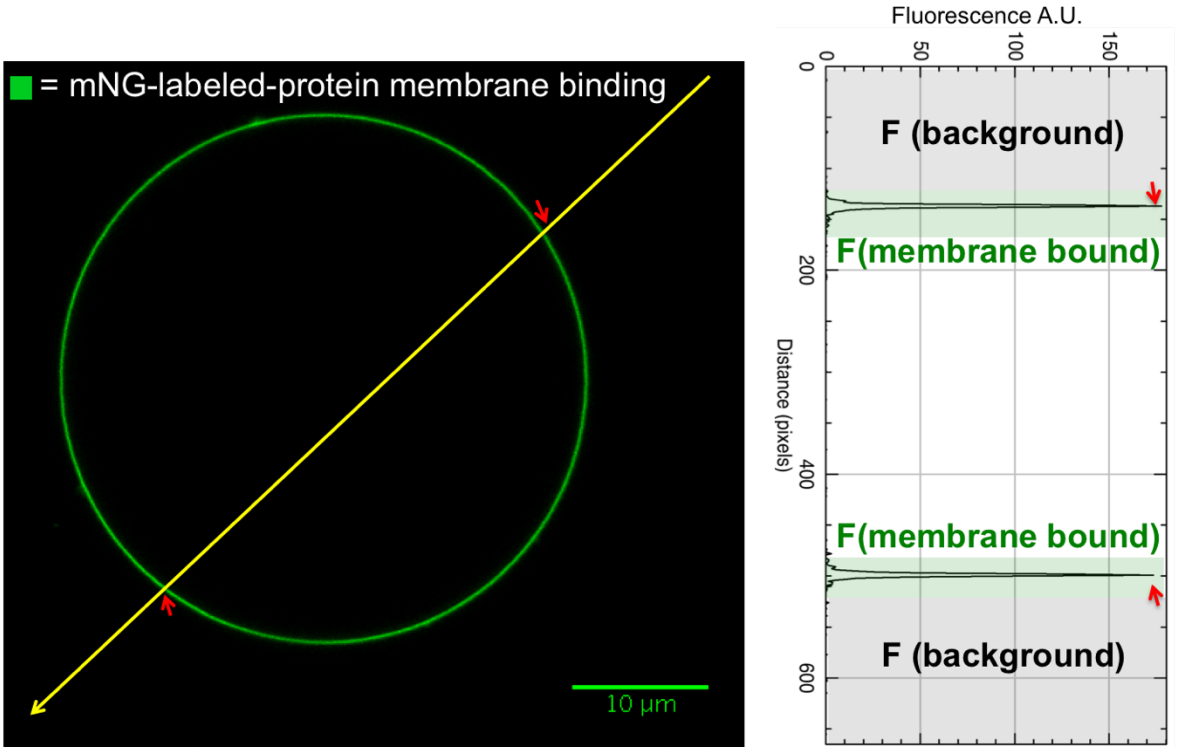

Fig 5.4 Example of protein-GUV binding quantification. mNG-labeled proteins were added to the outside of GUVs for membrane binding. Fluorescence intensity on the membrane above background fluorescence was analyzed by line scans across the perimeter of each GUV, which is used as a measurement of protein-membrane binding (see Material & Methods for details).

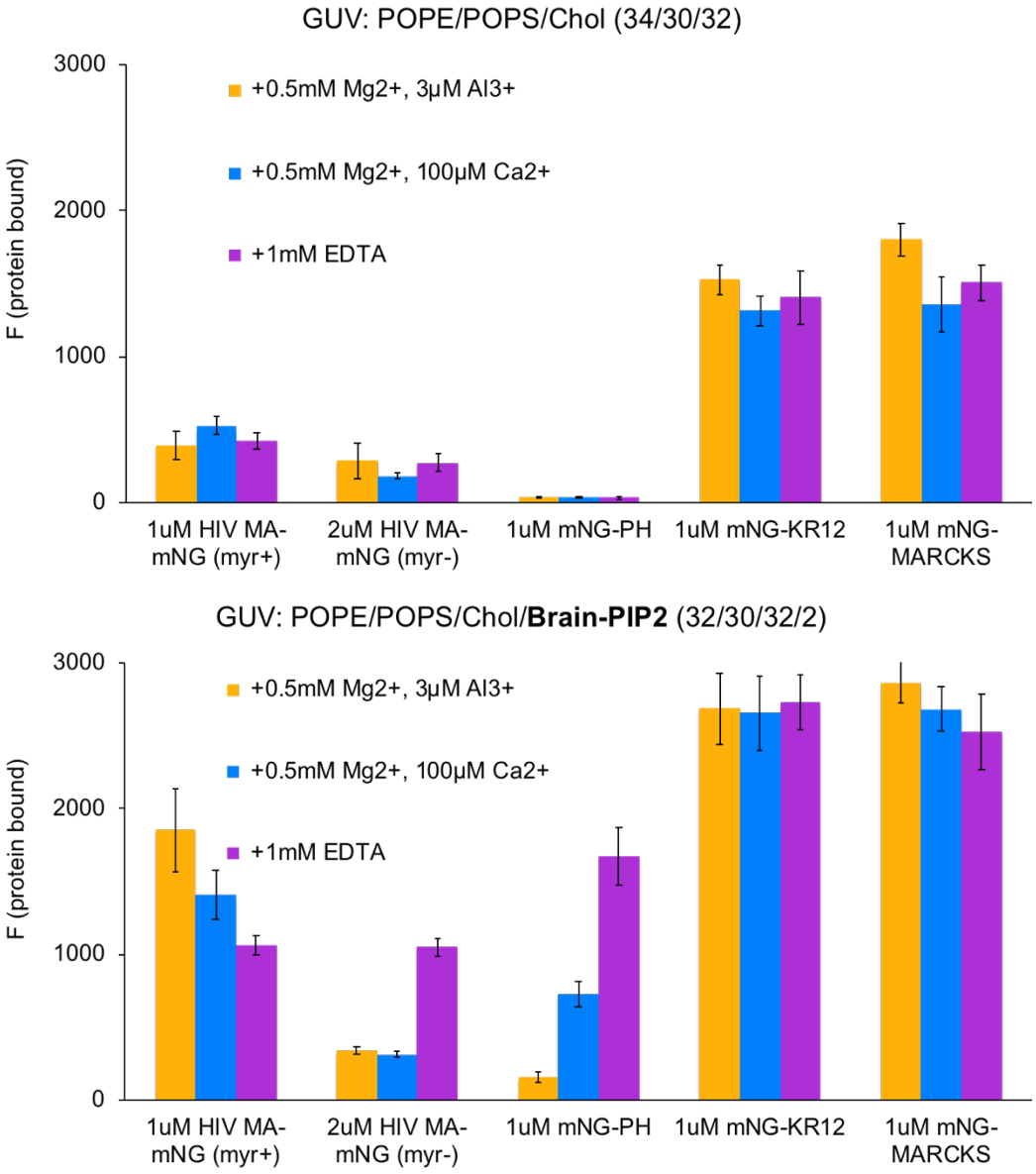

Fig 5.5 Protein can sense PIP2 lateral distributions on GUVs. (top) Protein binding to GUVs in the absence of PIP2; GUV composition: POPE/POPS/Chol (34/30/36); (bottom) protein binding to GUVs in the presence of PIP2; GUV composition: POPE/POPS/Chol/Brain-PIP2 (32/30/36/2). The final concentration for each protein in the binding assay is 1 μM, except HIV-1 MA (myr-) as 2μM. The 3 buffer conditions tested are based on 100mM KCl, 20mM HEPES, pH=7.2, with additional multivalent cations to induce PIP2 clusters, or with EDTA to eliminate PIP2 clusters.

highest affinity to membranes containing strongly clustered PIP2, and had the lowest affinity to membranes containing free PIP2, with almost a 2-fold difference (Fig. 5.5). I interpret these data to mean that HIV-1 MA prefers binding to clustered PIP2 over free PIP2. Strikingly, HIV-1 MA without the N-terminal 14-carbon myristate exhibited the opposite trend, with the highest affinity to membranes containing free PIP2. In the absence of myristoylation, HIV-1 MA showed inhibited membrane binding to both moderately and strongly clustered PIP2, with only about one third of the binding seen for free PIP2. Currently, we don't have an explanation why HIV-1 MA preference for PIP2 clusters depends on the myristoylation. Since non-myristoylated HIV-1 MA barely binds to membranes at 1 μM at 100mM KCl, in the experiments described in Fig. 5.5, I doubled the protein concentration to 2 μM for better visualization.

The phospholipase Cδ1 PH domain (mNG-PH) is the best characterized specific PIP2 binding protein with a structured binding pocket for the PIP2 headgroup. Interestingly, mNG-PH exhibited the highest affinity to free PIP2, approximately 5-fold higher binding than to moderately clustered PIP2, and almost 10-fold higher than binding to strongly clustered PIP2 (Fig. 5.5). Thus, it appears that cation-bridged PIP2 clusters hinder specific PH binding. This result agrees with a previous study showing that Ca^{2+} can confine the PIP2 headgroup tilt angle and can inhibit PH recognition and binding, as evidenced both by liposome experiments and molecular dynamics simulations (82). In addition, both the electrostatic sensor protein with 12 alternating K/R (mNG-KR12) and the MARCKS peptide (mNG-MARCKS) were not sensitive to PIP2 clustering behavior, with equal membrane affinity for all three PIP2 clustering

conditions (Fig. 5.5). Together, these results suggest that in vivo the myristoylated HIV-1 MA domain of Gag targets PIP2 clusters in membranes.

HIV-1 MA induces PIP2 to cluster due to trimerization

Previous studies have provided evidence of cellular proteins sequestering PIP2. For example, MARCKS is reported to sequester three PIP2 headgroups upon binding (83-86). Clustering of membrane-bound Syntaxin-1 can lead to formation of PIP2 clusters by electrostatic interactions with membrane-proximal basic residues (87, 88). The Bin1/amphiphysin/Rvs167 (BAR) domain-containing proteins have been shown to induce stable PIP2-BAR domain cluster formation upon oligomerization of BAR proteins (89-92). Thus, it is possible that viral proteins containing a basic patch, such as HIV-1 MA, could sequester PIP2 as well. To test this hypothesis, I subjected purified viral proteins and 100 nm LUVs with an inner leaflet lipid composition (POPE/POPS/Chol/PIP2 (32/30/36/2)) to fluorometric measurements. Of the 2 mol% total brain-PIP2, a fraction was substituted with the fluorescently labeled PIP2, TF-PIP2, which contains a fluorophore on the sn-2 chain. Similar to the multivalent cation-induced clustering described in Chapter 4, I assayed the ability of protein to induce PIP2 to cluster based on fluorescence self-quenching, see Fig. 5.6. An optimal ratio of 30% TF-PIP2 and 70% brain-PIP2 was used for all self-quenching experiments described here (Fig. 5.7). I first performed the binding assay in pure buffer without any multivalent cations. PIP2 should be mostly free in this buffer. TF-PIP2 at 30% of total PIP2 exhibits a modest fluorescence signal for detection of fluorescence changes. I next determined the optimal protein concentration

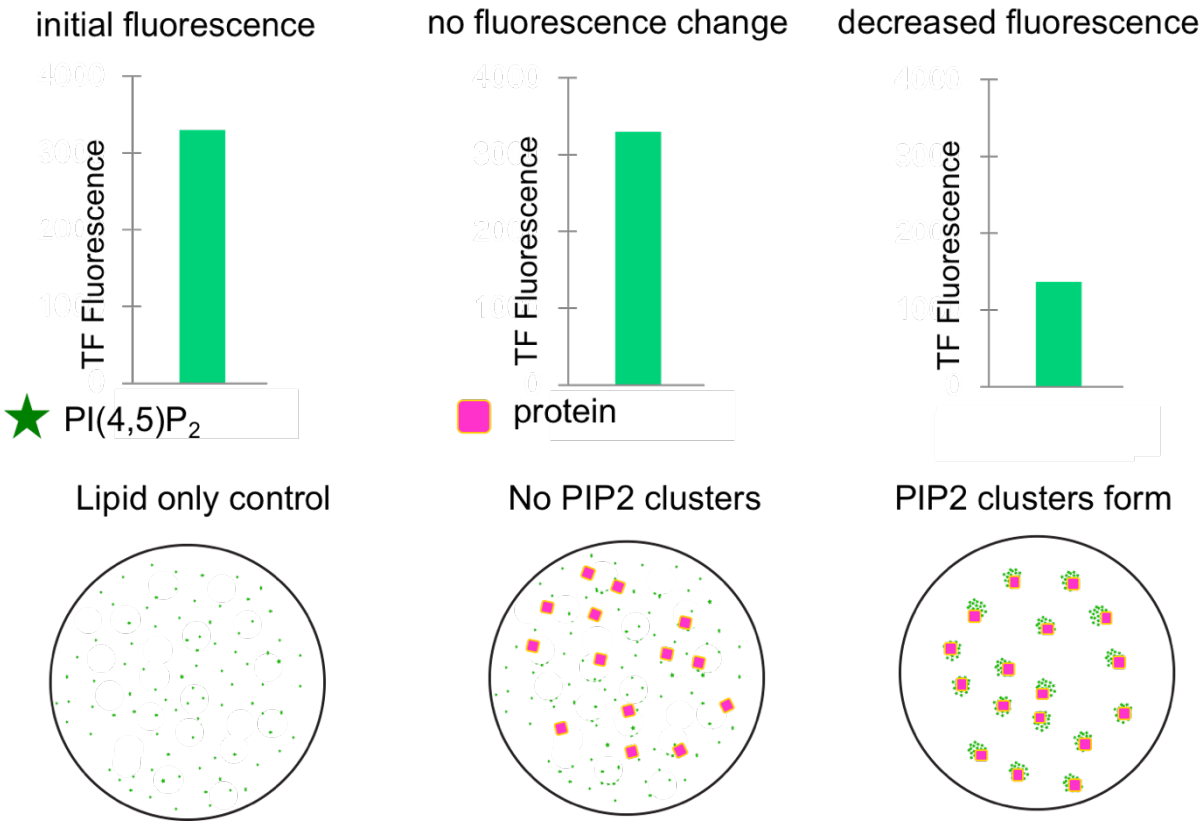

Fig 5.6 Schematic depiction of fluorescence self-quenching assay. (left) Initial fluorescence of lipid only control is measured. (middle) Upon adding proteins, no change of fluorescence indicates no protein-induced PIP2 clusters form. (right) Upon adding proteins, a decrease of fluorescence indicates protein induces PIP2 to form clusters.

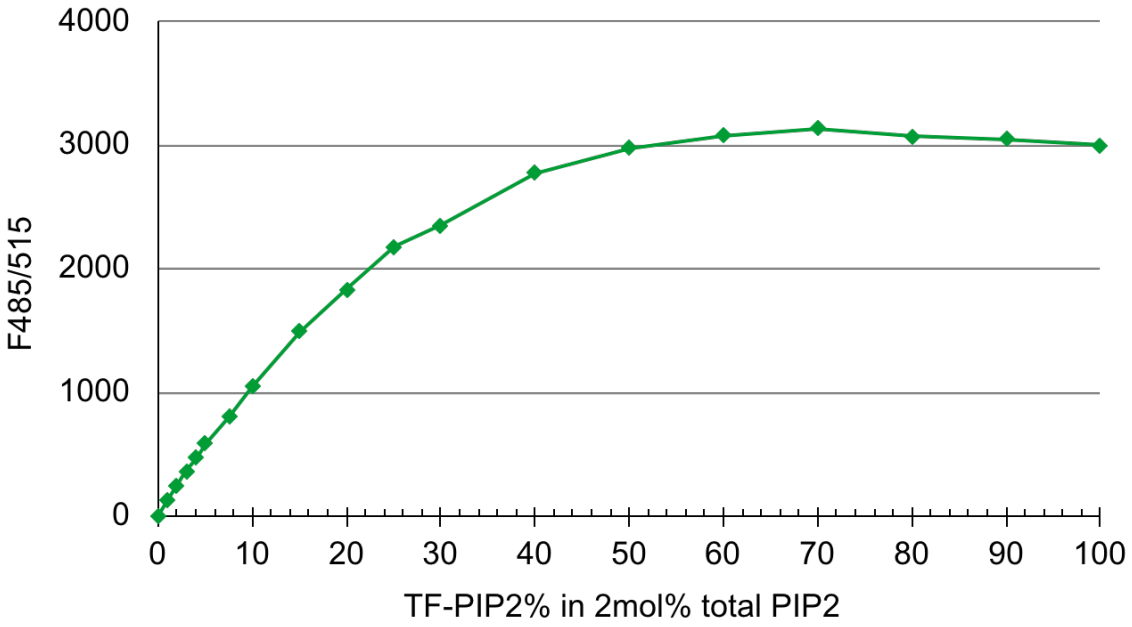

Fig 5.7 Optimize TF-PIP2/Brain-PIP2 ratio for self-quenching assay. Varying TF-PIP2/brain-PIP2 from 0/100 to 100/0 at a fixed 2 mol% total PIP2 in model membranes POPE/POPS/Chol/PIP2 (32/30/36/2).

for the assay using the RSV MASP+6 protein, which mimics the properties of Gag and which is reported to multimerize on PIP2-containing membranes (93). A concentration range for RSV MASP+6 from 0.4 μM up to 40 μM was tested (Fig. 5.8). The fluorescence emission (F485/515) of TF-PIP2 decreased upon the addition of RSV MASP+6, in a concentration-dependent manner. At both 20 μM and 40 μM, RSV MASP+6 binding was near saturation, and so I chose 20 μM as a fixed protein concentration for the following experiments (Fig. 5.8). For all proteins tested, membrane binding should be near saturation at this concentration, which would maximize the effect of protein on PIP2 reorganization.

Compared with the lipid only control, HIV-1 MA but not RSV MA led to significant PIP2 self-quenching, i.e. clustering (Fig. 5.9). HIV-1 MA is naturally myristoylated, but RSV MA is not. To determine if the effect of HIV MA on clustering was due to the myristoylation, I also tested non-myristoylated HIV MA. Remarkably, the capacity of HIV-1 MA to induce PIP2 clustering was not due to the N-terminal myristate, since both myrisotylated and non-myristoylated HIV MA proteins caused similar self-quenching (Fig. 5.9). I hypothesized that the HIV MA-induced PIP2 clustering is due to protein trimerization. One of the earliest crystal structures of HIV MA was of an MA trimer (Fig. 5.1) (46-48). Also, 2D crystallography of HIV MA revealed that the protein formed a lattice composed of hexamers of trimers on PIP2-containing membranes (51). More recent studies demonstrate that mutating residues at the trimer interface results in a decrease of trimerization of MA, both in vivo and vitro (Fig. 5.1) (53). To test the model that MA trimerization influences PIP2 clustering, I mutated residues positioned at the MA

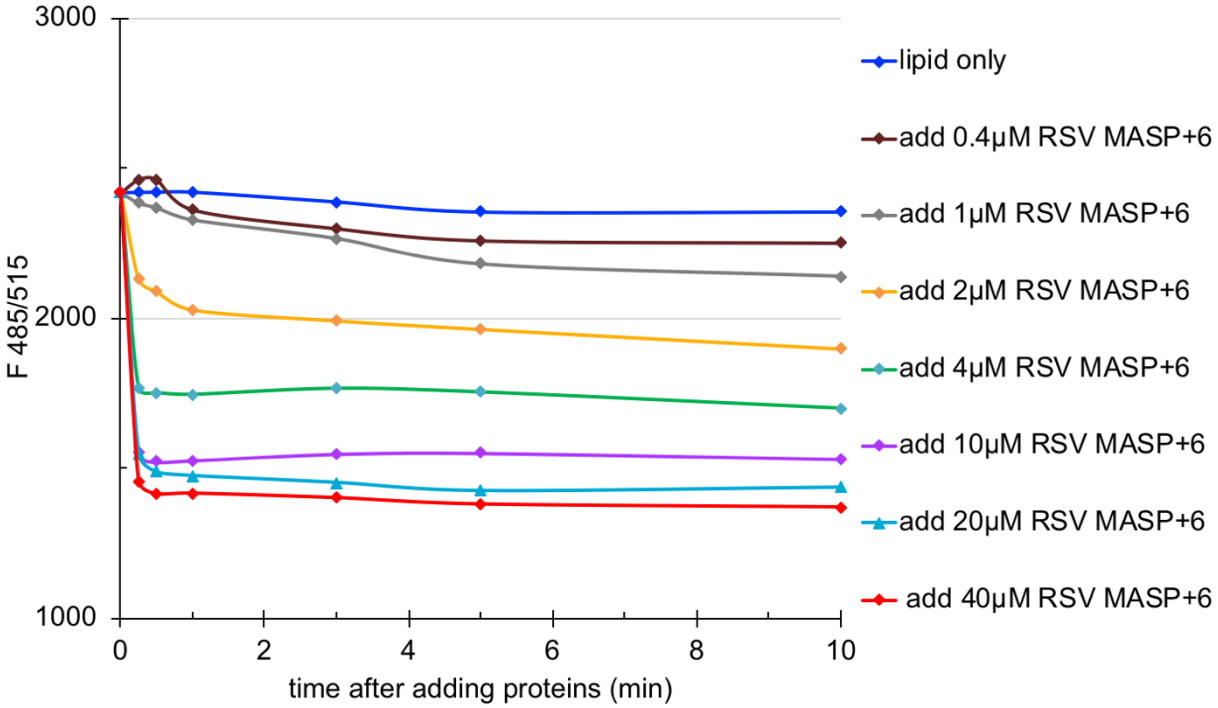

Fig 5.8 Testing the effect of protein concentrations on PIP2 clustering. RSV MASP+6 was added to LUVs at range of concentrations from 0.4 μM up to 40 μM. Lipid only is a negative control without added proteins. All proteins were added at zero time point after the initial fluorescence measurement, then the protein-LUV mixtures were subject to measurements at 0.2, 0.5, 1, 3, 5, and 10min post adding proteins.

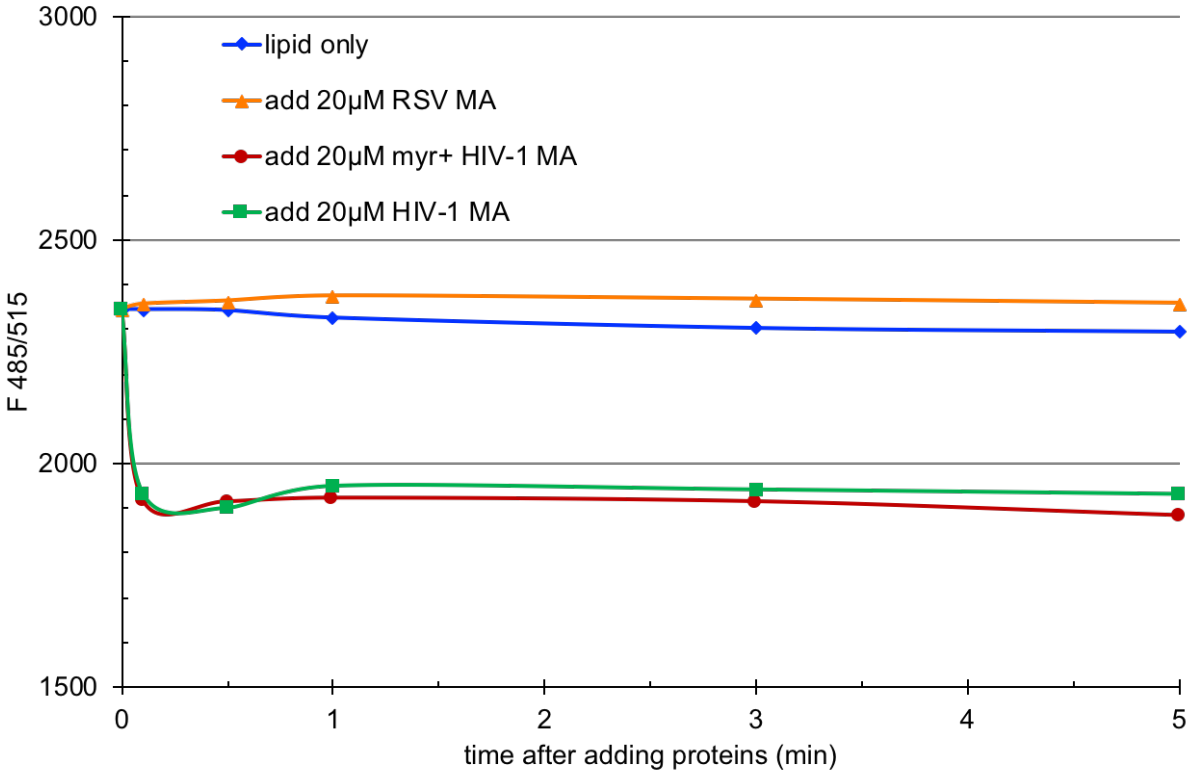

Fig 5.9 HIV-1 MA but not RSV MA promotes PIP2 clustering. RSV MA, myr+ HIV-1 MA and HIV-1 MA without myristate were added to LUVs at a final 20 μM, then each protein-LUV mixture was subject to measurements at 0.2, 0.5, 1, 3, and 5 min post adding proteins.

trimer interface. Three single mutant proteins (69TR, 69TD, 74LE) and a double mutant (69TR+74LE) were tested. No self-quenching of TF-PIP2 was observed for all four HIV-1 MA trimer-defective mutants in Fig. 5.10. To rule out the possibility that the lack of induced PIP2 clustering is due to a loss of membrane binding for all the HIV-1 MA trimer-defective mutants, I performed liposome pelleting assays. According to SDS-PAGE gel staining, all four HIV-1 MA trimer-defective mutants bound to liposomes, but only about half as well as did wild type HIV-1 MA (data not shown). To further address whether an increased membrane binding leads to PIP2 clustering, we repeated the protein-membrane assay for all proteins at a lower ionic strength, 50mM KCl. The known enhanced electrostatic interactions at lower ionic strength did not change TF-PIP2 self-quenching (Fig. 5.11). Thus, in summary, the lack of induced PIP2 clustering of the trimer mutants is likely due to the loss of HIV-1 MA trimer formation. Taken together, these results imply that HIV-1 MA promotes PIP2 clustering, which is due to MA trimerization, not to myristoylation.

Multimerization of HIV-1 and RSV Gag promote PIP2 clustering

Gag-membrane association and Gag-Gag multimerization enhance each other, leading to the formation of the Gag lattice and ultimately to the virus particle. For both HIV-1 and RSV, the CA and SP domains contribute to intermolecular Gag-Gag interactions (1, 94, 95). The RSV protein with most of the NC domain removed, MASP+6, has previously been shown to multimerize on membranes (79). I predict that the analogous protein for HIV, MASP, would also multimerize on membranes. As shown in Fig. 5.12, both HIV-1 MASP and RSV MASP+6 binding resulted in

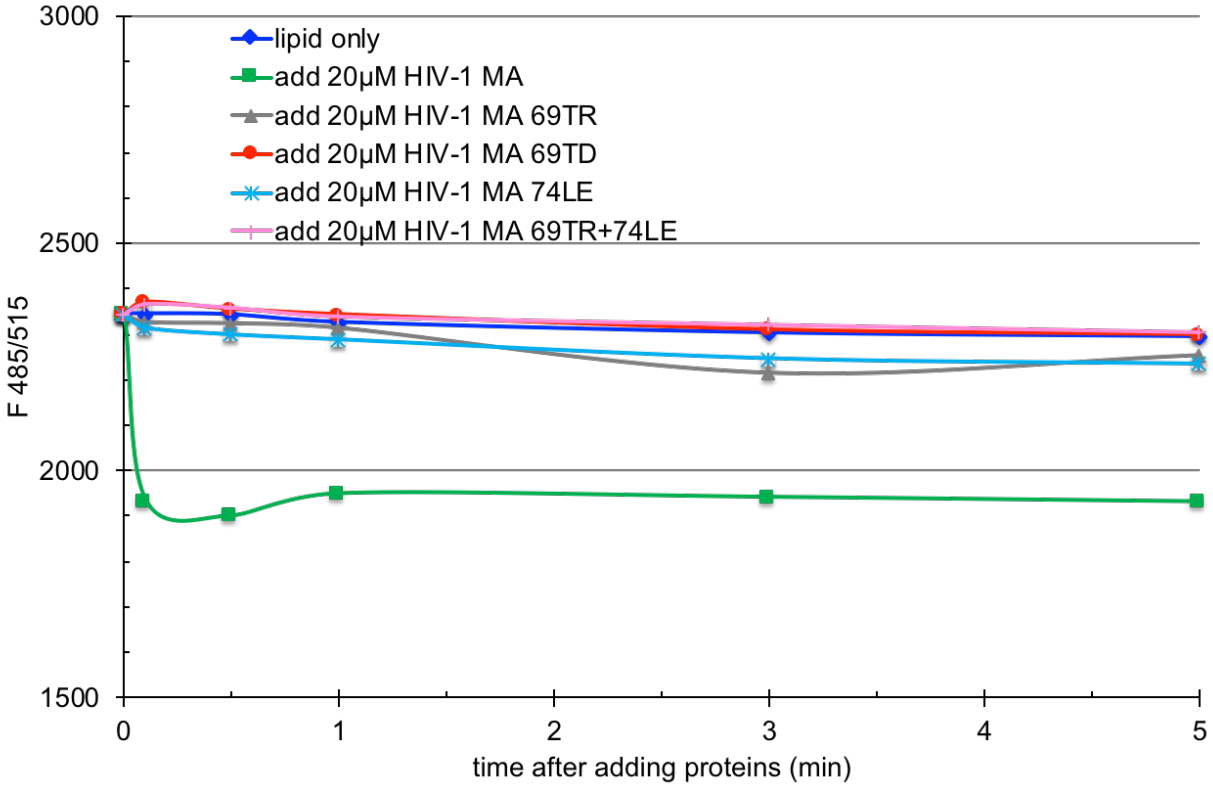

Fig 5.10 Loss of HIV-1 MA trimerization abolishes induced PIP2 cluster. HIV-1 MA WT and all four mutants were added to LUVs at a final 20 μM, then each protein-LUV mixture was subject to measurements at 0.2, 0.5, 1, 3, and 5 min post adding proteins.

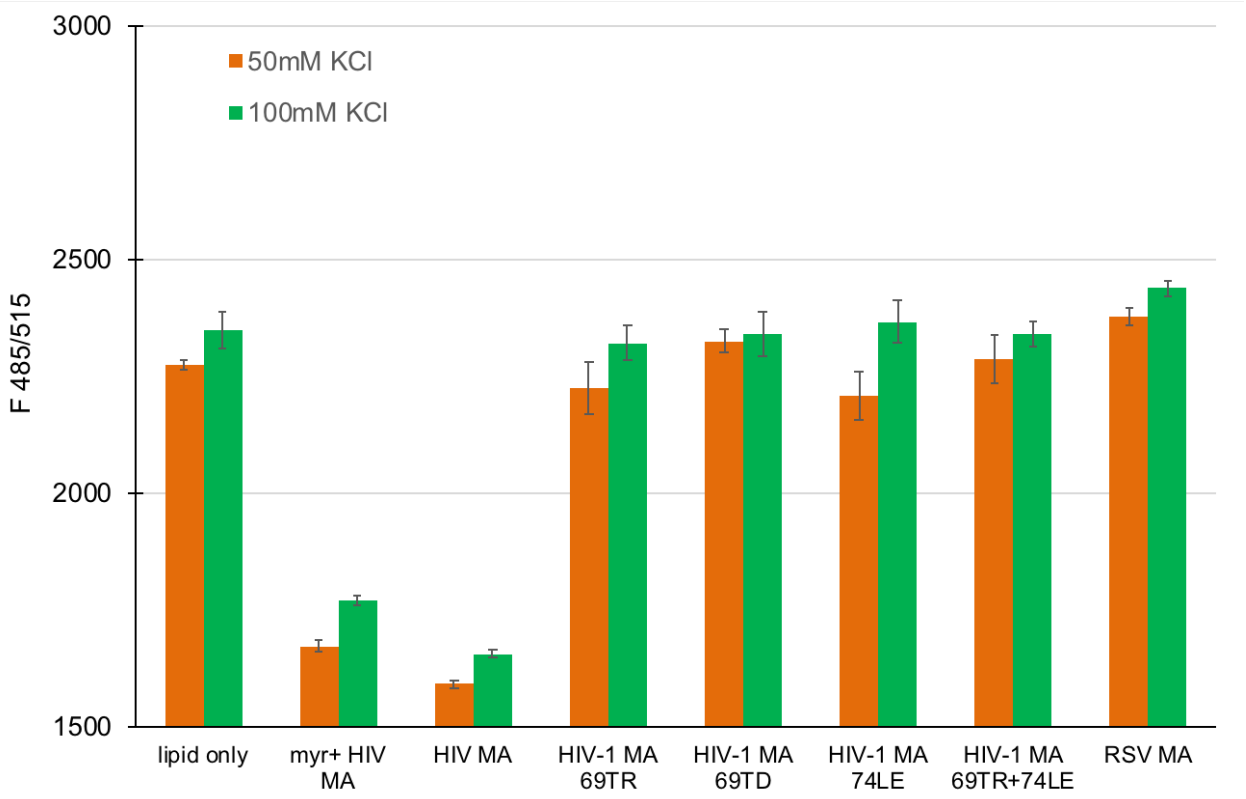

Fig 5.11 Effects of ionic strength on protein-induced PIP2 clustering. All protein-membrane binding was performed at both 50 mM and 100mM KCl. Each protein was added to LUVs at a final 20 μM, then each protein-LUV mixture was subject to measurements after 5min.

dramatic self-quenching, implying PIP2 clustering. For HIV, the quenching was greater than that observed for MA (see Fi. 5.9 and Fig. 5.12), which I interpret to indicate a greater degree of protein multimerization. A single mutation I475A in RSV MASP+6 has previously been identified to abolish in vitro assembly of VLPs (79, 96), because it disrupts the ability of the SP sequence to form a six-helix bundle by eliminating hydrophobic interactions with the neighboring helix. Indeed, this single amino acid mutant form of the RSV protein showed a significant recovery of TF-PIP2 fluorescence (Fig. 5.13), consistent with the predicted defect in hexamer formation. The effect was similar at both 50mM KCl and 100mM KCl (data not shown)

To further explore the effect of protein multimerization on PIP2 clustering I purified and tested an artificial chimera of RSV MA that forms hexamers. The RSV MA-CcmK4 protein is fused at its C-terminus to the hexameric carboxysome shell protein CcmK4 (93, 97, 98). I found that hexamerized RSV MA led to the strongest degree of TF-PIP2 self-quenching among all proteins tested (Fig. 5.14). In summary, multimerization of both HIV-1 and RSV Gag and Gag derivatives drives PIP2 clustering.

SUMMARY

This study shows that (1) HIV-1 MA prefers to bind to PIP2 clusters compared with free PIP2, and this preference is dependent on the N-terminal myristate; and that (2) HIV-1 Gag multimerization further promotes PIP2 clustering. HIV-1 viral membranes are found to be enriched in PIP2 compared with the host PM. My study supports the hypothesis that HIV-1 targets pre-existing PIP2-rich domains as assembly

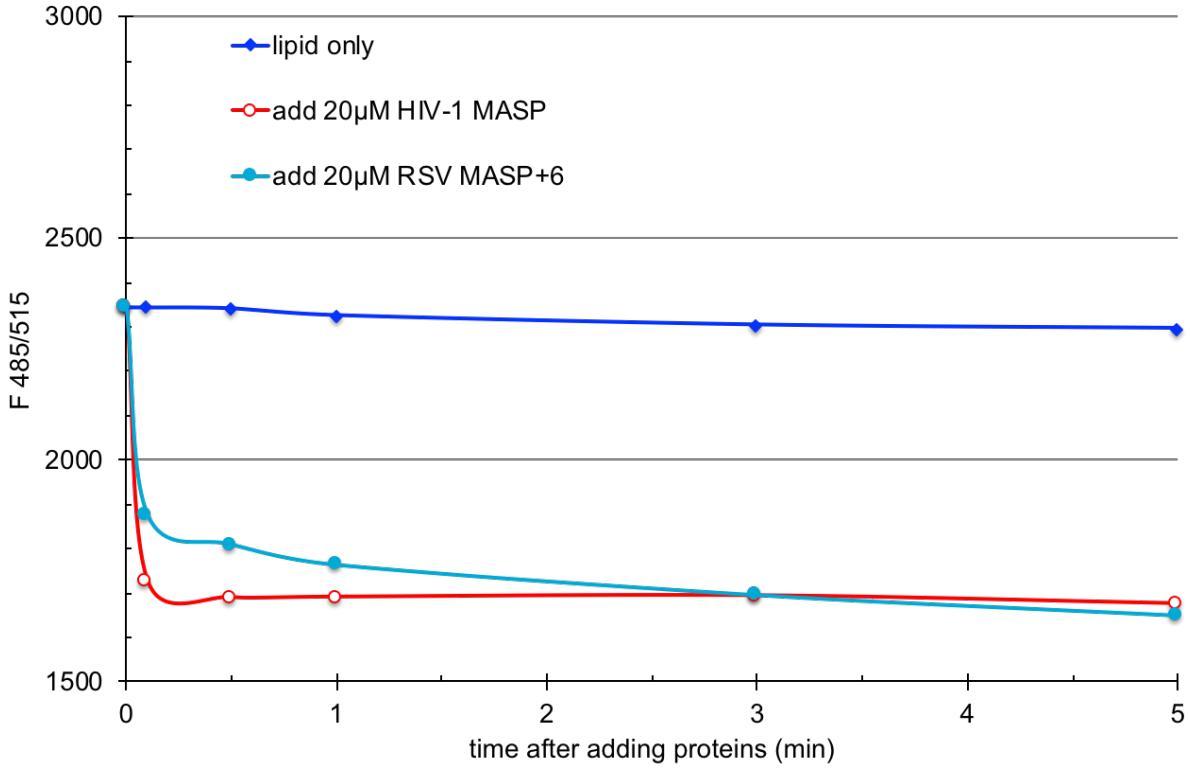

Fig 5.12 Both HIV-1 MASP and RSV MASP+6 induce significant PIP2 clustering. HIV-1 MASP and RSV MASP+6 were added to LUVs at a final 20 μM, then each protein-LUV mixture was subject to measurements at 0.2, 0.5, 1, 3, and 5 min post adding proteins.

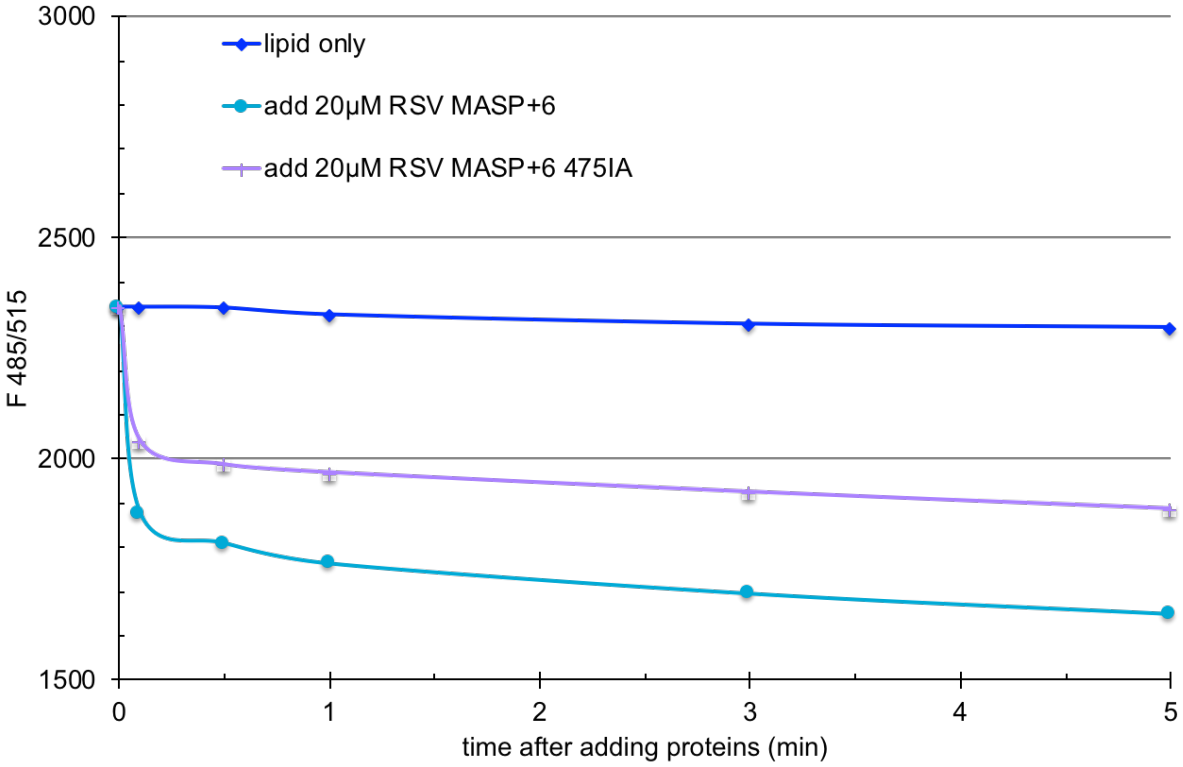

Fig 5.13 A multimerization-defective RSV Gag mutant exhibits reduced PIP2 clustering ability. Both RSV MASP+6 WT and 475IA mutant were added to LUVs at a final 20 μM, then each protein-LUV mixture was subject to measurements at 0.2, 0.5, 1, 3, and 5 min post adding proteins.

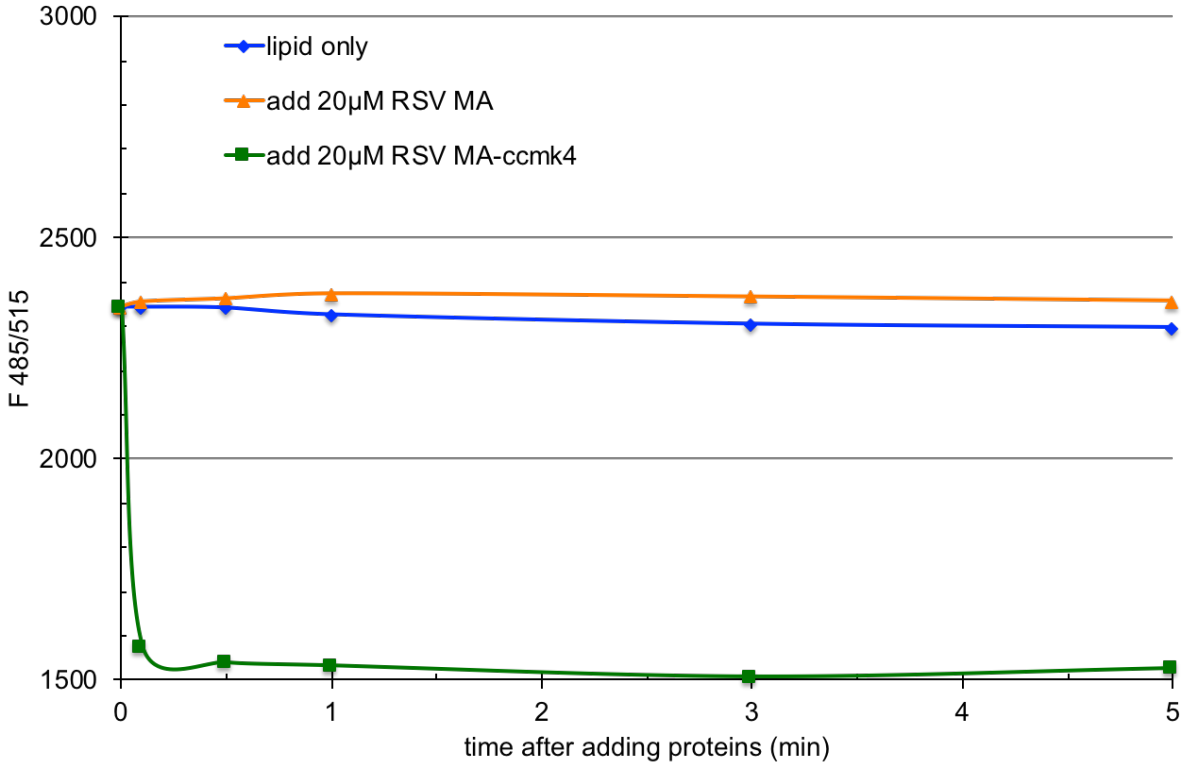

Fig 5.14 Forced hexameric RSV MA promotes significant PIP2 clustering. Both RSV MA and hexameric RSV MA-ccmK4 were added to LUVs at a final 20 μM, then each protein-LUV mixture was subject to measurements at 0.2, 0.5, 1, 3, and 5 min post adding proteins.

sites, and there further enriches PIP2 as Gag multimerizes to form the protein lattice that underlies the viral membrane.

In the future, I plan to test the HIV-1 Gag protein MACA, which does not contain the SP domain and thus cannot form the six-helix bundle that is essential for formation of hexamers. Similarly, I will also test several HIV-1 MASP mutants that abrogate assembly, including mutants that wreck the CA-CTD dimer interface (316WA+317MA), and mutants that abolish SP dependent hexamerization (363LA, 367MA, 363LA+367MA, 363LR+367MR) (Fig. 5.2). In addition, I also would like to test, in the context of MASP, the MA trimer enhancement mutant 62QR, a PIP2-binding defective mutant (HBR/RK switch), and all of the HIV-1 MA trimer-defective mutants. I predict that mutants that decrease the ability of the protein to multimerize will reduce the ability of the protein to induce PIP2 clusters.

REFERENCES

1. Sundquist WI, Krausslich HH-G, Kräusslich HG. 2012. HIV-1 Assembly , Budding , and Maturation. Cold Spring Harb Perspect Med. 2: a006924.
2. Briggs JAG, Riches JD, Glass B, Bartonova V, Zanetti G, Krausslich H-G. 2009. Structure and assembly of immature HIV. Proc Natl Acad Sci. 106:11090-11095.
3. Pettit SC, Lindquist JN, Kaplan AH, Swanstrom R. 2005. Processing sites in the human immunodeficiency virus type 1 (HIV-1) Gag-Pro-Pol precursor are cleaved by the viral protease at different rates. Retrovirology. 2:66.
4. Mattei S, Tan A, Glass B, Müller B, Kräusslich H-G, Briggs JAG. 2018. High-resolution structures of HIV-1 Gag cleavage mutants determine structural switch for virus maturation. Proc Natl Acad Sci. 115:E9401-E9410.
5. Briggs JAG, Grünewald K, Glass B, Förster F, Kräusslich HG, Fuller SD. 2006. The mechanism of HIV-1 core assembly: Insights from three-dimensional reconstructions of authentic virions. Structure. 14:15-20.
6. Dick RA, Vogt VM. 2014. Membrane interaction of retroviral Gag proteins. Front Microbiol. :187.
7. M. Resh. 1999. Fatty acylation of proteins: new insights into membrane targeting of myristylated and palmitoylated proteins. Biochim Biophys Acta - Mol Cell Res 1451:1-16.
8. Peitzsch RM, McLaughlin S. 1993. Binding of acylated peptides and fatty acids to phospholipid vesicles: pertinence to myristoylated proteins. Biochemistry 32:10436-10443.
9. Bouamr F, Scarlata S, Carter C. 2003. Role of myristylation in HIV-1 Gag assembly. Biochemistry. 42:6408-6417.
10. Barros M, Heinrich F, Datta SAK, Rein A, Karageorgos I, Nanda H, Lösche M. 2016. Membrane binding of HIV-1 matrix protein: dependence on bilayer composition and protein lipidation. J Virol. 90:4544-4555.
11. Li H, Dou J, Ding L, Spearman P. 2007. myristoylation is required for human immunodeficiency virus type 1 Gag-Gag multimerization in mammalian cells. J

Virol. 81:12899-12910.

12. Provitera P, El-Maghrabi R, Scarlata S. 2006. The effect of HIV-1 Gag myristoylation on membrane binding. Biophys Chem. 119:23-32.
13. Chukkapalli V, Ono A. 2011. Molecular determinants that regulate plasma membrane association of HIV-1 Gag. J Mol Biol. 410:512-524.
14. Cannon PM, Matthews S, Clark N, Byles ED, Iourin O, Hockley DJ, Kingsman SM, Kingsman AJ. 1997. Structure-function studies of the human immunodeficiency virus type 1 matrix protein, p17. J Virol. 71:3474-83.
15. Chukkapalli V, Hogue IB, Boyko V, Hu W-S, Ono A, Hogue IB, Chukkapalli V, Hu W-S, Boyko V, Hogue IB, Boyko V, Hu W-S, Ono A. 2007. Interaction between the human immunodeficiency virus type 1 gag matrix domain and phosphatidylinositol-(4,5)-bisphosphate is essential for efficient Gag membrane binding. J Virol. 82:2405-2417.
16. Lorizate M, Krausslich H-G, Kräusslich HG. 2011. Role of lipids in virus replication. Cold Spring Harb Perspect Biol. 3a004820.
17. Waheed AA, Freed EO. 2018. The role of lipids in retroviral replication. in retrovirus-cell interactions. Academic Press. 353-399.
18. Olety B, Ono A. 2014. Roles played by acidic lipids in HIV-1 Gag membrane binding. Virus Res. 193:108-115.
19. Ono A, Orenstein JM, Freed EO. 2002. Role of the Gag matrix domain in targeting human immunodeficiency virus type 1 assembly. J Virol. 74:2855-2866.
20. Vlach J, Saad JS. 2015. Structural and molecular determinants of HIV-1 Gag binding to the plasma membrane. Front Microbiol. 6:232.
21. Saad JS, Miller J, Tai J, Kim A, Ghanam RH, Summers MF. 2006. Structural basis for targeting HIV-1 Gag proteins to the plasma membrane for virus assembly. Proc Natl Acad Sci. 103:11364-11369.
22. Mercredi PY, Bucca N, Loeliger B, Gaines CR, Mehta M, Bhargava P, Tedbury PR, Charlier L, Floquet N, Muriaux D, Favard C, Sanders CR, Freed EO, Marchant J, Summers MF. 2016. Structural and molecular determinants of

membrane binding by the HIV-1 matrix protein. J Mol Biol. 428:1637-1655.
23. Llewellyn GN, Grover JR, Olety B, Ono A. 2013. HIV-1 Gag associates with specific uropod-directed microdomains in a manner dependent on its MA highly basic region. J Virol. 87:6441-6454.
24. Alfadhli A, Barklis E. 2014. The roles of lipids and nucleic acids in HIV-1 assembly. Front Microbiol. 5:253.
25. Chukkapalli V, Oh SJ, Ono A. 2010. Opposing mechanisms involving RNA and lipids regulate HIV-1 Gag membrane binding through the highly basic region of the matrix domain. Proc Natl Acad Sci. 107:1600-1605.
26. Ono A, Ablan SD, Lockett SJ, Nagashima K, Freed EO. 2004. Phosphatidylinositol (4,5) bisphosphate regulates HIV-1 Gag targeting to the plasma membrane. Proc Natl Acad Sci. 101:14889-14894.
27. Chan R, Uchil PD, Jin J, Shui G, Ott DE, Mothes W, Wenk MR. 2008. Retroviruses Human Immunodeficiency Virus and Murine Leukemia Virus Are Enriched in Phosphoinositides. J Virol. 82:11228-11238.
28. Brugger B, Glass B, Haberkant P, Leibrecht I, Wieland FT, Krausslich H-G. 2006. The HIV lipidome: A raft with an unusual composition. Proc Natl Acad Sci. 103:2641-2646.
29. Lorizate M, Sachsenheimer T, Glass B, Habermann A, Gerl MJ, Kräusslich H-GG, Brügger B. 2013. Comparative lipidomics analysis of HIV-1 particles and their producer cell membrane in different cell lines. Cell Microbiol. 15:292-304.
30. Tedbury PR, Freed EO. 2014. The role of matrix in HIV-1 envelope glycoprotein incorporation. Trends Microbiol. 22:372-378.
31. Checkley MA, Luttge BG, Freed EO. 2011. HIV-1 envelope glycoprotein biosynthesis, trafficking, and incorporation. J Mol Biol. 410:582-608.
32. Wyma DJ, Jiang J, Shi J, Zhou J, Lineberger JE, Miller MD, Aiken C. 2004. Coupling of human immunodeficiency virus type 1 fusion to virion maturation: a novel role of the gp41 cytoplasmic tail. J Virol. 78:3429-3435.
33. Jiang J, Aiken C. 2007. Maturation-dependent human immunodeficiency virus type 1 particle fusion requires a carboxyl-terminal region of the gp41

cytoplasmic tail. J Virol. 81:9999-10008.

34. Muranyi W, Malkusch S, Müller B, Heilemann M, Kräusslich H-GG. 2013. Super-resolution microscopy reveals specific recruitment of HIV-1 envelope proteins to viral assembly sites dependent on the envelope C-terminal tail. PLoS Pathog. 9:e1003198.
35. Wyma DJ, Kotov A, Aiken C. 2002. Evidence for a stable interaction of gp41 with Pr55Gag in immature human immunodeficiency virus type 1 particles. J Virol. 74:9381-9387.
36. Freed EO, Martin MA. 1995. Virion incorporation of envelope glycoproteins with long but not short cytoplasmic tails is blocked by specific, single amino acid substitutions in the human immunodeficiency virus type 1 matrix. J Virol. 69:1984-1989.
37. Davis MR, Jiang J, Zhou J, Freed EO, Aiken C. 2006. A mutation in the human immunodeficiency virus type 1 Gag protein destabilizes the interaction of the Envelope protein subunits gp120 and gp41. J Virol. 80:2405-2417.
38. Mammano F, Kondo E, Sodroski J, Bukovsky A, Göttlinger HG. 1995. Rescue of human immunodeficiency virus type 1 matrix protein mutants by envelope glycoproteins with short cytoplasmic domains. J Virol. 69:3824-3830.
39. Tedbury PR, Ablan SD, Freed EO. 2013. Global rescue of defects in hiv-1 envelope glycoprotein incorporation: implications for matrix structure. PLoS Pathog. 9:e1003739.
40. Murakami T, Freed EO. 2002. Genetic evidence for an interaction between human immunodeficiency virus type 1 matrix and alpha -helix 2 of the gp41 cytoplasmic tail. J Virol. 74:3548-3554
41. Tedbury PR, Mercredi PY, Gaines CR, Summers MF, Freed EO. 2015. Elucidating the mechanism by which compensatory mutations rescue an hiv-1 matrix mutant defective for gag membrane targeting and envelope glycoprotein incorporation. J Mol Biol. 427:1413-1427.
42. Cosson P. 1996. Direct interaction between the envelope and matrix proteins of HIV-1. EMBO J. 15:5783-5788.

43. West JT, Weldon SK, Wyss S, Lin X, Yu Q, Thali M, Hunter E. 2002. Mutation of the dominant endocytosis motif in human immunodeficiency virus type 1 gp41 can complement matrix mutations without increasing Env incorporation. J Virol. 76:3338-3349.
44. Postler TS, Desrosiers RC. 2012. The tale of the long tail: the cytoplasmic domain of HIV-1 gp41. J Virol. 87:2-15.
45. Roy NH, Chan J, Lambele M, Thali M. 2013. Clustering and mobility of HIV-1 Env at viral assembly sites predict its propensity to induce cell-cell fusion. J Virol. 87:7516-7525.
46. Hill CP, Worthylake D, Bancroft DP, Christensen AM, Sundquist WI. 1996. Crystal structures of the trimeric human immunodeficiency virus type 1 matrix protein: implications for membrane association and assembly. Proc Natl Acad Sci. 93:3099-3104.
47. Massiah MA, Starich MR, Paschall C, Summers MF, Christensen AM, Sundquist WI. 1994. Three-dimensional structure of the human immunodeficiency virus type 1 matrix protein. J Mol Biol. 244:198-223.
48. Massiah MA, Worthylake D, Christensen AM, Sundquist WI, Hill CP, Summers MF. 1996. Comparison of the NMR and X-ray structures of the HIV-1 matrix protein: Evidence for conformational changes during viral assembly. Protein Sci. 5:2391-2398.
49. Rao Z, Belyaev AS, Fry E, Roy P, Jones IM, Stuart DI. 1995. Crystal structure of SIV matrix antigen and implications for virus assembly. Nature. 378:743-747.
50. Alfadhli A, Barklis RL, Barklis E. 2009. HIV-1 matrix organizes as a hexamer of trimers on membranes containing phosphatidylinositol-(4,5)-bisphosphate. Virology. 387:466-472.
51. Alfadhli A, Huseby D, Kapit E, Colman D, Barklis E. 2006. Human immunodeficiency virus type 1 matrix protein assembles on membranes as a hexamer. J Virol. 81:1472-1478.
52. Huseby D, Barklis RL, Alfadhli A, Barklist E. 2005. Assembly of human

immunodeficiency virus precursor Gag proteins. J Biol Chem. 280:17664-17670.

53. Tedbury PR, Novikova M, Ablan SD, Freed EO. 2015. Biochemical evidence of a role for matrix trimerization in HIV-1 envelope glycoprotein incorporation. Proc Natl Acad Sci. 113:E182-E190.

54. Sanders RW, Vesanen M, Schuelke N, Master A, Schiffner L, Kalyanaraman R, Paluch M, Berkhout B, Maddon PJ, Olson WC, Lu M, Moore JP. 2002. Stabilization of the soluble, cleaved, trimeric form of the envelope glycoprotein complex of human immunodeficiency virus type 1. J Virol. 76:8875-8889.

55. Zhu P, Chertova E, Bess J, Lifson JD, Arthur LO, Liu J, Taylor KA, Roux KH. 2003. Electron tomography analysis of envelope glycoprotein trimers on HIV and simian immunodeficiency virus virions. Proc Natl Acad Sci. 100:15812-15817.

56. Alfadhli A, Mack A, Ritchie C, Cylinder I, Harper L, Tedbury PR, Freed EO, Barklis E. 2016. Trimer enhancement mutation effects on HIV-1 matrix protein binding activities. J Virol. 90:5657-5664.

57. Datta SAK, Clark PK, Fan L, Ma B, Harvin DP, Sowder RC, Nussinov R, Wang Y-X, Rein A. 2016. Dimerization of the SP1 region of HIV-1 Gag induces a helical conformation and association into helical bundles: implications for particle assembly. J Virol. 90:1773-1787.

58. Datta SAK, Temeselew LG, Crist RM, Soheilian F, Kamata A, Mirro J, Harvin D, Nagashima K, Cachau RE, Rein A. 2011. On the role of the SP1 domain in HIV-1 particle assembly: a molecular switch? J Virol. 85:4111-4121.

59. Schur FKM, Obr M, Hagen WJH, Wan W, Jakobi AJ, Kirkpatrick JM, Sachse C, Kräusslich HG, Briggs JAG. 2016. An atomic model of HIV-1 capsid-SP1 reveals structures regulating assembly and maturation. Science. 353:506-508.

60. Liang C, Hu J, Russell RS, Roldan A, Kleiman L, Wainberg MA. 2002. Characterization of a putative -helix across the capsid-sp1 boundary that is critical for the multimerization of human immunodeficiency virus type 1 Gag. J Virol. 76:11729-11737.

61. Guo X, Roldan A, Hu J, Wainberg MA, Liang C. 2005. Mutation of the sp1 sequence impairs both multimerization and membrane-binding activities of human immunodeficiency virus type 1 Gag. J Virol. 79:1803-1812.
62. Guo X, Liang C. 2005. Opposing effects of the M368A point mutation and deletion of the SP1 region on membrane binding of human immunodeficiency virus type 1 Gag. Virology. 335:232-241.
63. Accola MA, Höglund S, Göttlinger HG. 1998. A putative alpha-helical structure which overlaps the capsid-p2 boundary in the human immunodeficiency virus type 1 Gag precursor is crucial for viral particle assembly. J Virol. 72:2072-2078.
64. von Schwedler UK, Stray KM, Garrus JE, Sundquist WI. 2003. Functional surfaces of the human immunodeficiency virus type 1 capsid protein. J Virol. 77:5439-5450.
65. Ganser-Pornillos BK, von Schwedler UK, Stray KM, Aiken C, Sundquist WI. 2004. Assembly properties of the human immunodeficiency virus type 1 CA protein. J Virol. 78:2545-2552.
66. Zhao G, Perilla JR, Yufenyuy EL, Meng X, Chen B, Ning J, Ahn J, Gronenborn AM, Schulten K, Aiken C, Zhang P. 2013. Mature HIV-1 capsid structure by cryo-electron microscopy and all-atom molecular dynamics. Nature. 497:643-646.
67. Gres AT, Kirby KA, KewalRamani VN, Tanner JJ, Pornillos O, Sarafianos SG. 2015. X-ray crystal structures of native HIV-1 capsid protein reveal conformational variability. Science. 349:99-103.
68. Adamson CS, Jones IM. 2004. The molecular basis of HIV capsid assembly - Five years of progress. Rev Med Virol. 14:107-121.
69. Gamble TR, Yoo S, Vajdos FF, Von Schwedler UK, Worthylake DK, Wang H, McCutcheon JP, Sundquist WI, Hill CP. 1997. Structure of the carboxyl-terminal dimerization domain of the HIV-1 capsid protein. Science. 278:849-853.
70. Ivanov D, Tsodikov O V., Kasanov J, Ellenberger T, Wagner G, Collins T.

2007. Domain-swapped dimerization of the HIV-1 capsid C-terminal domain. Proc Natl Acad Sci. 104:4353-4358.

71. Ganser-Pornillos BK, Cheng A, Yeager M. 2007. Structure of full-length HIV-1 CA: a model for the mature capsid lattice. Cell. 131:70-79.
72. Wagner JM, Zadrozny KK, Chrustowicz J, Purdy MD, Yeager M, Ganser-Pornillos BK, Pornillos O. 2016. Crystal structure of an HIV assembly and maturation switch. Elife. 5:e17063.
73. Wen Y, Vogt VM, Feigenson GW. 2018. Multivalent cation-bridged PI(4,5)P2 clusters form at very low concentrations. Biophys J. 114:2630-2639.
74. Dalton AK, Ako-adjei D, Murray PS, Murray D, Vogt VM. 2007. Electrostatic interactions drive membrane association of the human immunodeficiency virus type 1 Gag MA domain. J Virol. 81:6434-6445.
75. Malakhov MP, Mattern MR, Malakhova OA, Drinker M, Weeks SD, Butt TR. 2004. SUMO fusions and SUMO-specific protease for efficient expression and purification of proteins. J Struct Funct Genomics. 5:75-86.
76. Kingsley PB, Feigenson GW. 1979. The synthesis of a perdeuterated phospholipid: 1,2-dimyristoyl-sn-glycero-3-phosphocholine-d72. Chem Phys Lipids. 24:135-147.
77. Wang T. 2010. Inductively coupled plasma optical emission spectrometry analytical instrumentation handbook, 2nd edition.
78. Buboltz JT, Feigenson GW. 1999. A novel strategy for the preparation of liposomes: Rapid solvent exchange. Biochim Biophys Acta - Biomembr 1417:232-245.
79. Dick RA, Barros M, Jin D, Lösche M, Vogt VM. 2015. Membrane binding of the Rous sarcoma virus Gag protein is cooperative and dependent on the spacer peptide assembly domain. j virol. 90:2473-2485.
80. Wen Y, Dick RA, Feigenson GW, Vogt VM. 2016. Effects of membrane charge and order on membrane binding of the retroviral structural protein Gag. J Virol. 90:9518-9532.
81. Kwiatkowska K. 2010. One lipid, multiple functions: How various pools of

PI(4,5)P2 are created in the plasma membrane. Cell Mol Life Sci. 67:3927-3946.

82. Bilkova E, Pleskot R, Rissanen S, Sun S, Czogalla A, Cwiklik L, Róg T, Vattulainen I, Cremer PS, Jungwirth P, Coskun Ü. 2017. Calcium directly regulates phosphatidylinositol 4,5-bisphosphate headgroup conformation and recognition. J Am Chem Soc. 139:4019-4024.

83. Zaitseva I, Cafiso DS, Wang J, Murray D, Gambhir A, Pentyala SN, Smith SO, Mclaughlin S, Hangyas-Mihalyne G, Zaitseva I, Cafiso DS, Wang J, Murray D, Pentyala SN, Smith SO, Mclaughlin S, Gambhir A, Pentyala SN, Smith SO, Mclaughlin S. 2004. Electrostatic sequestration of PIP2 on phospholipid membranes by basic/aromatic regions of proteins. Biophys J. 86:2188-2207.

84. Rauch ME, Ferguson CG, Prestwich GD, Cafiso DS. 2002. Myristoylated alanine-rich C kinase substrate (MARCKS) sequesters spin-labeled phosphatidylinositol 4,5-bisphosphate in lipid bilayers. J Biol Chem. 277:14068-14076.

85. Wang J, Gambhir A, Hangyás-Mihályné G, Murray D, Golebiewska U, McLaughlin S. 2002. Lateral sequestration of phosphatidylinositol 4,5-bisphosphate by the basic effector domain of myristoylated alanine-rich C kinase substrate is due to nonspecific electrostatic interactions. J Biol Chem. 277:34401-34412.

86. Wang J, Arbuzova A, Hangyas-Mihalyne G, McLaughlin S. 2001. The Effector domain of myristoylated alanine-rich c kinase substrate binds strongly to phosphatidylinositol 4,5-bisphosphate. J Biol Chem. 276:5012-5019.

87. Van Den Bogaart G, Meyenberg K, Risselada HJ, Amin H, Willig KI, Hubrich BE, Dier M, Hell SW, Grubmüller H, Diederichsen U, Jahn R. 2011. Membrane protein sequestering by ionic protein-lipid interactions. Nature. 479:552-555.

88. Honigmann A, Van Den Bogaart G, Iraheta E, Risselada HJ, Milovanovic D, Mueller V, Müllar S, Diederichsen U, Fasshauer D, Grubmüller H, Hell SW, Eggeling C, Kühnel K, Jahn R. 2013. Phosphatidylinositol 4,5-bisphosphate clusters act as molecular beacons for vesicle recruitment. Nat Struct Mol Biol.

20:679-686.

89. Picas L, Viaud J, Schauer K, Vanni S, Hnia K, Fraisier V, Roux A, Bassereau P, Gaits-Iacovoni F, Payrastre B, Laporte J, Manneville JB, Goud B. 2014. BIN1/M-Amphiphysin2 induces clustering of phosphoinositides to recruit its downstream partner dynamin. Nat Commun. 5:5647
90. Yoon Y, Zhang X, Cho W. 2012. Phosphatidylinositol 4,5-bisphosphate (PtdIns(4,5)P2) specifically induces membrane penetration and deformation by Bin/Amphiphysin/Rvs (BAR) domains. J Biol Chem. 287:34078-34090.
91. Lappalainen P, Koskela EV V., Tkach V, Drubin DGG, Michelot A, Stamou D, Zhao H, Michelot A, Koskela EV V., Tkach V, Stamou D, Drubin DGG, Lappalainen P. 2013. Membrane-sculpting BAR domains generate stable lipid microdomains. Cell Rep. 4:1213-1223.
92. Saarikangas J, Zhao H, Pykäläinen A, Laurinmäki P, Mattila PK, Kinnunen PKJ, Butcher SJ, Lappalainen P. 2009. Molecular mechanisms of membrane deformation by I-BAR domain proteins. Curr Biol. 19:95-107.
93. Dick RA, Kamynina E, Vogt VM. 2013. Effect of multimerization on membrane association of Rous sarcoma virus and HIV-1 matrix domain proteins. J Virol. 87:13598-13608.
94. Bush DL, Vogt VM. 2014. In vitro assembly of retroviruses. Annu Rev Virol. 1:561-580.
95. Ganser-Pornillos BK, Yeager M, Sundquist WI. 2008. The structural biology of HIV assembly. Curr Opin Struct Biol. 18:203-217.
96. Bush DL, Monroe EB, Bedwell GJ, Prevelige PE, Phillips JM, Vogt VM. 2014. Higher-order structure of the rous sarcoma virus SP assembly domain. J Virol. 88:5617-5629.
97. Kerfeld CA, Kerfeld CA, Sawaya MR, Tanaka S, Nguyen C V, Phillips M, Beeby M, Yeates TO. 2005. Protein structures forming the shell of primitive bacterial organelles. Science. 309:936-938.
98. Pornillos O, Ganser-Pornillos BK, Kelly BN, Hua Y, Whitby FG, Stout CD, Sundquist WI, Hill CP, Yeager M. 2009. X-Ray structures of the hexameric

building block of the HIV capsid. Cell. 137:1282-1292.

APPENDIX

SUMMARY

Myristoylated HIV-1 Gag and MA are sensitive to lipid acyl chain types, favoring disordered membranes (Ld) (1). However, I found that RSV Gag, like electrostatic sensor proteins, did not exhibit a preference for membrane order when an equal amount of negatively charged lipids PS are present in both disordered (Ld) and ordered membranes (Lo). RSV Gag membrane binding is primarily based on electrostatic interactions. The difference between these HIV-1 and RSV Gag sensitivity to membrane order could be due to the insertion of the hydrophobic myristate group into membranes. In my previous study, control proteins MARCKS and PS sensor Ev2 showed a strong preference to Ld over Lo. The MARCKS peptide binds to membrane via both electrostatic interactions from the 13 basic residues, and hydrophobic interactions from the 5 phenylalanine residues. I speculate that hydrophobic residues in both MARCKS and Ev2 are inserted into the inner core of the bilayer, and that this insertion is disfavored in the tightly packed Lo phase.

EIAV Gag is not naturally myristoylated, but showed dramatic sensitivity to membrane order, strongly preferring Ld over Lo according to liposome pelleting data (data not shown). Further in vitro investigations reveal that EIAV Gag-membrane association is partially dependent on the presence of the NC domain (data not shown). HIV-1 NC has been reported to be also engaged in membrane binding in addition to the MA domain (2). Interestingly, the NC domain is required for EIAV Gag sensitivity to Ld, as EIAV MA and MASP+5 failed to show any response to different membrane

order (data not shown). Amino acid analysis of the NC domains of these three retroviruses suggests that both HIV-1 and EIAV NC domains harbor 4-5 hydrophobic residues, while RS NC domain only contains 2 (Fig. A1). It indicates that these hydrophobic residues in HIV and EIAV NC might play a role in membrane order preference.

To further elucidate whether protein preference for Ld is due to the hydrophobic components, such as N-terminal myristoylation and hydrophobic residues, I mutated the hydrophobic residues to alanine in EIAV NC, HIV-1 NC, and MARCKS peptide, and also mutated the second glycine to alanine (F2A) in HIV-1 MA to block myristoylation. All proteins were purified as fluorescent proteins with mNG fused at the C-terminus. I prepared GUVs DSPC/DPPS/DOPC/DOPS/Chol (18/12/30/15/25) with resulting 24 mol% PS in both Ld and Lo phases. LR-DOPE, a red fluorescent marker was added to label the Ld phase. The protein-membrane binding assay was performed at 50mM KCl by the use of confocal microscopy. In Fig. A1, mNG-KR12 , an electrostatic sensor protein, was tested as a negative control, as it only follows the membrane charge, not membrane order. Both EIAV and HIV-1 wild type (WT) NC domains exhibited 4-fold higher binding to Ld than to Lo, while EIAV and HIV-1 NC with all hydrophobic residues mutated (F2A) lost their sensitivity to membrane order. Similarly, MARCKS WT bound to Ld significantly higher than to Lo, and F2A mutations completely abolished this preference. These results imply that the insertion of side chains of hydrophobic residues in EIAV NC, HIV-1 NC, and MARCKS is responsible for the Ld preference. Consistent with previous finding, myristoylated HIV-1 MA favored binding to Ld over Lo. The loss of the N-terminal

myristate led to the loss of the 4-fold preference binding to Ld. HIV-1 MA without myristate lost the preference to membrane order. RSV NC only slightly preferred Ld. This result indicates that the myristate insertion, another form of hydrophobic interaction, is responsible for HIV-1 Gag preference for Ld. In summary, I showed that proteins containing hydrophobic components, either a patch of hydrophobic residues or hydrophobic fatty acid modifications such as myristate, have preference for disordered membranes.

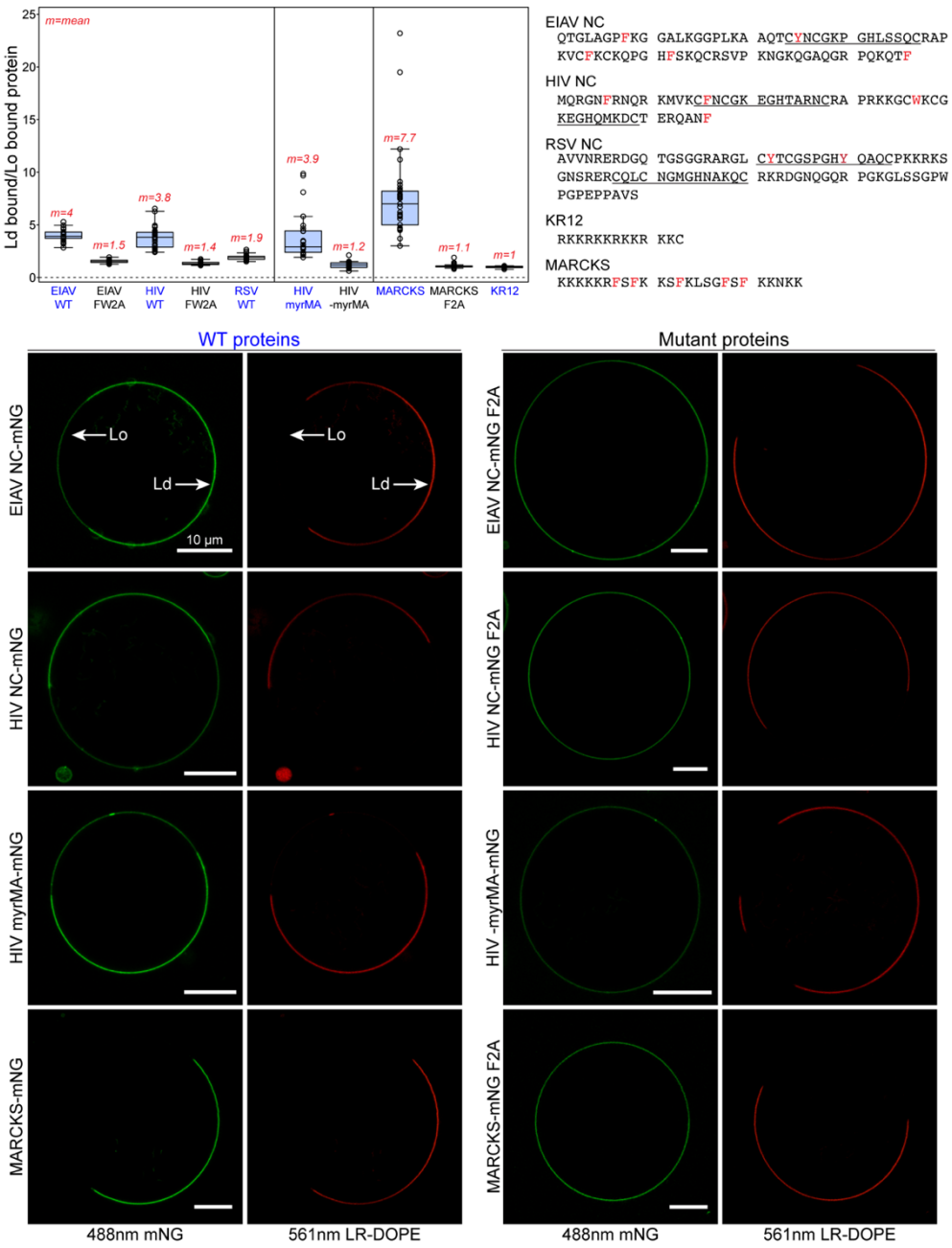

Fig. A1 Proteins with hydrophobic components favor disordered membranes on GUVs. GUVs: DSPC/DPPS/DOPC/DOPS/Chol (18/12/30/15/25) with 24 mol% PS in both Ld and Lo phases; buffer: 50mM KCl, 20mM Tris, pH=7.2; protein final concentration=1 µM. (Top, Left) The ratio of mNG-labeled protein binding to Ld/Lo. (Top, Right) Amino acid sequences of proteins tested with hydrophobic residues marked in red. (Bottom) Representative confocal images of protein-GUV binding. Red channels: LR-DOPE labeling the Ld phase; green channel: mNG-labeled proteins.

REFERENCES

1. Dick, R. A., Goh, S. L., Feigenson, G. W., & Vogt, V. M. (2012). HIV-1 Gag protein can sense the cholesterol and acyl chain environment in model membranes. Proc Natl Acad Sci.109:18761-18766.

2. 2. Datta, S. A., Heinrich, F., Raghunandan, S., Krueger, S., Curtis, J. E., Rein, A., & Nanda, H. (2011). HIV-1 Gag extension: conformational changes require simultaneous interaction with membrane and nucleic acid. J. Mol Biol. 406:205-214.